NJ

NASA CONTRACTOR REPORT
NASA CR-165574

UTRC REPORT
R81-915540-9

NASA

MASS AND MOMENTUM TURBULENT TRANSPORT EXPERIMENTS WITH CONFINED COAXIAL JETS

(NASA-CR-165574) MASS AND MOMENTUM TURBULENT TRANSPORT EXPERIMENTS WITH CONFINED COAXIAL JETS Interim Report, 18 Feb. - 18 Oct. 1981 (United Technologies Research Center) 157 p HC A08/MF A01

N82-19496

Unclas
G3/34 09270

By B.V. Johnson
J.C. Bennett

Prepared by
UNITED TECHNOLOGIES RESEARCH CENTER
East Hartford, CT 06108

For
NATIONAL AERONAUTICS AND SPACE ADMINISTRATION
LEWIS RESEARCH CENTER
CLEVELAND, OHIO
NOVEMBER 1981

MASS AND MOMENTUM TURBULENT
TRANSPORT EXPERIMENTS WITH
CONFINED COAXIAL JETS

Table of Contents

Table of Contents
(Continued)

MASS AND MOMENTUM TURBULENT TRANSPORT EXPERIMENTS WITH CONFINED COAXIAL JETS

B. V. Johnson
J. C. Bennett

SUMMARY

An experimental study of mixing downstream of coaxial jets discharging in an expanded duct was conducted to obtain data for the evaluation and improvement of turbulent transport models currently used in a variety of computational procedures throughout the propulsion community for combustor flow modeling. The study used laser velocimeter (LV) and laser induced fluorescence (LIF) techniques to measure velocities and concentration and flow visualization techniques to qualitatively determine the time dependent characteristics of the flow and the scale of the turbulent structure.

Flow visualization studies showed four major shear regions occurring; a wake region immediately downstream of the inner jet inlet duct, a shear region further downstream between the inner and annular jets, a recirculation zone, and a reattachment zone.

A combination of turbulent momentum transport rate and two velocity component data were obtained from simultaneous measurements with a two color LV system. Axial, radial and azimuthal velocities and turbulent momentum transport rate measurements in the r-z and r-θ planes were used to determine the mean value, second central moment (or rms fluctuation from mean), skewness and kurtosis for each data set probability density function (p.d.f.).

A combination of turbulent mass transport rate, concentration and velocity data were obtained from simultaneous measurements with an LV and LIF system. Velocity and mass transport in all three directions as well as concentration distributions were used to obtain the mean, second central moments, skewness and kurtosis for each p.d.f. These LV/LIF measurements also exposed the existence of a large region of counter-gradient turbulent axial mass transport in the region where the annular jet fluid was accelerating the inner jet fluid. These results also showed that for high transport rate regions, the transport rate p.d.f.s, skewness and kurtosis were similar to those occurring in turbulent boundary layers but that in low transport regions (including the recirculation region) these were higher than previously measured for the wake regions of turbulent boundary layers.

INTRODUCTION

Background

Computational procedures to predict combustion processes are being developed and refined by a number of researchers (e.g., see Ref. 19 and surveys in Refs. 20, 21, 22). These computational procedures predict the velocity, species, concentration, temperature and reaction rate distribution within the combustors which are used to determine combustor liner heat load, engine performance (combustion efficiency), pollution emissions (reactant products) and pattern factor (temperature distribution at turbine inlet). Because most combustors of practical interest have turbulent flow, the calculation procedures usually include mathematical models for the turbulent transport of mass (or species), momentum and heat. However, the prediction of combustion processes is very sensitive to the modeling of the mass and momentum transport processes and improper models result in inadequate predictions of combustion efficiency, liner heat load, emissions and exit temperature pattern factor.

The recent prediction of recirculating combusting flows typical of those found in aircraft gas turbines, have produced qualitative results which "provide insight into the nature of the combustion process rather than quantitative design information" (Ref. 19). Although the insight is helpful in diagnosing problems, the long term goal of the combustion modelers is to decrease combustor development costs by using accurate combustor design procedures. The deficiencies in the current computational procedures have been attributed to weaknesses in the mathematical models, including the transport models, and in the numerical methods. One recommendation from a NASA workshop on combustion modeling was that the mathematical models used in the calculation procedures be validated using experiments specifically designed to provide the required input data (Ref. 19). The first step in this process is the validation of the mass and momentum turbulent transport models for constant density flow.

The data used to formulate and validate the turbulent transport models have been obtained primarily from velocity and momentum transport measurements because only a limited amount of concentration and mass transport data is available. The mass (species) transport data presently available are not sufficient to determine where inadequacies exist in the present models or to formulate improvements for the models. One reason for this situation is that the method for simultaneously obtaining turbulent mass (species) and momentum transport data often have been indirect, requiring compromising assumptions. To overcome these limitations a new technique has been developed to simultaneously measure concentration and velocity and, therefore mass transport data which can be used to evaluate and improve combustion oriented turbulent transport models for scalars such as concentration of species and and temperature.

A review of techniques to measure instantaneous velocity, temperature and species concentration at a point is presented in Ref. 2. The current discussion will be limited to concentration measurement techniques. There are several intrusive techniques for simultaneously measuring velocity and concentration. Libby (e.g., Ref. 3) has successfully used two hot wires in air-helium mixtures; however, hot wire techniques are generally limited to flows without recirculation and have not been used extensively for gaseous mixtures other than helium and air which have large variations in thermal conductivity and density. Other methods require two probes which are often bulky and preclude 'point' measurements.

Several non-intrusive measurement techniques have been proposed to obtain simultaneously velocity and concentration measurements in recirculating flows (e.g., Ref. 4). Raman scattering, marker nephelometry (Ref. 5), and the laser induced fluorescence (LIF) of a trace material are three techniques previously used for obtaining the concentration portion of these measurements. Raman scattering has applications for combustion studies but has sensitivity limitations for room temperature fluid mechanics studies. Marker nephelometry requires high seed rates and probe volumes for LDV velocity measurements orders of magnitude smaller than the probe volume for concentration measurements. Laser induced fluorescence of trace dyes or gases offers an experimental method which is compatible with LDV measurements.

The use of fluorescein dye as a trace element in water was chosen for use in the current study of mixing between constant density fluids for several reasons. These reasons are: (1) that the dye and water are relatively inexpensive, (2) the wavelength required to excite the dye is compatible with current LDV equipment, and (3) the fluids are convenient to use. This choice restricts the measurement technique to the acquisition of constant density transport data. Although the combustion process has variable density gases mixing in a reacting environment, the mathematical transport models for combustors are expected to be based on the turbulent transport phenomena found in constant density mixing with modifications for variable density and reacting flows.

A preliminary effort at UTRC to obtain quantitative concentration measurements with fluorescent dye in 1975 was described by Owen (Paper 28 of Ref. 4). The current effort at UTRC was initiated in 1978 and makes use of improved optics, data handling capabilities and operative procedures. Initial results from the current effort were presented in Ref. 6. These measurements were limited in scope as only mean and fluctuating axial and radial velocities and radial mass transport measurements were obtained. The experimental capability for the present study was expanded to include measurement of the mass transport in the axial (z) and azimuthal (θ) directions and the momentum transport in the z-r and z-θ planes. Data acquisition and storage techniques were used in the present study which allowed the calculation of the higher moments of the velocity, concentration and turbulent transport rate probability density functions.

The current application of the combined LV/LIF measurement techniques along with the available data handling procedures provides an opportunity to obtain data which can be used to evaluate a number of computation methods and turbulent transport models. Results from the present study can be used to evaluate (1) the presently used two-equation turbulence model, (2) the Reynolds stress transport model and (3) the probability density function formulation for predicting turbulent transport and concentration fluctuations.

Outline of Present Study

Turbulent mixing of confined coaxial jets is being studied because of its similarity to the combustor situation and thus its value in the mathematical modeling of combustor flow fields. Surveys of previous experimental studies were presented in Refs. 7 and 8. The turbulent mixing characteristics of confined coaxial jets are applicable to the combustion fluid mixing process because the flow field has the same features found in gas turbine combustors and furnaces. The coaxial jets provide a method of introducing fuel and air into the combustion chamber. The recirculating flow zones associated with coaxial jets in enlarged ducts provide the pilot region usually required to maintain flame in a combustor over a range of operating conditions.

The Reynolds number ($Re = \rho Vd/u$) of flow injected through various sections of aircraft gas turbine combustors vary from 10^4 to 10^6 and, therefore, the flows are generally turbulent. Lower Reynolds numbers occur for flow through cooling holes at engine idle conditions. Higher Reynolds numbers occur for flow through swirlers or dilution jets at engine takeoff conditions. The flow conditions selected for the detailed data acquisition in the present study have Reynolds numbers of 15,900 and 47,500 for the inner and annular streams, respectively. These Reynolds numbers are factors of 5 to 20 greater than the transitional Reynolds number range and in the range occurring in aircraft gas turbines. Therefore, turbulent transport phenomena measured in the present experiment are also expected to be typical of the transport phenomena occurring in gas turbines.

The shear regions of coaxial jets confined in an enlarged duct are presented in Fig. 1. The discussion of the results from the present study will be related to each region as applicable. The terms and symbols shown on the figure will be used throughout the report.

The extent of each region shown in Fig. 1 has been previously shown to depend upon the dimensions of the coaxial jets and ducts, the velocities in the two streams and the fluid properties. The length of the wake region depends upon the jet inlet velocity profiles and the development of the shear layer between the jets. The length of the shear layer between the jets will depend upon the ratio U_i/U_a, and the dimensions of the jets. The length and velocities in the recirculation region will depend on the jet and duct dimensions and the velocity of the annular jet. The flow characteristics in the reattachment region are likely to be influenced by the characteristics in the shear layer between jets before reattachment. Thus, the flow field is relatively complex with interaction between several regions.

The present study was initiated with a flow visualization study to qualitatively determine the effects of velocity regio, U_i/U_a, and Reynolds number on the flow characteristics of the shear regions cited in Fig. 1. These tests were conducted for one inlet and duct geometry. Results from the study were also used to determine streamwise locations for obtaining detailed velocity, concentration, and transport rate measurements.

The major focus of this study was on the acquisition, reduction and analysis of velocity, concentration, mass transport rate and momentum transport rate measurements at seven axial locations within the duct test section. Single component velocity data and inner jet fluid concentration data were obtained simultaneously to determine the local mass (or scalar) transport rate. Two velocity components were obtained simultaneously to determine the local momentum transport rates. As a result, the concentration and principle velocity distributions were obtained during at least two nonconsecutive data acquisition runs. The data set for each point measurement was analyzed and reduced to obtain the mean and three central moments from each probability density function (p.d.f.), i.e., the mean values, the rms deviation from the mean, the skewness of the p.d.f., and the flatness factor (or kurtosis) of the p.d.f. The averages and central moments were obtained for the mass and momentum transport p.d.f.s as well as the velocity and concentration p.d.f.s. The reduced results for each data point set are tabulated and presented in this report. Graphical presentations of representative results are also included to aid in the discussion of the results.

Although the flow condition of the data reported in Ref. 6 was the same as that for the present study, the additional measurements of the present study produced several interesting and important results. Flow visualization showed the secondary vortex pairs superimposed on the conventional large scale turbulent structure in the shear layer between the jets. The axial mass transport results showed countergradient mass transport rates larger than the radial mass transport rates in a large central region of the flow. With regard to the evaluation of the mass and momentum transport models, the third and fourth central moments of the concentration and mass transport rate were found to be larger than those for the velocities and momentum transport rate. These results provide the turbulent transport modelers with much needed detail to (1) determine differences between the current models and experiments or (2) formulate improved models.

DESCRIPTION OF APPARATUS AND PROCEDURES

Flow System

A sketch of the test section along with the inlet and exhaust sections is shown in Fig. 2. The working fluid for this experiment was water with a temperature of approximately 20C. The test section consisted of a 122 mm inside diameter by 1 m long, thin-wall glass tube mounted in an optical box. Flow to the test section entered through an annular duct and a smaller center tube (Fig. 3). Flow exhausted through the exit duct, up over a weir and flowed to the drain. The top end of the duct containing the weir was open to the atmosphere. The atmospheric pressure at the weir prevented the test section from becoming overpressurized. In order to decrease the optical distortion obtained when conducting flow visualization and optical experiments in circular tubes thorugh water-glass-air interfaces, a flat-faced optical box surrounded the circular test section which was filled with water. The inlet plenum for the annular duct contained three perforated plates to produce approximately uniform flow and an honeycomb section to remove swirl from the flow. No flow straightening devices were used for the inner jet tube which was approximately 25 mm (1 in.) dia. and was fed with the same diameter duct and hose for the lengths of over 10 ft.

A schematic of the flow components used in the experiment is presented in Fig. 4. For the laser velocimeter tests, flow was circulated by a pump from the storage tank, through metering valves and flow measuring devices to the center jet inlet and annular jet inlet of the inlet plenum. The flow from the annular duct and center tube entered the test section, mixed, discharged into the exhaust ducts, and returned to the storage tank. For the LV/LIF tests and flow visualization tests where fluorescein dye was used as a tracer, the water from the exhaust was discharged into the city sanitary sewer and fresh water replenished the system.

For tests with dye, the dye was added to the inner jet fluid in a mixing chamber a short distance from the innet jet metering valve. Uniform flow of the dye was obtained by metering the dye through a micrometering valve with a 20 to 40 psi pressure drop. This pressure drop was large compared to other pressure drops in the system to ensure a uniform dye concentration in the inner jet fluid. A magnetic rotating mixer was used to keep the dye well stirred. An inline filter was required to prevent the dye micrometering valve from clogging.

Flow Visualization

Sketches of the optical arrangements used to obtain flow visualization photographs and motion pictures of the flow pattern in the r-z and r-θ planes are shown in Figs. 5 and 6, respectively. An argon ion laser with a principle line of 0.4880 μm wavelength (or all lines operating) and a 1 mm dia. beam was used as the light source. The laser beam was passed through a cylindrical lens (a glass or plastic round rod) causing the beam to diverge in one plane while maintaining a beam thickness of approximately 1 mm. The glass rod was positioned with the axis vertically to illuminate the r-z plane through the test section axis and with the axis horizontally to illuminate r-θ planes at selected axial locations. Cameras were used to view the flow with the camera optical axis at right angles to the plane being illuminated (Figs. 5 and 6). Relatively high concentrations of dye were used in the inner jet for these flow visualization studies. In general, the dye concentration was increased until the fluorescent light level was high enough for good photographic contrast; too high dye concentrations caused nonuniform light absorption along the light path.

LV/LIF Instrumentation

Overview

The laser velocimeter (LV) and laser induced fluorescence (LIF) measurements were obtained primarily using commercially available components and conventional laser velocimetry practices. Some electronic components, which were not commercially available when first required at UTRC, were designed and fabricated by the UTRC instrumentation group. The equipment utilized for each measurement will be described as the technique is discussed.

The LV measurement systems employed in these experiments used the dual beam LV optics concept. The laser-Doppler velocimeter dual beam operating principle is based on the scattering of light from a small particle traversing the measurement or probe volume. When the seed particle is traveling with the fluid flow, the flow velocity is also determined. The probe volume occurs at the intersection of two equal-intensity coherent laser light beams. The LV optics were arranged to obtain the minimum beam waist diameter (and therefore the highest beam intensity) at the probe volume location. The intersection of two coherent laser light beams at the probe volume caused an interference fring pattern to occur with a fringe spacing, $d_f = \lambda/[2 \sin (\phi/2)]$, where λ is the laser light wavelength and ϕ is the angle between the two laser light beams. Light scattered from the particle traversing the probe volume was collected and focused onto a photomultiplier. The frequency of the light intensity, f_D, arriving at the photodetector was related to one component of the particle velocity component, $f_D = U_i/d_f$, where U_i is the velocity component perpendicular to the optical axis and in the plane of the two laser light beams. Further descriptions of dual beam laser doppler velocimetry including the frequency shift used to prevent flow direction ambiguity are presented in Ref. 10.

Each LV system was comprised of components or subsystems which perform specific functions and which can usually be interchanged with equipment from various manufacturers. A laser-velocimeter system consists of the following components: (1) a laser, (2) a sending and receiving optical subsystem, (3) a signal processor(s), (4) a data handling subsystem, (5) a traverse system to position the probe volume, and (6) a scattering particle generator or seeder. Following are short descriptions of the components used for both the LV/LIF and two component LV systems.

For all the measurements reported, the particles naturally occurring in the East Hartford water supply were used as LV seeds (Item No. 6). The traverse system consisted of a milling machine base with three directions of motion and relative traverse position accuracies of ≈ 0.1 mm (Item No. 5).

The laser-Doppler velocimeter signal processors (Item No. 3) amplify and filter the signals from the photomultiplier, validate the Doppler frequency samples, and finally compute the Doppler period which is the reciprocal of the Doppler frequency. The SCIMETRICS Model 800A signal processors measured the elapsed time for 8 Doppler cycles. The processor counter records the pulses from a 125 MHz crystal during the 8 cycle period. In order to check the validity of the LDV signal, the processor also measured the pulses for 4 and 5 Doppler cycles and compares with the 8 cycle result to ensure the LDV signal is a valid one-particle signal. The integer number transmitted to the computer is the period of the Doppler frequency in nanoseconds. Two signal processors are required for the UTRC system (one for each velocity component).

A minicomputer data handling system (Item 4) was used to acquire, store and reduce the data on line. This sytem consisted of (1) a data handling interface (constructed by UTRC), (2) a DEC PDP10/11 minicomputer with a dual disk operating system, (3) a DEC Laboratory Peripheral Systems (LPS) with an A/D signal converter, and (4) a DECwriter III teletype printer. Specific functions of the data handling interface and the A/D converter will be described when applicable to a specific measurement.

Two Component LV Measurements

A list of the equipment employed for the two-component LV measurements is presented in Table I-A. A sketch of the optical arrangement used for the two component laser velocimeter measurements is shown in Fig. 7. The milling machine used to position the probe volume within the test section had a range of approximately 240 mm in the streamwise direction. The ranges for the vertical and cross stream directions were greater than the dimension of the test section.

A sketch of the optical components and beam paths used for the two component velocity measurements is presented in Fig. 8. This system was operated in a direct backscattering mode. The 0.5145 μm wavelength beams were used for the streamwise velocity measurements. The 0.4880 μm wavelength beam were used for the radial and azimuthal velocity measurements. A Bragg cell was used for both velocity components to eliminate the flow direction ambiguity. This optical subsystem provided signal to noise ratios greater than 20 except near the test section walls.

The LV Data Handling Interface was used to accept only those data points when the two velocity components were obtained within a period of time of 1 msec. However, data acquisition rate tests showed that almost all of the sets of two component data were obtained from a single particle. This time period was considered appropriate for a probe volume of length ≈ 1 mm and for typical velocities of 1 m/sec. The time from a clock within the data handling system was also recorded at each data acquisition.

LV/LIF Measurements

A list of the equipment employed for the laser velocimeter/laser induced fluorescence measurements is presented in Table I-B. A sketch showing the arrangement of the optical components used for the LV/LIF measurements is shown in Fig. 9. The LV measurements were obtained in a forward scattering mode while the LIF measurements were obtained in a direct backscattering mode where the light was sent and received through the same lens.

The 0.4880 μm wavelength of the argon ion laser was used both to excite the fluorescence of the fluorescein dye for the LIF measurement and to scatter light from particles for the LV measurements. The laser beam intensity used was monitored during bench tests to determine power fluctuations. The peak to peak power drift over a 20 minute period was less than 0.5 percent.

Fluorescein dye was made from fluorescein disodium salt with a chemical formula $C_{20}H_{10}O_5Na_2$. This dye is used extensively for water pollution studies and is available from chemical supply houses in powder form. Absorption and emission spectra data for fluorescein dye can be obtained from Ref. 11. A liquid dye concentrate was formed by dissolving 2.5 gms of dye powder in 1 tablespoon of alcohol and then mixing with 1 liter water. A dilute solution of dye was made by mixing 1 ml of concentrate with 3.5ℓ of water. The dilute solution was added to the inner jet fluid in ratios of 1 part dilute solution to 760 parts water. The dye in the dilute mixture was stirred for over one hour and can be considered uniformly mixed. The dilute concentration was mixed "inline" with the inner jet fluid. Variation in dye concentrations at the inner jet inlet location can be attributed to the last mixing process. A current-to-voltage converter was used to convert the current through the LIF photomultiplier tube to a voltage. The signal from the photomultiplier also was filtered with a 2 KHz low pass filter to remove the shot noise associated with photomultiplier tubes. The 2KHz filtering was compatible with the typical velocity of 1 m/sec and probe length of 1 mm. The LIF analog signal was processed through an A/D voltage converger each time an acceptable LV signal was obtained. The LV and LIF data were stored as pairs along with the data acquisition time by the Data Handling subsystem.

LF/LIF Data Reduction

Conventional LV data interpretation techniques were used to process and store the data. Listings of the program used to edit the two component velocity data and the LV/LIF data are presented in Tables V-1 and 2, respectively. The data from the LV signal processors and the LIF signals have been stored and will be available through the NASA Project Manager for researchers who wish to obtain other information from the data than the momemts and correlations obtained in the current editing process.

FLOW VISUALIZATION RESULTS

Flow visualization studies were conducted to determine the scale of the turbulent structure of the flow within the test section duct (Figs. 2 and 3). The flow visualization was obtained by adding fluorescein dye to the inner jet fluid. The strucutre and scale of the turbulent eddies was deduced from the interface between high and low concentrations of dye recorded on high speed motion pictures (Figs. 5 and 6).

These flow visualization studies were also conducted to determine if the flow field was swirl free, axisymmetric, and statistically stationary before data acquisition was initiated. This experiment was conducted to obtain a data base that can be used to evaluate axisymmetric flow calculation procedures and it is critical that the flow have these forementioned characteristics. Good axisymmetric characteristics are also required because data from the same radial location are obtained at several azimuthal locations. The transport models developed for the computational procedures are based on time-independent statistics. Therefore, it is important that the experimental data used to evaluate these models be obtained from statistically steady or stationary flows.

Motion pictures were obtained in the r-z plane with the center of illumination at z = 100 and 200 mm and in the r-θ plane at z = 51, 102, 152 and 203 mm. The forementioned set of planes were photographed at 500 frames/sec for five flow conditions. The characteristics of Flow Condition 1, that condition selected for detail data acquisition, are described in the following paragraph. The characteristics of the other flow conditions are described in Appendix I.

The photographs for Flow Condition 1 are presented in Fig. 10. This flow condition was the same as that for which data was acquired in Ref. 6. In the upper left photograph, the classical large eddy structure associated with shear layers could be discerned. The dyed inner jet fluid was moving slower than the annular jet; hence the eddies were "rolling" faster than the inner jet fluid. These eddies were associated with the shear layer between jets (Fig. 1). The upper right photograph shows the scale of the eddies containing inner jet fluid which occurred immediately upstream of the reattachment region (Fig. 1). The inner jet fluid intermittently filled most of the duct cross section. The r-θ plane photograph at z = 51 mm, shows the size of the eddy structure in the wake region. At z = 102 mm, which was in the shear layer between the jets, the radial scale of turbulence was increased and vortex pairs were similar to the vortex pairs observed by the California Institute of Technology fluid mechanics research group. The vortex pairs appeared to occur randomly both timewise and azimuthally in the shear layer between jets. At z = 152 mm, in shear layer between jets, the inner jet fluid distribution became more three dimensional than at the upstream locations. The largest scale structure with high dye concentrations occurred at z = 203 mm. This location was immediately upstream of the reattachment zone where the annular jet fluid began to decelerate the flow toward the duct wall. At further downstream locations, the peak concentrations of the inner jet fluid were lower and the dye concentration more uniform across the duct r-θ cross section.

The flow visualization study showed the flows were as axisymmetric and swirl free as could be determined visually. Although the scale of the turbulent structure was relatively large, the eddies were not axisymmetric or periodic. The large scale waves and eddies appeared to have a range of wavelengths. The flows did not have bistable modes or preferred azimuthal turbulent eddy orientations at any location including the reattachment region. However, the scale of the turbulent structure near the reattachment region was large which will require relatively long data acquisition times to acquire stationary data sets.

DISCUSSION OF MEAN AND FLUCTUATING VELOCITY AND CONCENTRATION RESULTS

Foreword to Presentation of Results

The use of computerized data acquisition storage, reduction and analysis techniques permitted numerous quantities to be determined from the data obtained in this study in addition to the mean and fluctuating velocity components and concentrations usually obtained. These included (1) calculation of parameters which can be used to characterize the probability density functions (p.d.f.s) of the velocity components, the concentrations, the mass transport rates and the momentum transport rates; and (2) the various correlations and cross correlations required to evaluate the modeling of a turbulent transport process.

The determination of all parameters and correlations obtainable from the experimental data was beyond the scope of this study. However, the most universally used terms have been calculated and are included in this report. The parameters presented include the mean and three central moments of the velocity and concentration probability density functions (i.e., the mean, rms variation from the mean, skewness and kurtosis or flatness factor), the mean and three central moments of the mass and momentum turbulent transport rate probability density functions, and the correlation coefficients for the mass and momentum turbulent transport rates.

The calculated parameters for each data point set are tabulated in Tables IV-XX with the terms XX used to denote run number. The number of velocity/velocity or velocity/concentration data pairs used to calculate the parameters for each data point set vary from 239 to 1000 and are also tabulated in Table IV-XX. The number of data pairs used to calculate the parameters for each data point are usually less than 250, 500, or 1000, the number of data pairs acquired for each data point. Data pairs were eliminated from the data set when one of the data pair appeared to be spurious. Spurious data was defined as data well outside the 3σ region of the probability density function and was believed to occur when the laser velocimeter signal processor passed "bad" data. The run numbers are tabulated in Table II as a function of axial location and direction of mass transport or plane or momentum transport.

Not all the data was stored on floppy disks due to a malfunction of the disk drive. When the data was not stored, it could not be editored to eliminate spurious LV data points and the third and fourth central moments were not considered accurate enough to be included in the data set. Not all combinations of data were obtained at all axial stations; the azimuthal transport terms were determined to be negligible in an initial set of runs and were not obtained when significant data acquisition time could be eliminated.

A tabulation of the figure numbers on which a particular result may be found is presented in Table III. The mean and fluctuating velocity and concentration data and the principle mass and momentum transport rate data for all axial stations are presented in graphical form. Representative results of other parameters were also plotted and are presented.

The results are presented and discussed in the following order. The mean and fluctuating velocity and concentration results are presented first, the turbulent mass and momentum transport rates and correlations second, the higher moments of velocity and concentrations, the autocorrelations of the concentration signal, and the higher moments of the turbulent transport rates are presented in later sections.

Detailed measurements were obtained for Flow Condition 1, described in the flow visualization section. This flow condition is the same condition used in the previous, less extensive data acquisition experiments sponsored by UTRC (Ref. 6).

Velocity Results

Mean and fluctuating velocity profiles were obtained at the seven axial stations as part of both the mass and momentum turbulent transport measurements. Consequently, each velocity profile is comprised of data from two or four azimuthal locations and two or more runs. The coordinate system employed for this study is presented in Fig. 3. The results will be related to the shear regions shown in Fig. 1.

Mean Axial Velocity

The mean axial velocity profiles are presented in Fig. 11. The velocity profile at the upstream measurement location closest to the inlet, $z = 13$ mm (0.5 in.), had several significant features. First, the peak velocities from the inner jet were approximately one-half the peak velocities from the annular jet. Second, there was a wake region at radius ratio, $r/R_o \approx 0.25$, from the flow adjacent to the inner tube. In addition, the axial velocity profile was observed to be axisymmetric.

The change in the axial velocity profile from $z = 13$ mm to successive locations downstream document the development of the various shear regions within the test region. The shear caused by the wake of the inner jet tube resulted in a decrease in the peak centerline velocity from $z = 13$ to 51 mm. This wake region disappeared at $z = 102$ mm.

The shear layer between jets occurred between $z = 51$ mm and 203 mm. In this shear region, the annular jet flow accelerated the inner jet flow. At $z = 254$ mm, the velocity profile in the center of the duct was approximately flat.

A third shear region occurred between the annular jet flow and the recirculation region. Note that the radial extent of back flow ($U < 0$) in this region decreased from $r/R_o = 0.54$ to 1.0 at $z = 13$ mm to $r/R_o \approx 0.85$ to 1.0 at $z = 203$ mm. The end of the recirculation cell and reattachment of the annular jet to the peripheral wall occurred near $z = 254$ mm. Note that the measured peak negative velocities occurred at $z = 102$ mm and had a value of -0.075 m/sec. This negative velocity was 17 percent of the peak streamwise axial velocity at that location. This ratio of reverse flow velocity to streamwise velocity is typical of that which occurs in free shear layers downstream of backward facing steps.

The axial variation of mean axial velocity along the centerline is shown in Fig. 12. The data presented shows the effects of the shear layers described previously. First, a decrease in centerline velocity occurred from z = 0 to 100mm due to the inner jet fluid mixing with the flow in the wake from the inner jet tube. Second, an increase in centerline velocity from z = 100 to 175 mm occurred as the fluid from the annular stream accelerated the fluid from the inner jet. Third, the deceleration of the centerline velocity from z = 200 mm to larger values of z occurred as the flow from the annular jet attached to the duct wall and closed the recirculation cell.

Radial Mean Velocity

The profiles of mean radial velocity are presented in Fig. 13. Note the velocity scale is changed by a factor of ten compared to that used for the axial velocity profiles. Positive velocities indicate flow radially outward from the test section centerline.

Rapid changes in the profiles of the radial velocity occurred from z = 13 mm, the flow from the inner jet and the annular stream was directed into the center tube wake region (+V for $r/R_o < 0.25$ and -V for $r/R_o > 0.25$). The negative radial velocities at radius ratios from 0.5 to 0.8 were attributed to the flow radially inward at the upstream end of the annular recirculation region. At z = 51 mm, the radial velocities for $r/R_o < 0.2$ were positive but near zero and indicated the relatively low, mass flux from the center jet to the tube wake region. Radial velocities inward for $0.2 < r/R_o < 0.45$ indicated fluid motion from the annular jet into the tube wake region. Radial velocities outward for $0.45 < r/R_o \lesssim 0.6$ indicated fluid moving from the annular jet into the shear layer between the annular jet and the recirculation zone.

At z = 102 mm, the radial profiles indicated (1) radial inward flow occurred for $r/R_o < 0.35$ where the outer annular flow was accelerating the inner region, (2) radial outward flow occurred for $0.35 < r/R_o < 0.7$ where the annular jet velocity decreased and flow was entrained into the recirculation cell and (3) radial flow inward occurred for $r/R_o < 0.7$ due to radial flow inward in the outer half of the recirculation cell. Similar descriptions are applicable at z = 152 mm. At z = 203, 254 and 305 mm, the flow had a positive radial component at all radius ratios. There was a trend toward decreasing radial velocity from z = 254 to 305 mm as the reattached flow begins to develop into turbulent duct flow.

The run to run variations are more apparent in the radial velocity profiles than the axial velocity profiles. These variations were attributed to the sensitivity of the radial flow pattern to small changes in velocity ratio and geometry. The flow condition selected had interesting features (wake, shear layer between jets, recirculation, reattachment--see Fig. 1) which occurred over a short distance. The fact that the flow was basically axisymmetric is significant (i.e., data for $\theta = 0$ and 180 are the same).

Azimuthal Mean Velocity

The mean azimuthal velocity profiles are presented in Fig. 14. These data are plotted with the same scale as the radial velocity profiles. For these experiments with axial coaxial jets, a mean azimuthal velocity equal zero was expected. However, it is difficult to obtain a completely swirl-free flow. The results presented here document the local magnitude of the swirl in the test section.

At $z = 13$ mm, the flow from the center jet, $r/R_o < 0.25$, had negligible swirl (i.e., $\tan^{-1} 0.01/0.8 = 0.7$ deg.), however, the recirculation region adjacent to the end wall had mean swirl velocity of 0.1 m/sec. The higher values of W at $z = 13$ mm occurred where the recirculating flow is impinging on the upstream wall, $r/R_o > 0.5$. The tendency toward rotation in the recirculation region was increased as the recirculating flow approaches the upstream wall. As will be shown in subsequent figures these mean azimuthal velocities were less than the rms fluctuation of the velocity component. At further downstream locations, the azimuthal velocity components indicated mean swirl angles of up to 1.5 deg. In all cases, the mean azimuthal velocity was less than the rms of the azimuthal fluctuating velocity and could not be discerned in flow visualization tests.

Fluctuating Velocities

Fluctuating axial, radial and azimuthal velocity profiles are presented in Figs. 15, 16 and 17, respectively. The changes in the intensity of the fluctuations between axial locations were well behaved and can be attributed to the developing shear layers. At $z = 13$ mm, the peak fluctuating velocities occurred in the wake from the center tube and the shear layer outside the annular jet. The fluctuation intensities at the center of the center and annular jets were 5 to 10 percent of the local velocities which is compatible with previous measurements in ducts and annulus (e.g., Ref. 18). The intensities of the fluctuating velocities increased and decreased with the development of the shear layers (1) between the center and annular jets, (2) between the annular jet and the recirculation zone, and (3) in the reattachment zone. The intensity of the axial velocity fluctuations were greater than those of the radial or azimuthal velocity components in the shear regions. As the local shear rate decreased, the ratio of the intensities, v'/u' and w'/u' tended toward 1.0 (i.e., at $z = 203$ and 254 mm and $r/R_o = 0$).

Concentration Results

A small amount of fluorescein dye was added to the inner jet fluid to differentiate the inner jet fluid from the annular jet fluid. Both fluids were water in the experiment. The intensity of the light emitted by the fluorescence of dye from the laser velocimeter probe volume was proportional to the concentration of dye in the probe volume. The local concentration of the inner jet fluid, $\bar{f}$, was defined to be the ratio of light emitted locally to the light emitted at the inner jet inlet where $\bar{f} = 1.0$ by definition. In the discussion of the experimental results the symbol $\bar{f}$ and term "concentration" refer to the concentration of inner jet fluid as defined. The term "mass transport" refers to the turbulent transport of the inner jet fluid.

Mean Concentration

The axial variation of the concentration along the centerline is shown in Fig. 12b. These data were obtained in two sets. The first set from $z = 25$ to 250 mm used the inlet-jet-fluid concentration $\bar{f} = 1$ at $z = 0$ to 50 mm as reference. The streamwise traverse range of 225 mm was the maximum obtainable with the available optics and traverse table. The second set of data were obtained from $z = 150$ to 350 mm. The LIF voltage signals from these data were ratioed to the upstream set of data at locations where the data sites overlap occurred. The LIF voltage signals for the individual concentration profiles presented in Fig. 18 were ratioed to the results from Fig. 12 to obtain a mean centerline concentration level.

The axial variation of the concentration along the centerline (Fig. 12b) showed small decreases occurred from $\bar{f} = 1.0$ for $z < 75$ mm. The end of the inner tube wake region occurred between $z = 50$ and 75 mm. The centerline concentrations decreased rapidly for 100 mm $< z <$ 200 mm which is the region where the inner jet fluid is being accelerated by the annular jet flow (see Fig. 11a). The decrease of the centerline concentration with axial distance became more gradual for $z > 200$ mm and the centerline concentration approached within 0.01 of the mass flow averaged concentration level within the duct, $\bar{f}_{ave} = 0.104$, at $z = 356$ mm.

The mean concentration profiles are presented in Fig. 18. At $z = 13$ and 51 mm, the mean concentration along the centerline was 1.0. The variations in $\bar{f}$ from 1.0 for $z = 13$ mm and $r/R_o \leq 0.15$ indicate the level of scatter in the value of mean concentration for a given high concentration measurement. These variations are attributed to (1) defects in the glass used for the duct and glass plates used for optical box plates, (2) small air bubbles or dirt on these surfaces that are occasionally formed during the course of a test and (3) a variation in trace material flow rate over the time period required to obtain a profile. At $z = 13$ mm and for $0.30 < r/R_o < 0.45$, the incoming fluid should have zero concentration. These data scattered about the $\bar{f} = 0$ value with a variation of less than 0.02. The values of $\bar{f} = 0.03$ at $z = 13$ mm and 51 mm and $r/R_o > 0.6$ were due to the inner jet fluid being convected from downstream stations upstream into the recirculating zone.

The concentration profiles showed the rapid decrease in peak concentration between 51 mm and 203 mm. Between $z = 203$ and 305 mm, the decrease in concentration level was more gradual. At $z = 305$ mm, the mean concentration profile was close to the mass-flow-averaged concentration level within the duct, $\bar{f}_{ave}$. The peak concentration was only 0.04 above $\bar{f}_{ave}$ at this axial location.

The concentration profiles were reasonably axisymmetric and repeatable from run to run. These data were obtained as part of the mass transport measurements in three directions. Each profile contains data which was obtained over a two to four week period.

Fluctuating Concentration

The concentration fluctuations, f', are presented in Fig. 19. Note the peak f' values increased from 0.15 at z = 13 to 0.30 at z = 152 mm. The peak values of the fluctuation intensity at z = 13, 51 and 102 mm, occurred in the high concentration gradient region between the inner jet and the annular jet. At z = 152 and 203 mm, the peak values of the concentration fluctuation intensities were near the centerline. The peak concentration fluctuation in the profiles occurred along the centerline for $z \geq 152$ mm. The peak concentration fluctuations also decreased with distance from the inlet plane for $z > 152$ mm. The ratio of concentration fluctuations, f', to mean concentration, $\bar{f}$, at z = 152 was approximately 0.50 which indicated a large fraction of the fluctuations was due to "all annular jet" to "all inner jet" concentration variations.

DISCUSSION OF TURBULENT TRANSPORT RESULTS

Momentum Transport

z-r Plane

The momentum transport rate profile in the z-r plane, $\overline{uv}$, are presented in Fig. 20. Because most of the momentum transport in this plane is due to the radial variation of the axial velocity, the discussion of the turbulent momentum transport rate distribution will be related to the axial velocity profiles (Fig. 11a) and the shear regions presented in Fig. 1.

At z = 13 and 51 mm, a weak momentum transport radially outward (i.e., $\overline{uv} > 0$) occurred for $r/R_o < 0.18$ and 0.12, respectively. This momentum flux was due to the shear of the inner jet fluid on the wake region downstream of the inner jet tube. For z = 13 mm and $0.18 < r/R_o < 0.3$, the momentum flux was radially inward, i.e., $\overline{uv} < 0$, due to the transport of momentum from the annular jet fluid to the wake region downstream of the inner jet tube. At z = 51 mm, the region with negative $\overline{uv}$ was enlarged to $0.12 < r/R_o < 0.33$. The wake region downstream of the inner jet tube disappeared at z = 102 mm, i.e., no region of $\overline{uv} > 0$ for $r/R_o < 0.3$.

The negative momentum transport rate for $r \lesssim 0.030$ and z = 102, 152 and 203 mm was due to the radial inward transport of axial momentum which accelerated the inner jet fluid. The magnitude of the negative transport rate decreased with increasing z from z = 102 mm and was essentially zero at z = 254 mm. The location of the zero momentum flux toward the center probably occurred at the axial location with peak axial velocities, i.e., z = 170 mm (Fig. 11a).

Radial outward momentum transport for r > 0.35 occurred in the free shear layer between the annular stream and the recirculating fluid at all axial locations. At the upstream end of the recirculation zone, z = 13 mm and 51 mm, the radial transport in the backward flowing region of the recirculation cell had approximately zero transport. At locations further downstream (z > 100 mm), the low or zero transport rate locations were estimated to lie closer to the wall.

At z = 305 mm, the shear stress distribution was approximately linear as expected for fully developed pipe flow. However, the ratio of the wall shear stress rate (extrapolated) to the kinetic energy of the flow was approximately 0.1. This value compares with a value of 0.002 to 0.003 previously obtained for fully developed pipe flow at these Reynolds numbers (e.g., Ref. 18). From this comparison and the high level of the turbulence intensity ($\simeq$ 60 percent), it can be concluded that the turbulent structure at z = 305 mm was far from equilibrium.

The correlation coefficients, R_{uv}, obtained from the turbulent transport measurements are presented in Fig. 21. The correlation coefficients, $R_{uv} = \overline{uv}/(u'v')$, have the same sign as the turbulent momentum transport rate, $\overline{uv}$. However, the shapes of the correlation profiles are easier to interpret at values of the momentum transport rate near zero. At z = 13 and 51 mm, the correlation coefficient profiles for r/R_o < 0.2 show that the peak radial outward coefficients were 0.35 and 0.2, which was only a factor of two less than the coefficients for the inward transport, i.e., the negative R_{uv} at r/R_o = 0.25. However, the ratio of the inward/outward momentum flux into the wake region was greater than 10 at that location (Fig. 23a). Although the correlation coefficients at r/R_o = 0 were not identically equal to 0.0 as expected for axisymmetric flow, a profile constructed through zero would not result in significant deviations of the data from the profile. The deviations which occurred can be attributed to spatial uncertainties in the measurement location and the location of the jet centerline. The absolute values of the peak transport correlation coefficients in each shear region were 0.35 and 0.55. These values are in the range previously measured for turbulent free shear momentum transport (e.g., Ref. 18). The correlations were higher in regions where the shear layers are stable and lower in the reattaching and recirculation zones where the turbulent structure (1) does not appear to be "ordered", or (2) had longer time-dependent characteristics.

z-θ Plane

The axial/tangential turbulent transport rate and correlation profiles obtained at z = 102 mm are presented in Fig. 22. As expected for this nominally axisymmetric flow, the transport rates were negligible compared to the axial/radial transport rates. The levels measured, $\overline{uw}$ < 0.004 m^2/s^2 and $|R_{uw}|$ < 0.04 are the levels of uncertainty which probably occurred in the transport measurements and their associated correlation coefficients.

Mass Transport

Radial Direction

The measured radial mass transport rate profiles are presented in Fig. 23. The radial mass transport rate is generally associated with the radial gradients of the mean concentration profiles (Fig. 18). Discussions of the mass transport measurements will be related to these profiles, to the shear regions, and flow visualization results.

The radial mass transport at z = 13 and 51 mm was concentrated at the interface between the inner jet and annular jet stream. Relatively low peak mass transport rates occurred at these locations even though the radial concentration gradients were the highest in the flow field. Flow visualization of this region showed that coherent waves occurred in this region but that the fluid generally was not mixed. The peak transport rates at z = 102 and 152 mm were higher by a factor of 4 compared to the peak levels at z = 51 mm. The radial extent of the high radial mass transport rate spread inward and outward at z = 102 and 152 mm. The radial profiles at z = 203 through 305 mm approached those associated with the self-preserving profiles of free jet mixing.

The correlation coefficient, R_{vf}, profiles are presented in Fig. 24. At z = 13 and 52 mm, the peak correlation coefficients were 0.25. These occurred in a region with growing waves but upstream of the region with turbulent eddies. At z = 102 mm, the peak correlation coefficients were 0.55 to 0.6. These occurred where large waves are beginning to break into eddies. The peak correlation coefficients decreased monotonically with increasing z from z = 102 mm. The radial mass transport was radially outward in all regions except in the recirculation region where negative correlations occurred, corresponding to convective mass transport radially inward. The extent of this region can be more easily discerned from the correlation, R_{vf} profiles (Fig. 24) than from the radial mass transport profiles (Fig. 23) because the inward mass transport rates are low.

Axial Direction

Turbulent scalar (mass) transport is generally associated with the scalar (concentration) gradients and a transport diffusion coefficient, $\dot{m}_i = -\varepsilon_m (\partial\bar{f}/\partial x_i)$. However for some classes of flows with turbulent transport, notably atmospheric transport of heat, the scalar transport can be opposite the direction of the scalar gradient. This class of scalar transport is denoted "countergradient" transport and requires a "Reynolds stress" formulation to calculate the scalar (mass) transport rate (e.g., Ref. 12). Some of the axial mass transport rate measurements obtained in this study fall into the "countergradient diffusion transport" category. Discussion of these flows will relate the measured axial mass transport to the velocity shear field which produces the mass transport mechanism.

The axial mass transport rate, $\overline{uf}$, profiles are presented in Fig. 25. The most important feature on these figures is the negative mass turbulent transport which occurred in the central region of the test section at z = 51, 102, 152 and 203 mm from the inlet plane. Note the axial mass transport rate decreased from near zero at z = 13 mm to a minimum level at z = 152 mm from the inlet plane. Through the region of the test section, the inner stream mass concentration decreased with increasing axial location (see Fig. 18). Note that the peak absolute values of the axial transport rates were higher than the values for the radial transport (Fig. 23) even though the peak radial concentration gradients were approximately five times the axial concentration gradients.

The countergradient transport processes can be explained by considering the shape of the axial velocity profiles in the countergradient transport region (Fig. 11) and the eddy structure associated with the momentum transport. In the region where the inner jet was being accelerated by the annular jet, the large eddies in that velocity shear layer near the centerline were rolling with the negative fluctuating axial velocities near the inner jet fluid. The result was that preferred rotational orientation of these eddies retard the flow in a streamwise direction and consequently resulted in $\overline{uf} < 0$ and hence countergradient mass transport.

Sketches of the regions with both countergradient and gradient axial mass turbuelnt transport and both axial velocity accelerations are shown in Fig. 26. The region with countergradient mass turbulent transport (M2) was apparently larger than the region where the flow from the inner jet was accelerated by the flow from the annular jet (V2). This difference in region size may be due to the response time or distance required to change the character of the turbulent structure.

The correlation coefficient, R_{uf}, profiles presented in Fig. 27 show the development of the axial mass transfer distribution at the low axial turbulent mass transfer rate more clearly than the local transport rate measurements. At $z = 13$ mm, all the axial transport for $r/R_o < 0.3$ was downstream. At $z = 51$ mm, the axial turbulent transport was downstream in the portions of the shear layer, $r/R_o < 0.14$, where the inner jet is accelerating the shear layer between the inner and annular jet. The axial turbulent transport was negative (upstream) in the inner jet-annular stream shear layer where the annular stream fluid was accelerating the shear layer fluid. The peak negative value of the correlation coefficient increases from -0.6 at $z = 102$ to +0.25 at $z = 305$ mm. Note that the peak of the negative correlation coefficients, R_{uf}, occurred near the maximum radial gradient in the concentration profiles.

Azimuthal Direction

The azimuthal mass transport rate and the correlation coefficient profiles at $z = 102$ and 203 mm are presented in Fig. 28. As expected for this nominally axisymmetric flow, the transport rate was close to zero and the correlation coefficients at $z = 203$ mm were the order of the scatter observed in the radial and axial mass transport results. The correlation coefficient at $z = 102$ mm near $r/R_o = 0$ may be high due to errors in location or small asymmetries in the location of the physical centerline of the jet. The radial mass transport data was obtained with the same optical setup but with a traverse vertically through the test section center. Misalignments of 0.5 mm (or 1/2 the probe volume length) could have caused the radial mass transport correlation coefficient to be approximately 0.2 at $z = 102$ mm (see Fig. 24). No explanation for the values of $R_{wf} = 0.15$ for $z = 102$ and $r/R_o = 0.3$ is apparent except that the overall mass transport at that location is low.

DISCUSSION OF SKEWNESS, KURTOSIS AND AUTOCORRELATION RESULTS FOR VELOCITY AND CONCENTRATION PROBABILITY DENSITY FUNCTIONS

Although mean and fluctuating velocity and concentration distributions and transport rate distributions are required to evaluate the accuracy of predictions with a given turbulent transport model, they do not provide the insight required to determine where the deficiencies in a turbulent transport model are located. Examination of the probability density functions for each data set (data acquired for each location) can show if the experimental conditions are compatible with the assumptions in current or proposed models. The experimental techniques and the computer based data acquisition systems employed in this study permitted the examination of these p.d.f.s and the determinations of their skewness and kurtosis parameters used to characterize the shape of the p.d.f.s. Typical results from this portion of the study are presented in this and the following section. The skewness and kurtosis for each available data set are presented in Table IV.

Typical Probability Density Functions

Velocity and concentration probability density functions (p.d.f.s) were plotted for data sets obtained at selected radial locations at $z = 103$ mm from the inlet plane. This axial location was chosen for more detailed analysis of the flow characteristics because the momentum and mass transfer rates are high at this location. These data were obtained as part of the momentum and mass transfer data acquisition; consequently the axial and radial velocity p.d.f.s were comprised of data from two different runs. The concentration p.d.f.s are comprised of data from the mass transport rate measurement in three directions. The mean quantity, rms variation from the mean, the skewness and the kurtosis (or flatness factors) tabulated are averages from the number of runs cited in each figure. The data from the runs was plotted to present a composite picture of the p.d.f. at each location.

The mean values and central moments of each parameter were defined using the nomenclature of Ref. 13. The specific definitions for each term are presented in Appendix II.

The axial velocity p.d.f.s (Fig. 29) showed significant changes with radial location. Several apparent relationships between the skewness and kurtosis for the shear layers at $z = 102$ and 203 mm can also be discerned. First, the p.d.f.s at $r/R_0 = 0.0$ and 0.1 were skewed to the higher velocity region. On the average, flow at these locations was accelerated axially. At $r/R_0 = 0.35$, the p.d.f. was skewed toward the lower velocities. On the average, fluid at this radius was decelerated by the shear layer between the jets. At radius ratios of 0.5 and 0.6, the p.d.f.s were more symmetric and had kurtosis close to that for Gaussian profiles. This latter region had an almost constant velocity gradient and almost constant turbulent momentum transport rate.

Although the radial velocity p.d.f.s (Fig. 30) showed less variation with radial location than the axial velocity p.d.f.s, they did have several varying features. At $r/R_o = 0.0$, the p.d.f. was sharply peaked at $v = 0$. Approximately 80 percent of the radial velocity samples lie between $\pm$ .1 m/s. The tails on each side of the peak cause the kurtosis to be relatively high, i.e., $K_v = 7.2$. The second central moment, u', increased as r/R_o increases.

The azimuthal velocity p.d.f.s (Fig. 31) had less variation with radial location than either the axial or radial velocity p.d.f.s. The only significant change was the increase in w' with increasing radius (as did u' and v').

The inner-jet fluid concentration p.d.f.s are presented in Fig. 32. These profiles show the range of the concentration fluctuations which occurred at four radial locations. Each of the profiles shows unique features which were characteristic of specific regions of the flow. At $r/R_o = 0.1$, the p.d.f. had a double peak. This measurement location occurred in a region where the large eddies had high or low concentration of inner jet fluid. The mean concentration value was 0.69 which occurred between the two peaks. The skewness factor was -5.1 which is a value larger than any obtained for the velocity profiles. However, the kurtosis had a value of only 2.2, which is closer to the value of 1.8 for a square p.d.f. profile than the value of 3.0 for a Gaussian p.d.f. profile.

The concentration p.d.f.s at $r/R_o = 0.0$ and 0.35 were obtained from measurements on the inner and outer edges, respectively, of the mean concentration profiles. At $r/R_o = 0$, the most probable inner jet fluid concentration was near 1.0. The tail of the p.d.f. was skewed toward the lower concentrations. The values of S_f and K_f were -2.6 and 12., respectively. At $r/R_o = 0.35$, the most probable inner stream concentration was 0.0. However, the tail of the p.d.f. was skewed toward values near 0.5. The skewness and kurtosis were 4.4 and 37.0, respectively. Note the precipitious slope of the concentration p.d.f. at values of less than 0.0 which was the shape expected for an ideal seed and measurement system.

The inner jet fluid concentration p.d.f.s show probabilities, $N(f)/N_o$, greater than 1.0 and less than 0.0, the limits for the inner jet concentration. The concentration measurements less than 0.0 were attributed to photomultiplier raise and temporal shifts in the photomultiplier dark current. The concentration measurements greater than 1.0 were attributed to nonuniformity of the dye/inner-jet water mixture and shifts in the inlet dye concentration as well as zero shift and dark current. The maximum magnitude of these effects can be estimated from the concentration fluctuation measurements presented in Fig. 19 for $z = 13$ mm. For $r/R_o < 0.1$, the inner jet concentration should be uniform at 1.0; the measured concentration fluctuation values were 0.05 to 0.06 for $0.3 < r/R_o < 0.4$. The concentration should be uniform; at 0.0; the measured concentration fluctuations were approximately 0.01.

Typical Skewness and Flatness Distributions

The skewness and flatness factors for the axial, tangential and azimuthal velocity and the inner jet concentration distributions at $z = 102$ and 205 mm for the inlet plane are presented in Figs. 33 through 35. These axial locations had relatively high and moderate momentum transport rates, respectively, and were therefore, suitable for comparison. Researchers requiring more insight into the radial variation of the skewness and kurtosis of the velocity components and concentrations at other axial locations can obtain the data from Table IV.

Axial Velocity

The skewness and kurtosis profiles for the axial velocity measurements at z = 102 mm (Fig. 33) show that the velocity p.d.f.s had positive skewness in the center region ($r/R_o < 0.20$). This indicated the longer tails of the p.d.f.s are in the positive velocity direction; a few eddies of fluid with higher axial velocities penetrated into the inner jet region to accelerate the flow. The skewness factors for $0.2 < r/R_o < 0.55$ are negative which indicates the longer tails of the p.d.f.s were in the lower velocity direction. The kurtosis tended to be greater than 3.0, the value for a Gaussian distribution, when the skewness factor deviated from zero. The kurtosis, K_u, for $r/R_o \approx 0.2$ and 0.65 were less than 3.0 which indicates a tendency toward a flat top on the p.d.f. (see Fig. 29, $r/R_o = 0.2$).

The axial velocity skewness and flatness factor profiles at z = 203 mm had less variation from 0.0 and 3.0 respectively, than the profiles for z = 102 mm. Note that the axial velocity profile at 203 mm (Fig. 14) had less shear than the profile at z = 102 mm. The same relationships between S_u and K_u as described for z = 102 mm appear to have occurred at z = 203 mm. For $0.15 < r/R_o < 0.6$, the S_u values are negative for $0.1 < r/R_o < 0.6$ but with a much smaller magnitude than at z = 102 mm. The variation of the skewness and kurtosis from 0 and 3 was in the same direction as for z = 102 but with less deviation.

The variation of the skewness and kurtosis, from the values for a Gaussian p.d.f., appeared to be correlated to the local curvature of the axial velocity profile. The relationship is that $S_u > 0$ if $\partial^2U/\partial r^2 > 0$ and $S_u < 0$ if $\partial^2U/\partial r^2 < 0$. The kurtosis is also related to the curvature of the axial velocity profile. When the absolute value of curvature is high, the kurtosis is also higher than occurs for a Gaussian p.d.f. When the curvature passes through zero, the kurtosis decreases and the p.d.f. becomes flatter. The magnitude of the deviations from the values for a Gaussian p.d.f. also appears to be proportional to the magnitude of $\partial^2U/\partial r^2$.

The forementioned relationships may not be universal but existed for the flow at these two axial locations. The positive skewness, $S_u > 0$, at z = 102 mm occurred where the curvature of axial velocity profile is positive, i.e., $\partial^2U/\partial r^2 > 0$. The negative skewness occurred when the curvature of the axial velocity profile is negative, i.e., $\partial^2U/\partial r^2 < 0$. Likewise, the values of the kurtosis at z = 102 mm were less than 3.0 where the curvature was near zero, i.e., $\partial^2U/\partial r^2 \approx 0$ at $r/R_o \approx 0.2$ and 0.6. The deviation of S_u and K_u from 0 and 3 respectively, at z = 203 mm were not as large as at z = 102 mm but were compatible with the stated hypothesis. Near $r/R_o = 0$, the curvature of the axial velocity profiles was positive but the magnitude was small. The composite skewness profile at $r/R_o = 0$ appears to be equal or greater than zero which is also compatible with the stated hypothesis.

Radial Velocity

The skewness and kurtosis of the radial velocity profiles are presented in Fig. 34. The skewness factor of the radial velocity p.d.f.s approached zero at $r/R_o = 0$, as expected for axisymmetric flow. At $z = 102$ mm, the skewness was negative or near zero for the region $r/R_o < 0.5$ where the radial velocity curvature was less than zero, i.e., $\partial^2U/\partial r^2 < 0$. Values of kurtosis greater than the Gaussian value of 3.0 occurred when the skewness deviated appreciably from zero.

Azimuthal Velocity

As might be expected for axisymmetric flow, the skewness factor, S_w, profiles for the azimuthal velocities at both $z = 102$ and 203 mm were near zero at all radii (Fig. 35). However, the flatness factors, K_w, deviated from the Gaussian value of 3.0 in the regions where the axial and radial velocity profiles had nonzero values for skewness and had flatness factors greater than 3.0.

Inner Jet Concentration

The skewness and flatness factor profiles obtained from the concentration data at $z = 102$ and 203 mm are presented in Fig. 36. These data were obtained from two sets of mass transport concentration measurements: uf and vf.

At $z = 102$ mm, the values of S_f for $r/R_o < 0.15$ were negative, indicating the tails of the concentration p.d.f.s were toward low values of f (see Fig. 32). At $z = 102$ mm and $r/R_o = 0.4$ the skewness factor reached a value of 4 to 6. These values were higher than the skewness factors obtained for the velocity p.d.f.s. At $z = 203$ mm, the skewness factor was positive with a value of approximately 1 or more all radius ratios. Thus the tails of the p.d.f.s indicated a few occurrences of high inner-jet fluid concentration.

The flatness factor or kurtosis profile at $z = 102$ mm has an interesting variation. Near $r/R_o = 0$, K_f was approximately 20, decreased to approximately 2 at $r/R_o =$ 0.1, increased to approximately 50 at $r/R_o = 0.4$, and decreased to approximately $r/R_o < 0.6$, the mean concentration level was 0.04 to 0.05 and the concentration fluctuations, r', had the same level. The motion picture frames (Fig. 10) from the flow visualization study, photographically show the magnitude of the eddy size and the variation in inner jet concentration.

Autocorrelation Measurements of Concentration

Autocorrelation measurements of the concentration photomultiplier signal were obtained at several radial locations for $z = 102$ mm in an attempt to obtain a quantitative measure of the axial scale of the large eddies. Results obtained at $r/R_o =$ 0.0, 0.10 and 0.21 are presented in Fig. 37. Although the large eddy structure was discernible in the flow visualization motion pictures and on the LIF photomultiplier output, the autocorrelations did not show that a dominant frequency occurred in the flow. The correlation $R_f(\tau) = 0$ occurred at 20 to 25 ms for all three radial locations. At $r/R_o = 0.1$, a secondary peak in the autocorrelation occurred at $\tau = 50$ ms. This period for large scale eddies was in the range observed in the motion pictures, i.e., wavelengths of 20 to 100 mm with convective velocities of 1 to 1.5 m/sec. From the autocorrelations it was difficult to determine other times, τ, where significant peaks in the correlation coefficients occur.

Stability studies of this axisymmetric flow are currently being conducted at UTRC under Corporate sponsorship. The preliminary results indicate several axisymmetric disturbance modes with high spatial growth rates can occur with the velocity profile at $z = 102$ mm. The results also indicate that growth rate remains constant over a large range of cyclic frequencies, rather than reaching a peak and decreasing toward a cutoff frequency as occurs for the plane shear layer (e.g., Ref. 14). A tentative conclusion from the analytical results is that this coaxial flow with recirculation does not have a preferential large eddy wavelength but rather a range of disturbance wavelengths which can develop into large eddy structure.

DISCUSSION OF SKEWNESS AND FLATNESS RESULTS FOR MASS AND MOMENTUM TRANSFER PROBABILITY DENSITY FUNCTIONS

Typical Transport Rate Probability Density Functions

Data from the turbulent momentum and transport measurement at z = 102 mm were plotted for the same data sets used in the presentation of the velocity of the velocity and concentration p.d.f.s. The locations selected include data typical of that obtained at high turbulent mass and momentum transport rate locations.

Momentum Transport

The probability density functions for the momentum transport in the r-z plane are presented in Fig. 38. These p.d.f.s all had the peaked distributions about the zero uv momentum transport rate. This shape of momentum rate p.d.f. also occurs in turbulent boundary layers (Ref. 15). The p.d.f.s all had the two highest probability of occurences, $N(uv)/N_o$, in the probability bins adjacent to uv = 0.

Radial Mass Transport

Probability density functions of the radial mass transport data re presented in Fig. 39. The data obtained at $r/R_o = 0.1$ and 0.2 had high mean turbulent mass transport radially outward. The mean turbulent radial mass transport rates at $r/R_o = 0$, 0.35, 0.5 and 0.6 were an order of magnitude less than the highest rates at $r/R_o =$ 0.1 and 0.2. Although the p.d.f.s for $r/R_o = 0.1$ and 0.2 were skewed toward positive values, the most probable occurrence was the negative bin adjacent to the zero transport rate. For all the data shown, the peak transport rate occurred at the smallest values of vf near zero with the sign opposite the mean turbulent radial transport direction. For the locations with the high mean turbulent transport rates, the p.d.f.s and the higher amounts, S_{vf} and K_{vf}, were well behaved and in the general range expected from Gaussian p.d.f.s of the velocity and concentration distributions with reasonable correlation coefficients. Although the p.d.f. at $r/R_o = 0.35$ had the same general shape as these at $r/R_o = 0.1$ and 0.2, the skewness and kurtosis, S_{vf} and K_{vf}, were large. These large values may have been due to the low turbulent intermittency factor for the mass transport that occurred as a result of the large eddy structure at this location (see Fig. 10 for flow visualization of this phenomena).

Axial Mass Transport

Probability density functions (p.d.f.s) of the axial turbulent mass transport rate for five radial locations are presented in Fig. 40. At all radial locations, the net mass transport was negative and the skewness factors were negative. For four of the five p.d.f.s including the two with high turbulent transport, the most probable turbulent transport rate was the smallest positive transport rate bin, uf = +0.02 m/s. For the two locations with the highest transport rate ($r/R_o = 0.1$ and 0.2), 60 percent of all the transport occurrences were at that rate. For $r/R_o = 0.1$ and 0.2, the probability of occurrences, $N(uf)/N_o$ at uf = 0.02 was also more than twice as high as at uf = -0.02. These statements were also true for the radial transport at the same location.

Azimuthal Mass Transport

Probability density functions for the turbulent azimuthal mass transport data are presented in Fig. 41. Compared to the radial and axial mass transport p.d.f.s, the distributions on either side of wf = 0 were reasonably symmetric. For a non-swirling axisymmetric flow, the mean azimuthal mass transport rate and the skewness should be zero at all locations; the kurtosis would be expected to be the same order of magnitude as the kurtosis for the turbulent axial and mass transport p.d.f.s.

Typical Transport Results

Momentum Transport

The second central moment (or rms fluctuation from the mean) of the turbulent transport in the r-z plane, σ_{uv}, are presented in Fig. 42. This quantity previously was used to analyze and evaluate the turbulent transport process in boundary layers, e.g., Ref. 16. A comparison of the values of σ_{uv} with $\overline{uv}$ from Fig. 24 show that σ_{uv} was always at least a factor of two greater than $\overline{uv}$. Ratios of $\sigma_{uv}/\overline{uv}$ approximately equal 3 were previously reported for boundary layers (Ref. 16). At z = 13 and 51 mm, the minimum values of $_{uv}$ occurred in the core regions of the inner and annular jets. In these regions, the large scale eddy structure with accompanying large values of σ_{uv} were not yet developed.

Skewness and kurtosis profiles (S_{uv} and K_{uv}) for z = 102 and 203 mm are presented in Fig. 43. At z = 102 mm, the skewness factor varied across the shear layer depending on the local shear direction. The skewness factor should have approached zero at r/R_o = 0 due to the zero shear stress at that location and symmetry of the flow. At z = 203 mm, the peak value of the skewness factor occurred at $r/R_o \approx 0.3$ although the peak shear stress rate occurred at $r/R_o \approx 0.7$ (Fig. 22). The flatness factors, K_{uv} at z = 102 mm varied across the shear layer. The values for $r/R_o \approx 0.0$ ranged from 30 to 70. The values of K_{uv} at $r/R_o \approx 0.2$, which was the location with the peak negative shear, decreased to values of approximately 10. Near the zero shear location, $r/R_o \approx 0.3$, the flatness factor K_{uv} increased to 50. At z = 203 mm, the flatness factor varied from 10 for r/R_o near zero to 25 at $r/R_o \approx 0.7$ (the peak shear region).

These flatness factor results are similar to the results obtained in a turbulent boundary layer by Gupta and Kaplan (Ref. 17). For the boundary layer, values of the flatness factors were approximately 3 in the logarithmic shear region and increased to values above 40 in the low shear region at the edge of the boundary layer.

Radial Mass Transport

The second central moments of the turbulent axial mass transport rate p.d.f.s obtained at z = 102 and 203 mm are presented in Fig. 44. These second moments, σ_{vf} were generally less than the second moments for the axial mass transport rate, σ_{uf}. This result was compatible with higher rms fluctuations being obtained for the axial velocity component than for the radial velocity component (Figs. 15 and 16).

The skewness of the radial mass transport rate profiles (Fig. 45) show that large values of skewness were obtained for S_{vf} than either S_{uf} or S_{uv}. This increase in skewness was greatest where the radial mass transport rates were low, at r/R_o = 0.05 and 0.35 at z = 203 mm. The kurtosis, K_{vf}, was also high where the skewness was large. At z = 203 mm, the skewness increased from a value of zero at r/R_o = 0 and reached values of 4 to 6 for $r/R_o \approx 0.5$ (locations where the concentration, $\bar{f}$, is low and the concentration fluctuation, f', are relatively high). The kurtosis also increased from values of approximately 8 at r/R_o = 0 to values above 40 for $r/R_o \approx 0.5$.

Axial Mass Transport

Profiles of σ_{uf}, the rms variation from the mean turbulent axial transport, $\overline{uf}$, at z = 102 and 203 are presented in Fig. 46. The peak values of $_{uf}$ were approximately twice the values of the peak values of $\overline{uf}$ (Fig. 25). This ratio was less than the corresponding ratio for the momentum transport measurements. These relationships may be associated with the result that the peak correlation coefficients for the axial mass transport were greater than the correlation coefficients for the momentum transport measurements.

The skewness and flatness factor profiles for the turbulent axial mass transport measurements at z = 102 and 203 mm are presented in Fig. 47. At z = 102 mm, where the axial mass transport was in the countergradient direction, the skewness factors were negative. The peak flatness factors were 50 to 200, the largest values obtained in this study and occur at $r/R_o \approx 0$ and 0.4 where the axial mass transport rate was negligible. The minimum kurtosis occurred at $r/R_o \approx 0.2$, where the axial mass transport rate was high. At z = 203 mm, the skewness factors in the high axial mass transport region were 1 or less. However, S_{uf} increased to 2 in the region where the shear was high and the axial mass transport was low. The kurtosis of the turbulent axial mass transport rate p.d.f.s varied from 7 to 10 in the high axial mass transport rate region to more than 20 at r/R_o = 0.65 where the axial mass transport rates and mean concentrations were low.

Azimuthal Mass Transport

The second central moment, skewness and kurtosis for several turbulent azimuthal mass transport p.d.f.s at z = 102 mm are presented in Fig. 48. The central moment results were approximately equal to those for the radial mass transport (Fig. 44). The skewness results were near zero at all radii except for R/R_o = 0 where the value of -2.8 was obtained. For an axisymmetric flow, skewness values equal zero were expected. The large skewness at $r/R_o = 0$ was attributed to possible errors in probe volume location. Recall the skewness vlaues for vf increased to large values near zero (Fig. 45) and the optical arrangements for the radial and azimuthal mass transport rate measurements are identical with the exception of the traverse path. The kurtosis for wf was in the same range as that obtained for uf.

SUMMARY OF RESULTS

Qualitative and quantitative studies were conducted of the flow downstream of coaxial jets discharging into an expanded duct. The ratio of annular jet diameter and duct diameter to the inner jet diameter were 2 and 4, respectively. The inner jet peak velocity was approximately one-half the annular jet peak velocity. Results from the studies were related to the four shear regions within the duct: (1) wake region downstream of the inlet, (2) shear layer between the jets, (3) recirculation region, and (4) reattachment region.

Flow visualization studies were conducted using dye as a trace material and high-speed motion pictures to record the dye patterns in selected r-z and r-θ planes. Following are the principal results from this study:

1. The flow was as axisymmetric and swirl-free as could be determined visually.

2. The larger scales of the turbulent structure were observed to grow from the width of the wake region downstream of the inner jet tube to a large fraction of the duct diameter immediately upstream of the reattachment zone.

3. The turbulent eddies were <u>not</u> axisymmetric or periodic at any location within the duct. The large scale waves and eddies appeared to have a range of wave lengths.

4. Vortex pairs of secondary eddies were observed in the r-θ plane in the region where the shear layer between the jets was developing.

A detailed map of the velocity, concentration, mass transport rate and momentum transport rate distribution within the duct was obtained to provide data for the evaluation and improvement of turbulent transport models. Data sets of two velocity components pairs were obtained simultaneously to determine momentum transport rate and velocities. Data sets of velocity and concentration pairs were obtained simultaneously to determine mass transport rate, concentration, and velocity. Probability density functions (p.d.f.s) of all the forementioned parameters were obtained from the data sets. Mean quantities, second central moments, skewness and kurtosis were calculated to characterize each data set. Following are the principal results from this study:

5. The axial and radial velocity profiles documented the changes in the shear regions within the duct.

6. The mean and fluctuating concentration profiles documented the inner jet fluid distribution within the duct.

7. The turbulent momentum transport rate measurements in the r-z plane documented the local momentum fluxes due to turbulent mixing. Correlation coefficients were determined for each measurement location and data set.

8. Countergradient turbulent axial mass transport was measured in the shear region between jets. The peak axial mass transport rates were greater than the peak radial mass transport rates even though the axial concentration gradients were approximately one-fifth the radial gradients.

9. The countergradient turbulent axial mass transport was related to the general direction of the eddies between the inner and annular jets. The countergradient axial mass transport occurred when the annular jet was accelerating the inner jet fluid.

10. Turbulent axial mass transport correlation coefficients as high as 0.6 were measured. These correlation coefficients were greater than the peak momentum transport or radial mass transport correlation coefficients.

11. The skewness and kurtosis of the momentum transport p.d.f.s in the peak shear region were approximately the same as previously measured in turbulent boundary layers. However, the kurtosis in the low shear region was greater than previously measured in the wake region of the turbulent boundary layers.

12. The skewness of the axial velocity p.d.f.s was related to the curvature of the axial velocity profiles. $S_u < 0$ was obtained for $\partial^2 U/\partial r^2 < 0$; $S_u > 0$ was obtained for $\partial^2 U/\partial r^2 > 0$. The skewness was also proportional to the magnitude of $\partial^2 U/\partial r^2$.

13. The peak values of kurtosis for the mass transport p.d.f.s were greater than the peak values for the momentum transport p.d.f.s.

14. The kurtosis for all the transport rate p.d.f.s were an order of magnitude greater in the low transport rate regions, including the recirculation region, than in the high transport rate regions.

REFERENCES

1. Launder, B. E. and D. B. Spalding: Mathematical Models of Turbulence. Academic Press, 1972.

2. Demetriades, A.: Probes for Multivariant Flow Characteristics. Proceedings of the Dynamic Flow Conference, 1978.

3. Libby, P. A.: Studies in Variable-Density and Reacting Turbulent Shear Flows, Studies in Convection, Vol. 2, Academic Press, 1977.

4. -----: Application of Non Intrusive Instrumentation in Fluid Flow Research. AGARD Conference Proceedings No. 193, May 1976.

5. Becker, H. A.: Mixing Concentration Fluctuations, and Marker Nephelometry Studies in Convection, Vol. 2, Academic Press, 1977.

6. Johnson, B. V. and J. C. Bennett: Velocity and Concentration Characteristics and Their Cross Correlations for Coaxial Jets in a Confined Sudden Expansion; Symposium on the Fluid Mechanics of Combustion Systems, 1981 ASME Fluids Engineering Division Meeting, Boulder, CO, June 22-24, 1981. Also issued as UTRC Report UTRC81-16, March 1981.

7. Habib, M. A. and J. H. Whitelaw: Velocity Characteristics of Confined Coaxial Jets With and Without Swirl. ASME Journal of Fluids Engineering, Vol. 102, pp. 47-53 (1980).

8. Schetz, J. A.: Injection and Mixing in Turbulent Flow, Vol. 68, Progress in Astronautics and Aeronautics, AIAA, 1980.

9. Habib, M. A. and J. H. Whitelaw: Velocity Characteristics of a Confined Coaxial Jet. ASME Journal of Fluids Engineering, Vol. 101, pp. 521-529, December 1979.

10. Durst, F., A. Melling and J. H. Whitelaw: Principles and Practices of Laser-Doppler Anemometry. Academic Press, NY, 1976.

11. -----: Data for Dye Lasers. Kodak Publication No. JJ-169, March 1972.

12. Lumley, J. L.: Computational Modeling of Turbulent Flows. Advances in Applied Mechanics. Vol. 18, Academic Press (1978).

13. Tennekes, H., and J. L. Lumley: A First Course in Turbulence, Chapter 6, MIT Press, 1972.

14. Michalke, A.: On Statial Growing Disturbances in an Inviscid Shear Layer, Journal of Fluid Mechanics, Vol. 23, Part 3, 1965, pp. 521-544.

15. Lu, S. S. and W. W. Willmarth: Measurements of the Structure of the Reynolds Stress in a Turbulent Boundary Layer, J. Fluids Mechanics, Vol. 60, Part 3, pp. 481-511 (1973).

16. Willmarth, W. W.: Structure of Turbulence in Boundary Layers, Advances in Applied Mechanics, Vol. 15, Academic Press, NY, 1975.

17. Gupta, A. K. and R. E. Kaplan: Statistical Characteristics of Reynolds Stress in a Turbulent Boundary Layer, Phys. Fluids, Vol. 15, pp. 981.

18. Hinze, J. O.: Turbulence, McGraw-Hill, NY, 1959, Chapter 7.

19. Gerstein, M. (Ed): Fundamentals of Gas Turbine Combustion, NASA Conference Publication 2087, 1979.

20. Hudson, D. A.: Combustion Modeling Needs for the 80's. AIAA Preprint 80-1288.

21. Mellor, A. M.: Turbulent-Combustion Interaction Models for Practical High Intensity Combustors: Seventeenth Symposium on Combustion, p. 377, Combustion Institute, 1979.

22. Dryburgh, D. and R. B. Edelman: Technical Evaluation Report on the Propulsion and Energetics Panel 54th Meeting on Bomcustio Modeling. AGARD Advistory Report No. 153, March 1980.

APPENDIX I

FLOW VISUALIZATION RESULTS FOR ALL FLOW CONDITIONS

Flow visualization studies were conducted prior to the selection of the flow condition for detailed data acquisition to determine the effects of the velocity ratio, V_i/V_a, on the flow characteristics within the test section.

Motion pictures were obtained in the r-z plane with the center of illumination at z = 100 and 200 mm and in the r-θ plane at z = 51, 102 and 203 mm. Motion pictures with a frame speed of 500 per second were obtained for each flow condition for the following five conditions:

Flow Condition	Inner Jet Velocity, V_i m/s	Annular Jet Velocity, V_a m/s	Inner Jet Flow Rate gpm	Annular Jet Flow Rate gpm
1	0.52	1.66	6.2	52.8
2	0.27	1.66	3.2	52.8
3	2.08	1.66	24.6	52.8
4	0.94	1.51	11.1	48.0
5	0.94	2.87	11.1	94.8

In the following paragraphs, the photographs presented in Figs. 10 and 49 to 52 will be discussed. Discussion about the characteristics of Flow Condition 1 is repeated to form a basis for comparison. Where possible, the turbulent structure will be related to the shear regions shown schematically in Fig. 1. The motion picture frames chosen from each sequence were selected to show the largest scale of turbulence which occurred at each location. For some locations the large scale structure was intermittent.

The photographs of Flow Condition 1 are presented in Fig. 10. This flow condition was the same as that for which data was acquired in Ref. 6. In the upper left photograph, the classical large eddy structure associated with shear layers could be discerned. The dyed inner jet fluid was moving slower than the annular jet; hence the eddies were "rolling" faster than the inner jet fluid. These eddies were associated with the shear layer between jets (Fig. 1). The upper right photograph shows the scale of the eddies containing inner jet fluid which occurred immediately upstream of the reattachment region (Fig. 1). The inner jet fluid intermittently filled most of the duct cross section. The r-θ plane photograph for z = 51 mm shows the size of the eddy structure in the wake region. At z = 102 mm, which was in the shear layer between the jets, the radial scale of turbulence was increased and vortex pairs could be discerned from observation of the motion picture sequences. These vortex pairs were similar to the vortex pairs observed by the California Institute of Technology fluid mechanics research group. The vortex pairs appeared to occur randomly both timewise and azimuthally in the shear layer between jets. At z = 152 mm the inner jet fluid distribution became more three dimensional than at the upstream locations. This location was also in shear layer between jets. The largest scale structure with high dye concentrations occurred at z = 203 mm. This location was immediately upstream of the reattachment zone where the annular jet fluid began to decelerate and flow toward the duct wall. At further downstream locations, the peak concentrations of the inner jet fluid were lower and the dye concentration more uniform across the duct r-θ cross section.

The inner jet velocity, V_i, for Flow Condition 2 was approximately half that of Flow Condition 1. As a result the wake region length was decreased and the classical large eddy structure of the shear layer between jets occurred at z = 51 mm. The r-θ plane photograph showed dye filaments at the edge of the inner jet fluid which were associated with the vortex pair phenomena described for Flow Condition 1. The lack of axisymmetry in the shape of the inner jet fluid also occurred at z = 102 mm rather than at z = 153 mm for Condition 1. At z = 203 mm the radial extent of the diffuser inner jet fluid spanned the entire duct diameter.

For Flow Condition 3, the inner jet velocity, V_i, was four times that for Flow Condition 1. Thus, the inner jet was flowing faster than the annular stream. In the upper left photograph, the shape of the eddies in the shear layer between jets seem to be different than occurred for Flow Condition 1 or 2. The eddies were observed to roll in the opposite direction with a wave speed less than the inner jet fluid. In the right r-z plane photograph, the size of the turbulent eddies was smaller than for the previous case. The reattachment zone was also moved downstream compared to Flow Conditions 1 and 2. At z = 51 mm and 102 mm the double-vortex structure could be discerned. At z = 203 mm the inner jet fluid concentration was decreased in some locations, but the large scale structure which occurred upstream of the reattachment zone had not yet formed.

Flow Condition 4 was chosen to obtain approximately equal peak velocities in the inner jet and annular stream. The flow rates were determined by ratioing the peak velocities and flow rates from Ref. 6 to the desired velocity ratio. The r-z photograph for z ≈ 100 mm showed eddies in the shear region layer between jets that did not have a single "roll" direction. Observation of the motion pictures showed rolls in both directions but with most of the direction previously associated with higher annular jet velocities. At z ≈ 200 mm, the inner jet had large eddy structures similar to that for Flow Condition 1. The reattachment zone for Flow Condition 4 was approximately 4 mm downstream of that for Condition 1. The turbulent structure in the r-θ planes at z = 102, 157 and 203 mm had slightly smaller eddy sizes than at the same axial locations for Flow Condition 1.

Flow Condition 5 has approximately 75 percent greater velocity in both jets than Flow Condition 1. Within the ability to discern flow characteristics from the high speed motion pictures, the turbulent structure of Flow Condition 5 was the same as Flow Condition 1.

The flow visualization study showed the flows were as axisymmetric and swirl free as could be determined visually. Although the scale of the turbulent structure was relatively large, the eddies were not axisymmetric or periodic. The large scale waves and eddies appeared to have a range of wavelengths. The flows did not have bistable modes or preferred azimuthal turbulent eddy orientations at any location including the reattachment region. However, the scale of the turbulent structure near the reattachment region was large which will require relatively long data acquisition times to acquire stationary data sets.

APPENDIX II

DEFINITIONS OF SKEWNESS AND KURTOSIS FOR VELOCITY, CONCENTRATION, AND TRANSPORT PROBABILITY DENSITY FUNCTIONS

Terms in this appendix for the velocity components and concentrations are defined using the notation of Ref. 13 and conventional statistical methods.

$\tilde{u}$ — Local instantaneous axial velocity component

$B(\tilde{u})$ — Probability density function (p.d.f.) of $\tilde{u}$ with properties $B(\tilde{u}) \geq 0$ and $\int_{-\infty}^{\infty} B(u)\,du = 1.0$

U — Mean value of axial velocity component defined: $U = \int_{-\infty}^{+\infty} \tilde{u}\, B(\tilde{u})\, d\tilde{u}$

u — Local instantaneous axial velocity fluctuation from the mean, defined: $u = \tilde{u} - U$

σ_u or u' — Second central moment of velocity u defined: $\sigma_u{}^2 = u'^2 = \int_{-\infty}^{-\infty} u^2\, B(\tilde{u})\, d\tilde{u}$ Will also be denoted as rms fluctuation.

$\overline{u^n}$ — nth central moment of velocity u defined: $\overline{u^n} = \int_{-\infty}^{\infty} u^n\, B(\tilde{u})\, d\tilde{u}$

S_u — Skewness of velocity component, u, p.d.f. defined: $S_u = \overline{u^3}/\sigma_u{}^3$

K_u — Kurtosis (or flatness factor) of velocity component, u, p.d.f. defined: $K_u = \overline{u^4}/\sigma_u{}^4$

In like manner, the mean, rms fluctuation, skewness, and kurtosis for the radial velocity, azimuthal velocity and concentration are defined.

The second moments, skewness and kurtosis for the momentum and mass transport rates are defined in a similar manner.

$u\tilde{v}$ — Local instantaneous momentum turbulent transport rate: $(\tilde{u}-U)(\tilde{v}-V)$

$B(uv)$ — Probability density function (p.d.f.) of uv with properties $B(uv) > 0$ and $\int_{-\infty}^{+\infty} B(uv)\, d(uv) = 1.0$

$\overline{uv}$ — Mean value of turbulent momentum transport rate defined: $uv = \int_{-\infty}^{\infty} (\tilde{u}-U)(\tilde{v}-V)\, b(uv)\, d(uv)$

$(uv)'$ — Local instantaneous fluctuation of momentum transport rate from mean, defined: $(uv)' = uv - \overline{uv}$

σ_{uv} Second central moment of momentum transport rate: $\sigma_{uv} = \int_{-\infty}^{\infty} (uv)'^2 \, B(uv) \, d(uv)$

$(uv)^n$ nth central moment of momentum transport rate: $(uv)^n = \int_{-\infty}^{\infty} (uv)'^n \, B(uv) \, d(uv)$

S_{uv} Skewness of momentum transport rate: $S_{uv} = (\overline{uv})^3/\sigma_{uv}^3$

K_{uv} Kurtosis of momentum transport rate: $K_{uv} = (\overline{uv})^4/\sigma_{uv}^4$

In a like manner, the mean, second central moment, skewness and kurtosis for the momentum transport in the r-z plane and the mass transport in three directions are defined.

TABLE I-1

Components Used for Two-Component LV Measurements

I. Laser Light Source

Argon Ion Laser (Lexel Model 95)
- All lines, 1.0 watt power
- Etalon installed
- TEM_{oo} mode

II. LV Optics

DISA Model 5500 Optics
- Beamsplitters (2)
- Bragg cell: 1 mHz effective frequency offset
- Backscatter unit: 2 color
- Optical filters 0.5145 and 0.4880 μm wavelengths
- Field stop unit
- Beam spacing unit
- Beam expander
- Achromatic lens: 310 mm FL
- Photomultiplier tubes (2)

III. Electronics

LV Signal Processors - 2 (SCIMETRICS Model 800A)
- 0.4 to 2.0 mHz range
- 3% data window
- 4/8 and 5/8 comparison for "good signals"

Oscilloscope - 2 (Tektronics Model 465B)

LV Data Handling Interface (UTRC design)
- Clock
- Coincidence check

Computer (PDP 11/10)
- Floppy disk
- DECwriter III (1200 baud rate)

TABLE I-2

Components Used for LV/LIF Measurements

I. Light Source
- Argon Ion Laser (Spectra Physics Model 164)
  - 0.4880 μm wavelength
  - 0.5 watts power

II. LV/LIF Optics
- Transmitting Optics
  - Polarization rotator (TSI 9102 12)
  - Beamsplitter (TST 9115)
  - Bragg cell: 1.0 mHz frequency offset (TSI 9180)
  - Beam spacer (TSI 9113-22)
  - Beam expander (TSI 9188)
  - Transmitting lens (ϕ = 7.57 deg.) (TSI 9110)
- Concentration Data Acquisition Optics
  - Backscatter unit (TSI 9140)
  - Photomultiplier tube (RCA 7265)
  - Wratten filter (Kodak #15)
- Velocity Data Acquisition Optics
  - Backscatter unit (TSI 9140)
  - Photomultiplier (TSI 9160)
  - Collecting lens: 250 mm F.L. (TSI 9118)

III. LV Electronics
- LV Signal Processor (SCIMETRICS Model 800A)
  - 0.4 to 2 mHz range
  - 3% data window
  - 4/8 and 5/8 comparison for "good signals"
- Oscilloscope (Tektronics Model 465b)
  - 2 units
- Minicomputer (PDP 11/10)
  - Floppy disk
  - DECwriter III (1200 baud rate)

IV. LIF Electronics
- Current-to-Voltage Converter (UTRC design)
- Low Pass Filter
  - 2 KHz (Kronhite Model 3202)
- Oscilloscope (Tektronics Model 465B)
- A/D Converter (PDP LPS Unit)
  - Computer controlled
- Digital Voltmeter (HP Model 3465A)
- Minicomputer (PDP 11/10)
  - Same as for LV electronics
- LV Data Interface (UTRC design)
  - Clock

TABLE II

Table of Run Numbers from Which Data was Utilized for Tables and Figures

Velocity Component or Transport Measurement Obtained	Traverse Direction	C_L	Axial Location, z-mm						
			13	51	102	152	203	254	305
U, V, $\overline{uv}$	Vertical		44,8	17	16,15	20	21	72	74
U, W, $\overline{uw}$	Horizontal		9	14	18,23	19,24	22	71	73
U, C, $\overline{uc}$	Vertical	59,68	60	61	62	63	64	66	67
V, C, $\overline{vc}$	Vertical	55	45	47	52	51	50	69	70
W, C, $\overline{wc}$	Horizontal		57	58	53	54	56		
U (only)	± 45 deg		10,11						

TABLE III

Figures on Which Results are Displayed

Quantity	Direction or plane	Central Moment	Symbol	C_L	Axial Location, z-mm						
					13	51	102	153	203	254	305
Velocity	z	1	U	12	11	11	11	11	11	11	11
		2	u'		15	15	15	15	15	15	15
		3	S_u				33		33		
		4	K_u				33		33		
	r	1	V		13	13	13	13	13	13	13
		2	v'		16	16	16	16	16	16	16
		3	S_v				34		34		
		4	K_v				34		34		
	θ	1	W		14	14	14	14	14	14	14
		2	w'		17	17	17	17	17	17	17
		3	S_w				35		35		
		4	K_w				35		35		
Concentration		1	f	12	18	18	18	18	18	18	18
		2	f'		19	19	19	19	19	19	19
		3	S_f				36		36		
		4	K_f				36		36		
Momentum Transport	z-r	1	$\overline{uv}$		20	20	20	20	20	20	20
			R_{uv}		21	21	21	21	21	21	21
		2	σ_{uv}				42		42		
		3	S_{uv}				43		43		
		4	K_{uv}				43		43		
	z-θ	1	$\overline{uw}$				22				
			R_{uw}				22				
Mass Transport	z	1	$\overline{uf}$		25	25	25	25	25	25	25
			R_{uf}		27	27	27	27	27	27	27
		2	σ_{uf}				46		46		
		3	S_{uf}				47		47		
		4	K_{uf}				47		47		
	r	1	$\overline{vf}$		23	23	23	23	23	23	23
			R_{vf}		24	24	24	24	24	24	24
		2	σ_{vf}				44		44		
		3	S_{vf}				45		45		
		4	K_{vf}				45		45		
	θ	1	$\overline{wf}$				28				
			R_{wf}				28				
		2	σ_{wf}				48				
		3	S_{wf}				48				
		4	K_{wf}				48				

TABLE IV-14

AXIAL AND AZIMUTHAL VELOCITY DATA AND CORRELATIONS

Test Date: 6/15/81 Run No.: 14 Flow Condition: 1 Geometry: 1

Axial Location: 51 mm (2.0 in.); $x/R_o = 0.83$

Pt No.	r mm +(θ=270) -(θ=90)	r/R_o	U m/s	u' m/s	S_u	K_u	W m/s	w' m/s	S_w	K_w	$\overline{uw}$ m^2/s^2	R_{uw}	σ_{uw} m^2/s^2	S_{uw}	K_{uw}	N
1	0.7	.011	0.717	.051			.007	.044								
2	3.7	.061	0.676	.069			.000	.050								
3	6.8	.111	0.616	.079			.004	.054								
4	9.8	.161	0.658	.134			.008	.082								
5	12.9	.211	0.888	.188			.003	.148								
6	15.9	.261	1.243	.169			.024	.132								
7	19.0	.311	1.443	.091			.007	.060								
8	22.0	.361	1.491	.064			-.020	.045								
9	25.1	.411	1.474	.083			-.030	.063								
10	28.1	.461	1.241	.203			-.026	.159								
11	31.2	.511	0.865	.225			-.027	.215								
12	34.2	.561	0.443	.292			-.031	.199								
13	37.3	.611	0.110	.198			-.029	.176								
14	40.3	.661	-0.015	.141			-.003	.129								
15	46.4	.761	-0.078	.139			-.011	.127								
16	52.5	.861	-0.075	.141			-.023	.119								
17	0.7	.011	0.706	.057			-.002	.041								
18	-2.4	-.039	0.724	.049			-.002	.037								
19	-5.4	-.089	0.700	.065			.002	.045								
20	-8.5	-.139	0.649	.087			.002	.079								
21	-11.5	-.189	0.845	.170			.023	.139								
22	-14.6	-.239	1.195	.190			.073	.138								
23	-17.6	-.289	1.438	.105			.069	.080								
24	-20.7	-.338	1.486	.069			.021	.054								
25	-23.7	-.388	1.483	.097			.005	.071								
26	-26.7	-.438	1.324	.194			.008	.121								
27	-29.8	-.488	0.901	.276			.001	.191								
28	-32.8	-.538	0.487	.283			.020	.200								
29	-35.9	-.588	0.187	.259			.038	.161								
30	-38.9	-.638	-0.030	.135			.016	.138								
31	-45.0	-.738	-0.067	.122			.029	.098								
32	-51.1	-.837	-0.128	.141			.020	.081								
33	0.7	.011	0.737	.053			.004	.042								

TABLE IV-15

AXIAL AND RADIAL VELOCITY DATA AND CORRELATIONS

Test Date: 6/16/81 Run No.: 15 Flow Condition: 1 Geometry: 1

Axial Location: 102 mm (4.0 in.); $x/R_o = 1.66$

Pt No.	r mm +(θ=0) -(θ=180)	r/R_o	U m/s	u' m/s	S_u	K_u	V m/s	v' m/s	S_v	K_v	$\overline{uv}$ m^2/s^2	R_{uv}	σ_{uv} m^2/s^2	S_{uv}	K_{uv}	N
1	0.5	.008	.780	.123	1.318	7.53	-.019	.123	-1.627	12.99						491
2	3.6	.058	.784	.123	1.017	5.83	-.067	.125	—	—						499
3	6.6	.108	.860	.170	.799	3.39	-.067	.129	-.870	6.25						497
4	9.7	.158	1.005	.194	.409	2.70	-.055	.143	-.399	3.33						499
5	12.7	.208	1.212	.201	-.072	2.35	-.078	.148	-.244	3.81						499
6	15.7	.258	1.370	.187	-.719	2.94	-.046	.144	-.013	4.04						999
7	18.8	.308	1.491	.146	-1.284	5.36	-.018	.140	-.127	4.44						998
8	21.8	.358	1.372	.184	-1.760	6.94	.008	.149	-.878	5.80						999
9	24.9	.408	1.264	.244	-1.198	4.80	.028	.174	-.604	4.12						999
10	27.9	.458	1.069	.276	—	—	.043	.198	—	—						
11	31.0	.508	.821	.309	-.336	3.09	.055	.223	-.180	2.92						997
12	34.0	.558	.586	.319	-.159	2.88	.040	.232	.510	4.72						499
13	37.1	.608	.342	.321	-.028	2.70	.025	.237	.916	5.71						249
14	43.2	.708	-.032	.279	.576	3.40	.018	.196	.744	4.00						249
15	49.3	.808	-.187	.228	.897	4.40	-.028	.134	.726	5.06						248
16	0.5	.008	.732	.119	.927	4.97	-.014	.114	-.896	11.65						498
17	-2.5	-.042	.742	.136	1.068	5.36	-.058	.155	-2.537	15.01						499
18	-5.6	-.092	.782	.143	.817	3.58	-.061	.154	-3.312	24.91						499
19	-8.6	-.142	.889	.170	.632	3.16	-.070	.143	-.771	4.91						498
20	-11.7	-.192	1.047	.193	.059	2.46	-.070	.145	-.046	3.00						498
21	-14.7	-.241	1.229	.179	-.492	3.00	-.060	.156	-1.435	12.41						999
22	-17.8	-.291	1.351	.161	-.904	4.05	-.031	.150	-1.059	9.77						999
23	-20.8	-.341	1.396	.169	-1.476	6.29	-.013	.155	-.862	6.73						997
24	-23.9	-.391	1.316	.212	-1.272	4.90	.028	.171	-.537	4.03						998
25	-26.9	-.441	1.133	.268	-.819	3.59	.040	.217	-.778	4.96						998
26	-30.0	-.491	.880	.304	-.255	2.85	.067	.226	-.230	2.81						999
27	-33.0	-.541	.629	.321	-.076	3.09	.043	.240	.024	2.77						499
28	-36.1	-.591	.461	.340	—	—	.044	.207	—	—						
29	-42.2	-.691	.079	.338	—	—	-.013	.145	—	—						
30	-48.3	-.791	.029	.202	—	—	-.094	.096	—	—						
31	0.5	.008	.723	.088	—	—	-.001	.063	—	—						

TABLE IV-16

AXIAL VELOCITY, RADIAL VELOCITY, AND MOMENTUM TURBULENT TRANSPORT DATA AND CORRELATIONS

Test Date: 6/17/81 Run No.: 16 Flow Condition: 1 Geometry: 1

Axial Location: 102 mm (4.0 in.); x/R_o = 1.66

Pt No.	r mm +(θ=0) -(θ=180)	r/R_o	U m/s	u' m/s	S_u	K_u	V m/s	v' m/s	S_v	K_v	$\overline{uv}$ m^2/s^2	R_{uv}	σ_{uv} m^2/s^2	S_{uv}	K_{uv}	N
1	0.5	0.008	.768	.124	1.118	6.38	.001	.117	.163	8.99	.0005	.003	.030	1.28	41.23	498
2	3.6	0.058	.768	.131	1.409	7.36	-.026	.106	-1.019	5.89	-.0049	-.355	.025	-3.14	31.49	499
3	6.6	0.108	.840	.158	.903	3.80	-.043	.119	-.752	3.97	-.0088	-.470	.023	-2.69	15.73	499
4	9.7	0.158	.976	.199	.394	2.67	-.065	.146	-.401	2.87	-.0167	-.576	.032	-1.85	10.08	499
5	12.7	0.208	1.172	.204	-.140	2.67	-.071	.137	-.059	2.92	-.0142	-.508	.030	-2.14	11.90	499
6	15.7	0.258	1.368	.187	-.797	3.24	-.047	.146	-.065	3.86	-.0082	-.300	.032	-1.07	19.01	999
7	18.8	0.308	1.493	.135	-1.492	6.97	-.017	.134	-.025	4.17	-.0006	-.035	.028	2.31	50.58	999
8	21.8	0.358	1.459	.176	-1.434	5.80	.013	.149	-.281	5.02	.0064	.244	.039	3.94	49.91	999
9	24.9	0.408	1.333	.253	-1.288	5.44	.046	.173	-.678	5.23	.0167	.381	.063	3.82	36.09	999
11	31.0	0.508	.894	.311	-.423	3.17	.068	.222	-.193	3.40	.0277	.402	.077	1.15	13.24	998
12	34.0	0.558	.663	.319	-.345	3.12	.059	.224	.029	3.51	.0271	.379	.078	1.70	9.71	499
13	37.1	0.608	.454	.355	-.040	2.70	.049	.216	.327	4.00	.0379	.494	.085	2.42	11.58	249
14	43.2	0.708	.006	.348	.135	2.19	.008	.211	.611	3.81	.0320	.436	.072	2.37	18.72	249
15	49.3	0.808	-.205	.229	.723	3.40	-.031	.143	.663	3.57	.0126	.384	.036	2.27	12.71	249
16	0.5	0.008	.761	.126	1.041	5.45	.001	.112	.017	5.26	.0004	.025	.022	1.48	25.26	497
17	-2.5	-0.041	.785	.126	1.077	6.04	-.042	.121	-1.234	5.41	-.0034	-.225	.020	-1.45	23.51	499
18	-5.6	-0.091	.842	.156	.833	4.30	-.070	.141	-.812	3.58	-.0096	-.436	.029	-1.79	21.51	499
19	-8.6	-0.141	.957	.186	.566	2.97	-.072	.151	-.493	3.46	-.0119	-.424	.033	-3.73	39.55	499
20	-11.7	-0.191	1.132	.205	.196	2.46	-.068	.164	-.436	4.35	-.0138	-.410	.031	-0.90	6.92	499
21	-14.7	-0.241	1.292	.192	.547	3.05	-.058	.148	-.010	4.21	-.0089	-.313	.031	-0.26	15.49	999
22	-17.8	-0.291	1.422	.176	.752	3.53	-.034	.152	-.450	5.84	-.0010	-.037	.037	3.03	48.19	999
23	-20.8	-0.341	1.473	.171	1.329	6.06	.006	.151	-.348	5.38	.0054	.208	.044	5.44	66.56	999
24	-23.9	-0.391	1.381	.237	-1.356	5.07	.022	.182	-.807	4.70	.0197	.457	.060	3.68	23.45	999
25	-26.9	-0.441	1.168	.299	-.651	3.11	.051	.206	-.267	2.99	.0314	.509	.068	2.74	17.49	999
26	-30.0	-0.491	.955	.319	-.398	3.38	.075	.227	-.093	3.16	.0321	.443	.082	0.38	18.81	999
27	-33.0	-0.541	.707	.326	-.173	3.22	.069	.253	.392	3.42	.0349	.424	.093	1.64	12.76	499
28	-36.1	-0.591	.468	.358	-.209	3.17	.059	.257	-.040	2.52	.0371	.404	.086	1.53	7.24	248
29	-42.2	-0.691	.074	.334	.178	2.42	.002	.208	.753	3.99	.0268	.386	.077	1.43	9.09	249
30	-48.3	-0.791	-.209	.227	.621	3.58	-.047	.132	1.352	7.30	.0108	.362	.043	4.63	32.22	249
31	0.5	0.008	.772	.111	.815	7.11	-.002	.105	-.403	7.94	-.0008	-.070	.023	-4.23	67.05	499

TABLE IV-17

AXIAL VELOCITY, RADIAL VELOCITY, AND MOMENTUM TURBULENT TRANSPORT DATA AND CORRELATIONS

Test Date: 6/18/81 Run No.: 17 Flow Condition: 1 Geometry: 1

Axial Location: 51 mm (2.0 in.); x/R_o = 0.83

Pt No.	r mm +(θ=0) -(θ=180)	r/R_o	U m/s	u' m/s	S_u	K_u	V m/s	v' m/s	S_v	K_v	$\overline{uv}$ m^2/s^2	R_{uv}	σ_{uv} m^2/s^2	S_{uv}	K_{uv}	N
1	0.0	.000	.762	.054	-.253	2.97	.002	.041	.131	3.28	-.0002	-.090	.002	-0.05	8.69	499
2	3.0	.050	.754	.055	-.438	3.29	.001	.039	-.005	3.72	.0001	.062	.002	-0.83	18.36	499
3	6.1	.100	.723	.066	-.480	3.34	.002	.049	-.337	3.29	.0006	.175	.003	2.77	22.61	499
4	9.1	.150	.694	.116	1.137	6.36	-.039	.114	-.620	3.23	-.0047	-.353	.017	-4.04	31.24	499
5	12.2	.200	.927	.174	.371	2.92	-.049	.136	-.211	2.58	-.0112	-.473	.025	-1.47	7.68	499
6	15.2	.250	1.297	.185	-.517	2.75	-.058	.130	.367	3.05	-.0116	-.484	.026	-1.82	8.06	999
7	18.3	.300	1.551	.087	-1.753	8.39	-.029	.082	.788	5.47	-.0017	-.235	.011	-5.94	69.40	998
8	21.3	.350	1.569	.066	-.849	1.90	-.026	.076	-.760	6.52	.0014	.273	.006	3.29	25.64	997
9	24.4	.400	1.506	.124	-1.342	7.47	-.009	.103	-1.111	8.33	.0050	.394	.021	5.77	55.86	998
11	30.5	.500	1.254	.228	-.672	3.28	.029	.156	-.809	4.44	.0145	.409	.048	3.66	29.89	999
12	33.5	.550	.841	.276	-.056	3.03	.052	.200	-.211	2.71	.0232	.421	.058	1.72	11.86	499
13	36.6	.600	.482	.256	.108	2.91	.051	.209	-.091	3.00	.0262	.489	.054	1.35	6.50	249
14	42.7	.699	-.039	.198	.427	4.43	-.021	.136	1.405	8.37	.0075	.278	.034	2.25	15.83	249
15	48.8	.799	-.134	.154	-.204	2.95	-.034	.092	.337	4.74	.0018	.127	.013	-0.12	7.14	247
16	0.0	.000	.747	.055	-.545	3.34	-.004	.045	-.075	3.20	.0000	.006	.003	0.54	10.27	498
17	-3.0	-.050	.743	.059	-.373	2.79	-.002	.045	-.468	4.39	.0004	.136	.003	2.66	23.75	499
18	-6.1	-.100	.724	.066	-.528	3.53	-.001	.048	-.353	3.06	.0007	.229	.004	3.17	27.71	499
19	-9.1	-.150	.689	.099	.682	4.55	-.039	.098	-1.078	4.85	-.0029	-.297	.014	-4.58	35.80	499
20	-12.2	-.200	.906	.158	.313	2.90	-.065	.139	-.622	4.75	-.0091	-.413	.022	-1.04	8.24	498
21	-15.2	-.250	1.249	.170	-.334	2.76	-.062	.127	.517	3.38	-.0092	-.427	.023	-2.24	13.38	998
25	-27.4	-.450	1.281	.227	-.732	3.50	-.031	.155	-.724	4.46	.0143	.406	.045	5.69	72.36	999
26	-30.5	-.500	.826	.285	-.210	2.81	-.048	.208	-.091	3.15	.0302	.510	.065	1.76	9.04	999
27	-33.5	-.550	.413	.268	-.152	3.14	-.027	.211	.239	3.03	.0241	.427	.061	1.92	8.90	499
28	-36.6	-.600	.090	.268	.442	3.08	-.024	.174	.657	3.35	.0222	.475	.053	1.79	9.80	249
29	-42.7	-.699	-.136	.161	-.053	2.78	-.051	.092	.936	7.78	.0049	.333	.017	2.16	10.20	249
30	-48.8	-.799	-.131	.155	-.121	2.97	-.032	.069	-.209	4.36	.0026	.242	.013	2.19	25.43	248
31	-51.8	-.849	-.111	.148	-.458	3.69	-.027	.093	2.272	18.65	.0023	.170	.010	1.38	9.97	239
32	0.0	.000	.753	.057	-.248	2.71	-.002	.041	.210	3.22	.0001	.058	.002	0.01	10.97	498

TABLE IV-18

AXIAL AND AZIMUTHAL VELOCITY DATA AND CORRELATIONS

Test Date: 6/22/81 Run No.: 18 Flow Condition: 1 Geometry: 1

Axial Location: 102 mm (4.0 in.); x/R_o = 1.66

Pt No.	r mm +(θ=270) -(θ=90)	r/R_o	U m/s	u' m/s	S_u	K_u	W m/s	w' m/s	S_w	K_w	$\overline{uw}$ m^2/s^2	R_{uw}	σ_{uw} m^2/s^2	S_{uw}	K_{uw}	N
1	0.5	0.008	0.771	0.154	1.428	6.98	-0.004	0.144	0.377	5.16						496
2	3.6	0.058	0.783	0.141	0.681	4.27	-0.002	0.125	0.162	4.46						498
3	6.6	0.108	0.881	0.201	0.734	3.89	-0.001	0.144	0.044	3.89						499
4	9.7	0.158	1.004	0.198	0.333	2.82	0.019	0.150	0.057	3.58						499
5	12.7	0.208	1.173	0.218	-0.066	2.48	-0.002	0.153	0.057	3.44						499
6	15.7	0.258	1.332	0.187	-0.508	2.82	-0.001	0.132	0.186	3.37						997
7	18.8	0.308	1.451	0.170	-1.324	5.55	-0.004	0.115	-0.126	3.75						993
8	21.8	0.358	1.469	0.187	-1.512	5.71	-0.019	0.130	-0.046	5.44						996
9	24.9	0.408	1.363	0.247	-1.223	4.52	-0.019	0.179	0.126	5.08						997
11	27.9	0.508	1.150	0.296	-0.548	2.71	-0.005	0.222	-0.052	3.33						499
12	31.0	0.558	0.900	0.308	-0.286	2.56	-0.002	0.244	-0.131	3.48						499
13	34.0	0.608	0.694	0.333	-0.250	3.10	-0.005	0.247	0.094	3.19						499
14	37.1	0.658	0.472	0.327	-0.301	2.96	-0.041	0.218	0.170	3.29						249
15	43.2	0.708	0.097	0.300	0.206	2.59	-0.011	0.196	-0.018	2.69						249
16	49.3	0.808	-0.150	0.246	0.721	4.41	-0.020	0.151	-0.181	3.57						249
17	0.5	0.008	0.768	0.163	0.882	3.95	-0.025	0.150	-0.244	4.90						497
18	-2.5	-0.041	0.790	0.130	1.157	6.07	0.010	0.120	-0.179	6.61						498
19	-5.6	-0.091	0.842	0.159	0.700	4.52	0.004	0.134	-0.016	4.81						497
20	-8.6	-0.141	0.939	0.179	0.224	3.91	0.021	0.146	-0.094	3.79						498
21	-11.7	-0.191	1.140	0.214	0.173	2.44	0.027	0.153	-0.193	3.00						497
22	-14.7	-0.241	1.294	0.205	-0.386	2.67	0.031	0.148	-0.176	3.83						993
24	-20.8	-0.341	1.465	0.177	-1.299	5.46	0.022	0.132	0.270	5.13						999
25	-23.9	-0.391	1.396	0.229	-1.092	4.06	0.028	0.177	0.165	4.69						998
26	-26.9	-0.441	1.253	0.271	-0.811	3.31	0.012	0.220	-0.064	3.78						997
27	-30.0	-0.491	0.982	0.335	-0.507	3.22	0.005	0.252	0.257	3.09						499
28	-33.0	-0.541	0.754	0.341	-0.102	2.92	0.024	0.263	-0.068	2.75						499
29	-36.1	-0.591	0.520	0.359	-0.310	3.26	-0.003	0.242	-0.072	3.21						496
30	-39.1	-0.641	0.355	0.388	-0.158	2.68	0.053	0.255	-0.283	2.69						249
31	-45.2	-0.741	0.001	0.292	0.309	2.70	0.031	0.205	-0.102	3.59						249
32	-51.3	-0.841	-0.231	0.221	0.646	3.91	0.041	0.148	0.147	3.15						249
33	0.5	0.008	0.753	0.132	0.543	3.62	0.001	0.141	-0.107	6.25						491

TABLE IV-19

AXIAL AND AZIMUTHAL VELOCITY DATA AND CORRELATIONS

Test Date: 6/19/81 Run No.: 19 Flow Condition: 1 Geometry: 1

Axial Location: 152 mm (6.0 in.); x/R_o = 2.50

P_t No.	r mm +(θ=270) −(θ=90)	r/R_o	U m/s	u' m/s	S_u	K_u	W m/s	w' m/s	S_w	K_w	$\overline{uw}$ m^2/s^2	R_{uw}	σ_{uw} m^2/s^2	S_{uw}	K_{uw}	N
1	1.8	.029	.898	.188	.230	2.82	.002	.164	.343	4.78						499
2	4.8	.079	.939	.216	.098	2.80	.016	.168	.042	4.19						499
3	7.9	.129	.983	.199	.135	2.49	.014	.155	.243	.412						497
4	10.9	.179	1.043	.213	-.104	2.48	.010	.150	.163	4.09						499
5	14.0	.229	1.149	.212	-.260	2.92	-.009	.142	.068	3.63						498
6	17.0	.279	1.205	.219	-.691	3.89	.003	.152	-.116	5.06						998
7	20.1	.329	1.326	.218	-.738	3.22	.005	.158	.156	5.25						998
8	23.1	.379	1.286	.261	-1.127	5.02	.005	.183	.036	6.21						999
9	26.2	.429	1.203	.279	-.862	3.79	.007	.210	-.109	4.90						999
10	29.2	.479	1.068	.304	-.616	3.37	.015	.231	.045	4.40						999
11	32.3	.529	.899	.355	-.649	3.24	.010	.276	-.152	4.03						499
12	35.3	.579	.777	.373	-.522	3.27	.023	.270	-.113	4.36						498
13	38.4	.629	.564	.413	-.289	2.74	.006	.279	-.067	3.68						499
14	41.4	.679	.357	.384	-.074	2.10	-.009	.281	.032	3.09						249
15	47.5	.779	.045	.328	.437	2.73	-.014	.228	.356	3.76						248
16	53.6	.878	-.181	.277	.475	3.19	.028	.196	.385	3.32						248
17	1.8	.029	.969	.188	.351	2.81	.034	.167	.315	3.86						499
18	-1.3	-.021	.959	.171	.367	3.09	-.001	.165	.018	3.75						499
19	-4.3	-.071	.996	.192	.315	3.02	.019	.156	.447	4.96						499
20	-7.4	-.121	1.062	.199	.254	2.67	.032	.153	.048	3.97						498
21	-10.4	-.171	1.143	.200	-.205	2.52	.024	.159	-.185	5.06						499
23	-16.5	-.271	1.213	.220	-.341	2.84	.039	.161	-.046	4.03						998
24	-19.6	-.321	1.263	.223	-.775	3.78	.035	.163	-.183	4.26						999
25	-22.6	-.371	1.284	.238	-1.099	5.40	.034	.179	.259	4.31						998
26	-25.7	-.420	1.198	.269	-.786	3.66	-.010	.215	-.079	3.83						999
27	-28.7	-.470	1.112	.309	-.787	3.81	.020	.234	-.040	3.26						499
28	-31.8	-.520	.976	.337	-.889	4.08	.010	.249	-.103	3.48						499
29	-34.8	-.570	.868	.350	-.645	3.46	-.004	.260	-.057	3.81						498
30	-37.8	-.620	.680	.354	-.354	2.91	.048	.279	-.015	3.14						249
31	-43.9	-.720	.278	.411	.141	2.65	.030	.260	.326	3.68						249
32	-50.0	-.820	.040	.361	.553	3.09	.026	.236	.097	3.02						249

TABLE IV-20

AXIAL VELOCITY, RADIAL VELOCITY, AND MOMENTUM TURBULENT TRANSPORT DATA AND CORRELATIONS

Test Date: 6/23/81 Run No.: 20 Flow Condition: 1 Geometry: 1

Axial Location: 152 mm (6.0 in.); x/R_o = 2.50

Pt No.	r mm +(θ=0) −(θ=180)	r/R_o	U m/s	u' m/s	S_u	K_u	V m/s	v' m/s	S_v	K_v	$\overline{uv}$ m^2/s^2	R_{uv}	σ_{uv} m^2/s^2	S_{uv}	K_{uv}	N
1	0.8	.012	0.936	0.193	0.313	3.03	−0.011	0.185	0.068	3.02	−0.0030	−0.086	0.034	−0.61	8.34	499
2	3.8	.062	0.979	0.214	0.185	2.63	−0.045	0.167	−0.327	4.10	−0.0124	−0.348	0.034	−1.33	8.10	498
3	6.9	.112	1.033	0.207	0.046	2.72	−0.050	0.167	−0.405	3.65	−0.0122	−0.353	0.033	−1.14	9.13	499
4	9.9	.162	1.101	0.226	−0.050	2.76	−0.046	0.183	−0.133	3.79	−0.0119	−0.287	0.040	0.20	9.34	499
5	13.0	.212	1.197	0.224	−0.272	2.38	−0.046	0.177	−0.473	3.44	−0.0088	−0.221	0.040	0.05	8.25	499
6	16.0	.262	1.247	0.222	−0.624	3.44	−0.008	0.187	−0.497	4.10	0.0003	0.008	0.054	2.62	23.89	999
7	19.1	.312	1.284	0.229	−0.773	3.55	0.007	0.193	−0.535	3.73	0.0066	0.150	0.053	2.66	19.65	999
8	22.1	.362	1.244	0.258	−1.028	4.99	0.048	0.213	−0.602	4.04	0.0141	0.257	0.074	3.64	24.44	999
9	25.1	.412	1.156	0.294	−0.897	4.01	0.065	0.230	−0.479	3.41	0.0219	0.324	0.089	4.25	37.68	999
10	28.2	.462	1.052	0.322	−0.885	3.95	0.088	0.241	−0.360	3.07	0.0314	0.405	0.093	2.31	16.17	998
11	31.2	.512	0.898	0.361	−0.691	3.64	0.106	0.268	−0.303	3.31	0.0414	0.428	0.103	2.09	10.28	999
12	34.3	.562	0.725	0.398	−0.432	2.70	0.105	0.290	0.001	2.63	0.0568	0.492	0.107	0.95	4.71	499
13	37.3	.612	0.547	0.381	−0.507	3.32	0.045	0.297	0.133	2.54	0.0412	0.364	0.102	0.50	4.36	249
14	43.4	.712	0.193	0.398	0.054	2.24	0.010	0.265	0.079	4.13	0.0276	0.261	0.098	0.90	7.12	248
15	49.5	.812	−0.119	0.298	0.624	3.34	0.007	0.228	0.289	3.09	0.0269	0.396	0.074	1.45	14.13	247
16	52.6	.862	−0.177	0.245	0.384	3.37	−0.019	0.188	0.173	5.39	0.0090	0.196	0.043	1.30	10.56	241
17	0.8	.012	0.920	0.194	0.257	2.84	−0.002	0.163	−0.312	4.59	0.0017	0.055	0.034	1.37	14.87	499
18	−2.3	−.037	0.916	0.200	0.268	2.78	−0.017	0.178	−0.079	3.88	−0.0039	−0.109	0.037	0.30	15.16	497
19	−5.3	−.087	0.993	0.208	0.106	2.50	−0.038	0.165	0.100	3.62	−0.0078	−0.229	0.034	0.01	8.43	498
20	−8.4	−.137	1.066	0.235	−0.163	2.77	−0.040	0.178	−0.276	3.83	−0.0115	−0.274	0.042	0.70	17.49	498
21	−11.4	−.187	1.171	0.217	−0.250	2.54	−0.040	0.175	−0.215	3.18	−0.0069	−0.181	0.036	−0.50	5.63	499
22	−14.5	−.237	1.234	0.225	−0.530	2.96	−0.016	0.182	−0.282	3.91	−0.0005	−0.012	0.051	4.07	60.43	999
23	−17.5	−.287	1.288	0.212	−0.486	3.04	0.010	0.178	−0.182	4.00	0.0005	0.014	0.042	3.08	46.51	998
24	−20.6	−.337	1.261	0.264	−0.809	3.63	0.023	0.201	−0.341	3.96	0.0125	0.235	0.064	2.20	17.49	999
25	−23.6	−.387	1.220	0.278	−0.900	3.88	0.057	0.222	−0.354	3.98	0.0210	0.341	0.072	3.37	26.78	999
26	−26.7	−.437	1.085	0.305	−0.604	3.35	0.066	0.232	−0.080	3.24	0.0268	0.379	0.074	1.40	16.12	998
27	−29.7	−.487	0.970	0.321	−0.369	2.87	0.095	0.236	−0.216	3.39	0.0324	0.427	0.088	3.57	28.52	998
28	−32.8	−.537	0.767	0.354	−0.375	3.57	0.076	0.267	−0.054	3.40	0.0377	0.399	0.106	1.45	9.44	499
29	−35.8	−.587	0.549	0.412	−0.424	2.84	0.030	0.317	−0.558	4.54	0.0595	0.456	0.132	1.33	7.64	248
30	−41.9	−.687	0.265	0.412	0.181	2.97	0.063	0.274	−0.321	2.70	0.0547	0.484	0.120	2.10	10.77	249
31	−48.0	−.787	−0.038	0.364	0.567	3.54	−0.023	0.261	−0.906	6.33	0.0247	0.260	0.082	1.48	8.90	246
32	−51.1	−.837	−0.174	0.250	0.750	3.55	0.007	0.200	0.519	4.08	0.0140	0.280	0.054	2.79	17.57	239

TABLE IV-21

AXIAL VELOCITY, RADIAL VELOCITY, AND MOMENTUM TURBULENT TRANSPORT DATA AND CORRELATIONS

Test Date: 6/24/81 Run No.: 21 Flow Condition: 1 Geometry: 1

Axial Location: 203 mm (8.0 in.); x/R_o = 3.33

Pt No.	r mm +(θ=0) −(θ=180)	r/R_o	U m/s	u' m/s	S_u	K_u	V m/s	v' m/s	S_v	K_v	$\overline{uv}$ m^2/s^2	R_{uv}	σ_{uv} m^2/s^2	S_{uv}	K_{uv}	N
1	0.8	.013	.968	.205	-.087	2.73	-.003	.175	-.058	3.93	-.0013	-.038	.039	0.57	12.94	498
2	3.8	.063	.976	.201	-.211	2.83	.000	.194	-.077	3.75	-.0061	-.156	.045	-.073	14.87	499
3	6.9	.113	.991	.209	-.314	3.37	.009	.179	-.298	3.96	-.0030	-.001	.039	0.60	15.75	499
4	9.9	.163	1.030	.213	-.127	2.46	.011	.179	-.387	3.38	-.0035	-.092	.039	0.24	7.97	499
5	13.0	.213	1.021	.238	-.259	3.05	.007	.201	-.574	4.75	.0015	.031	.058	1.90	13.93	499
6	16.0	.263	1.035	.245	-.452	3.66	.026	.206	-.748	4.08	.0052	.102	.062	2.04	19.17	999
7	19.1	.313	1.051	.253	-.541	4.11	.031	.200	-.610	4.28	.0056	.110	.060	3.87	43.95	999
8	22.1	.363	1.013	.276	-.621	3.32	.067	.203	-.372	3.64	.0105	.188	.065	2.05	15.28	999
9	25.2	.413	.976	.300	-.799	4.26	.083	.231	-.312	3.55	.0185	.267	.047	2.86	23.70	999
10	28.2	.463	.891	.315	-.732	3.87	.082	.237	-.302	3.54	.0206	.276	.084	1.99	14.35	999
11	31.3	.513	.797	.332	-.585	3.45	.120	.260	-.300	3.26	.0269	.311	.099	1.94	14.58	999
12	34.3	.563	.684	.351	-.329	2.96	.115	.269	-.192	2.85	.0324	.345	.106	2.23	13.28	499
13	37.4	.613	.575	.336	—	—	.136	.258	—	—	—	—	—	—	—	—
14	43.5	.713	.308	.363	—	—	.107	.266	—	—	—	—	—	—	—	—
15	49.6	.813	.031	.288	—	—	.054	.259	—	—	—	—	—	—	—	—
16	52.6	.863	-.054	.261	—	—	.039	.226	—	—	—	—	—	—	—	—
17	0.8	.013	1.007	.208	—	—	-.023	.183	—	—	—	—	—	—	—	—
18	-2.3	-.038	1.004	.203	-.008	2.55	-.003	.177	.089	3.21	-.0021	-.059	.034	-0.23	8.02	499
19	-5.4	-.088	1.018	.205	.081	2.95	-.002	.184	.072	3.43	-.0031	-.082	.036	0.09	7.35	498
20	-8.4	-.138	1.013	.214	-.270	3.42	.001	.194	-.335	3.58	-.0010	-.025	.049	0.04	16.55	496
21	-11.5	-.188	1.045	.222	-.514	3.46	-.002	.189	-.236	3.57	.0009	.022	.052	-1.50	20.09	499
22	-14.5	-.238	1.077	.230	-.336	3.52	.002	.197	-.543	4.00	.0070	.155	.055	3.53	29.32	999
23	-17.6	-.288	1.061	.244	-.572	4.15	.029	.199	-.419	3.55	.0086	.177	.054	2.34	15.68	999
25	-23.7	-.388	.966	.291	-.538	3.30	.061	.235	-.213	3.12	.0218	.319	.079	2.26	13.57	999
26	-26.7	-.438	.897	.313	-.624	3.57	.050	.249	-.394	3.12	.0301	.387	.094	2.95	23.88	999
27	-29.7	-.488	.841	.319	-.413	3.22	.096	.258	-.596	3.64	.0302	.367	.089	1.47	11.03	999
28	-32.8	-.538	.734	.356	-.523	3.26	.070	.296	-.475	3.02	.0391	.371	.103	1.06	6.96	498
29	-35.8	-.588	.603	.385	-.364	2.91	.078	.272	-.137	2.46	.0488	.466	.104	1.20	5.33	249
30	-41.9	-.688	.383	.413	-.225	2.36	.093	.304	.137	2.55	.0640	.510	.116	1.01	4.26	249
31	-48.0	-.788	.107	.367	.384	2.41	.022	.312	-.768	5.13	.0488	.426	.111	1.59	7.60	241
32	-51.1	-.838	.032	.293	—	—	.184	.446	—	—	—	—	—	—	—	—
33	0.8	.013	.979	.213	-.052	2.70	.001	.179	-.081	3.18	-.0019	-.049	.037	-0.32	6.46	498

TABLE IV-22

AXIAL AND AZIMUTHAL VELOCITY DATA AND CORRELATIONS

Test Date: 6/25/81 Run No.: 22 Flow Condition: 1 Geometry: 1

Axial Location: 203 mm (8.0 in.); x/R_o = 3.33

Pt. No.	r mm +(θ=270) −(θ=90)	r/R_o	U m/s	u' m/s	S_u	K_u	W m/s	w' m/s	S_w	K_w	$\overline{uw}$ m^2/s^2	R_{uw}	τ_{uw} m^2/s^2	S_{uw}	K_{uw}	N
1	2.5	0.042	.975	.206	.000	2.609	.0096	.169	.021	3.205						498
2	5.6	0.092	1.009	.219	.013	2.675	.0069	.175	.013	2.902						495
3	8.6	0.142	1.025	.209	−.245	2.610	.0049	.172	.087	3.610						496
4	11.7	0.192	1.042	.230	−.194	2.760	.0091	.169	.239	3.346						493
5	14.7	0.241	1.078	.217	−.297	2.694	.0016	.174	−.029	3.224						496
6	17.8	0.291	1.085	.229	−.295	2.731	.0004	.193	.144	3.409						985
7	20.8	0.341	1.056	.254	−.462	3.040	−.0067	.188	.022	3.037						986
8	23.9	0.391	1.035	.273	−.442	3.063	.0012	.216	−.148	3.519						994
9	26.9	0.441	.982	.279	−.446	2.836	−.0198	.244	.209	3.282						991
10	30.0	0.491	.900	.288	−.234	2.803	.0085	.251	−.075	2.925						982
11	33.0	0.541	.779	.318	−.328	2.600	−.0159	.252	.099	2.818						490
12	36.1	0.591	.659	.337	−.175	2.736	−.0220	.289	−.260	3.223						492
13	39.1	0.641	.540	.374	−.257	2.649	−.0049	.271	−.276	2.997						495
14	42.2	0.691	.389	.369	.011	2.367	.0079	.298	−.136	3.032						244
15	48.3	0.791	.152	.374	.268	2.441	.0159	.236	.060	2.713						241
16	54.4	0.891	−.065	.280	.328	2.420	−.0020	.245	−.081	3.437						248
17	2.5	0.042	.977	.197	−.140	2.720	−.0134	.188	−.324	4.268						495
18	−0.5	−0.008	.963	.163	.095	2.629	.0038	.160	−.102	3.109						493
19	−3.6	−0.058	.990	.201	−.131	2.721	.0034	.175	−.310	3.603						492
20	−6.6	−0.108	.970	.212	−.084	2.617	.0340	.182	−.112	3.513						493
21	−9.7	−0.158	1.007	.219	−.145	3.054	.0287	.172	−.131	3.523						495
22	−12.7	−0.208	1.015	.218	−.286	3.375	.0401	.181	.402	4.143						994
23	−15.7	−0.258	1.060	.220	−.183	2.792	.0315	.179	−.043	3.806						991
24	−18.8	−0.308	1.050	.238	−.506	3.797	.0274	.188	−.032	3.419						990
25	−21.8	−0.358	1.039	.251	−.521	3.354	.0161	.211	−.107	3.585						992
26	−24.9	−0.408	1.012	.280	−.669	3.691	.0236	.225	.067	3.493						996
27	−29.9	−0.458	.977	.280	−.572	3.038	.0297	.235	.044	3.308						496
28	−31.0	−0.508	.875	.301	−.527	3.174	.0265	.257	.050	3.053						498
29	−34.0	−0.558	.706	.372	−.497	3.004	.0041	.266	.047	3.284						499
30	−37.1	−0.608	.694	.37[illegible]	−.444	3.254	.0391	.283	.045	2.825						247
31	−43.2	−0.708	.498	.340	−.190	2.657	−.0089	.295	−.115	2.891						249
32	−49.3	−0.808	.213	.378	−.066	2.319	.0177	.257	.073	2.588						249

TABLE IV-23

AXIAL VELOCITY, AZIMUTHAL VELOCITY, AND MOMENTUM TURBULENT TRANSPORT DATA AND CORRELATIONS

Test Date: 6/26/81 Run No.: 23 Flow Condition: 1 Geometry: 1

Axial Location: 102 mm (4.0 in.); x/R_o = 1.66

Pt No.	r mm +(θ=270) -(θ=90)	r/R_o	U m/s	u' m/s	S_u	K_u	W m/s	w' m/s	S_w	K_w	$\overline{uw}$ m^2/s^2	R_{uw}	σ_{uw} m^2/s^2	S_{uw}	K_{uw}	N
1	0.00	0.00	.777	.138	1.035	5.07	.011	.135	.230	7.48	.0045	-0.024	.0301	3.145	27.89	496
2	6.10	0.10	.879	.170	.552	3.15	.002	.157	-.406	4.53	.0011	-0.040	.0295	.775	11.93	498
3	12.19	0.20	1.171	.206	-.153	2.63	.010	.159	.112	2.94	.0005	-0.015	.0313	.943	10.60	499
4	18.29	0.30	1.458	.170	-1.344	6.22	-.001	.116	-.036	4.64	.0004	-0.022	.0218	-.883	13.93	999
5	21.34	0.35	1.485	.183	-1.714	7.28	.018	.137	.466	6.59	-.0011	.043	.0405	-1.446	37.67	999
6	30.48	0.50	.880	.340	-.475	3.65	.009	.258	.184	4.05	-.0018	.021	.0866	-.893	12.65	499
7	36.58	0.60	.480	.336	-.243	3.13	.042	.278	-.202	4.01	.0068	-.072	.0947	.168	7.86	499

TABLE IV-24

AXIAL VELOCITY, AZIMUTHAL VELOCITY, AND MOMENTUM TURBULENT TRANSPORT DATA AND CORRELATIONS

Test Date: 6/26/81 Run No.: 24 Flow Condition: 1 Geometry: 1

Axial Location: 152 mm (6.0 in.); $x/R_o = 2.50$

Pt No.	r mm +(θ=270) −(θ=90)	r/R_o	U m/s	u' m/s	S_u	K_u	W m/s	w' m/s	S_w	K_w	$\overline{uw}$ m^2/s^2	R_{uw}	σ_{uw} m^2/s^2	S_{uw}	K_{uw}	N
1	0.0	.00	.946	.208	.187	2.76	.006	.197	−.716	6.25	.0055	−.134	.041	0.62	10.17	499
2	6.1	.10	1.042	.214	.059	2.62	.018	.177	.403	4.26	.0034	−.089	.040	−0.76	12.26	499
3	12.2	.20	1.193	.226	−.145	2.63	.002	.181	.202	3.62	.0004	−.011	.039	0.24	9.20	499
4	18.3	.30	1.293	.238	−.887	4.96	.016	.189	.350	4.21	−.0014	.030	.053	−2.32	41.54	998
5	24.4	.40	1.272	.239	−.840	4.10	.006	.201	−.054	5.55	−.0020	.041	.061	−1.89	34.91	998
6	30.5	.50	.931	.331	−.463	3.21	.010	.282	−.024	3.81	.0034	−.036	.099	0.56	19.23	499
7	36.6	.60	.574	.377	−.298	3.09	.031	.280	.263	2.75	.0036	−.034	.107	0.30	5.79	498

TABLE IV-44

AXIAL VELOCITY, RADIAL VELOCITY, AND MOMENTUM TURBULENT TRANSPORT DATA AND CORRELATIONS

Test Date: 7/29/81 Run No.: 44 Flow Condition: 1 Geometry: 1

Axial Location: 13 mm (0.5 in.); $x/R_o = 0.21$

Pt No.	r mm +(θ=0) -(θ=180)	r/R_o	U m/s	u' m/s	S_u	K_u	V m/s	v' m/s	S_v	K_v	$\overline{uv}$ m^2/s^2	R_{uv}	σ_{uv} m^2/s^2	S_{uv}	K_{uv}	N
1	0.0	.000	.790	.064	-.144	3.17	.005	.049	.147	3.40	-.0002	-.050	.003	-.046	10.82	487
2	3.0	.050	.792	.062	-.167	2.99	.011	.048	-.010	4.33	.0002	.054	.003	1.84	13.07	475
3	6.1	.100	.744	.075	-.586	4.66	.012	.051	.144	4.23	.0008	.218	.004	3.56	46.70	467
4	9.1	.150	.647	.091	-.094	2.80	.013	.060	-.318	4.87	.0014	.260	.006	1.77	14.26	487
5	12.2	.200	.526	.137	.640	3.49	-.063	.148	-.626	3.98	-.0069	-.342	.025	-2.94	24.80	497
6	15.2	.250	1.230	.216	-.255	2.72	-.066	.163	1.106	6.48	-.0149	-.423	.039	-1.53	13.26	992
7	18.3	.300	1.582	.065	-.364	-1.56	-.040	.057	.420	3.87	-.0005	-.130	.004	-2.42	26.47	992
8	21.3	.350	1.588	.054	-.072	-5.29	-.045	.051	.254	4.12	.0000	.010	.003	-0.16	17.38	994
9	24.4	.400	1.542	.083	-.656	2.78	-.029	.064	.703	15.87	.0010	.184	.006	0.36	33.74	995
10	27.4	.450	1.340	.129			-.010	.085								
11	30.5	.500	.694	.235			.028	.172								
12	33.5	.550	-.005	.144			-.032	.104								
13	36.6	.600	-.063	.113	-.127	3.38	-.040	.071	.403	4.74	.0020	.244	.009	1.45	11.67	241
14	42.7	.699	-.079	.120	-.385	3.30	-.035	.069	.156	3.19	.0013	.161	.009	1.32	10.77	241
15	48.8	.799	-.055	.107	-.633	3.99	-.033	.080	-.118	3.70	.0013	.157	.009	2.34	16.77	239
16	0.0	.000	.780	.059	-.494	3.40	.010	.046	.013	3.92	-.0004	-.148	.003	-1.58	11.15	494
17	-3.0	-.050	.749	.065	-.312	3.11	-.005	.047	-.394	4.98	-.0006	.189	.003	1.65	15.73	495
18	0.0	.000	.802	.061	-.223	2.82	-.008	.040	.111	3.20	-.0001	.030	.003	-0.19	14.17	493
19	-6.1	-.100	.722	.084	-1.292	11.52	.001	.045	-.375	4.26	-.0006	.155	.004	-2.44	28.29	495
20	-9.1	-.150	.646	.096	-.311	2.71	-.001	.050	-.281	3.68	-.0016	.340	.005	1.94	12.15	494
21	-12.2	-.200	.509	.115	.396	3.32	-.038	.107	-.706	3.65	.0004	-.029	.015	-1.69	18.15	498
22	-15.2	-.250	1.060	.207	-.086	2.76	-.085	.160	.414	3.26	.0154	-.465	.035	-1.25	11.31	999
23	-18.3	-.300	1.563	.081	-1.175	3.28	-.068	.052	.264	4.35	.0009	-.212	.006	-0.57	49.40	998
24	-21.3	-.350	1.603	.048	-.926	-5.48	-.060	.038	.521	4.63	.0004	-.206	.003	-4.98	41.97	999
25	-24.4	-.400	1.611	.044	-.034	-15.66	-.058	.038	-.017	4.75	.0000	.000	.002	-2.45	41.96	999
26	-27.4	-.450	1.505	.111	-.794	3.65	-.046	.068	-.459	3.90	-.0020	.269	.009	-3.23	27.27	999
27	-30.5	-.500	.774	.253	-.097	2.83	.026	.179	-.172	2.96	-.0211	.465	.049	1.91	10.63	997
28	-33.5	-.550	-.009	.134	.834	4.63	-.044	.097	.906	6.53	-.0057	.440	.020	5.14	39.03	498
29	-36.6	-.600	-.065	.109	-.187	3.34	-.048	.060	-.358	5.94	-.0017	.266	.007	2.23	11.39	239
30	-42.7	-.699	-.040	.112	-.534	4.10	-.033	.073	.033	3.38	-.0007	.085	.010	-1.75	21.11	246
31	-48.8	-.799	-.036	.100	-1.144	4.93	-.021	.074	.661	8.34	.0002	-.022	.006	-0.16	5.89	244
32	0.0	.000	.805	.053	-.518	2.68	.008	.037	.165	3.37	-.0001	-.062	.002	-0.17	10.46	498

TABLE IV-45

RADIAL VELOCITY, CONCENTRATION AND MASS TRANSPORT DATA AND CORRELATIONS

Test Date: 7/31/81 Run No.: 45 Flow Condition: 1 Geometry: 1

Axial Location: 13 mm (0.5 in.); $x/R_o = 0.21$

Pt No.	r mm +(θ=0) −(θ=180)	r/R_o	V m/s	v' m/s	S_v	K_v	$\overline{f}$	f'	S_f	K_f	$\overline{vf}$ m/s	R_{vf}	σ_{vf} m/s	S_{vf}	K_{vf}	N
2	.00	.000	.006	.032	.280	3.82	1.051	.065	.019	3.06	−.0001	.045	.002	−.583	7.76	500
3	1.52	.025	.010	.034	−.099	3.45	1.018	.062	.106	3.22	.0001	.029	.002	.287	9.07	500
4	3.05	.050	.011	.035	−.170	3.38	.998	.066	−.038	3.02	.0000	.014	.002	−.089	7.64	500
5	4.57	.075	.014	.038	−.240	3.11	.949	.061	.108	2.88	.0000	−.021	.002	−.198	6.89	500
6	6.10	.100	.018	.035	−.236	3.49	1.084	.067	.224	3.36	.0000	.048	.002	.627	10.17	500
8	9.14	.150	.017	.042	−.253	3.06	1.007	.062	.029		.0000	.006	.003	.128	6.75	500
9	10.67	.175	.019	.053	−.425	4.53	.989	.067	−.046	3.25	.0001	.022	.004	1.286	18.35	500
10	12.19	.200	.016	.087	−1.233	7.61	.850	.094	−.845	4.07	.0018	.228	.010	3.902	50.71	1000
11	15.24	.250	−.049	.149	−.080	3.91	.198	.114	.700	3.87	.0045	.267	.016	1.315	8.36	1000
12	18.29	.300	−.046	.049	.237	4.01	.009	.014	.366	3.17	.0000	−.049	.001	−.354	7.64	1000
13	21.34	.350	−.031	.042	−.638	3.46	.015	.014	.370	3.09	.0000	−.015	.001	−1.044	14.90	1000
14	24.38	.400	−.017	.036	−1.803	7.15	.015	.014	.274	3.14	.0000	−.021	.001	.616	22.11	1000
15	27.43	.450	−.011	.067	−.584	4.26	.006	.013	.265	3.05	.0000	.013	.001	−.440	13.22	1000
16	30.48	.500	.029	.140	−.014	5.01	.021	.016	.506	3.70	−.0001	−.051	.002	−.176	11.48	1000
17	33.53	.550	−.009	.043	−.153	13.25	.035	.017	.212	2.72	−.0000	−.060	.001	−.392	26.66	500
18	36.58	.600	.001	.005	−2.992	29.47	.035	.016	.298	2.95	.0000	.070	.000	1.268	12.82	500
25	−4.57	−.075	−.001	.039	.252	2.93	1.025	.065	−.055	3.78	.0001	.033	.002	−.198	5.70	500
29	−10.67	−.175	.006	.060	.902	7.07	.981	.066	−.112	2.92	.0000	.012	.004	−.396	19.98	500
32	−12.19	−.200	−.003	.106	1.188	6.45	.970	.149	−1.046	3.77	.0031	.200	.019	−3.640	28.05	999
33	−15.24	−.250	−.074	.144	−.654	4.67	.172	.119	.796	3.35	.0043	.251	.018	−2.051	18.31	1000
34	−18.29	−.300	−.050	.049	−.578	5.21	.006	.015	.225	2.93	.0000	.022	.001	.294	8.94	1000

TABLE IV-47

RADIAL VELOCITY, CONCENTRATION AND MASS TRANSPORT DATA AND CORRELATIONS

Test Date: 8/3/81 Run No.: 47 Flow Condition: 1 Geometry: 1

Axial Location: 51 mm (2.0 in.); x/R_o = 0.83

Pt No.	r mm +(θ=0) -(θ=180)	r/R_o	V m/s	v' m/s	S_v	K_v	$\overline{f}$	f'	S_f	K_f	$\overline{vf}$ m/s	R_{vf}	σ_{vf} m/s	S_{vf}	K_{vf}	N
3	0.0	.000	.007	.032	.248	3.85	0.992	.059			-.0001	-.037				500
4	0.0	.000	.009	.031	.286	3.52	1.008	.064			-.0001	-.038				500
5	0.0	.000	.005	.034	-.004	3.73	1.000	.059			.0000	.015				499
6	3.0	.050	.006	.034	-.090	3.71	1.008	.063			.0000	.003				500
7	6.1	.100	.006	.042	-.482	4.17	1.016	.085			.0004	.115				500
8	9.1	.150	.005	.060	-.278	5.61	0.807	.205			.0011	.088				500
9	10.7	.175	-.003	.084	-1.287	7.82	0.627	.224			.0037	.196				500
10	12.2	.200	-.006	.092	-.203	5.91	0.418	.190			.0046	.265				1000
11	15.2	.250	-.015	.080	-.029	5.36	0.150	.129			.0024	.231				1000
12	18.3	.300	-.012	.053	-.089	5.57	0.011	.050			.0002	.075				1000
14	18.3	.300	-.015	.052	-.064	5.21	0.009	.039			.0003	.012				1000
15	21.3	.350	-.007	.048	-.538	6.66	0.000	.015			-.0001	-.083				999
16	24.4	.400	.007	.055	.334	7.78	0.001	.016			-.0001	-.067				998
17	27.4	.450	.022	.095	-.376	6.09	0.006	.016			-.0002	-.123				999
18	30.5	.500	.011	.108	.894	10.58	0.011	.016			-.0001	-.034				1000
19	33.5	.550	.005	.086	.986	13.28	0.021	.018			-.0001	-.062				500
20	36.6	.600	-.003	.045	.185	5.91	0.025	.017			.0001	.059				500
21	42.7	.699	-.008	.034	-1.490	10.96	0.025	.016			.0000					500
22	48.8	.799	.000	.010	-1.930	20.03	0.021	.018			.0000					500
26	0.0	.000	.008	.034	.175	3.74	1.000	.060			.0000					500
27	0.0	.000	.008	.034	.225	3.74	1.000	.069			.0000					499
28	-3.0	-.050	-.004	.035	.044	3.26	1.017	.060			.0001	.024				500
29	-6.1	-.100	-.003	.046	.115	5.33	1.015	.080			.0004	.109				500
30	-9.1	-.150	-.006	.065	.468	5.57	0.845	.182			.0017	.141				499
31	-10.7	-.175	-.008	.075	.904	6.06	0.667	.217			.0028	.236				500
32	-12.2	-.200	-.028	.099	1.200	5.81	0.451	.193			.0043	.229				1000
33	-15.2	-.250	-.034	.094	-.036	5.04	0.174	.124			.0032	.276				1000
34	-18.3	-.300	-.029	.058	-.216	5.85	0.026	.056			.0004	.014				1000
35	-21.3	-.350	-.020	.059	.943	8.18	-0.002	.018			.0000					500
36	-24.4	-.400	-.006	.074	.081	7.96	-0.002	.014			.0000					500
37	-27.4	-.450	.010	.116	.717	6.45	0.001	.015			-.0003	-.158				500
38	-30.5	-.500	.003	.126	-.685	8.39	0.004	.015			-.0002	-.103				500
39	-33.5	-.550	.002	.095	-.918	8.03	0.014	.018			.0000	.000				499
41	-42.7	-.699	-.023	.052	.573	3.92	0.019	.018			.0000					500

TABLE IV-50

RADIAL VELOCITY, CONCENTRATION AND MASS TRANSPORT DATA AND CORRELATIONS

Test Date: 8/6/81 Run No.: 50 Flow Condition: 1 Geometry: 1

Axial Location: 203 mm (8.0 in.); x/R_o = 3.33

Pt No.	r mm +(θ=0) −(θ=180)	r/R_o	V m/s	v' m/s	S_v	K_v	$\bar{f}$	f'	S_f	K_f	$\overline{vf}$ m/s	R_{vf}	σ_{vf} m/s	S_{vf}	K_{vf}	N
9	0.0	.000	-.008	.169	-.121	3.78	.287	.160	.708	3.71	.0008	.030	.027	0.09	10.33	1000
10	3.0	.050	.004	.169	-.150	3.67	.280	.174	—	—	.0028	.095	—	—	—	1000
11	6.1	.100	.017	.171	-.173	3.52	.272	.167	.842	3.90	.0056	.197	.028	0.80	8.45	1000
12	9.1	.150	.005	.169	-.601	5.11	.233	.160	.953	4.34	.0076	.280	.026	1.87	12.49	1000
14	12.2	.200	.010	.191	-.303	4.09	.192	.151	1.090	4.41	.0082	.285	.026	1.39	9.20	999
15	15.2	.250	.039	.187	-.178	4.11	.150	.137	1.157	4.44	.0063	.246	.023	0.87	6.41	1000
16	18.3	.300	.043	.198	-.483	3.82	—	—	—	—	—	—	—	—	—	1000
17	21.3	.350	.062	.214	-.416	3.61	.086	.113	1.998	8.60	.0064	.267	.023	3.58	33.49	1000
18	24.4	.400	.077	.229	-.425	3.88	.058	.093	2.396	12.00	.0058	.275	.027	10.97	222.20	1000
19	27.4	.450	.088	.226	-.279	3.63	.038	.075	2.924	15.39	.0038	.228	.018	5.95	67.58	1000
20	30.5	.500	.114	.233	-.135	3.50	.025	.059	2.223	9.18	.0029	.211	.014	4.16	34.71	1000
21	33.5	.550	.095	.260	-.281	3.44	.021	.053	3.092	17.96	.0029	.210	.014	4.59	35.47	998
22	36.6	.600	.164	.252	.166	3.56	.026	.050	2.868	17.05	.0015	.116	.013	3.37	34.84	1000
23	42.7	.699	.051	.173	1.122	5.67	.019	.031	1.781	12.53	.0001	.016	.006	4.17	44.81	999
24	0.0	.000	-.005	.169	-.202	4.45	.274	.157	.790	3.83	.0004	.016	.026	0.20	10.32	1000
29	0.0	.000	-.003	.170	-.141	3.54	.280	.162	.787	3.59	.0005	.017	.026	0.21	6.84	1000
30	-3.0	-.050	.003	.182	.069	3.82	.203	.118	.936	4.73	.0019	.088	.020	0.14	8.27	1000
31	-6.1	-.100	.008	.181	.014	3.43	.263	.159	.915	4.18	.0044	.153	.027	0.48	7.47	1000
32	-9.1	-.150	.011	.182	-.137	3.68	.238	.156	.934	4.20	.0060	.213	.028	0.48	8.93	1000
33	-12.2	-.200	.016	.193	-.387	3.83	.198	.142	.913	3.76	.0074	.270	.026	0.90	7.35	999
34	-15.2	-.250	.030	.185	-.521	3.90	.181	.140	1.030	4.02	.0082	.316	.025	1.69	9.25	1000
35	-18.3	-.300	.038	.206	-.433	3.62	.135	.126	1.556	6.76	.0073	.282	.024	1.75	9.68	1000
36	-21.3	-.350	.048	.232	-.416	3.32	.121	.121	1.702	6.95	.0090	.319	.028	2.76	21.30	1000
37	-24.4	-.400	.071	.224	-.274	3.06	.089	.100	1.842	8.09	.0063	.282	.021	2.79	22.06	1000
38	-27.4	-.450	.079	.245	-.378	3.29	.066	.086	2.262	9.78	.0055	.259	.020	3.01	20.09	1000
39	-30.5	-.500	.091	.242	-.040	3.20	.056	.071	2.446	11.27	.0041	.235	.020	5.26	58.40	999
40	-33.5	-.550	.097	.243	-.137	3.22	.053	.065	3.087	17.51	.0031	.195	.018	6.45	72.01	1000
41	-36.6	-.600	.117	.250	-.061	2.98	.031	.049	3.342	23.26	.0018	.143	.012	4.54	42.06	999
42	-42.7	-.699	.097	.260	.125	2.99	.035	.036	2.581	18.08	.0003	.036	.010	5.75	77.82	1000
43	48.8	-.799	.120	.288	.443	2.97	.028	.036	2.591	18.38	.0005	.050	.012	6.58	86.73	999
44	0.0	.000	.001	.173	-.117	3.80	.280	.150	.748	3.89	.0001	.005	.025	0.11	9.54	1000

TABLE IV-51

RADIAL VELOCITY, CONCENTRATION AND MASS TRANSPORT DATA AND CORRELATIONS

Test Date: 8/10/81 Run No.: 51 Flow Condition: 1 Geometry: 1

Axial Location: 152 mm (6.0 in.); $x/R_o = 2.50$

Pt No.	r mm +(θ=0) -(θ=180)	r/R_o	V m/s	v' m/s	S_v	K_v	$\overline{f}$	f'	S_f	K_f	$\overline{vf}$ m/s	R_{vf}	σ_{vf} m/s	S_{vf}	K_{vf}	N
8	1.52	.025	0.001	.147	.390	5.18	.542	.267	.260	2.13	-.0023	-.058	.044	-1.286	15.23	1000
9	4.57	.075	-0.017	.144	-.585	4.16	.508	.257	.236	2.18	.0125	.338	.039	1.245	10.40	1000
10	7.62	.125	-0.021	.158	-.241	3.71	.398	.237	.606	2.60	.0165	.439	.036	0.897	8.78	1000
11	10.67	.175	-0.040	.167	-.319	3.40	.320	.216	.790	3.23	.0178	.494	.035	1.732	8.28	1000
12	13.72	.225	-0.018	.174	-.397	3.49	.249	.209	1.196	4.44	.0167	.459	.037	2.32	13.80	1000
14	16.76	.275	-0.019	.189	-.648	4.57	.167	.173	1.430	5.31	.0133	.409	.033	2.17	10.42	1000
15	19.81	.324	0.011	.199	-.422	3.87	.086	.127	2.142	8.28	.0078	.311	.027	2.91	16.55	1000
16	22.86	.375	0.009	.218	-.558	4.34	.045	.090	3.059	14.66	.0045	.227	.020	5.15	43.80	1000
17	25.91	.425	0.035	.229	-.538	3.70	.023	.056	3.543	21.20	.0021	.162	013	5.27	50.10	999
18	28.96	.475	0.018	.255	-.148	3.06	.017	.040	4.680	36.53	.0010	.011	.096	6.62	77.26	1000
19	32.00	.525	0.064	.243	-.202	4.10	.005	.026	3.438	40.70	-.0001	-.009	.006	3.02	36.44	1000
20	35.05	.575	0.066	.251	-.022	3.43	.007	.022	1.008	6.29	-.0000	-.002	.006	1.74	15.59	999
21	38.10	.624	0.041	.244	.180	3.99	.013	.022	.602	4.07	-.0004	-.067	.006	0.82	22.97	999
22	44.20	.724	0.003	.174	.353	4.75	.010	.022	.405	3.58	-.0004	-.114	.004	-0.36	13.40	1000
27	1.52	.025	0.011	.151	-.034	4.42	.547	.276	.235	2.17	-.0044	-.107	.046	-0.088	12.56	1000
28	-1.52	-.025	-0.005	.158	.318	5.10	.573	.289	.280	2.02	.0116	.253	.050	0.882	14.03	1000
29	-4.57	-.075	-0.010	.161	.432	4.29	.504	.289	.386	2.23	.0170	.365	.045	0.964	10.04	999
30	-7.62	-.125	-0.008	.160	.332	3.98	.408	.259	.676	2.87	.0176	.426	.040	1.397	10.03	1000
31	-10.67	-.175	-0.000	.163	.288	3.74	.327	.239	.938	3.76	.0166	.426	.038	1.150	7.30	1000
32	-13.72	-.225	0.011	.186	.291	3.52	.236	.213	1.218	4.57	.0177	.441	.042	1.764	9.41	999
33	-16.76	-.275	0.030	.189	.364	4.22	.158	.184	1.601	5.75	.0130	.375	.037	2.687	14.47	1000
34	-19.81	-.325	0.039	.208	.311	3.43	.101	.146	2.130	8.30	.0088	.289	.033	3.830	29.70	999
35	-22.86	-.375	0.061	.217	.193	3.45	.046	.091	3.311	18.94	.0040	.203	.020	4.628	49.12	1000
36	-25.91	-.425	0.066	.236	.337	3.02	.028	.066	4.321	27.73	.0024	.151	.015	5.22	48.94	999
37	-28.96	-.475	0.097	.259	.218	3.45	.026	.060	5.307	43.72	.0022	.141	.016	6.908	86.65	999
38	-32.00	-.525	0.095	.273	-.008	3.15	.002	.027	4.902	53.68	.0003	.036	.008	5.810	79.73	999
39	-35.05	-.575	0.086	.276	-.144	2.97	.005	.021	3.005	24.16	.0000	.001	.008	8.006	115.72	999
40	-41.15	-.675	0.065	.264	-.372	2.93	.012	.019	1.246	9.70	-.0005	.094	.006	2.478	31.99	1000
41	1.52	.025	-0.015	.151	-.089	4.01	.539	.272	.374	2.18	.0009	.022	.041	-0.263	9.42	1000

TABLE IV-52

RADIAL VELOCITY, CONCENTRATION AND MASS TRANSPORT DATA AND CORRELATIONS

Test Date: 8/10/81 Run No.: 52 Flow Condition: 1 Geometry: 1

Axial Location: 102 mm (4.0 in.); x/R_o = 1.66

PL No.	r mm +(θ=0) -(θ=180)	r/R_o	V m/s	v' m/s	S_v	K_v	$\bar{f}$	f'	S_f	K_f	$\overline{vf}$ m/s	R_{vf}	σ_{vf} m/s	S_{vf}	K_{vf}	N
2	0.0	.000	-.012	.064	-.068	5.32	.915	.128	-2.654	12.39	.0004	.051	.017	0.16	60.26	999
3	9.1	.150	-.035	.135	-.493	2.98	.429	.212	.355	2.44	.0152	.532	.029	1.66	7.92	1000
4	3.0	.050	-.011	.085	-1.642	9.10	.851	.184	-1.600	5.05	.0078	.498	.030	4.90	34.90	1000
5	6.1	.100	-.021	.111	-.991	4.60	.651	.240	-.444	2.07	.0139	.523	.032	2.60	15.69	1000
6	12.2	.200	-.054	.160	-.331	3.48	.262	.174	.848	3.78	.0165	.595	.028	2.23	10.36	1000
7	15.2	.250	-.054	.144	.105	3.59										1000
8	18.3	.300	-.052	.132	-.596	5.62	.033	.077	2.336	8.39	.0035	.339	.014	4.43	31.29	1000
9	21.3	.350	-.020	.157	-.296	4.60	.002	.038	6.377	64.09	.0010	.174	.011	15.96	340.84	1000
10	24.4	.400	.012	.161	-.940	6.05	-.002	.016	1.865	20.63	-.0001	-.055	.003	0.28	19.61	1000
14	33.5	.550	.041	.237	.134	3.87	.008	.016	.248	2.94	-.0004	-.115	.004	-0.20	8.49	1000
15	36.6	.600	.011	.202	.329	3.99	.010	.016	.220	3.46	-.0004	-.135	.003	-0.81	12.23	1000
16	42.7	.699	-.013	.202	.588	4.12	.009	.016	.290	3.38	-.0003	-.088	.003	-0.61	8.88	1000
17	48.8	.799	-.033	.134	.777	5.09	.005	.016	.377	3.56	-.0001	-.035	.002	-0.59	14.50	1000
18	0.0	.000	-.010	.068	1.286	14.25	.936	.140	-2.511	11.84	.0001	.011	.028	-10.45	175.69	1000
22	0.0	.000	.011	.074	-.353	13.11	.877	.132	-2.394	10.87	-.0005	.047	.025	2.33	92.75	1000
23	-3.0	-.050	.005	.087	-1.837	10.90	.829	.158	-1.987	7.48	.0063	.458	.032	7.96	87.11	1000
24	-6.1	-.100	-.004	.117	-1.199	5.62	.657	.222	-.707	2.54	.0146	.561	.038	3.95	28.59	1000
25	-9.1	-.150	-.015	.141	-.630	3.90	.481	.230	.128	2.09	.0179	.550	.034	2.10	12.72	1000
26	-12.2	-.200	-.017	.148	-.137	2.84	.320	.198	.715	3.21	.0168	.570	.029	1.82	7.74	1000
27	-15.2	-.250	-.015	.155	.053	3.37	.176	.151	1.023	3.94	.0131	.558	.025	2.26	11.37	1000
28	-18.3	-.300	-.003	.157	-.136	3.97										1000
29	-21.3	-.350	.014	.173	-.429	4.87	.027	.066	4.126	28.59	.0029	.252	.016	7.81	91.84	1000
30	-24.4	-.400	.037	.180	-.367	3.58	.008	.027	3.432	25.17	.0003	.057	.007	7.17	75.79	1000
31	-27.4	-.450	.054	.214	-.261	3.29	.007	.018	.508	4.71	-.0005	-.119	.004	-0.35	14.31	998
32	-30.5	-.500	.080	.220	-.067	3.03	.010	.018	.288	3.15	-.0005	-.137	.004	-0.59	7.65	1000
33	-33.5	-.550	.092	.242	.071	3.12	.012	.018	.388	3.39	-.0007	-.169	.004	-1.30	9.52	1000
34	-36.6	-.600	.070	.254	.331	3.01	.008	.018	.168	3.05	-.0007	-.152	.005	-1.16	9.35	998
35	-42.7	-.699	.025	.214	.533	3.09	.020	.018	.203	3.25	-.0003	-.064	.004	-0.36	7.66	996
36	0.0	.000	-.011	.067	.560	9.98	.953	.131	-2.668	12.94	.0007	.076	.020	5.92	142.96	999

TABLE IV-53

AZIMUTHAL VELOCITY AND CONCENTRATION DATA AND CORRELATIONS

Test Date: 8/11/81 Run No.: 53 Flow Condition: 1 Geometry: 1

Axial Location: 102 mm (4.0 in.); x/R_o = 1.66

Pt No.	r mm +(θ=270) -(θ=90)	r/R_o	W m/s	w' m/s	S_w	K_w	$\overline{f}$	f'	S_f	K_f	$\overline{wf}$ m/s	R_{wf}	σ_{wf} m/s	S_{wf}	K_{wf}	N
2	0.0	.000	.011	.063	.276	5.07	.916	.131	-2.588	11.37	-.0012	.140	.017	-2.66	63.51	1000
3	3.0	.050	.012	.082	.171	9.68	.871	.190								1000
4	6.1	.100	.008	.099	.181	4.95	.749	.256	-.486	2.08	-.0022	.086	.033	-.98	12.63	1000
5	9.1	.150	.010	.123	.385	3.98	.564	.257								998
6	12.2	.200	.018	.140	-.102	3.26	.336	.199	.844	3.82	-.0019	.068	.024	-.20	7.72	1000
7	18.3	.300	.030	.121	-.158	4.47	.096	.115	1.799	7.00	-.0022	.156	.016	-.72	19.39	1000
8	24.4	.400	.029	.170	-.263	5.49	.008	.034								999
9	30.5	.500	.032	.261	.101	3.78	.007	.016	.310	3.24	.0001	-.026	.005	.29	13.14	1000
10	36.6	.600	.041	.256	.118	3.50	.014	.017	.227	2.94	-.0001	.025	.004	-.34	8.19	999
11	42.7	.699	.019	.208	.148	3.35	.021	.017								995
12	0.0	.000	.009	.072	-.240	12.25	.912	.145								1000
16	0.0	.000	.008	.074	.253	6.83	.904	.141								999
17	-3.0	-.050	-.009	.075	.231	7.43	.905	.145								999
18	-6.1	-.100	.004	.093	.413	6.50	.615	.222								1000
19	-9.1	-.150	.009	.125	.115	4.21	.605	.249								1000
20	-12.2	-.200	.015	.144	.032	3.75	.404	.226								999
21	-18.3	-.300	.034	.122	-.172	3.97	.117	.124								1000
22	-24.4	-.400	.000	.158	-.124	5.88	.016	.026								1000
23	-30.5	-.500	-.005	.260	.058	3.52	.011	.016								1000
24	18.3	.300	-.033	.108	.011	4.62	.074	.093								1000
25	0.0	.000	-.013	.070	.245	5.16	.925	.143								1000

TABLE IV-54

AZIMUTHAL VELOCITY, CONCENTRATION AND MASS TRANSPORT DATA AND CORRELATIONS

Test Date: 8/12/81 Run No.: 54 Flow Condition: 1 Geometry: 1

Axial Location: 152 mm (6.0 in.); x/R_o = 2.50

Pt No.	r mm +(θ=0) -(θ=180)	r/R_o	$\bar{W}$ m/s	w' m/s	S_w	K_w	$\bar{f}$	f'	S_f	K_f	$\overline{wf}$ m/s	R_{wf}	σ_{wf} m/s	S_{wf}	K_{wf}	N
2	1.52	.025	.015	.156	.136	4.40	.578	.304			-.0038	.080				1000
3	1.52	.025	.010	.153	.042	4.04	.558	.304			-.0010	.021				1000
4	4.57	.075	.017	.152	.387	4.73	.510	.294			-.0060	.134				999
5	7.62	.125	.025	.152	.132	3.82	.448	.276			-.0060	.143				999
6	10.67	.175	.026	.157	.175	3.52	.343	.249			-.0040	.102				999
7	13.72	.225	.025	.162	.007	3.57	.266	.221			-.0035	.098				1000
8	19.81	.325	.031	.165	.043	4.27	.105	.155			-.0013	.051				1000
9	25.91	.425	.023	.216	.196	3.88	.013	.069			.0002	-.013				999
10	32.00	.525	.038	.267	-.102	3.38	-.010	.035			.0002	-.021				999
11	38.10	.625	.023	.290	.066	3.17	-.010	.022			.0002	-.031				999
12	44.20	.725	.030	.283	.059	3.33	-.008	.025			-.0000	.000				1000
14	1.52	.025	.004	.157	.017	4.33	.528	.289			-.0013	.029				1000
17	1.52	.025	.002	.159	-.147	4.56	.555	.296			-.0000	.000				999
18	-1.52	-.025	.004	.151	-.017	4.27	.551	.294			.0010	.016				998
19	-4.57	-.075	.007	.164	.302	6.51	.485	.274			-.0008	-.019				1000
20	-7.62	-.125	.013	.164	.084	3.70	.390	.251			-.0008	-.020				1000
21	-10.67	-.175	.019	.163	.278	3.73	.324	.229			-.0030	-.080				999
22	-16.76	-.275	.016	.177	.176	5.49	.151	.171			-.0016	-.052				999
23	-22.86	-.375	-.004	.203	-.084	4.51	.040	.101			.0002	.012				1000
24	-28.96	-.475	-.001	.273	.128	3.77	.001	.048			.0006	.046				1000
25	-35.05	-.575	.009	.296	.001	3.52	.000	.030			-.0002	-.027				999
26	1.52	.025	-.015	.151	-.108	4.48	.531	.286			.0014	.034				1000
27	1.52	.025	-.005	.149	.098	3.61	-.018	.020			.0000	.000				1000

TABLE IV-56

AZIMUTHAL VELOCITY, CONCENTRATION AND MASS TRANSPORT DATA AND CORRELATIONS

Test Date: 8/14/81 Run No.: 56 Flow Condition: 1 Geometry: 1

Axial Location: 203 mm (8.0 in.); x/R_o = 3.33

Pt No.	r mm +(θ=270) -(θ=90)	r/R_o	W m/s	w' m/s	S_w	K_w	$\overline{f}$	f'	S_f	K_f	$\overline{wf}$ m/s	R_{wf}	σ_{wf} m/s	S_{wf}	K_{wf}	N
2	.0	.000	.011	.182	.021	4.62										1000
3	3.0	.050	.014	.184	.150	3.80										1000
4	6.1	.100	.023	.179	.194	4.20										1000
5	9.1	.150	.029	.195	.088	4.54										1000
6	12.2	.200	.022	.182	.233	4.47										1000
7	18.3	.300	.010	.211	.039	3.60										1000
8	24.4	.400	.009	.231	-.047	3.84										1000
9	30.5	.500	.015	.267	-.237	3.79	.045	.059			.0005	-.032	.000			1000
10	36.6	.600	.016	.302	-.037	2.92	.035	.036			-.0000	.000	.001			1000
11	42.7	.699	.019	.285	-.005	2.94	.035	.029			.0002	-.025	.001			1000
12	.0	.000	.012	.185	-.062	3.61	.277	.148			-.0006	.022	.001			1000
16	.0	.000	.003	.183	.016	3.64	.273	.141			-.0018	.070	.001			1000
17	-3.0	-.050	-.007	.174	.306	4.64	.265	.157			.0000	.000	.001			1000
18	-6.1	-.100	.006	.176	.881	4.03	.256	.149			.0001	.004	.001			1000
19	-9.1	-.150	.013	.185	-.069	3.66	.243	.147			.0002	.007	.001			1000
20	-12.2	-.200	.019	.181	.221	3.86	.208	.138			-.0001	-.004	.002			1000
21	-18.3	-.300	.001	.191	.136	3.85	.151	.133			-.0003	-.012	.002			1000
22	-30.5	-.500	.013	.265	.189	3.38	.060	.078			.0001	.005	.002			1000
23	-42.7	-.699	.012	.317	-.060	3.20	.044	.042			.0003	.023	.001			1000
24	.0	.000	-.006	.173	.035	3.56	.288	.153			.0018	.068	.001			1000

TABLE IV-57

AZIMUTHAL VELOCITY, CONCENTRATION AND MASS TRANSPORT DATA AND CORRELATIONS

Test Date: 8/17/81 Run No.: 57 Flow Condition: 1 Geometry: 1

Axial Location: 13 mm (0.5 in.); $x/R_o = 0.21$

Pt No.	r mm +(θ=270) -(θ=90)	r/R_o	W m/s	w' m/s	S_w	K_w	$\overline{f}$	f'	S_f	K_f	$\overline{wf}$ m/s	R_{wf}	σ_{wf} m/s	S_{wf}	K_{wf}	N
1	.00	.000	.010	.033	.082	2.86										994
2	.00	.000	.009	.036	-.258	3.50										1000
3	.00	.000	.008	.034	-.294	3.45	1.002	.056								999
4	3.05	.050	.007	.037	.015	3.34	.999	.056								999
5	6.10	.100	.008	.042	-.208	3.32	1.000	.056								999
6	9.14	.150	.007	.047	.167	3.24	.998	.057								997
7	12.19	.200	.001	.074	.013	3.72	.837	.118								1000
8	18.29	.300	.027	.064	-.193	3.77	.015	.018								999
9	24.38	.400	.046	.028	-.016	3.39	.000	.014								1000
10	30.48	.500	.031	.220	.186	2.82	.006	.015								992
11	36.58	.600	.066	.124	.050	2.78	.033	.025								998
12	42.67	.700	.111	.123	-.120	2.89	.019	.019								996
13	.00	.000	.009	.036	-.199	3.25										998
14	.00	.000	.009	.035	-.256	3.30										1000
15	.00	.000	.008	.035	-.064	2.85			.371	3.10		-.058				994
16	.00	.000	.010	.035	.141	3.00			.060	2.63		.008				994
17	.00	.000	.007	.037	-.198	3.72			.182	3.08		-.019				999
18	-3.05	-.050	-.010	.035	-.072	2.98			.005	3.07		-.037				996
19	-6.10	-.100	-.012	.040	-.021	2.82			.093	3.81		-.025				997
20	-9.14	-.150	-.010	.051	-.076	2.87			.098	2.54		-.066				998
21	-12.19	-.200	-.011	.095	-.072	4.51			-.660	3.46		.098				997
22	-18.29	-.300	.052	.065	-.060	3.11			.810	5.90		.035				998
23	-24.38	-.400	-.013	.048	-.654	4.96			.309	3.61		.048				999
24	-30.48	-.500	-.017	.210	-.134	3.51			.296	3.05		.029				996
25	-36.58	-.600	.083	.132	-.410	2.96			.549	3.63		.047				992
26	-42.67	-.700	.116	.113	-.393	3.21			.272	3.15		.098				990
27	.00	.000	-.009	.036	.114	3.64			.067	1.82		-.000				1000
28	.00	.000	-.008	.037	.158	3.23			.397	3.23		.008				1000

TABLE IV-58

AZIMUTHAL VELOCITY, CONCENTRATION AND MASS TRANSPORT DATA AND CORRELATIONS

Test Date: 8/17/81 **Run No.:** 58 **Flow Condition:** 1 **Geometry:** 1

Axial Location: 51 mm (2.0 in.); $x/R_o = 0.83$

Pt No.	r mm +(θ=270) −(θ=90)	r/R_o	W m/s	w' m/s	S_w	K_w	$\overline{f}$	f'	S_f	K_f	$\overline{wf}$ m/s	R_{wf}	σ_{wf} m/s	S_{wf}	K_{wf}	N
2	.0	.000	.010	.038	.088	3.35	1.000	.051	-.400	5.18	-.0000	.011	.002	.08	6.44	1000
3	.0	.000	.008	.038	.169	3.64	.971	.054	-.163	2.58	-.0000	-.017	.002	.20	9.52	1000
4	3.0	.050	.010	.041	.203	3.08	.993	.053	-.235	3.84	-.0[illegible]	.000	.002	.06	6.34	999
5	6.1	.100	.008	.045	.132	3.52	1.021	.058	-1.605	9.57	-.0002	.070	.003	-1.79	22.36	1000
6	9.1	.150	.007	.068	.132	5.13	.860	.162	-1.046	3.88	-.0007	.059	.015	-3.96	79.97	1000
7	12.2	.199	.010	.133	.083	3.74	.467	.185	.423	2.75	-.0010	.040	.023	-.75	8.67	999
9	.0	.000	.012	.038	-.105	3.27	.971	.052								1000
10	.0	.000	.012	.038	-.194	3.45	1.028	.058								1000
11	18.2	.299	.028	.075	-.220	4.44	.054	.052								996
12	24.3	.399	.039	.078	.044	5.46	.018	.014								996
13	30.4	.498	.045	.222	.177	3.12	.025	.015								997
14	36.5	.598	.050	.192	.137	3.70	.035	.017								996
15	42.6	.698	.019	.138	.237	2.51	.040	.017	.457	3.77	.0001	-.054	.002	1.25	14.02	991
18	.0	.000	-.009	.038	.162	3.67	1.001	.074	.430	3.21	-.0002	-.079	.003	-.47	8.19	1000
19	-3.0	-.050	-.013	.037	-.042	3.23	.981	.056	.029	4.18	-.0000	-.010	.002	.18	7.19	1000
20	-6.1	-.100	-.010	.044	.089	3.07	1.026	.063	-.946	8.54	-.0000	-.009	.003	.35	15.49	999
21	-9.1	-.150	-.007	.058	.003	3.30	.933	.122								992
22	-12.2	-.199	-.006	.124	.090	3.76	.565	.205	.136	2.31	.0017	.067	.025	.25	7.46	1000
23	-18.2	-.299	.047	.090	.241	4.91	.072	.066	1.889	7.93	.0005	.081	.007	.62	19.55	1000
24	-24.3	-.399	-.014	.092	-.655	13.83	.021	.015	.361	3.21	-.0000	-.002	.002	-.99	54.09	1000
27	.0	.000	-.013	.035	.071	2.83	.998	.054								994
28	.0	.000	-.011	.039	-.006	3.23	.991	.053								998
29	-30.4	-.498	-.001	.217	-.141	3.19	.013	.015								998
30	-36.5	-.598	.046	.194	-.329	3.43	.024	.016								990
31	-42.6	-.698	.071	.140	-.252	3.10	.033	.018								993
32	.0	.000	-.011	.038	.144	3.14	1.002	.052								999

TABLE IV-60

AXIAL VELOCITY, CONCENTRATION AND MASS TRANSPORT DATA AND CORRELATIONS

Test Date: 8/19/81 Run No.: 60 Flow Condition: 1 Geometry: 1

Axial Location: 13 mm (0.5 in.); x/R_o = 0.21

Pt No.	r mm +(θ=0) -(θ=180)	r/R_o	U m/s	u' m/s	S_u	K_u	$\overline{f}$	f'	S_f	K_f	$\overline{uf}$ m/s	R_{uf}	σ_{uf} m/s	S_{uf}	K_{uf}	N
3	.00	.00	[illegible]	.053	-.543	3.72	.996	.053	-.380	3.17	.0000	.014	.003	-.003	10.13	999
4	3.05	.05	.803	.049	-.244	2.86	.948	.056	-.081	2.62	-.0000	-.016	.003	-.550	8.72	1000
5	6.10	.10	.759	.061	-.465	3.12	1.019	.048	-.670	4.48	-.0000	-.016	.003	.033	6.12	1000
6	9.14	.15	.674	.079	-.348	3.05	.983	.058	-.895	7.34	-.0002	.035	.005	-.711	13.73	999
7	12.19	.20	.503	.107	-.148	3.28	.806	.096	-.794	4.19	.0019	.186	.107	.063	10.69	988
8	18.29	.30	1.630	.057	-1.217	11.09	-.007	.013	.304	2.88	.0000	.034	.001	-.240	15.27	1000
9	24.38	.40	1.596	.062	-.832	11.26	-.008	.013	.331	3.08	-.0000	-.020	.001	-1.276	16.17	1000
10	30.48	.50	.702	.256	-.036	2.69	.001	.013	.195	2.94	-.0003	-.095	.003	-.433	5.63	1000
11	36.58	.60	-.047	.084	-.609	4.23	.006	.014	.142	2.92	-.0000	-.024	.001	-.158	12.75	999
12	42.67	.70	-.057	.089	-.827	5.12	-.001	.013	.288	3.29	-.0000	-.044	.001	-.530	14.14	1000
13	.00	.00	.816	.053	-.534	3.33	1.005	.052	-.457	3.34	.0000	.024	.003	.526	11.78	996
14	.00	.00	.813	.054	-.477	3.00						.029				996
15	.00	.00	.813	.054	-.461	3.66						-.154				998
16	.00	.00	.813	.054	-.458	3.18						.032				1000
17	.00	.00	.817	.054	-.431	3.36						.059				998
18	-3.05	-.05	.773	.064	-.490	3.19						.009				994
19	-6.10	-.10	.716	.076	-.273	3.05						.062				996
20	-9.14	-.15	.625	.092	-.166	2.78						.055				997
21	-12.19	-.20	.472	.116	.039	2.82						.272				998
22	-18.29	-.30	1.589	.071	-1.051	4.33						.004				425
23	-24.38	-.40	1.642	.042	-.647	11.73						-.015				1000
24	-30.48	-.50	.650	.276	-.040	[illegible]						-.092				1000
25	-36.58	-.60	-.036	.096	-.769	4.25						-.098				1000
26	-42.67	-.70	-.038	.094	-.491	3.08						-.088				999

TABLE IV-61

AXIAL VELOCITY, CONCENTRATION AND MASS TRANSPORT DATA AND CORRELATIONS

Test Date: 8/19/81 Run No.: 61 Flow Condition: 1 Geometry: 1

Axial Location: 51 mm (2.0 in.); x/R_o = 0.83

Pt No.	r mm +(θ=0) -(θ=180)	r/R_o	U m/s	u' m/s	S_u	K_u	$\overline{f}$	f'	S_f	K_f	$\overline{uf}$ m/s	R_{uf}	σ_{uf} m/s	S_{uf}	K_{uf}	N
2	0.5	0.008	.803	.054	-.463	3.48	1.000	.059	.054	3.10	.0001	.046	.003	.50	8.50	1000
3	3.6	0.058	.806	.051	-.290	3.43	.980	.063	.098	3.44	.0000	.013	.003	-.37	9.55	1000
4	6.6	0.108	.759	.076	-.429	3.25	1.013	.070	-.414	4.26	.0011	.204	.006	1.54	11.20	1000
5	9.6	0.158	.712	.098	.575	4.31	.772	.156	-.944	3.43	-.0017	-.113	.020	-2.86	20.44	1000
6	12.7	0.208	1.004	.219	.320	2.47	.367	.171	.600	2.91	-.0183	-.491	.034	-1.05	4.76	1000
7	18.8	0.308	1.629	.069	-.970	11.52	-.001	.032	3.803	25.60	-.0002	-.089	.005	-10.14	192.18	1000
8	24.9	0.408	1.519	.140	-1.191	5.40	-.007	.015	.139	2.94	-.0001	-.053	.002	-1.10	13.63	999
9	31.0	0.508	.775	.300	-.641	3.43	-.003	.015	.362	3.28	-.0005	-.120	.005	-.52	9.61	1000
10	37.1	0.608	.027	.167	—	—	—	—	—	—	—	—	—	—	—	—
11	43.2	0.708	-.079	.146	-.223	4.20	.010	.022	.418	3.15	-.0005	-.163	.003	-1.95	12.34	250
15	0.5	0.008	.792	.057	-.196	2.73	.979	.059	.065	3.24	.0000	.006	.003	.72	8.32	999
16	-2.5	-0.042	.753	.070	—	—	1.000	.059	—	—	—	—	—	—	—	1000
17	-5.6	-0.092	.693	.083	-.250	3.08	.918	.062	-.187	3.79	.0008	.157	.006	1.99	22.58	1000
18	-8.6	-0.142	.663	.092	.408	4.32	.870	.165	-.974	3.77	-.0001	-.005	.021	-4.22	40.81	1000
19	-11.7	-0.192	.886	.173	.336	2.80	.473	.190	.445	2.76	-.0142	-.429	.032	-1.15	6.41	999
20	-17.8	-0.291	1.581	.100	-1.039	5.71	.024	.050	3.594	23.12	-.0014	-.276	.010	-9.87	149.73	1000
21	-23.9	-0.391	1.571	.153	-2.444	12.84	.000	.014	.070	3.19	-.0002	-.074	.003	-4.53	57.11	500
22	-30.0	-0.491	.831	.328	-.427	3.82	.005	.015	.199	2.91	-.0007	-.151	.005	-1.32	10.36	498
23	-36.1	-0.591	.062	.187	1.091	6.64	.017	.016	.164	3.22	-.0004	-.125	.003	-.76	16.95	500
24	-42.2	-0.691	-.061	.123	-.435	3.89	.017	.015	.222	3.13	-.0002	-.124	.002	-.67	9.02	500

TABLE IV-62

AXIAL VELOCITY, CONCENTRATION AND MASS TRANSPORT DATA AND CORRELATIONS

Test Date: 8/20/81 Run No.: 62 Flow Condition: 1 Geometry: 1

Axial Location: 102 mm (4.0 in.); $x/R_o = 1.66$

Pt No.	r mm +(θ=0) -(θ=180)	r/R_o	U m/s	u' m/s	S_u	K_u	$\overline{f}$	f'	S_f	K_f	$\overline{uf}$ m/s	R_{uf}	σ_{uf} m/s	S_{uf}	K_{uf}	N
3	1.5	.025	.770	.090	.199	4.17	.934	.126	-2.458	11.76	-.0002	-.013	.018	-9.72	175.89	1000
4	4.6	.075	.784	.102	.790	6.51	.852	.163	-2.058	7.89	-.0018	-.111	.032	-9.08	131.17	1000
5	7.6	.125	.834	.145	1.192	5.77	.665	.225	-.569	2.30	-.0146	-.446	.044	-3.74	25.35	1000
6	10.7	.175	1.004	.201	.468	2.74	.447	.221	.291	2.28	-.0265	-.595	.042	-1.46	6.27	1000
7	13.7	.225	1.231	.228	-.157	2.48	.241	.166	[illegible]	4.31	-.0229	-.607	.044	-2.44	11.46	1000
8	19.8	.325	1.547	.141	-1.813	8.69	.028	.068	2.444	9.90	-.0021	-.220	.014	-5.06	54.60	1000
9	25.9	.425	1.349	.260	-1.535	7.19	.000	.036	5.466	42.57	-.0003	-.032	.010	-0.06	85.76	997
10	32.0	.525	.817	.361												1000
11	38.1	.624	.321	.342												1000
12	44.2	.724	-.010	.274												1000
13	1.5	.025	.766	.090	.067	3.24	.896	.121	-2.452	12.66	.0001	.012	.018	-5.33	54.23	999
17	1.5	.025	.779	.089	.159	3.78	.901	.118	-2.962	15.40	-.0002	-.018	.020	-7.42	92.99	1000
18	-1.5	-.025	.763	.098	.409	4.11	.885	.146	-2.046	7.60	.0003	.019	.023	-6.45	75.19	1000
19	-4.6	-.075	.788	.126	.865	4.60	.730	.227	-.809	2.69	-.0100	-.352	.039	-3.41	22.86	1000
20	-7.6	-.125	.920	.192	.790	3.32	.546	.262	.121	2.01	-.0291	-.578	.052	-2.22	11.13	998
21	-10.7	-.175	1.110	.211	.180	2.51	.351	.202	.614	3.11	-.0251	-.590	.042	-1.46	5.73	1000
22	-16.7	-.275	1.487	.179	-.950	4.08	.081	.117	2.004	8.15	-.0107	-.511	.033	-5.39	43.04	1000
23	-22.9	-.375	1.410	.260												999
24	-29.0	-.475	.940	.340												1000
25	-35.1	-.575	.424	.377	-.086	2.97	.001	.016	.364	3.06	-.0011	-.181	.006	-0.65	6.44	1000
26	-41.1	-.674	.023	.291	.269	2.89	-.002	.016	.294	3.04	-.0009	-.190	.005	-0.89	7.66	1000
27	1.5	.025	.775	.092	-.191	3.19	.929	.112	-3.392	18.97	.0003	.028	.016	-6.77	92.34	999

TABLE IV- 63

AXIAL VELOCITY, CONCENTRATION AND MASS TRANSPORT DATA AND CORRELATIONS

Test Date: 8/20/81 Run No.: 63 Flow Condition: 1 Geometry: 1

Axial Location: 152 mm (6.0 in.); x/R_o = 2.50

Pt No.	r mm +(θ=0) -(θ=180)	r/R_o	U m/s	u' m/s	S_u	K_u	$\overline{f}$	f'	S_f	K_f	$\overline{uf}$ m/s	R_{uf}	σ_{uf} m/s	S_{uf}	K_{uf}	N
16	1.5	.025	.911	.187	.548	3.01	.542	.274	.237	2.11	-.0226	-0.44	.050	-1.40	7.08	998
17	1.5	.025	.927	.196	.387	3.05	.502	.264	.304	2 18	-.0236	-0.46	.048	-1.03	6.03	1000
18	-1.5	-.025	.919	.196	.245	2.99	.507	.266	.335	2.16	-.0213	-0.41	.049	-0.90	5.23	999
19	-4.6	-.075	.973	.201	.271	2.59	.463	.261	.419	2.25	-.0241	-0.46	.048	-0.97	4.59	1000
20	-7.6	-.125	1.069	.235	.182	2.46	.401	.252	.702	2.92	-.0325	-0.55	.056	-1.17	4.66	999
21	-10.7	-.175	1.163	.239	-.112	2.65	.315	.232	.897	3.41	-.0293	-0.53	.054	-1.45	7.20	1000
22	-16.8	-.275	1.337	.241	-.728	3.58	.136	.152	1.401	4.73	-.0108	-0.29	.040	-2.03	14.74	999
23	-22.9	-.375	1.247	.311	-.877	3.92	.057	.095	2.792	12.45	.0038	0.01	.025	-1.48	18.82	1000
24	-29.0	-.475	.916	.390	-.519	2.84	.011	.048	7.195	78.77	.0006	0.03	.015	8.07	113.41	500
25	-35.1	-.575	.580	.412	-.246	2.73	.022	.024	1.849	11.76	-.0014	-0.14	.010	-0.61	15.27	500
26	-41.1	-.674	.168	.398	.266	2.55	.018	.019	.382	3.06	-.0016	-0.21	.009	-2.22	18.12	499
27	1.5	.025	.920	.198	.410	2.88	.537	.267	.246	2.09	-.0224	-0.43	.051	-1.19	6.04	998
28	4.6	.075	.977	.218	.427	3.25	.466	.267	.429	2.22	-.0275	-0.47	.056	-1.53	8.06	999
29	7.6	.125	1.046	.220	.236	2.53	.417	.255	.641	2.59	-.0289	-0.52	.050	-0.80	4.14	1000
30	10.7	.175	1.164	.231	-.126	2.52	.275	.197	.942	3.83	-.0244	-0.54	.046	-1.80	10.83	1000
31	13.7	.225	1.267	.245	-.405	2.72	.196	.171	1.043	3.93	-.0211	-0.50	.045	-1.78	10.35	1000
32	19.8	.325	1.349	.263	-1.339	5.43	.072	.115	2.164	8.00	-.0046	-0.15	.031	-3.29	24.66	1000
33	25.9	.425	1.192	.325	-1.056	4.37	.017	.053	4.073	24.20	.0005	0.03	.012	0.76	18.55	1000
34	1.5	.025	.908	.190	.370	2.99	.549	.273	.253	2.05	-.0216	-0.42	.049	-1.19	5.99	998

TABLE IV-64

AXIAL VELOCITY, CONCENTRATION AND MASS TRANSPORT DATA AND CORRELATIONS

Test Date: 8/21/81 Run No.: 64 Flow Condition: 1 Geometry: 1

Axial Location: 203 mm (8.0 in.); x/R_o = 3.33

Pt No.	r mm +(θ=0) −(θ=180)	r/R_o	U m/s	u' m/s	S_u	K_u	$\overline{f}$	f'	S_f	K_f	$\overline{uf}$ m/s	R_{uf}	σ_{uf} m/s	S_{uf}	K_{uf}	N
4	2.03	.033	.970	.208	-.224	3.46	.279	.170	.853	3.68	-.0090	-.254	.034	.522	10.83	999
5	5.08	.083	.989	.215	-.156	3.13	.261	.162	.922	4.27	-.0108	-.310	.035	-.646	13.67	999
6	8.13	.133	.998	.230	-.072	2.67	.252	.163	.734	3.56	-.0108	-.287	.037	-.409	5.78	1000
7	11.18	.183	1.076	.230	-.290	2.89	.205	.159	1.140	4.88	-.0108	-.295	.038	-1.056	10.00	1000
8	14.22	.233	1.115	.239	-.402	3.47	.151	.130	1.090	4.43	-.0068	-.219	.031	-.818	9.94	998
9	20.32	.333	1.108	.288	-.878	4.18	.090	.106	1.555	5.43	-.0010	-.032	.024	-.138	5.05	999
18	0.00	.000	.983	.211	-.106	2.85	.268	.158	.684	3.41	-.0105	-.313	.033	-.337	8.41	1000
19	-1.02	-.017	.973	.203	-.173	2.90	.281	.157	.756	3.81	-.0083	-.261	.030	-.639	8.05	1000
20	-4.06	-.067	.983	.220	-.192	2.93	.271	.171	.858	3.61	-.0099	-.264	.035	-.270	6.25	1000
21	-7.11	-.116	1.018	.217	-.184	3.04	.256	.167	.929	4.08	-.0110	-.304	.033	-.839	5.80	1000
22	-10.16	-.166	1.049	.239	-.404	3.66	.222	.154	.878	3.83	-.0088	-.240	.034	-.481	9.59	1000
23	-16.26	-.266	1.074	.262	-.506	3.46	.143	.131	1.114	3.95	-.0043	-.125	.032	-.120	6.44	1000
24	-22.35	-.366	.995	.307	-.584	3.39	.089	.102	1.953	7.76	.0026	.082	.026	-.288	17.78	1000
25	-28.45	-.466	.828	.355	-.578	3.29	.044	.072	3.730	24.81	.0014	.054	.016	1.049	10.71	1000
26	-34.54	-.566	.626	.372	-.408	2.78	.044	.056	4.620	37.82	.0000	-.002	.014	1.574	20.20	1000
27	-40.65	-.666	.347	.377	-.062	2.49	.030	.030	2.570	18.03	-.0001	.006	.012	2.882	27.43	1000
28	0.00	-.000	.980	.208	-.125	3.00	.272	.155	.831	3.92	-.0104	-.326	.030	-.711	6.67	1000

TABLE IV-66

AXIAL VELOCITY, CONCENTRATION AND MASS TRANSPORT DATA AND CORRELATIONS

Test Date: 8/24/81 Run No.: 66 Flow Condition: 1 Geometry: 1

Axial Location: 254 mm (10.0 in.); $x/R_o = 4.16$

Pt No.	r mm +(θ=0) −(θ=180)	r/R_o	U m/s	u' m/s	S_u	K_u	$\overline{f}$	f'	S_f	K_f	$\overline{uf}$ m/s	R_{uf}	σ_{uf} m/s	S_{uf}	K_{uf}	N
3	-0.76	-0.012	.885	.224	-.404	3.52	.200	.095	.676	3.52	.0009	.041	.021	0.68	7.88	1000
4	2.29	0.037	.859	.234	-.483	3.51	.182	.094	.745	3.50	.0017	.075	.021	0.39	6.07	1000
5	5.33	0.087	.850	.225	-.399	3.23	.180	.094	.759	3.73	.0011	.054	.020	0.33	5.91	1000
6	8.38	0.137	.847	.258	-.678	3.72	.160	.089	.915	3.99	.0030	.130	.021	1.05	8.02	1000
7	11.43	0.187	.846	.254	-.562	3.53	.151	.085	.740	3.37	.0024	.111	.020	0.48	6.17	1000
8	17.53	0.287	.800	.281	-.416	2.90	.124	.077	1.068	3.87	.0027	.124	.019	0.63	6.20	1000
9	23.62	0.387	.716	.306	-.319	2.79	.104	.067	1.460	5.70	.0031	.152	.017	0.48	6.50	1000
10	29.72	0.487	.549	.321	-.121	2.53	.080	.052	1.696	7.57	.0024	.142	.015	1.45	11.41	1000
11	35.81	0.587	.420	.327	-.025	2.64	.061	.039	2.032	10.52	.0014	.108	.013	2.65	21.12	1000
12	41.91	0.687	.272	.305	.394	2.86	.062	.034	1.641	8.56	.0005	.048	.011	2.46	21.26	1000
13	-0.76	-0.012	.870	.239	-.772	4.52	.180	.090	.894	4.54	.0014	.067	.020	1.08	7.72	1000
15	-0.76	-0.012	.848	.247	-.641	3.88	.195	.095	.750	3.72	.0025	.107	.023	1.29	8.53	1000
16	-3.81	-0.062	.866	.222	-.544	4.01	.207	.096	.538	2.98	.0012	.054	.021	0.91	8.07	1000
17	-6.86	-0.112	.842	.249	-.631	3.73	.195	.099	.732	3.80	.0030	.120	.024	0.99	7.17	999
18	-9.91	-0.162	.840	.250	-.725	4.01	.192	.100	.809	3.50	.0031	.123	.024	0.58	5.82	1000
19	-12.95	-0.212	.821	.265	—	—	.175	.095	—	—	.0041	.150	.024	—	—	1000
20	-19.05	-0.312	.804	.275	-.611	3.59	.149	.092	.961	3.79	.0032	.125	.022	0.39	6.19	1000
21	-25.15	-0.412	.709	.311	—	—	.125	.078	—	—	.0045	.171	.024	—	—	1000
22	-31.24	-0.512	.592	.323	-.230	2.62	.093	.059	1.951	10.06	.0027	.140	.016	0.73	9.55	1000
23	-37.34	-0.612	.463	.321	-.113	2.51	.091	.055	1.758	7.34	.0031	.177	.017	2.82	22.52	1000
24	-43.43	-0.712	.334	.328	-.014	2.60	.074	.041	2.158	12.68	.0016	.120	.015	3.59	32.06	1000
25	-0.76	-0.012	.863	.238	-.437	3.45	.186	.088	.488	2.98	.0016	.076	.021	0.54	6.74	1000

TABLE IV-67

AXIAL VELOCITY, CONCENTRATION AND MASS TRANSPORT DATA AND CORRELATIONS

Test Date: 8/24/81 Run No.: 67 Flow Condition: 1 Geometry: 1

Axial Location: 305 mm (12.0 in.); x/R_o = 5.00

Pt No.	r mm +(θ=0) −(θ=180)	r/R_o	U m/s	u' m/s	S_u	K_u	$\overline{f}$	f'	S_f	K_f	$\overline{uf}$ m/s	R_{uf}	σ_{uf} m/s	S_{uf}	K_{uf}	N
3	0.0	.000	.690	.243	−.451	2.91	.146	.056	.881	3.99	.0034	.250	.012	0.97	6.57	999
4	3.0	.050	.708	.238	−.384	2.83	.134	.050	.795	3.64	.0028	.237	.011	0.90	6.03	999
5	6.1	.100	.686	.244	−.345	2.94	.136	.050	.771	3.58	.0030	.240	.011	1.46	13.40	1000
6	9.1	.150	.659	.262	−.448	2.96	.130	.050	1.015	4.30	.0032	.239	.012	0.66	5.30	1000
8	18.3	.300	.636	.256	−.233	2.79	.121	.046	.974	4.43	.0029	.246	.010	0.69	5.92	1000
9	24.4	.400	.544	.268	−.142	2.53	.116	.045	1.442	6.60	.0027	.227	.012	1.55	16.22	1000
10	30.5	.500	.462	.264	−.004	2.58	.099	.036	.914	3.93	.0022	.239	.009	1.36	9.50	1000
11	36.6	.600	.388	.258	.121	2.41	.094	.035	1.164	5.09	.0015	.172	.009	1.93	15.50	1000
12	42.7	.699	.303	.248	.226	2.65	.090	.030	1.126	5.46	.0014	.186	.007	1.76	11.95	1000
13	0.0	.000	.720	.231	−.389	2.88	.140	.054	.992	4.06	.0028	.224	.011	0.77	6.96	1000
16	0.0	.000	.698	.243	−.440	3.18	.144	.060	.937	4.21	.0034	.233	.014	0.85	7.15	1000
17	−3.0	−.050	.699	.246	−.383	2.75	.141	.058	.849	3.91	.0038	.199	.012	0.57	5.25	1000
18	−6.1	−.100	.679	.247	−.457	2.95	.142	.058	.809	3.48	.0038	.262	.013	0.73	5.39	1000
19	−9.1	−.150	.688	.247	−.441	3.08	.141	.060	.773	3.39	.0033	.220	.013	0.71	6.69	1000
20	−12.2	−.200	.663	.244	−.336	2.99	.138	.059	.863	3.81	.0034	.238	.013	1.05	7.40	1000
21	−18.3	−.300	.634	.260	−.382	2.80	.129	.059	1.093	4.69	.0033	.217	.014	1.40	9.02	1000
22	−24.4	−.400	.548	.270	−.244	2.68	.122	.052	1.212	5.30	.0038	.271	.013	2.68	26.39	1000
23	−30.5	−.500	.476	.269	.025	2.52	.104	.046	1.231	5.57	.0029	.232	.011	1.41	10.86	1000
24	−36.6	−.600	.398	.262	.082	2.43	.101	.040	1.383	6.71	.0021	.194	.010	1.32	11.41	1000
25	−42.7	−.699	.306	.249	.329	2.80	.088	.037	1.463	7.20	.0018	.192	.010	1.58	13.21	1000
26	0.0	.000	.681	.248	−.452	2.89	.142	.064	.717	3.33	.0042	.270	.014	0.77	6.08	1000

TABLE IV-69

RADIAL VELOCITY, CONCENTRATION AND MASS TRANSPORT DATA AND CORRELATIONS

Test Date: 8/25/81 Run No.: 69 Flow Condition: 1 Geometry: 1

Axial Location: 254 mm (10.0 in.); x/R_o = 4.16

Pt No.	r mm +(θ=0) -(θ=180)	r/R_o	V m/s	v' m/s	S_v	K_v	$\bar{f}$	f'	S_f	K_f	$\overline{vf}$ m/s	R_{vf}	σ_{vf} m/s	S_{vf}	K_{vf}	N
3	1.52	.025	.023	.175	.028	3.87	.187	.100	.693	3.29	.0001	.006	.016	-.331	6.57	1000
4	4.57	.075	.030	.189	-.195	3.47	.183	.101	.648	3.47	.0030	.158	.018	.322	6.02	1000
5	7.62	.125	.035	.183	-.363	4.14	.173	.098	.895	4.47	.0024	.136	.017	.452	7.48	999
6	10.67	.175	.042	.189	-.307	3.46	.156	.091	.673	3.04	.0036	.210	.016	1.067	7.07	1000
7	13.72	.225	.045	.187	-.292	3.41	.146	.092	.744	3.13	.0036	.210	.016	.595	5.31	999
8	19.81	.325	.072	.196	-.188	2.92	.138	.098	1.409	6.24	.0047	.243	.017	.883	6.37	1000
9	25.91	.425	.100	.219	-.263	3.75	.087	.076	1.416	5.25	.0046	.277	.016	2.420	16.40	998
10	32.00	.524	.097	.229	-.245	3.24	.059	.059	1.924	8.27	.0030	.226	.014	3.838	33.22	1000
11	38.10	.624	.108	.236	.004	2.84	.041	.042	1.985	8.71	.0020	.204	.011	3.608	26.26	998
12	44.20	.724	.087	.222	.416	3.87	.031	.032	1.570	9.34	.0008	.119	.007	2.811	23.68	999
13	1.52	.025	.017	.168	-.177	3.78	.194	.101	.657	3.38	.0013	.075	.017	.766	8.74	1000
16	1.52	.025	.017	.180	-.099	3.90	.190	.091	.530	2.94	.0002	.011	.016	.321	7.63	999
17	-1.52	-.025	-.011	.179	-.141	3.95	.182	.093	.660	3.27	-.0001	.004	.016	-.183	7.95	1000
18	-4.57	-.075	.001	.175	.107	4.31	.175	.091	.580	3.14	.0015	.096	.016	.419	9.28	1000
19	-7.62	-.125	-.001	.170	.286	3.90	.164	.090	.994	5.33	.0032	.209	.015	.864	8.11	998
20	-10.67	-.175	.006	.190	.233	3.47	.151	.086	.736	3.46	.0035	.214	.015	.849	7.10	1000
21	-16.76	-.275	.037	.197	.143	4.09	.140	.083	.926	3.86	.0040	.243	.016	.922	6.64	1000
22	-22.86	-.375	.048	.205	.286	3.24	.106	.074	1.165	4.13	.0040	.263	.014	1.270	10.11	1000
23	-28.96	-.475	.066	.219	.081	3.21	.090	.061	1.604	6.20	.0033	.246	.012	2.283	16.67	1000
24	-35.05	-.574	.096	.224	.110	2.84	.061	.045	2.010	9.34	.0018	.178	.010	2.008	16.01	999
25	-41.15	-.674	.108	.236	-.046	2.92	.071	.043	1.955	9.62	.0017	.169	.010	2.596	20.06	997
26	1.52	.025	-.014	.180	.274	4.37	.185	.092	.678	3.24	.0006	.039	.016	.530	9.02	1000

TABLE IV-70

RADIAL VELOCITY, CONCENTRATION AND MASS TRANSPORT DATA AND CORRELATIONS

Test Date: 8/25/81 Run No.: 70 Flow Condition: 1 Geometry: 1

Axial Location: 305 mm (12.0 in.); x/R_o = 5.00

P_t No.	r mm +(θ=0) −(θ=180)	r/R_o	V m/s	v' m/s	S_v	K_v	$\bar{f}$	f'	S_f	K_f	$\overline{vf}$ m/s	R_{vf}	σ_{vf} m/s	S_{vf}	K_{vf}	N
3	0.00	.00	.020	.179	-.238	4.00	.142	.057	.734	3.81	.0003	.034	.010	.104	8.19	1000
4	3.05	.05	.021	.175	-.108	3.45	.143	.058	.646	3.13	.0013	.130	.010	1.156	9.82	1000
5	6.10	.10	.031	.169	-.019	3.63	.128	.055	.839	3.76	.0009	.096	.009	.758	13.10	1000
6	9.14	.15	.033	.171	-.209	3.74	.131	.055	.660	3.12	.0013	.140	.009	.769	9.86	1000
7	12.19	.20	.045	.174	-.240	3.38	.129	.056	.857	3.82	.0018	.187	.009	.728	9.12	1000
8	18.29	.30	.060	.192	-.192	3.48	.115	.052	.947	3.76	.0022	.219	.009	1.378	9.61	999
9	24.38	.40	.082	.206	-.226	3.05	.103	.047	1.339	5.69	.0022	.228	.009	1.533	10.67	1000
10	30.48	.50	.088	.205	-.103	2.93	.092	.040	1.407	5.80	.0021	.250	.007	1.698	10.74	1000
11	36.58	.60	.088	.214	.023	2.90	.085	.034	1.243	5.85	.0018	.250	.008	2.241	15.54	998
12	42.67	.70	.072	.210	.139	2.92	.068	.027	1.334	7.22	.0012	.214	.006	3.142	32.44	998
13	0.00	.00	.018	.179	-.088	3.35	.143	.058	.778	3.94	-.0001	-.010	.010	-.021	8.16	99[illegible]
16	0.00	.00	-.022	.170	.042	3.32	.149	.067	.707	3.23	.0002	.020	.011	.314	6.14	999
17	-3.05	-.05	-.001	.171	-.082	3.72	.140	.064	.736	3.45	.0002	.020	.011	-.241	9.28	1000
18	-6.10	-.10	-.002	.175	.072	3.51	.134	.060	.648	3.12	.0006	.054	.010	.649	8.96	999
20	-12.19	-.20	.016	.178	.109	3.02	.129	.063	.998	4.59	.0013	.118	.010	.390	7.24	999
21	-18.29	-.30	.021	.167	.069	3.10	.128	.060	.874	3.58	.0017	.172	.009	.405	6.53	1000
22	-24.38	-.40	.035	.188	-.020	3.22	.106	.058	.940	4.10	.0024	.243	.010	2.180	24.82	999
23	-30.48	-.50	.041	.204	-.048	3.03	.102	.048	1.063	4.64	.0022	.224	.009	1.046	8.38	1000
24	-36.58	-.60	.064	.194	-.022	3.13	.076	.041	1.286	5.56	.0018	.22[illegible]	.007	1.401	11.52	998
25	-42.67	-.70	.056	.195	-.094	2.83	.083	.040	1.281	5.90	.0015	.199	.008	1.855	14.37	999

TABLE IV-71

AXIAL AND AZIMUTHAL VELOCITY DATA AND CORRELATIONS

Test Date: 8/26/81 Run No.: 71 Flow Condition: 1 Geometry: 1

Axial Location: 254 mm (10.0 in.); $x/R_o = 4.16$

Pt No.	r mm +(θ=0) −(θ=180)	r/R_o	U m/s	u' m/s	S_u	K_u	W m/s	w' m/s	S_w	K_w	$\overline{uw}$ m^2/s^2	R_{uw}	σ_{uw} m^2/s^2	S_{uw}	K_{uw}	N
1	1.5	.025	.886	.219	-.631	4.15	-.041	.180	.175	4.77						993
2	4.6	.075	.876	.210	-.424	3.45	-.017	.218	1.834	13.22						991
3	7.6	.125	.880	.220	-.508	3.77	-.028	.186	.374	3.97						991
4	10.7	.175	.888	.209	-.634	3.90	.066	.395	2.413	9.37						998
5	13.7	.225	.886	.219	-.271	3.12	-.033	.198	.519	4.85						998
6	19.8	.325	.859	.242	-.424	3.35	-.010	.255	2.518	18.16						998
7	25.9	.425	.814	.271	-.314	2.84	-.012	.220	.239	3.48						994
8	32.0	.525	.746	.290	-.465	3.58	-.016	.245	.260	3.61						982
9	38.1	.624	.605	.305	-.349	3.40	-.014	.289	1.174	8.22						990
10	44.2	.724	.450	.318	-.476	3.70	.028	.317	1.464	8.91						492
11	-1.5	-.025	.898	.207	-.427	3.37	.040	.195	-.664	5.22						996
12	-4.6	-.075	.899	.231	-.574	3.92	.028	.187	-.206	3.77						997
14	-7.6	-.125	.874	.225	-.533	3.70	.040	.172	-.274	3.89						498
15	-10.7	-.175	.874	.238	-.583	3.72	.025	.195	-.339	3.27						498
16	-16.8	-.275	.845	.248	-.504	3.12	.042	.216	.169	3.88						497
17	-22.9	-.375	.794	.291	-.515	3.18	.007	.215	-.138	4.03						498
18	-29.0	-.475	.689	.289	-.175	3.07	.046	.244	.014	3.12						499
19	-35.1	-.575	.539	.288	-.081	2.75	.025	.255	-.196	2.63						498
20	-41.1	-.674	.406	.324	-.255	2.72	.042	.300	.722	4.24						499

TABLE IV-72

AXIAL VELOCITY, RADIAL VELOCITY, AND MOMENTUM TURBULENT TRANSPORT DATA AND CORRELATIONS

Test Date: 8/26/81 Run No.: 72 Flow Condition: 1 Geometry: 1

Axial Location: 254 mm (10.0 in.); x/R_o = 4.16

Pt No.	r mm +(θ=0) -(θ=180)	r/R_o	U m/s	u' m/s	S_u	K_u	V m/s	v' m/s	S_v	K_v	$\overline{uv}$ m^2/s^2	R_{uv}	σ_{uv} m^2/s^2	S_{uv}	K_{uv}	N
1	.0	.000	.873	.221	-.459	3.27	.058	.206	.644	4.31	-.0048	-.105				492
2	3.0	.050	.907	.219	-.307	3.42	.053	.194	-.004	6.20	.0019	.045				496
3	6.1	.100	.904	.211	-.301	3.23	.034	.177	-.296	3.34	.0023	.061				498
4	9.1	.150	.883	.225	-.573	3.59	.041	.188	-.483	4.89	.0029	.069				498
5	12.2	.200	.887	.227	-.326	3.05	.024	.216	-.791	4.12	.0066	.134				498
6	18.3	.300	.862	.266	-.312	2.86	.054	.203	-.356	3.48	.0125	.231				497
7	24.4	.400	.787	.298	-.440	3.43	.113	.210	-.313	3.00	.0086	.138	.059	.93	7.53	499
8	30.5	.500	.671	.301	-.160	3.28	.099	.235	-.457	3.50	.0212	.299	.071	2.18	13.16	495
9	36.6	.600	.559	.309	-.298	3.10	.129	.236	-.295	3.41	.0254	.349	.069	.87	6.63	493
10	42.7	.699	.369	.330	-.008	2.80	.119	.271	-.309	3.55	.0227	.254	.084	.59	6.57	247
11	-3.0	-.050	.901	.213	-.689	3.80	-.024	.173	-.102	4.05	.0027	.072	.043	1.28	16.55	496
12	-6.1	-.100	.887	.192	-.473	3.28	-.007	.190	.281	3.98	.0012	.033	.041	1.39	20.36	498
14	-9.1	-.150	.863	.214	-.321	3.37	.003	.187	.165	4.67	.0003	.009	.045	-.05	14.92	496
15	-12.2	-.200	.874	.229	-.449	2.96	.001	.181	-.139	3.88	.0012	.029	.049	1.48	12.76	494
16	-18.3	-.300	.859	.246	-.469	3.18	.026	.199	-.159	3.17	.0111	.226	.062	2.95	18.37	498
17	-24.4	-.400	.775	.280	-.436	3.46	.043	.223	-.196	3.51	.0151	.241	.070	2.51	17.42	498
18	-30.5	-.500	.681	.312	-.601	3.81	.085	.211	.078	3.11	.0165	.251	.075	1.59	13.62	249

TABLE IV-73

AXIAL AND AZIMUTHAL VELOCITY DATA AND CORRELATIONS

Test Date: 8/27/81 Run No.: 73 Flow Condition: 1 Geometry: 1

Axial Location: 305 mm (12.0 in.); x/R_o = 5.00

Pt No.	r mm +(θ=270) -(θ=90)	r/R_o	U m/s	u' m/s	S_u	K_u	W m/s	w' m/s	S_w	K_w	$\overline{uw}$ m^2/s^2	R_{uw}	σ_{uw} m^2/s^2	S_{uw}	K_{uw}	N
1	-2.03	.033	.774	.220	-.476	3.08	.003	.214	1.309	7.57						991
2	1.02	.017	.774	.217	-.492	8.16	.018	.254	2.656	16.16						999
3	4.06	.067	.774	.212	-.422	3.12	.014	.219	1.748	11.91						999
4	7.11	.116	.797	.221	-.674	3.93	.000	.198	1.361	10.32						997
5	10.16	.167	.768	.217	-.366	3.12	.007	.188	-.526	5.59						996
6	16.26	.266	.734	.232	-.431	3.42	-.006	.249	-.095	10.38						995
7	22.35	.366	.667	.246	-.332	3.20	.050	.383	1.231	11.01						998
8	28.45	.466	.614	.248	-.249	2.73	.148	.462	1.959	6.93						996
9	34.54	.566	.528	.247	-.206	2.87	-.014	.313	-1.223	12.09						996
10	40.64	.666	.450	.259	-.097	2.98	.005	.440	-.067	7.74						996
11	-2.03	-.033	.778	.214	-.432	3.21	-.013	.326	-1.354	10.66						996
12	-5.08	-.083	.756	.215	-.402	3.02	.015	.222	1.980	17.05						999
13	-8.13	-.133	.796	.214	-.615	3.73	.018	.193	.369	4.34						996
14	-11.18	-.183	.766	.224	-.401	3.26	.016	.217	1.459	10.80						999
15	-14.22	-.233	.756	.218	-.443	3.24	.007	.190	-.203	3.56						997
16	-20.32	-.333	.680	.242	-.423	3.05	.014	.208	.387	4.31						996
17	-26.42	-.433	.634	.240	-.224	3.01	.022	.264	2.595	19.16						996
18	-32.51	-.533	.561	.252	-.289	3.08	.016	.217	.009	3.26						977
19	-38.61	-.633	.475	.256	-.083	2.68	.041	.319	2.878	19.11						999
20	-44.70	-.733	.379	.248	-.110	2.86	.062	.338	2.59	14.34						992

TABLE IV-74

AXIAL VELOCITY, RADIAL VELOCITY, AND MOMENTUM TURBULENT TRANSPORT DATA AND CORRELATIONS

Test Date: 8/27/81 Run No.: 74 Flow Condition: 1 Geometry: 1

Axial Location: 305 mm (12.0 in.); $x/R_o = 5.00$

Pt No.	r mm +(θ=0) −(θ=180)	r/R_o	U m/s	u' m/s	S_u	K_u	V m/s	v' m/s	S_v	K_v	$\overline{uv}$ m^2/s^2	R_{uv}	σ_{uv} m^2/s^2	S_{uv}	K_{uv}	N
1	-1.27	-.021	.792	.203	-.359	3.16	.007	.175	-.082	3.60	[illegible]	-.024	.040	.431	15.93	499
2	1.78	.029	.777	.210	-.490	3.78	.014	.181	-.116	4.16	.0013	.035	.039	.575	9.19	497
3	4.83	.079	.786	.216	-.472	3.35	.027	.178	-.225	3.55	.0045	.117	.043	1.834	14.62	497
4	7.87	.129	.748	.214	-.159	2.53	.049	.194	-.277	3.50	.0017	.042	.043	-.107	8.07	496
5	10.92	.179	.752	.218	-.385	3.00	.030	.176	-.348	3.11	.0035	.092	.043	1.363	13.40	498
6	17.02	.279	.709	.231	-.615	4.09	.071	.198	-.298	3.73	.0078	.171	.047	2.719	21.57	498
7	23.11	.379	.684	.235	-.166	3.20	.089	.201	-.410	3.19	.0054	.114	.053	.327	11.54	499
8	29.21	.479	.603	.243	-.256	3.26	104	.222	-.039	3.28	.0132	.246	.056	2.187	13.75	498
9	35.31	.579	.519	.241	-.209	2.96	.126	.227	-.255	2.53	.0126	.229	.058	.902	7.11	499
10	41.40	.679	.392	.256	-.024	2.80	.102	.219	-.159	3.37	.0198	.354	.054	.830	6.20	497
11	-1.27	-.021	.773	.218	-.435	3.55	-.017	.177	.029	3.04	.0009	.023	.047	.504	18.88	499
12	-4.32	-.071	.776	.215	-.397	3.07	-.008	.182	-.154	3.72	.0055	.140	.043	1.064	10.74	499
14	-7.37	-.121	.757	.202	-.374	2.97	.004	.174	.024	3.28	-.0004	-.011	.038	-.535	9.47	498
15	-10.41	-.171	.747	.215	-.413	3.06	-.001	.230	-.322	6.91	.0051	.103	.051	1.181	15.92	494
16	-13.46	-.221	.733	.219	-.372	3.12	.014	.213	.112	4.78	.0057	.123	.049	1.655	15.32	497
17	-19.56	-.321	.701	.224	-.475	3.88	.041	.193	-.232	3.50	.0079	.183	.041	.931	7.38	494
18	-25.65	-.420	.609	.259	-.625	4.02	.024	.222	-.609	6.53	.0121	.211	.054	.779	9.87	495
19	-31.75	-.520	.571	.253	-.152	2.62	.067	.210	-.131	3.10	.0184	.361	.050	1.089	5.08	247
20	-37.85	-.620	.473	.251	-.300	3.00	.070	.220	.452	3.78	.0107	.193	.052	.293	6.68	248
21	-43.94	-.720	.374	.257	-.265	2.99	.096	.223	.327	3.24	.0194	.338	.061	-.472	11.81	247

TABLE V-A

LISTING OF BASIC PROGRAM USED TO EDIT
TWO-COMPONENT LV DATA STORED ON DISKS

```
10 D1$='DY1:R'
12 R1$='R'
14 P1$='P'
16 PRINT 'TWO-DIMENSIONAL DATA EDITING - CORRELATION'
20 PRINT
30 PRINT 'RUN #', \ INPUT R2$
35 PRINT 'DATE ', \ INPUT D0$
40 PRINT
50 DIM P2(2),P5(2),L1(2),L2(2),F0(2)
52 L1(1)=.5145 \ L1(2)=.488
54 PRINT 'P5=PULSE STRETCHER (GREEN 1 OR 100)='; \ INPUT P5(1)
56 PRINT 'P5=PULSE STRETCHER (BLUE 1 OR 100)='; \ INPUT P5(2)
58 PRINT 'P2=MIN. FREQ. SCALE (GREEN, MHZ)='; \ INPUT P2(1)
60 P3=125
62 PRINT 'P2=MIN. FREQ. SCALE (BLUE, MHZ)='; \ INPUT P2(2)
64 PRINT 'L2= DUAL BEAM INCLUDED ANGLE (GREEN, DEG.)='; \ INPUT L2(1)
66 PRINT 'L2= DUAL BEAM INCLUDED ANGLE (BLUE, DEG.)='; \ INPUT L2(2)
68 PRINT 'F0=FREQ. OFFSET (GREEN, MHZ)='; \ INPUT F0(1)
70 P4=8
72 PRINT 'F0=FREQ. OFFSET (BLUE, MHZ)='; \ INPUT F0(2)
73 PRINT 'CLOCK SCALE(MSEC)='; \ INPUT T1
74 PRINT 'VELOCITY COMPONENT (GREEN)='; \ INPUT A7$
76 PRINT 'VELOCITY COMPONENT (BLUE)='; \ INPUT A8$
77 P5=1 \ L1(1)=.5145 \ L1(2)=.488
78 PRINT 'POINT # ', \ INPUT P2$
79 PRINT 'POSITION='; \ INPUT A9$
80 DIM D1(1000),D2(1000),C1(1),C2(1)
81 DIM A(1000),B(1000)
82 OPEN D1$&R2$&P1$&P2$ FOR INPUT AS FILE #1
84 INPUT #1:N0
86 FOR I=1 TO 1000
88 D1(I)=0 \ D2(I)=0
90 NEXT I
110 K=1
111 FOR I=1 TO N0
112 INPUT #1:D1(I)
113 INPUT #1:C1(1)
114 INPUT #1:D2(I)
115 INPUT #1:C2(1)
116 NEXT I
117 CLOSE #1
119 P1=3.14159
120 C2=L1(K)/2/SIN(L2(K)/2*P1/180)
125 V3=C2*(P2(K)-F0(K))
130 V4=C2*(5*P2(K)-F0(K))
135 C1=100/(V4-V3)
140 PRINT 'COEF FOR DATA RED(FT/SEC/MHZ),C2=';C2
150 PRINT 'VMIN=';V3;'MPS','VMAX=';V4;'MPS'
```

```
250 DIM N1(100)
260 IF K=2 GO TO 296
291 N5=NO
292 PRINT 'RESULTS FOR VELOCITY COMPONENT='+A7$
294 GO TO 300
296 PRINT 'RESULTS FOR VELOCITY COMPONENT='+A8$
300 N9=0
305 F1=0
310 FOR I=1 TO 100 \ N1(I)=0 \ NEXT I
320 D1=1 \ D2=1
400 FOR N=1 TO NO
410 IF K=2 GO TO 416
412 E=D1(D1)
413 D1=D1+1
414 GO TO 440
416 E=D2(D2)
418 D2=D2+1
436 IF E=0 GO TO 480
440 F=P3*P4*P5(K)/E
445 V=C2*(F-FO(K))
451 IF V>V4 GO TO 454
452 IF V>=V3 GO TO 460
454 N9=N9+1
455 GO TO 480
460 I=INT((V-V3)*C1)
470 N1(I)=N1(I)+1
480 NEXT N
485 PRINT 'HISTOGRAM BASED ON';N;'SAMPLES'
495 FOR I=1 TO 100
500 IF N1(I)=0 GO TO 530
501 K3=V3+(I+.5)/C1
502 PRINT I,N1(I),K3
508 IF F1=1 GO TO 524
512 F1=1 \ T3=N1(I)
524 IF N1(I)<=T3 GO TO 530
526 T3=N1(I)
530 NEXT I
616 FOR I=1 TO 4 \ PRINT  \ NEXT I
618 FOR I=1 TO 100
619 Z=INT(N1(I)/T3*50)
620 IF (N1(I)/T3)<.01 GO TO 622
621 PRINT TAB(Z);I
622 NEXT I
623 PRINT 'INPUT N2,N3'; \ INPUT N2,N3
624 V9=N3/C1+V3
625 V8=N2/C1+V3
627 V0=(V9-V8)/20
628 U4=0
630 N4=0 \ V1=0 \ V2=0 \ U3=0
632 IF K=2 GO TO 640
634 M1=V8 \ M2=V0
636 GO TO 650
640 M3=V8 \ M4=V0
650 D1=1 \ D2=1
660 FOR N=1 TO NO
665 IF K=2 GO TO 687
670 E=D1(D1)
```

```
675 D1=D1+1
680 IF E=0 GO TO 740
686 GO TO 690
687 E=D2(D2)
688 D2=D2+1
689 IF E=0 GO TO 740
690 F=P3*P4*P5(K)/E
700 V=C2*(F-F0(K))
704 IF V<V8 GO TO 732
706 IF V>V9 GO TO 732
712 N4=N4+1
722 IF K=2 GO TO 728
724 A(N)=V
726 GO TO 740
728 B(N)=V
730 GO TO 740
732 IF K=2 GO TO 738
734 A(N)=-100
736 GO TO 740
738 B(N)=-100
740 NEXT N
741 K=K+1
742 IF K=2 GO TO 120
743 K=1 \ N4=0
744 FOR I=1 TO 100 \ N1(I)=0 \ NEXT I
745 FOR N=1 TO N0
746 IF A(N)=-100 GO TO 753
747 IF B(N)=-100 GO TO 753
748 IF K=2 GO TO 751
749 I=INT(A(N)/.1)+50
750 GO TO 752
751 I=INT(B(N)/.1)+50
752 N1(I)=N1(I)+1 \ N4=N4+1
753 NEXT N
754 U3=0 \ U4=0
755 IF K=2 GO TO 767
756 FOR I=1 TO 5 \ PRINT  \ NEXT I
757 PRINT '      ';A7$;' HISTOGRAM BASED ON';N4;'EDITED SAMPLES'
758 PRINT 'I','N1(I)','V(I)','P1(I)','P2(I)'
759 FOR I=1 TO 100
760 IF N1(I)=0 GO TO 765
761 K3=I*.1-4.95
762 R2=N1(I)/N4
763 U3=U3+R2
764 PRINT I,N1(I),K3,R2,U3
765 NEXT I
766 GO TO 778
767 FOR I=1 TO 5 \ PRINT  \ NEXT I
768 PRINT '      ';A8$;' HISTOGRAM BASEDON';N4;'EDITED SAMPLES'
769 PRINT 'I','N2(I)','V(I)','P1(I)','P2(I)'
770 FOR I=1 TO 100
771 IF N1(I)=0 GO TO 776
772 K3=I*.1-4.95
773 R2=N1(I)/N4
774 U4=U4+R2
775 PRINT I,N1(I),K3,R2,U4
776 NEXT I
```

```
777 FOR J=1 TO 5 \ PRINT  \ NEXT J
778 K=K+1 \ N4=0
779 IF K=2 GO TO 744
780 A1=0 \ A2=0 \ A3=0 \ A4=0
781 N5=0
782 B1=0 \ B2=0 \ B3=0 \ B4=0
784 U4=0 \ W2=0 \ W3=0 \ W4=0
790 FOR J=1 TO 100 \ N1(J)=0 \ NEXT J
792 FOR N=1 TO N0
794 IF A(N)=-100 GO TO 820
796 IF B(N)=-100 GO TO 820
798 A1=A1+A(N)
800 A2=A2+(A(N))^2
802 A3=A3+(A(N))^3
804 A4=A4+(A(N))^4
806 B1=B1+B(N)
808 B2=B2+(B(N))^2
810 B3=B3+(B(N))^3
812 B4=B4+(B(N))^4
814 N5=N5+1
820 NEXT N
830 A1=A1/N5
832 B1=B1/N5
834 A4=A4/N5-4*A1*A3/N5+6*(A1^2)*A2/N5-3*(A1^4)
836 B4=B4/N5-4*B1*B3/N5+6*(B1^2)*B2/N5-3*(B1^4)
838 A3=A3/N5-3*A1*A2/N5+2*(A1^3)
840 B3-B3/N5-3*B1*B2/N5+2*(B1^3)
842 A2=A2/N5-(A1^2)
844 A2=SQR(A2)
846 B2=B2/N5-(B1^2)
848 B2=SQR(B2)
860 PRINT '       RESULTS FOR RUN';R2$;'POINT';P2$
862 FOR J=1 TO 4 \ PRINT  \ NEXT J
864 PRINT '       RESULTS FOR COMPONENT   ';A7$
866 FOR J=1 TO 2 \ PRINT  \ NEXT J
868 PRINT 'VBAR=';A1;'MPS'
870 PRINT 'VRMS=';A2;'MPS'
872 PRINT 'THIRD MOMENT OF TURBULENCE=';A3;'MPS^3'
874 R3=A3/(A2^3)
876 PRINT '3RD CORRELATION COEFFICIENT=';R3
878 PRINT 'FOURTH MOMENT OF TURBULENCE=';A4;'MPS^4'
880 R4=A4/(A2^4)
882 PRINT '4TH CORRELATION COEFFICIENT=';R4
890 FOR J=1 TO 4 \ PRINT  \ NEXT J
892 PRINT '      RESULTS FOR COMPONENT  ';A8$
894 FOR J=1 TO 2 \ PRINT  \ NEXT J
896 PRINT 'VBAR=';B1;'MPS'
898 PRINT 'VRMS=';B2;'MPS'
900 PRINT 'THIRD MOMENT OF TURBULENCE=';B3;'MPS^3'
902 R3=B3/(B2^3)
904 PRINT '3RD CORRELATION COEFFICIENT=';R3
906 PRINT 'FOURTH MOMENT OF TURBULENCE=';B4;'MPS^4'
908 R4=B4/(B2^4)
910 PRINT '4TH CORRELATION COEFFICIENT=';R4
944 PRINT
```

```
946 PRINT
948 W2=0 \ W3=0 \ W4=0
949 N5=0 \ U4=0 \ R8=0
950 FOR N=1 TO NO
952 IF A(N)=-100 GO TO 972
954 IF B(N)=-100 GO TO 972
956 W1=(B(N)-B1)*(A(N)-A1)
960 I=INT(W1/.01)+50
962 IF I>99 GO TO 972
964 IF I<1 GO TO 972
966 N5=N5+1
967 U4=U4+W1
968 W2=W2+W1^2
969 W3=W3+W1^3
970 N1(I)=N1(I)+1
971 W4=W4+W1^4
972 NEXT N
974 U4=U4/N5
975 FOR I=1 TO 5 \ PRINT  \ NEXT I
980 PRINT 'UV HISTOGRAM BASEDON ';N5;'SAMPLES'
981 FOR I=1 TO 2 \ PRINT  \ NEXT I
983 PRINT 'I','N2(I)','UV(I)','P1(I)','P2(I)'
984 FOR J=1 TO 100
985 IF N1(J)=0 GO TO 994
986 K3=J*.01-.495
988 P9=N1(J)/N5
990 R8=R8+P9
992 PRINT J,N1(J),K3,P9,R8
994 NEXT J
996 FOR J=1 TO 5 \ PRINT  \ NEXT J
1000 PRINT '        UV CORRELATION RESULTS'
1004 FOR I=1 TO 4 \ PRINT  \ NEXT I
1008 W4=W4/N5-4*U4*W3/N5+6*(U4^2)*W2/N5-3*(U4^4)
1012 W3=W3/N5-3*U4*W2/N5+2*(U4^3)
1016 W2=W2/N5-(U4^2)
1020 PRINT 'UV CORRELATION =';U4;'MPS^2'
1024 PRINT '2ND MOMENT OF UV HISTOGRAM=';W2;'MPS^4'
1028 PRINT '3RD MOMENT OF UV HISTOGRAM=';W3;'MPS^6'
1032 PRINT '4TH MOMENT OF UV HISTOGRAM=';W4;'MPS^8'
1080 PRINT 'END OF RUN';R2$;'OINT';P2$
1085 FOR I=1 TO 10 \ PRINT  \ NEXT I
1090 GO TO 78
1100 STOP
```

TABLE V-B

LISTING OF BASIC PROGRAM USED TO EDIT
LV/LIF DATA STORED ON DISKS

```
10 D1$='DY1:R'
12 R1$='R'
14 P1$='P'
16 PRINT 'LDV - LIF DATA EDITING'
20 PRINT 'RUN #', \ INPUT R2$
30 PRINT  \ PRINT
40 PRINT
50 PRINT 'MIN FREQ SCALE(MHZ)', \ INPUT P2
60 P3=125
70 P4=8
80 PRINT 'P5= PULSE STRETCHER(1 OR 100)='; \ INPUT P5
90 PRINT 'L1=LASER WAVELENGTH(MICRONS)='; \ INPUT L1
100 PRINT 'L2= DUAL BEAM INC ANGLE(DEG)='; \ INPUT L2
110 PRINT 'FO=FREQ OFFSET,ZERO VEL(MHZ)='; \ INPUT FO
112 PRINT 'CBAR(NO DYE)='; \ INPUT CO
113 PRINT 'CBAR(CENTERLINE)='; \ INPUT C9
114 PRINT 'C-TO -F SCALING PARAMETER='; \ INPUT SO
115 PRINT 'DATE', \ INPUT DO$
119 P1=3.14159
120 C2=L1/2/SIN(L2/2*P1/180)
125 V3=C2*(P2-FO)
130 V4=C2*(5*P2-FO)
135 C1=100/(V4-V3)
140 PRINT 'COEF FOR DATA RED(MPS/MHZ),C2+';C2
150 PRINT 'VMIN=';V3;'MPS','VMAX=';V4;'MPS'
250 DIM N1(100),N3(100)
251 DIM E1(1000),E2(1000)
255 DIM D1(1000),C1(1)
257 DIM V1(1000),N2(100)
280 PRINT 'POINT #', \ INPUT P2$
281 PRINT 'POSITION', \ INPUT A9$
291 N5=NO
300 N9=0
305 F1=0
310 FOR I=1 TO 100 \ N1(I)=0 \ NEXT I
316 FOR I=1 TO 1000 \ D1(I)=0 \ NEXT I
318 FOR I=1 TO 1000 \ E2(I)=0 \ NEXT I
320 OPEN D1$&R2$&P1$&P2$ FOR INPUT AS FILE #1
324 INPUT #1:NO
326 FOR I=1 TO NO
328 INPUT #1:D1(I)
330 INPUT #1:C1(1)
332 INPUT #1:E1(I)
336 E2(I)=SO*(E1(I)-CO)/(C9-CO)
340 NEXT I
344 CLOSE #1
```

```
400 FOR N=1 TO NO
410 T2=D1(N)
420 IF T2=2.5 GO TO 410
440 F=F3*F4*F5/T2
445 V=C2*(F-FO)
446 V1(N)=V
451 IF V>V4 GO TO 454
452 IF V>=V3 GO TO 460
454 N9=N9+1
455 GO TO 480
460 I=INT((V-V3)*C1)
470 N1(I)=N1(I)+1
480 NEXT N
482 FOR J=1 TO 3 \ PRINT  \ NEXT J
485 PRINT 'HISTOGRAM BASED ON';N;'SAMPLES'
495 FOR I=1 TO 100
500 IF N1(I)=0 GO TO 540
501 K3=V3+(I+.5)/C1
502 PRINT I,N1(I),K3
505 C3=C3+1 \ C4=I
508 IF F1=1 GO TO 524
512 F1=1 \ T3=N1(I)
514 C5=I
524 IF N1(I)<=T3 GO TO 540
526 T3=N1(I)
540 NEXT I
560 FOR J=1 TO 3 \ PRINT  \ NEXT J
570 FOR I=1 TO 100
575 Z=INT(N1(I)/T3*50)
578 IF (N1(I)/T3)<.01 GO TO 590
580 PRINT TAB(Z);I
590 NEXT I
623 PRINT 'INPUT N2,N3'; \ INPUT N2,N3
624 V9=N3/C1+V3
625 V8=N2/C1+V3
627 V0=(V9-V8)/20
628 U4=0
629 Q3=0 \ Q4=0 \ W2=0 \ W3=0 \ W4=0
630 N4=0 \ V1=0 \ V2=0 \ U3=0
631 Q1=0 \ Q2=0 \ G1=0
632 G2=0
640 FOR I=1 TO 100 \ N1(I)=0 \ NEXT I
650 FOR J=1 TO 100 \ N2(J)=0 \ NEXT J
655 FOR J=1 TO 100 \ N3(J)=0 \ NEXT J
660 FOR N=1 TO NO
700 V=V1(N)
702 I=INT(V/.1)+50
704 IF V<V8 GO TO 740
706 IF V>V9 GO TO 740
708 N1(I)=N1(I)+1
710 V1=V1+V
720 V2=V2+V*V
725 U3=U3+V^3
726 U4=U4+V^4
730 N4=N4+1
731 Q1=Q1+E2(N)
```

```
732 Q2=Q2+E2(N)*E2(N)
733 G1=G1+V*E2(N)
734 Q3=Q3+(E2(N))^3
735 Q4=Q4+(E2(N))^4
740 NEXT N
750 V1=V1/N4
752 U4=U4/N4-4*V1*U3/N4+6*(V1^2)*V2/N4-3*(V1^4)
754 U3=U3/N4-3*V1*V2/N4+2*(V1^3)
755 Q1=Q1/N4
756 Q4=Q4/N4-4*Q1*Q3/N4+6*(Q1^2)*Q2/N4-3*(Q1^4)
757 Q3=Q3/N4-3*Q1*Q2/N4+2*(Q1^3)
760 V2=V2/N4-V1^2
761 U2=SQR(V2)
764 Q2=Q2/N4-Q1*Q1
765 Q2=SQR(Q2)
766 G1=G1/N4-Q1*V1
767 N6=0 \ P8=0 \ R9=0 \ N7=0 \ R8=0
768 IF (Q2/Q1)<1.00000E-03 GO TO 809
770 A1=Q2/3
771 B2=2*Q2*U2
772 FOR N=1 TO N0
774 IF V1(N)<V8 GO TO 808
776 IF V1(N)>V9 GO TO 808
778 J=INT(E2(N)/.02)+25
779 IF J<1 GO TO 808
780 IF J>99 GO TO 808
782 N2(J)=N2(J)+1
784 N6=N6+1
786 R2=((V1(N)-V1)*(E2(N)-Q1))-G1
787 J1=INT(R2/.04)+50
788 IF J1<1 GO TO 808
790 IF J1>99 GO TO 808
792 N3(J1)=N3(J1)+1
794 N7=N7+1
797 G2=G2+R2
798 W2=W2+R2^2
799 W3=W3+R2^3
800 W4=W4+R2^4
808 NEXT N
809 FOR N=1 TO 10 \ PRINT  \ NEXT N
810 PRINT 'DATA OUTPUT FOR RUN';R2$;' POINT';P2$
811 PRINT A9$
820 PRINT 'N0=';N0,'N4=';N4
821 G2=G2/N7
822 W4=W4/N7
824 W3=W3/N7
826 W2=W2/N7
827 W1=SQR(W2)
828 S3=W3/(W1^3)
829 S4=W4/(W1^4)
830 PRINT 'VBAR=';V1;'MPS'
850 PRINT 'VRMS=';U2;'MPS'
858 R3=U3/((U2)^3)
868 R4=U4/((U2)^4)
872 H3=S0*W1
874 PRINT 'FBAR=';Q1
```

```
875 PRINT 'FRMS=';Q2
877 PRINT 'F'V' BAR =';G1;'MPS'
878 PRINT 'F'V' RMS =';W1;'MPS'
880 PRINT 'DATE',D0$
885 PRINT 'DATA STORED AS FILE ';R1$&R2$&P1$&P2$
886 FOR I=1 TO 5 \ PRINT  \ NEXT I
888 PRINT 'VELOCITY HISTOGRAM BASED ON';N4;'SAMPLES'
890 PRINT 'I','N1(I)','V(I)','P1(I)','P2(I)'
892 FOR I=1 TO 100
894 IF N1(I)=0 GO TO 899
895 K3=I*.1-4.95
896 P9=N1(I)/N4
897 R9=R9+P9
898 PRINT I,N1(I),K3,P9,R9
899 NEXT I
900 FOR J=1 TO 5 \ PRINT  \ NEXT J
901 IF N6=0 GO TO 920
902 PRINT 'CONCENTRATION HISTOGRAM BASED ON';N6;'SAMPLES'
904 FOR J=1 TO 2 \ PRINT  \ NEXT J
906 PRINT 'I','N2(I)','C(I)','P1(I)','P2(I)'
907 FOR J=1 TO 100
908 K3=J*.02-.49
909 IF N2(J)=0 GO TO 914
910 P9=N2(J)/N6
911 P8=P8+P9
912 PRINT J,N2(J),K3,P9,P8
914 NEXT J
920 IF N7=0 GO TO 980
924 FOR J=1 TO 5 \ PRINT  \ NEXT J
928 PRINT 'C-V HISTOGRAM BASED ON';N7;'SAMPLES'
930 FOR J=1 TO 2 \ PRINT  \ NEXT J
932 PRINT 'I','N3(I)','CV(I)','P1(I)','P2(I)'
936 FOR J=1 TO 100
940 IF N3(J)=0 GO TO 960
944 K3=J*.04-1.98
948 P9=N3(J)/N7
952 R8=R8+P9
956 PRINT J,N3(J),K3,P9,R8
960 NEXT J
976 FOR J=1 TO 4 \ PRINT  \ NEXT J
985 PRINT
990 PRINT
992 PRINT '        MOMENTS OF PROBABILITY DISTRIBUTIONS'
994 FOR J=1 TO 3 \ PRINT  \ NEXT J
996 PRINT '                        VELOCITY'
997 PRINT  \ PRINT
998 PRINT 'THIRD MOMENT OF TURBULENCE=';U3;'MPS^3'
1000 PRINT '3RD CORRELATION COEFFICIENT=';R3
1002 PRINT 'FOURTH MOMENT OF TURBULENCE='U4;'MPS^4'
1004 PRINT '4TH CORRELATION COEFFICIENT=';R4
1010 FOR N=1 TO 5 \ PRINT  \ NEXT N
1012 PRINT '                    CONCENTRATION'
```

```
1014 PRINT  \ PRINT
1016 PRINT 'THIRD MOMENT OF CONCENTRATION=';Q3
1018 R3=Q3/(Q2^3)
1020 PRINT '3RD CORRELATION COEFFICIENT=';R3
1022 PRINT 'FOURTH MOMENT OF CONCENTRATION=';Q4
1024 R4=Q4/(Q2^4)
1026 PRINT '4TH CORRELATION COEFFICIENT=';R4
1028 FOR J=1 TO 5 \ PRINT  \ NEXT J
1030 PRINT '        VELOCITY-CONCENTRATION PRODUCT'
1032 PRINT  \ PRINT
1033 R3=G1/U2/Q2
1034 PRINT 'PRODUCT CORRELATION COEFFICIENT='R3
1035 PRINT 'SECOND MOMENT OF PRODUCT=';W2;'MPS^2'
1036 PRINT 'THIRD MOMENT OF PRODUCT=';W3;'MPS^3'
1038 PRINT '3RD CORRELATION COEFFICIENT=';S3
1040 PRINT 'FOURTH MOMENT OF PRODUCT=';W4;'MPS^4'
1042 PRINT '4TH CORRELATION COEFFICIENT=';S4
1044 PRINT 'G2=';G2
1078 PRINT  \ PRINT  \ PRINT
1080 PRINT 'END OF RUN';R2$;'POINT';P2$
1100 GO TO 280
```

SHEAR REGIONS OF COAXIAL JETS CONFINED IN AN ENLARGED DUCT

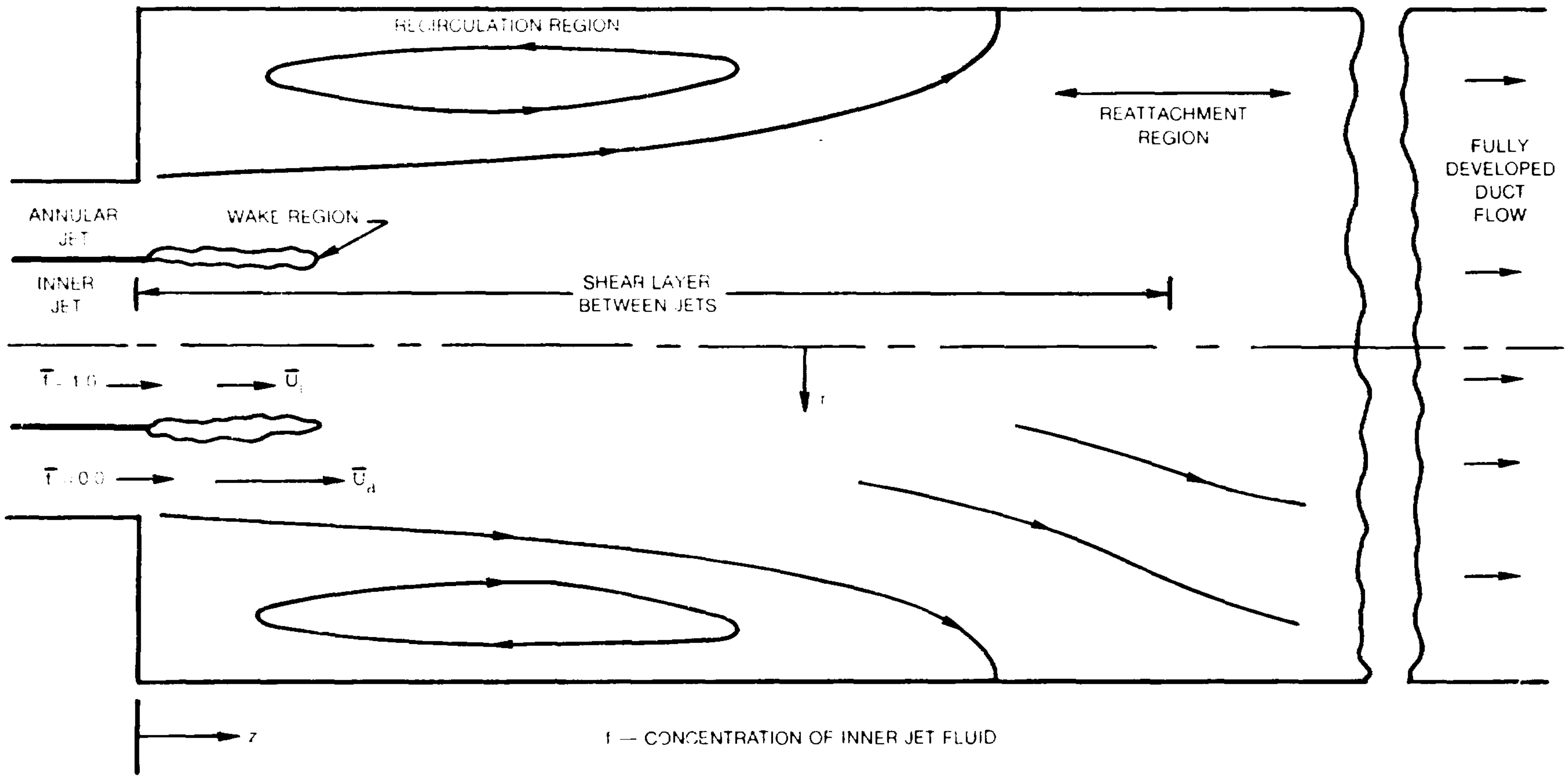

FIG. 1

81-12-38-1

SKETCH OF TEST SECTION

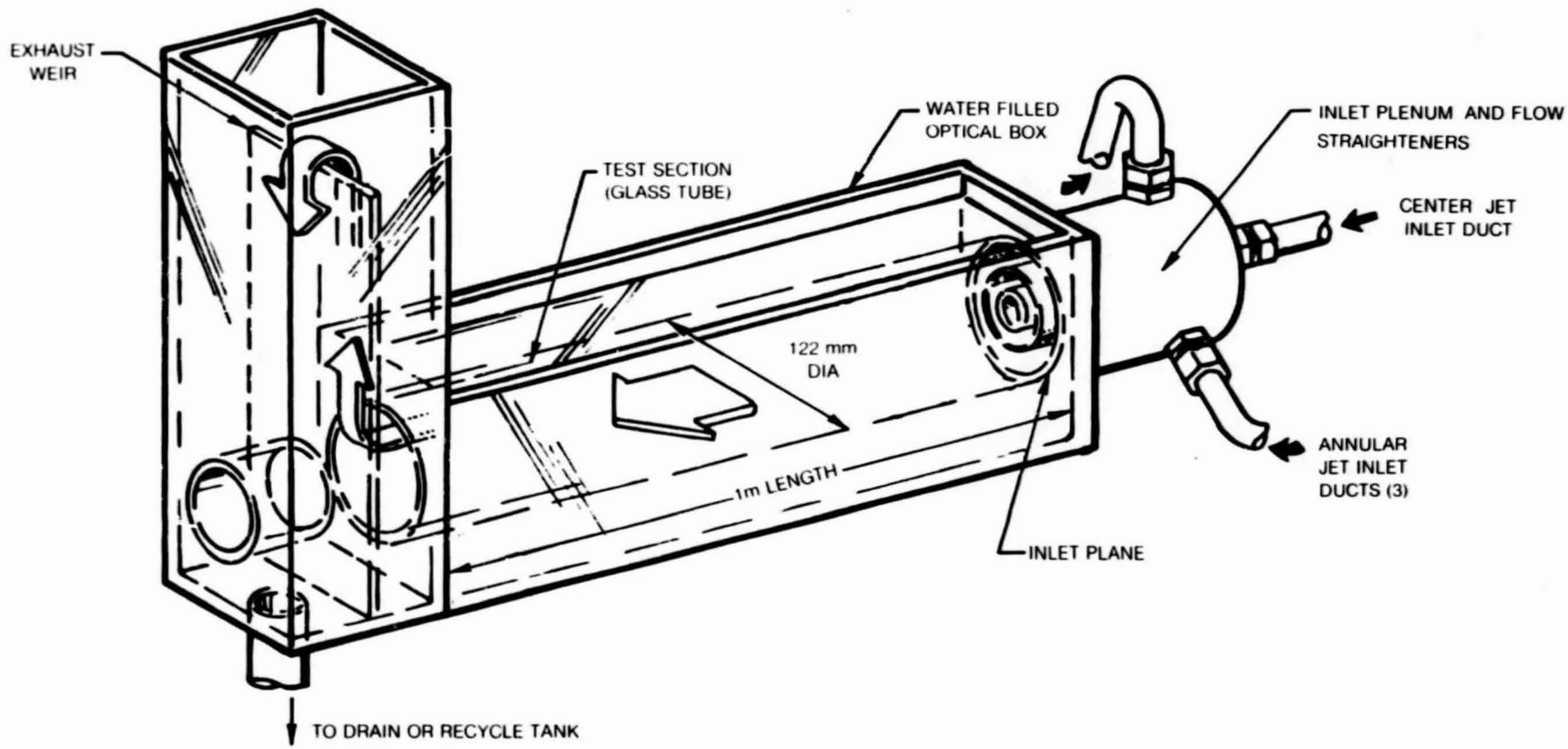

FIG. 2

81-12-38-2

SKETCHES OF TEST SECTION INLET REGION WITH VELOCITY AND COORDINATE SYSTEM

DIMENSION	R_{i1}	R_{i2}	R_a	R_o	L
LENGTH (mm)	12.5	15.3	29.5	61.0	1016
LENGTH (in.)	0.492	0.601	1.162	2.402	40

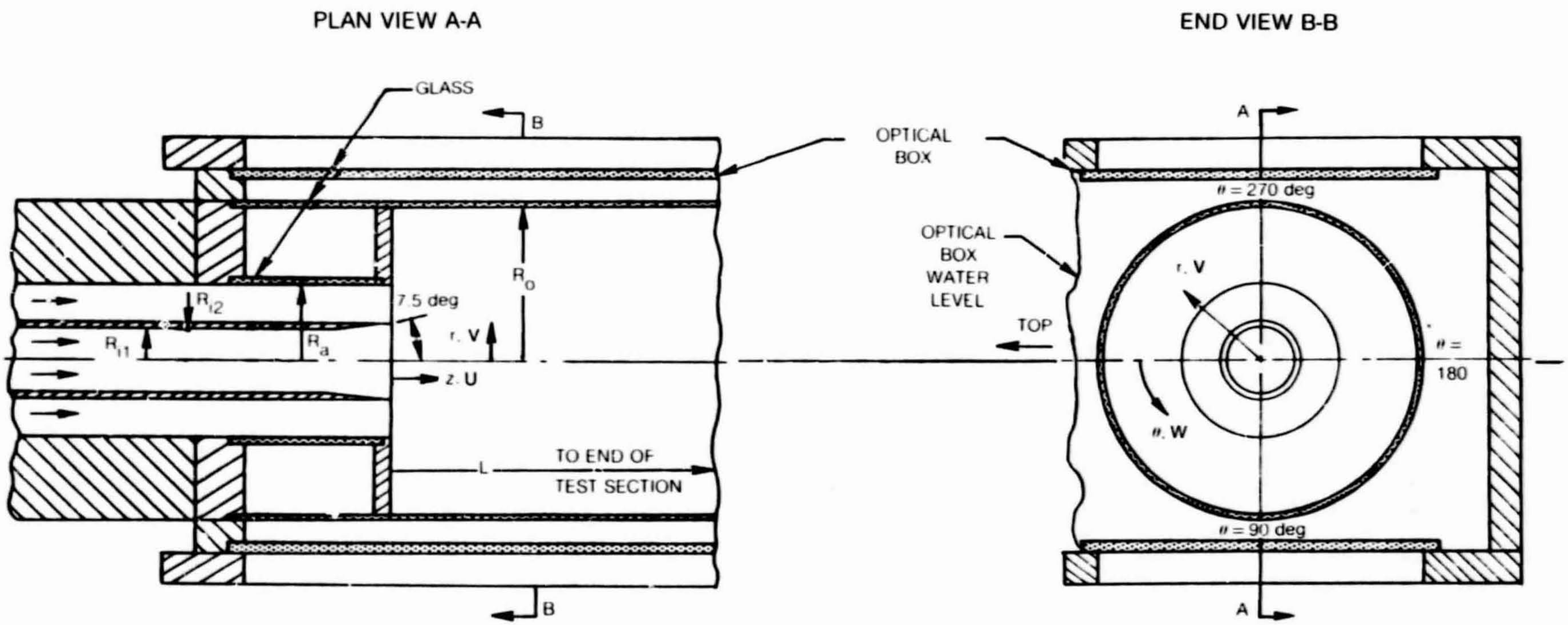

FIG. 3

81–12–38–3

SCHEMATIC OF FLOW COMPONENTS FOR TEST APPARATUS

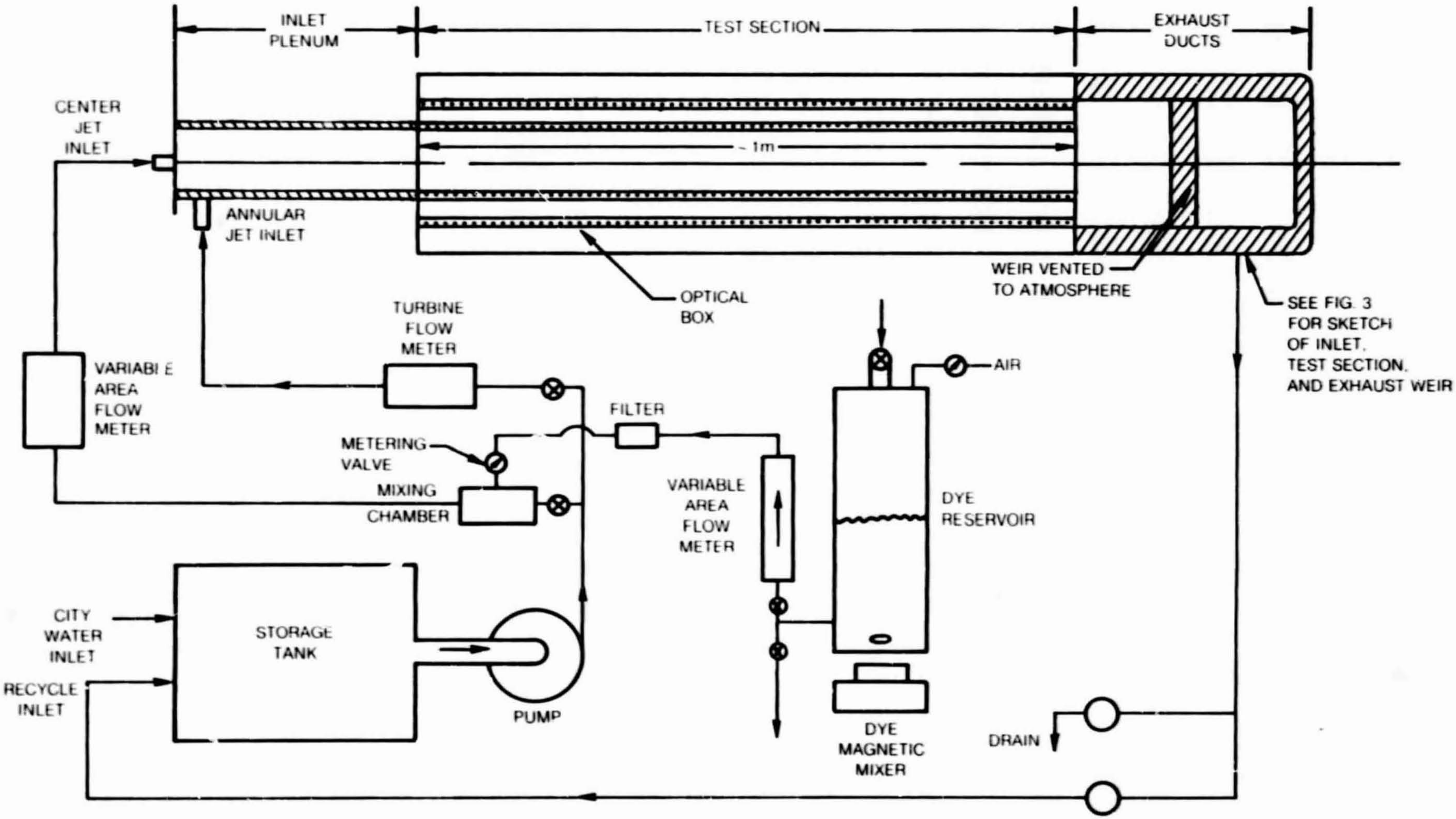

FIG. 4

81–12–38–4

OPTICAL ARRANGEMENT FOR FLOW VISUALIZATION PHOTOGRAPHS AND MOTION PICTURES IN r-z PLANE

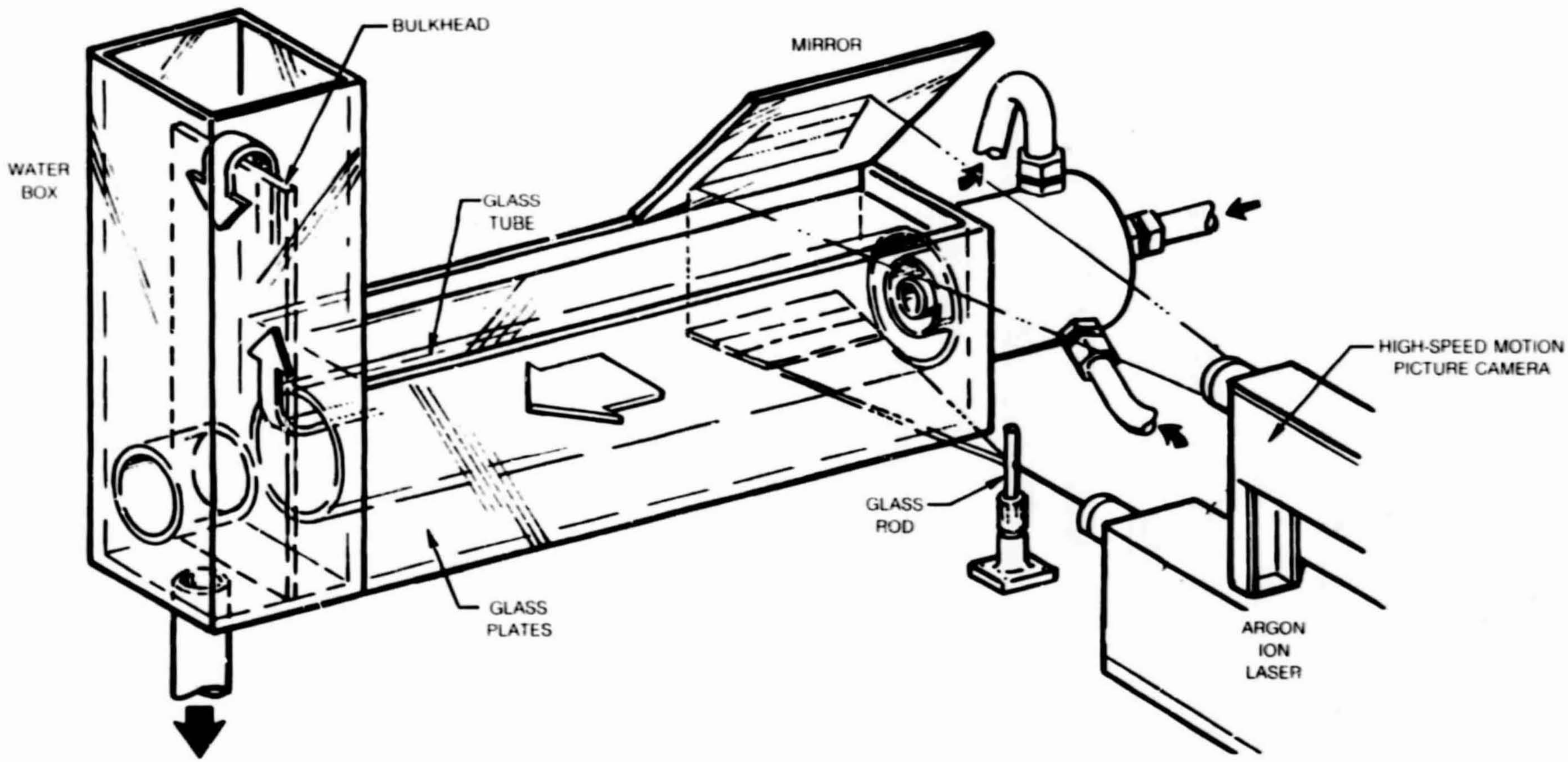

FIG. 5

81–12–38–5

OPTICAL ARRANGEMENT FOR FLOW VISUALIZATION PHOTOGRAPHS AND MOTION PICTURES IN r-θ PLANE

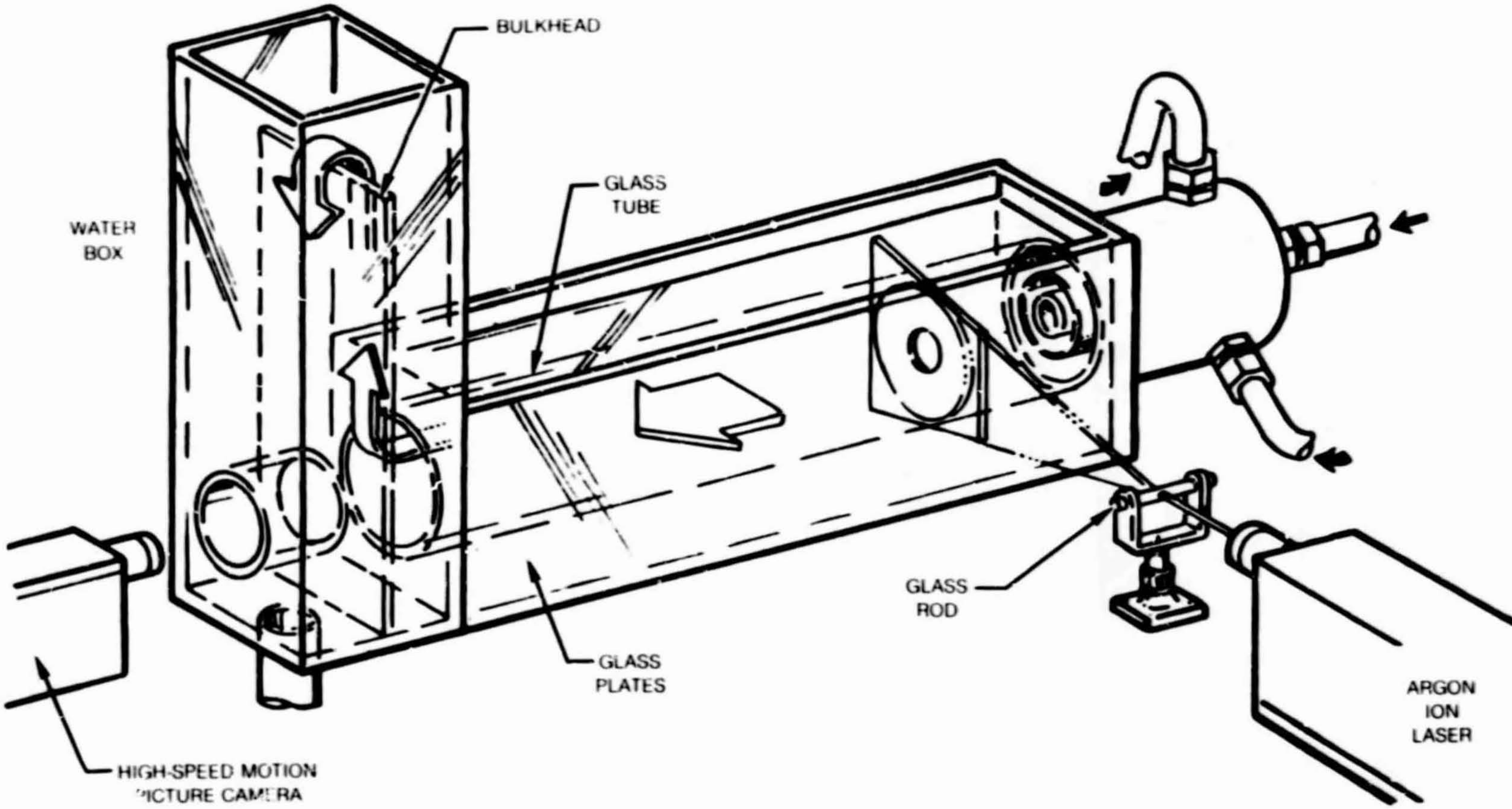

FIG. 6

81-12-38-6

R81-915540-9

OPTICAL ARRANGEMENT FOR TWO COMPONENT LV MEASUREMENTS

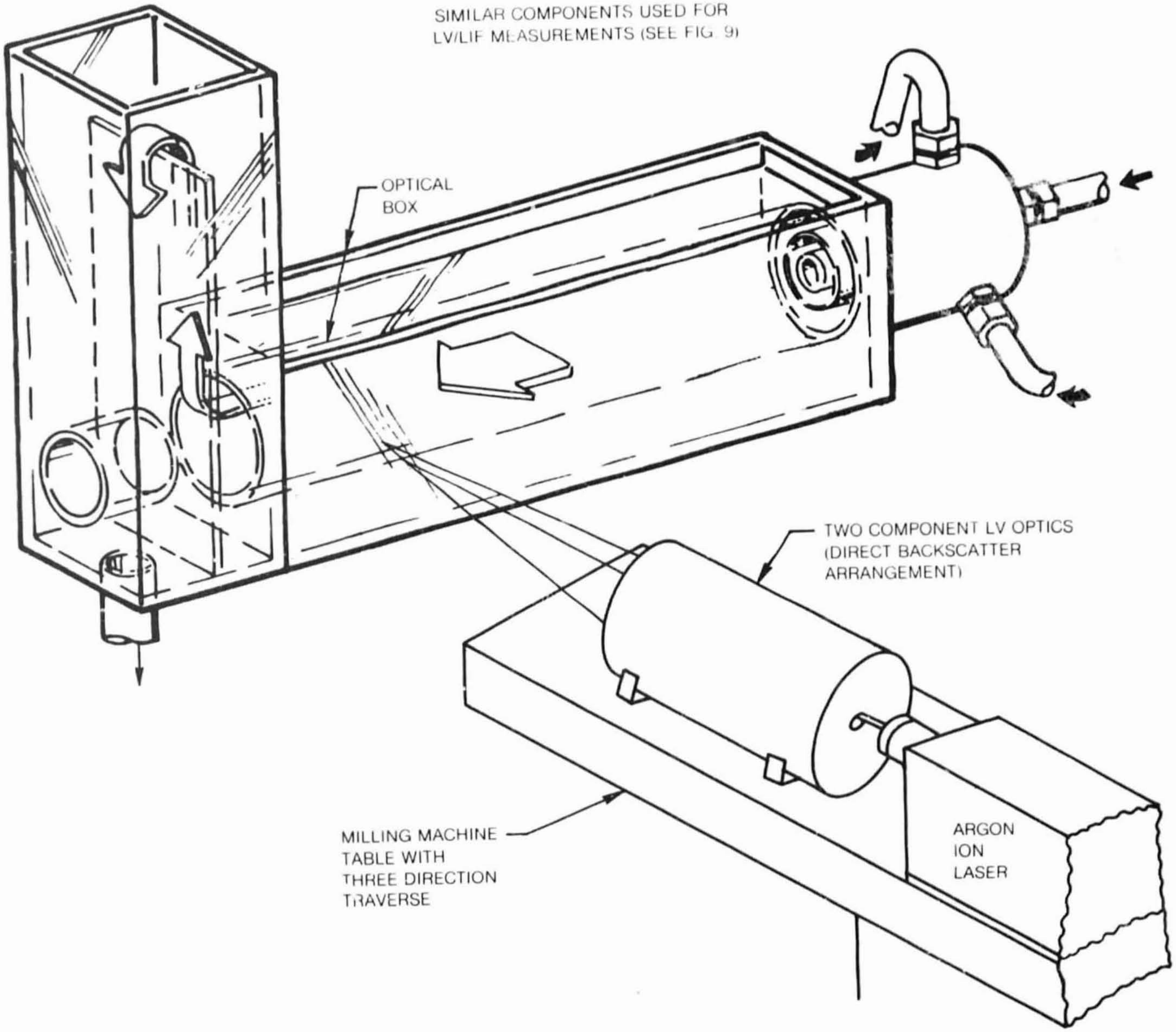

FIG. 7

C-2

81-12-38-7

SKETCH OF OPTICAL COMPONENTS AND BEAM PATHS USED FOR TWO COMPONENT VELOCITY MEASUREMENTS

DISA 55 × 00 OPTIC COMPONENTS

02 — BACKCOVER PLATE WITH POLARIZATION ROTATOR
03 — BEAM SPLITTER SECTION 1
04 — BRAGG CELL SECTIONS
05 — BEAM SPLITTER SECTION 2
06 — BACKSCATTER SECTION WITH GREEN LASER LINE FILTER
07 — BACKSCATTER SECTION WITH BLUE LASER LINE FILTER
08 — PHOTOMULTIPLIER TUBE
09 — LENS MOUNT
10 — PINHOLE SECTION
11 — BEAM TRANSLATOR
12 — BEAM EXPANDER

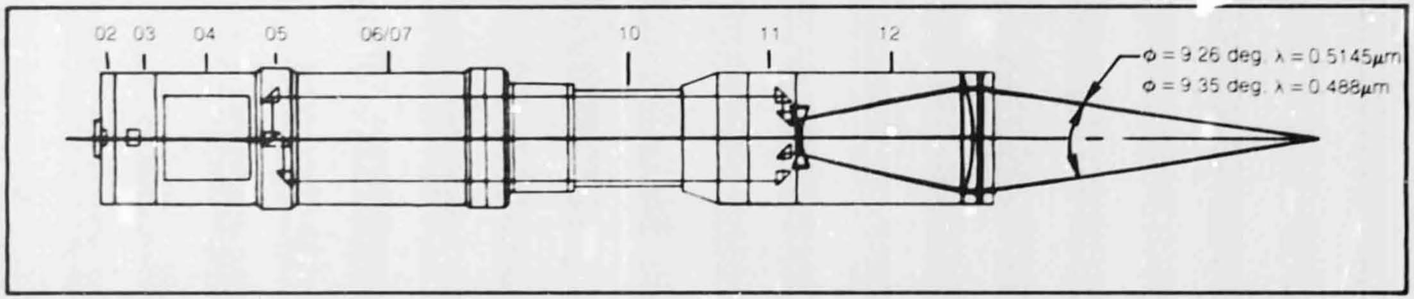

TRANSMITTER BEAM PATH

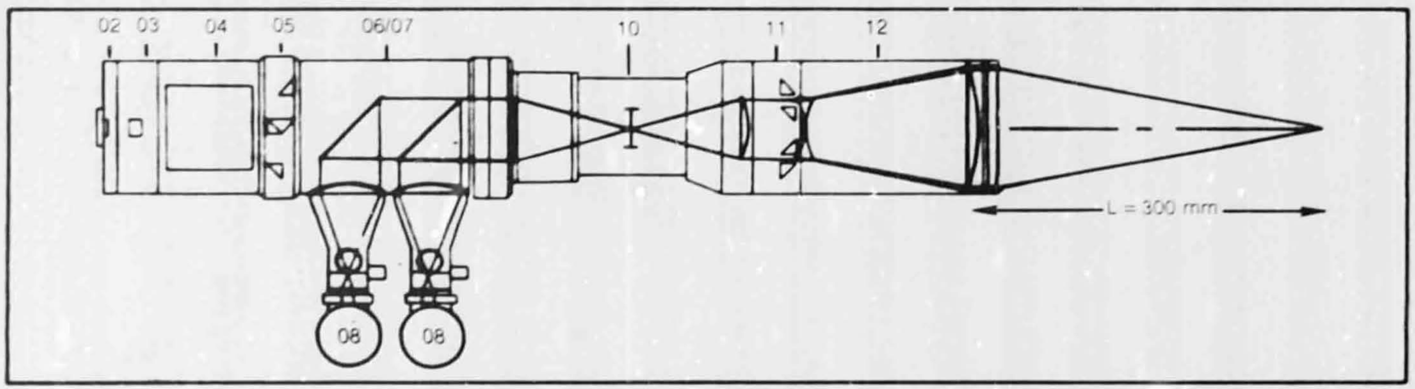

RECEIVER BEAM PATH

FIG. 8

SKETCH OF OPTICS COMPONENTS USED FOR LV/LIF MEASUREMENTS

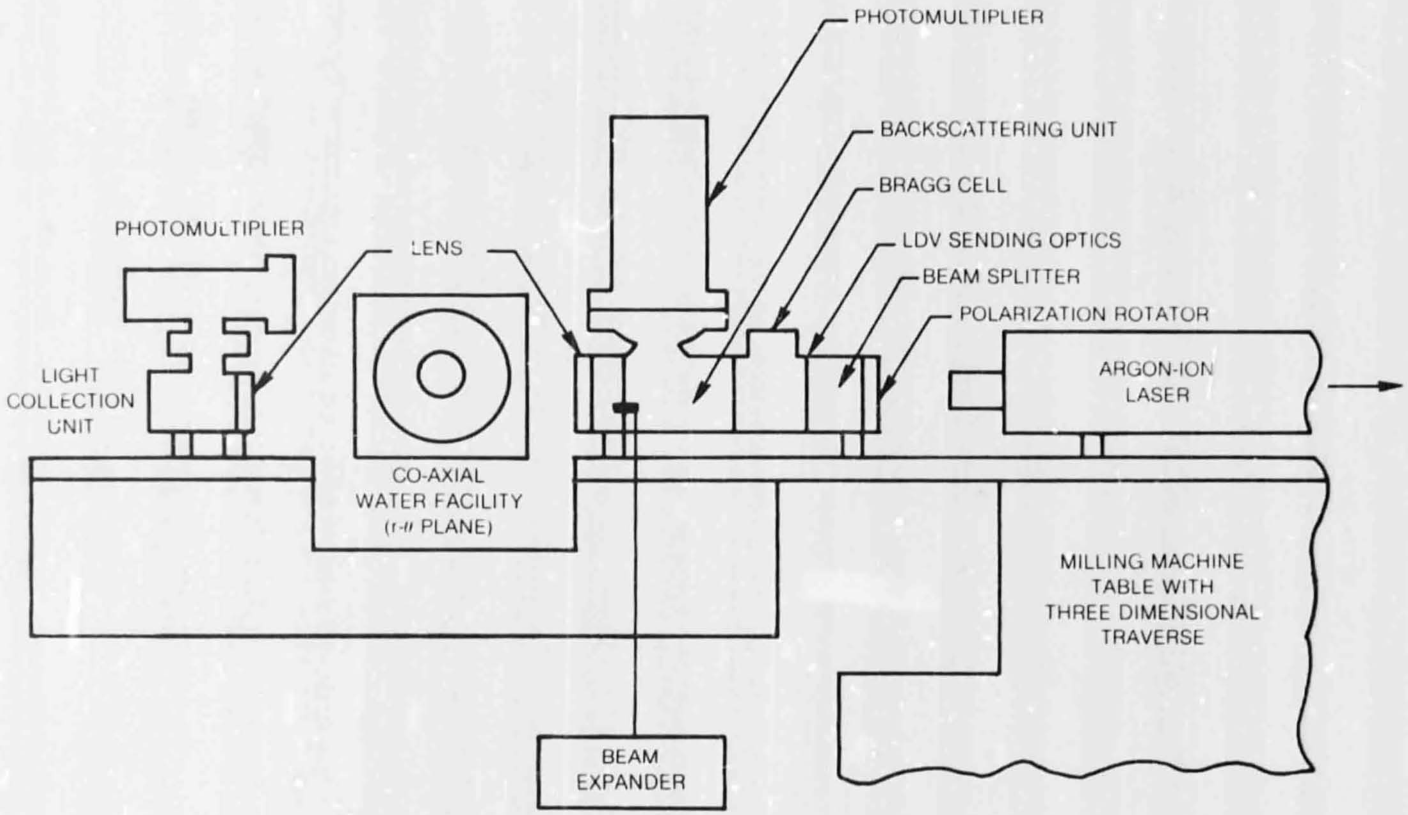

FIG. 9

81–12–38–9

ORIGINAL PAGE
BLACK AND WHITE PHOTOGRAPH

VISUALIZATION OF FLOW CONDITION 1 FROM HIGH SPEED MOTION PICTURES

$V_j = 0.52$ m/s $V_a = 1.66$ m/s
$Q_j = 6.2$ gpm $Q_a = 52.8$ gpm
DYE ADDED TO INNER JET FLUID

r-z PLANE

$0 < z < 125$ mm

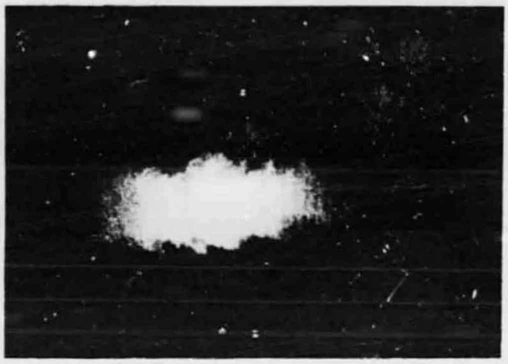

$125 < z < 250$ mm

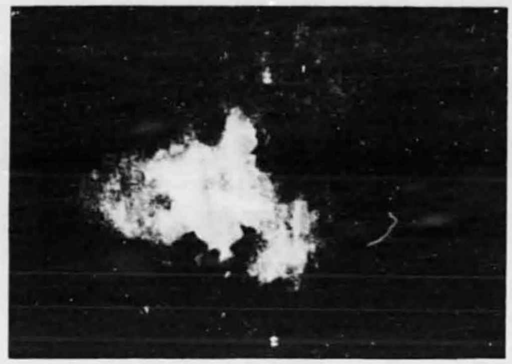

r-θ PLANE

z = 51 mm

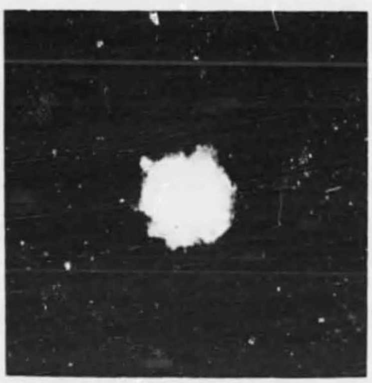

z = 102 mm

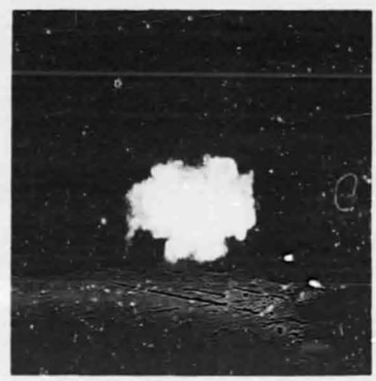

z = 153 mm

z = 203 mm

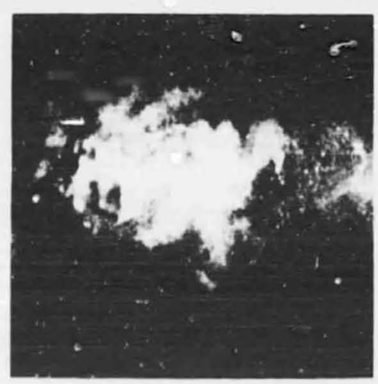

MEAN AXIAL VELOCITY PROFILES

SYMBOL	○	●	□	■	△	▲
LOCATION, θ	0	180	270	90	0	180
RUN NOS	44, 17, 16, 20		9, 14, 18, 19		60, 61, 62, 63	

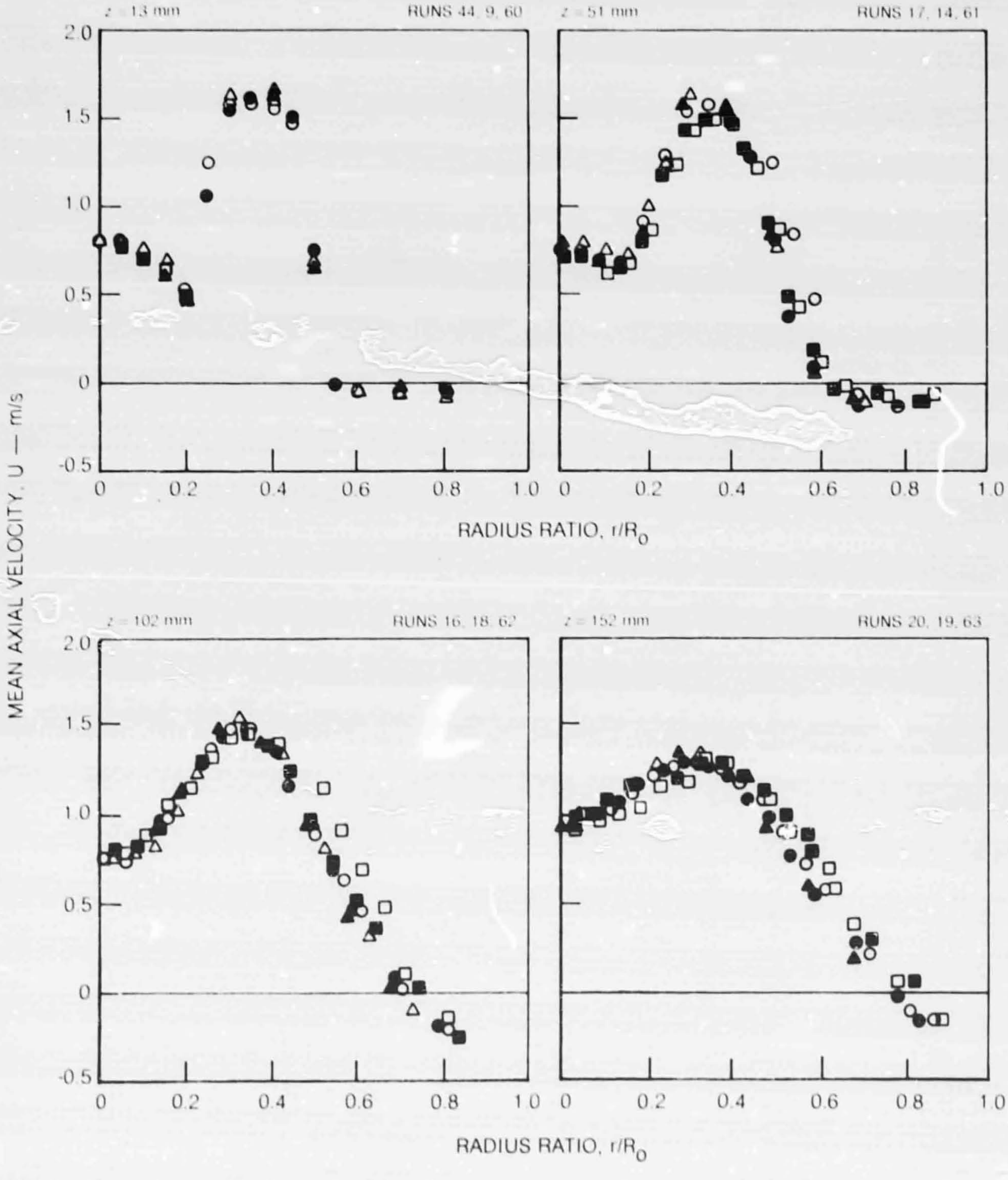

81-12-38-11

MEAN AXIAL VELOCITY PROFILES (CONT.)

SYMBOL	○	●	□	■	△	▲
LOCATION, θ	0	180	270	90	0	180
RUN NOS	21, 72, 74		22, 71, 73		64, 66, 67	

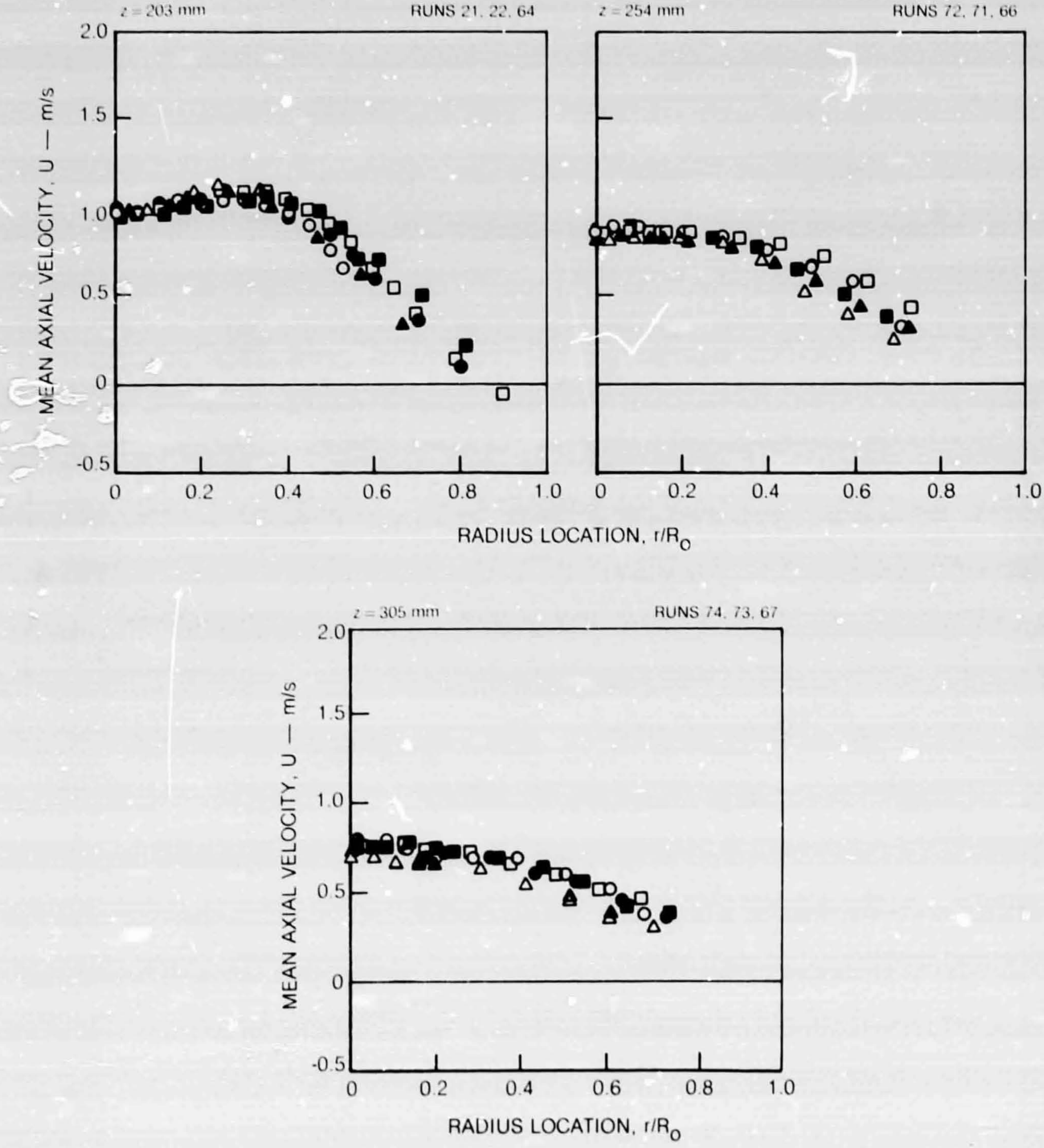

81–12–38–12

AXIAL VARIATION OF MEAN AXIAL VELOCITY AND MEAN INNER JET FLUID CONCENTRATION ALONG CENTERLINE

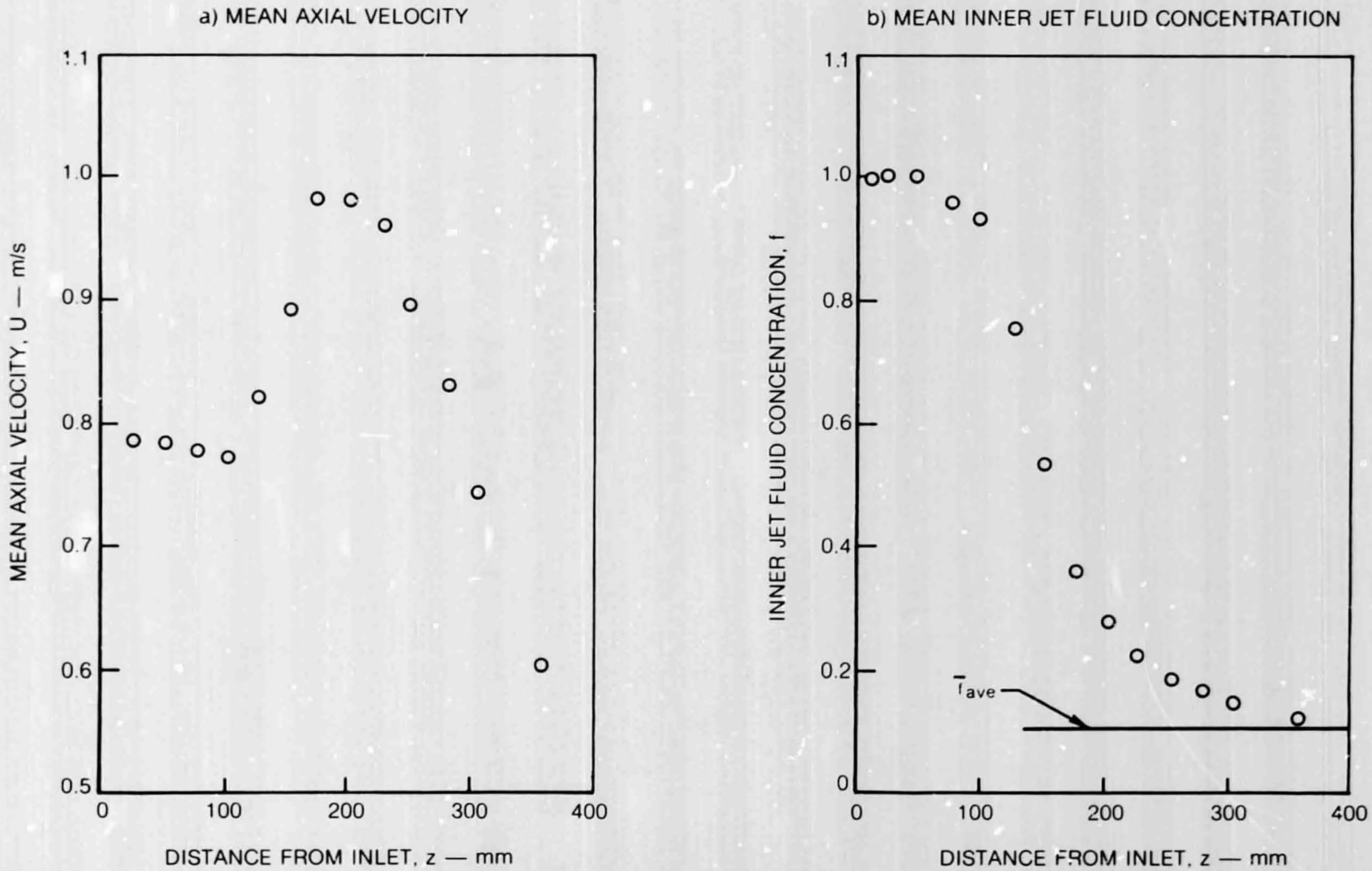

FIG. 12

81-12-38-13

MEAN RADIAL VELOCITY PROFILES

SYMBOL	○	●	◇	◆
LOCATION, θ	0	180	0	180
RUN NOS	44, 17, 16, 20		45, 47, 52, 51	

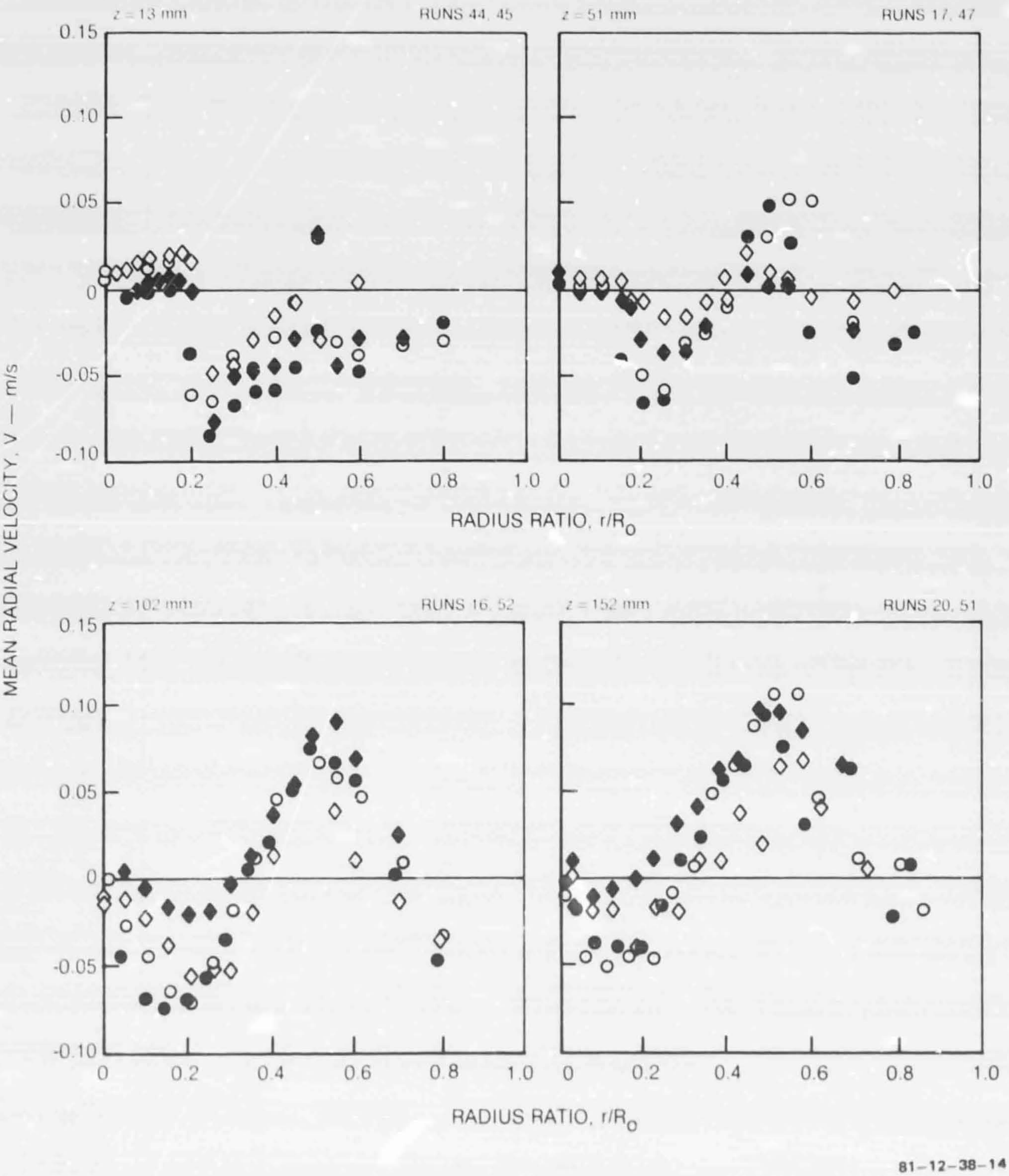

81-12-38-14

MEAN RADIAL VELOCITY PROFILES (CONT.)

SYMBOL	○	●	◇	◆
LOCATION, θ	0	180	0	180
RUN NOS.	21, 72, 74		50, 69, 70	

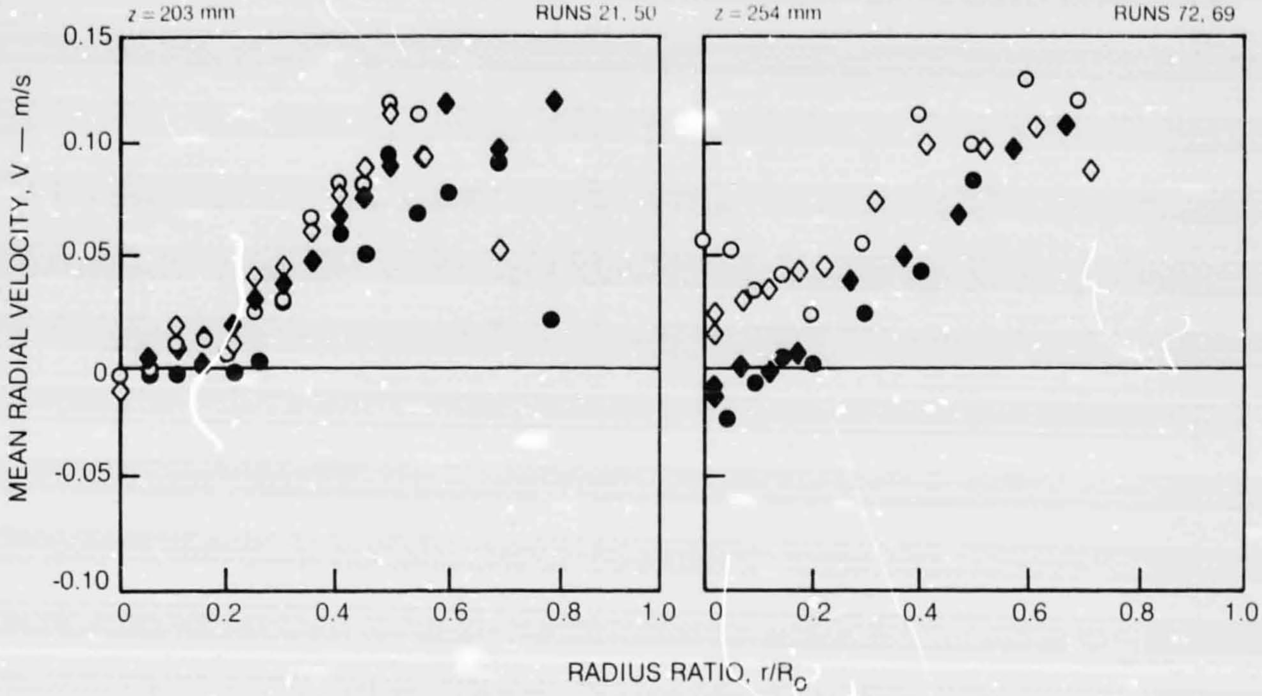

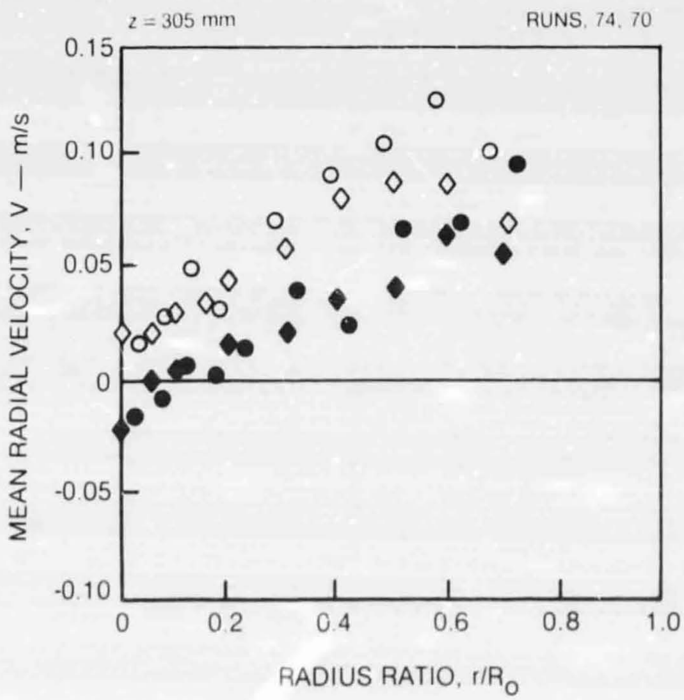

81–12–38–15

MEAN AZIMUTHAL VELOCITY PROFILES

SYMBOL	□	■	◪	◩	◺	◣
LOCATION, θ	270	90	270	90	270	90
RUN NOS.	14, 18, 19		23, 24		57, 58, 53, 54	

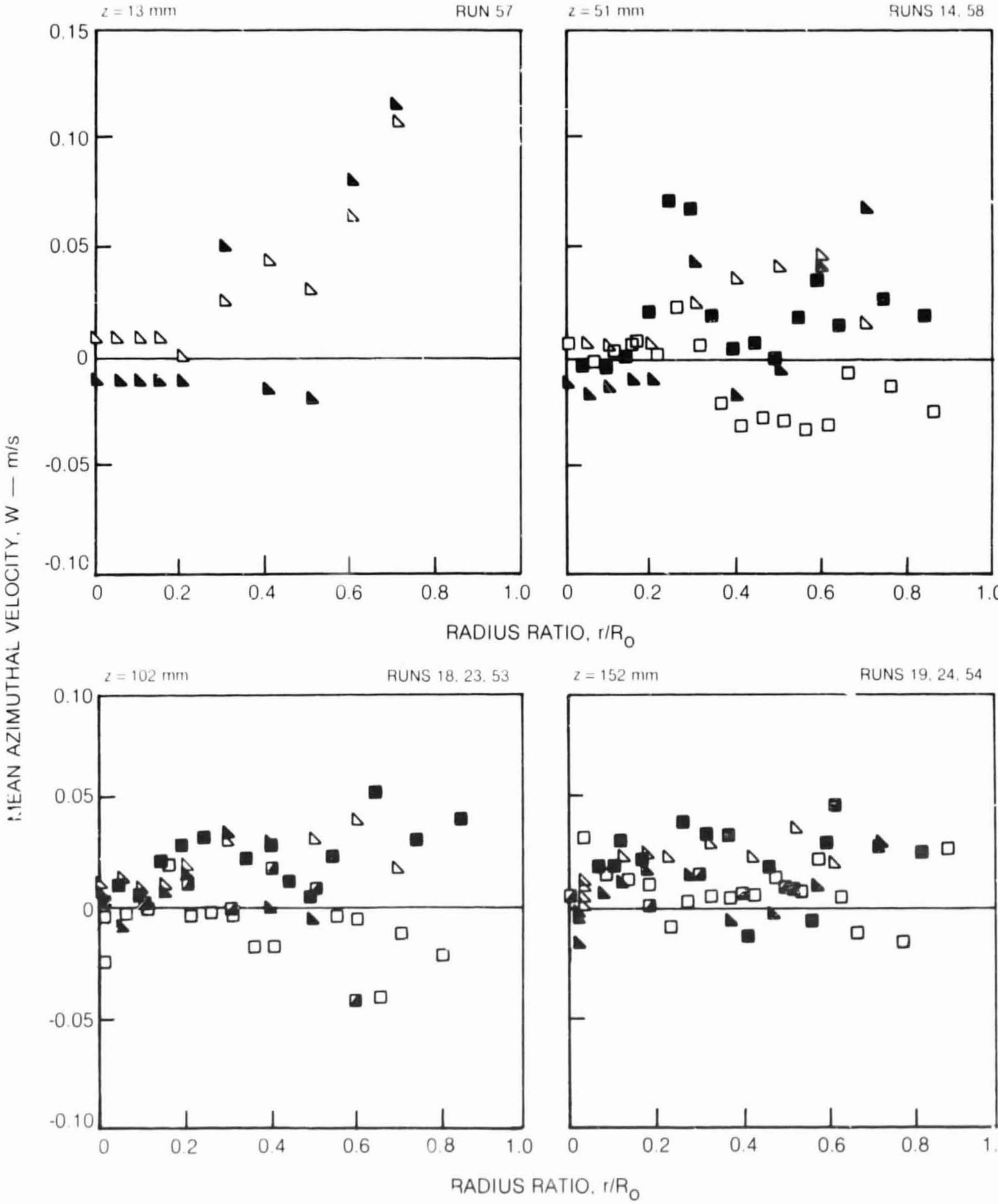

81-12-38-16

MEAN AZIMUTHAL VELOCITY PROFILES (CONT.)

SYMBOL	□	■	◺	◣
LOCATION, θ	270	90	270	90
RUN NOS.	22, 17, 73		56	

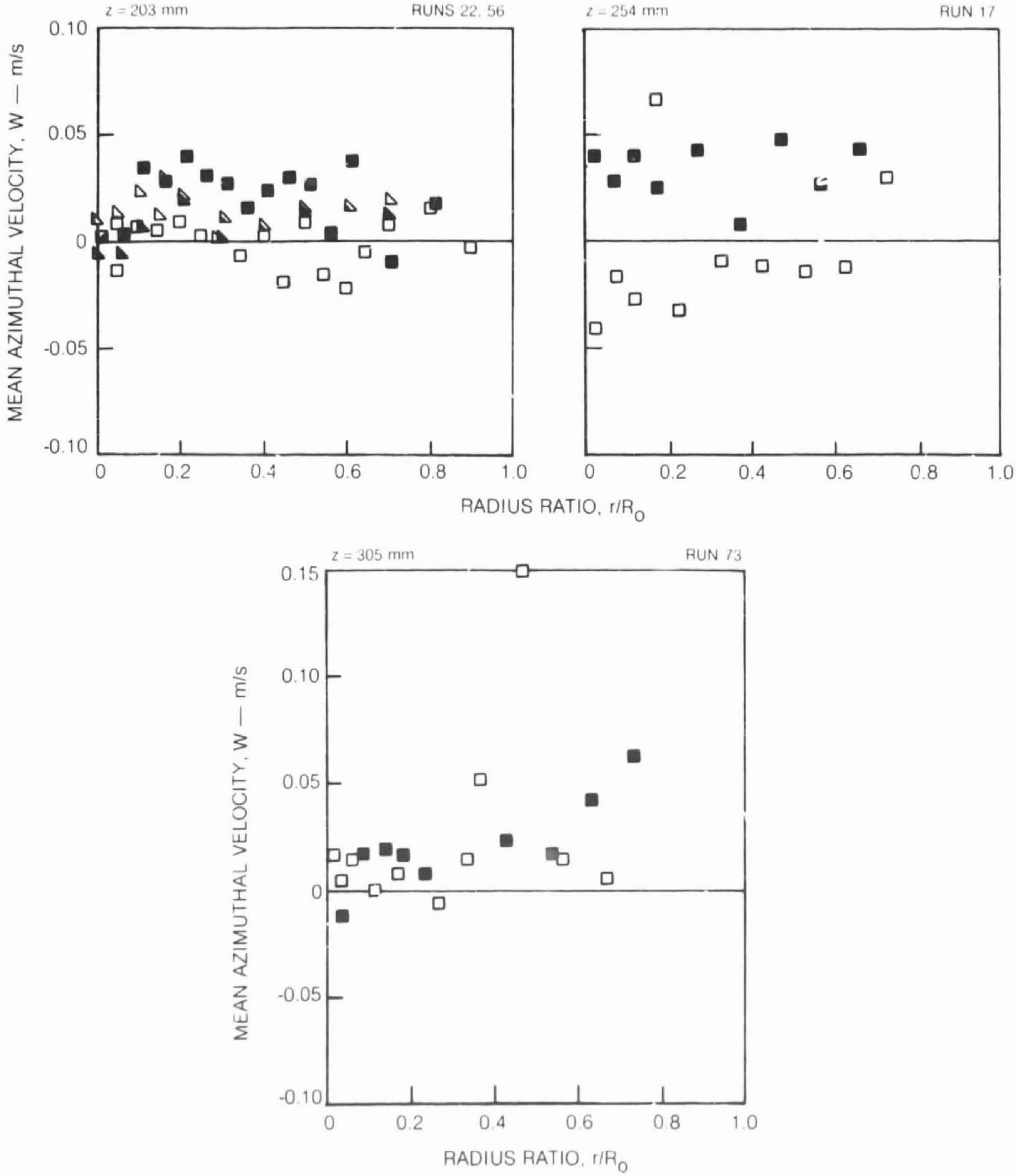

81–12–38–17

FLUCTUATING AXIAL VELOCITY PROFILES

SYMBOL	○	●	□	■	△	▲
LOCATION, θ	0	180	270	90	0	180
RUN NOS.	44, 17, 16, 20		9, 14, 18, 19		60, 61, 62, 63	

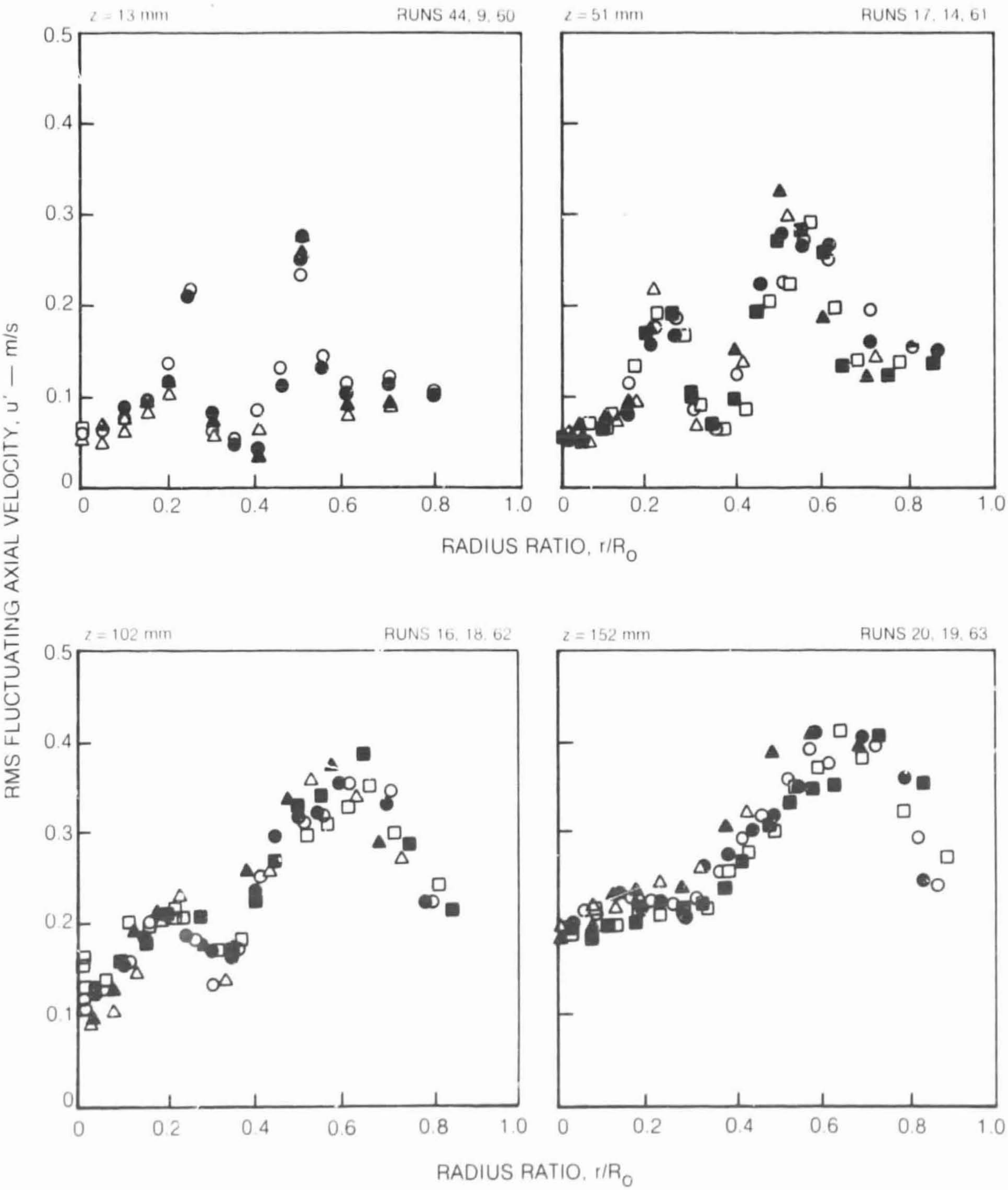

81-12-38-18

FLUCTUATING AXIAL VELOCITY PROFILES (CONT.)

SYMBOL	○	●	□	■	△	▲
LOCATION, θ	0	180	270	90	0	180
RUN NOS.	21, 72, 74		22, 71, 73		64, 66, 67	

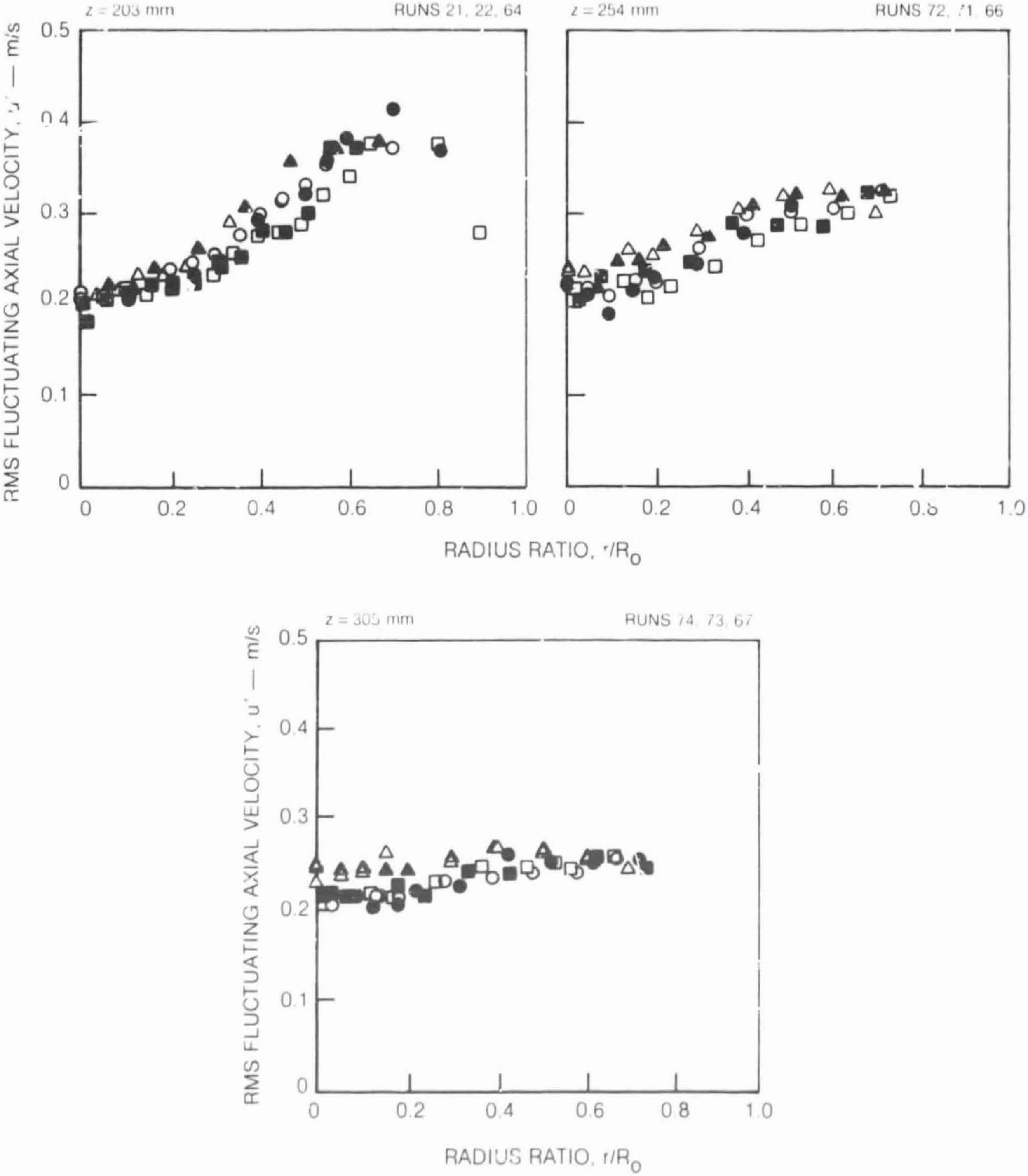

81-12-38-19

FLUCTUATING RADIAL VELOCITY PROFILES

SYMBOL	○	●	◇	◆
LOCATION, θ	0	180	0	180
RUN NOS	44, 17, 16, 20		45, 47, 52, 51	

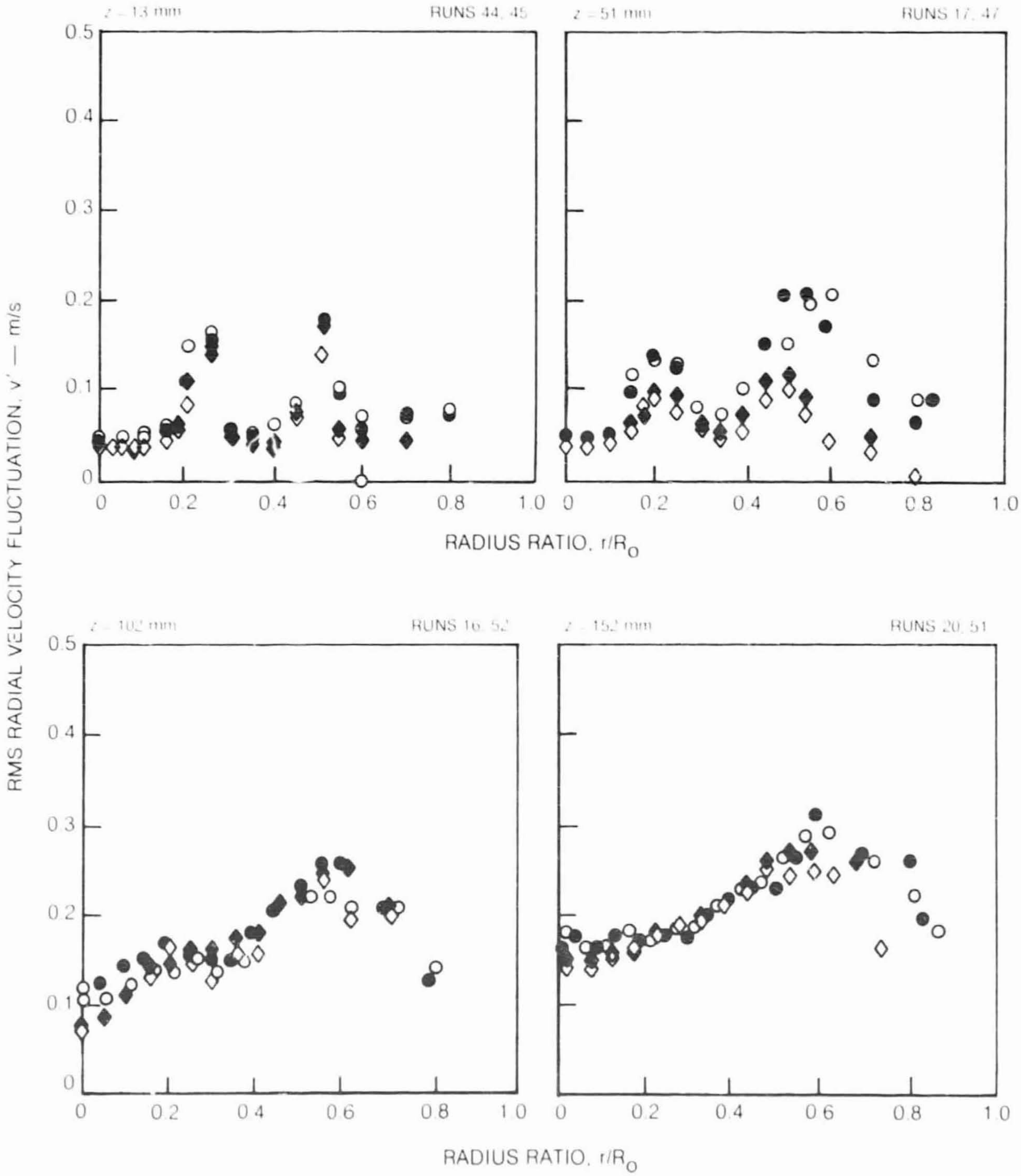

81-12-38-20

FLUCTUATING RADIAL VELOCITY PROFILES (CONT.)

SYMBOL	○	●	◇	◆
LOCATION, θ	0	180	0	180
RUN NOS.	21, 72, 74		50, 69, 70	

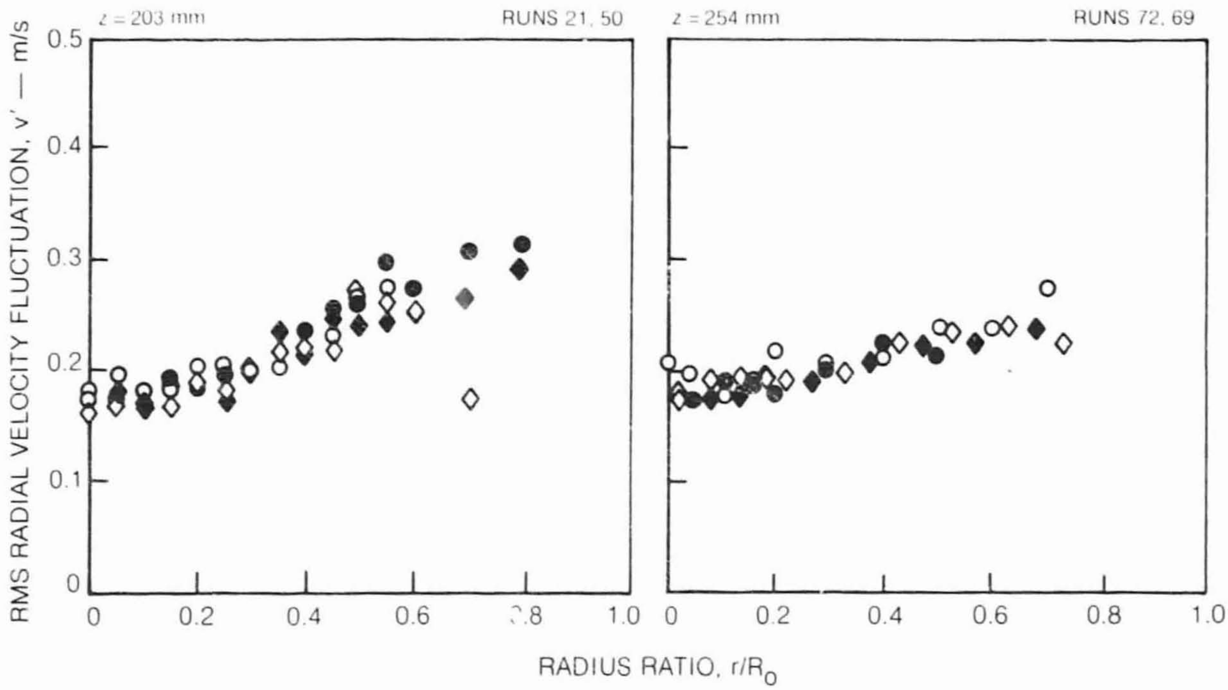

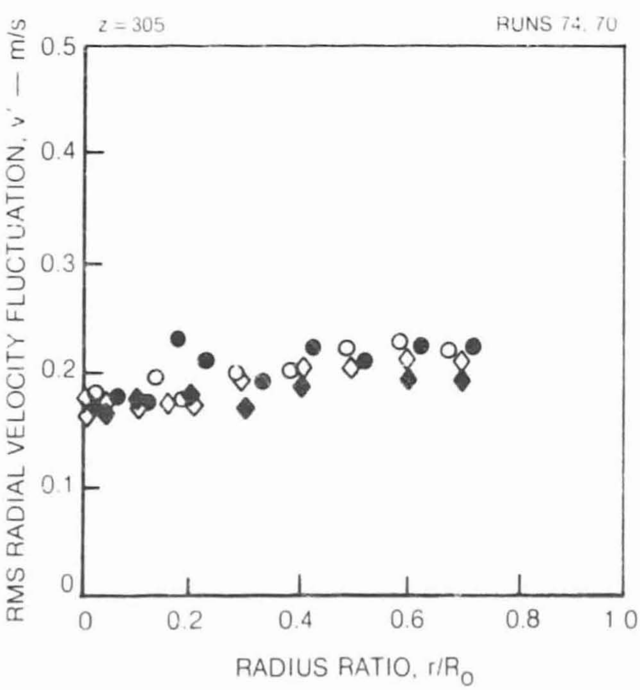

81-12-38-21

FLUCTUATING AZIMUTHAL VELOCITY PROFILES

SYMBOL	□	■	◺	◣
LOCATION, θ	270	90	270	90
RUN NOS	9, 14, 18, 19		57, 58, 53, 54	

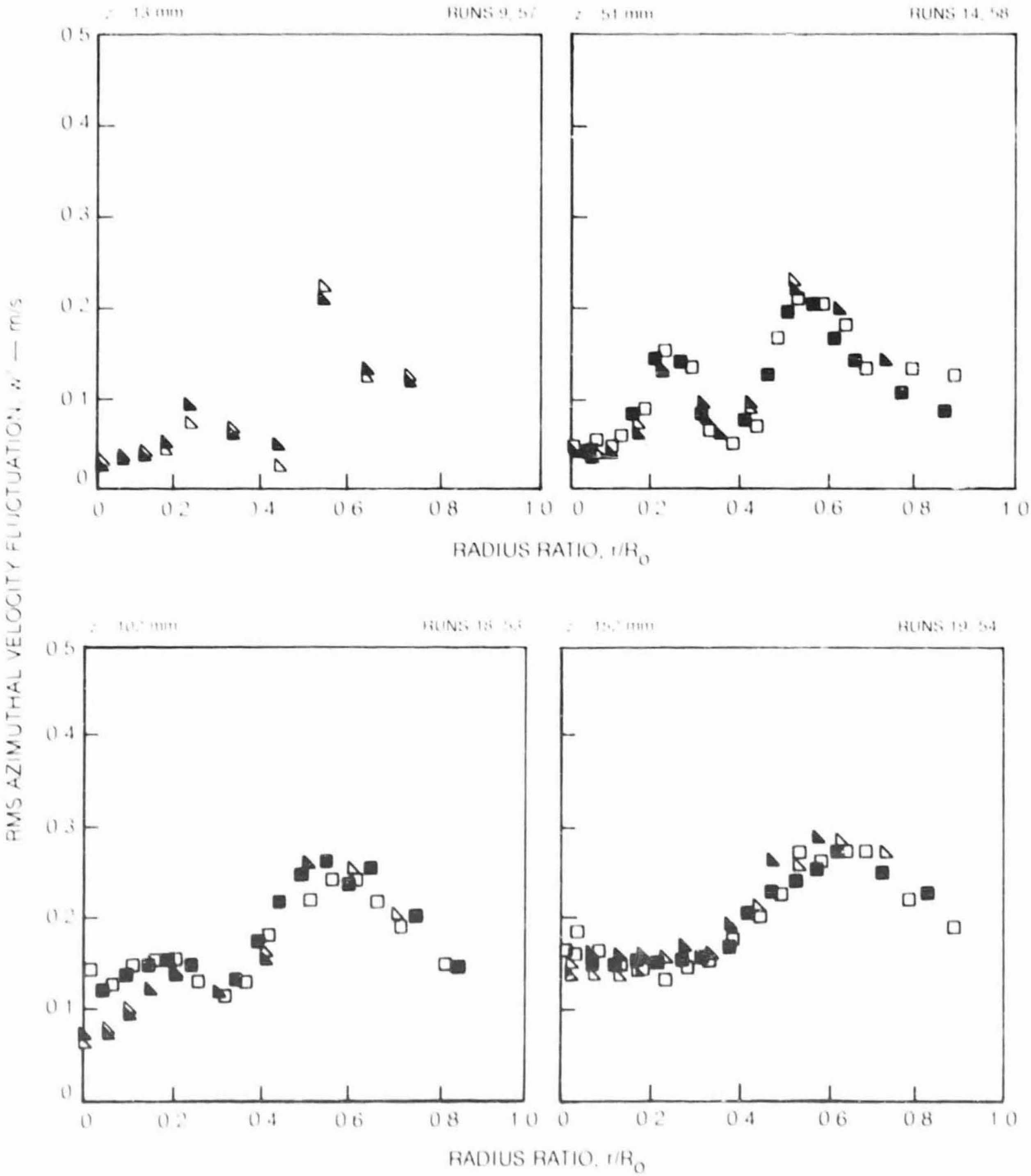

81-12-38-22

FLUCTUATING AZIMUTHAL VELOCITY PROFILES (CONT.)

SYMBOL	□	■	△	◣
LOCATION, θ	270	90	270	90
RUN NOS	22, 71, 73		56	

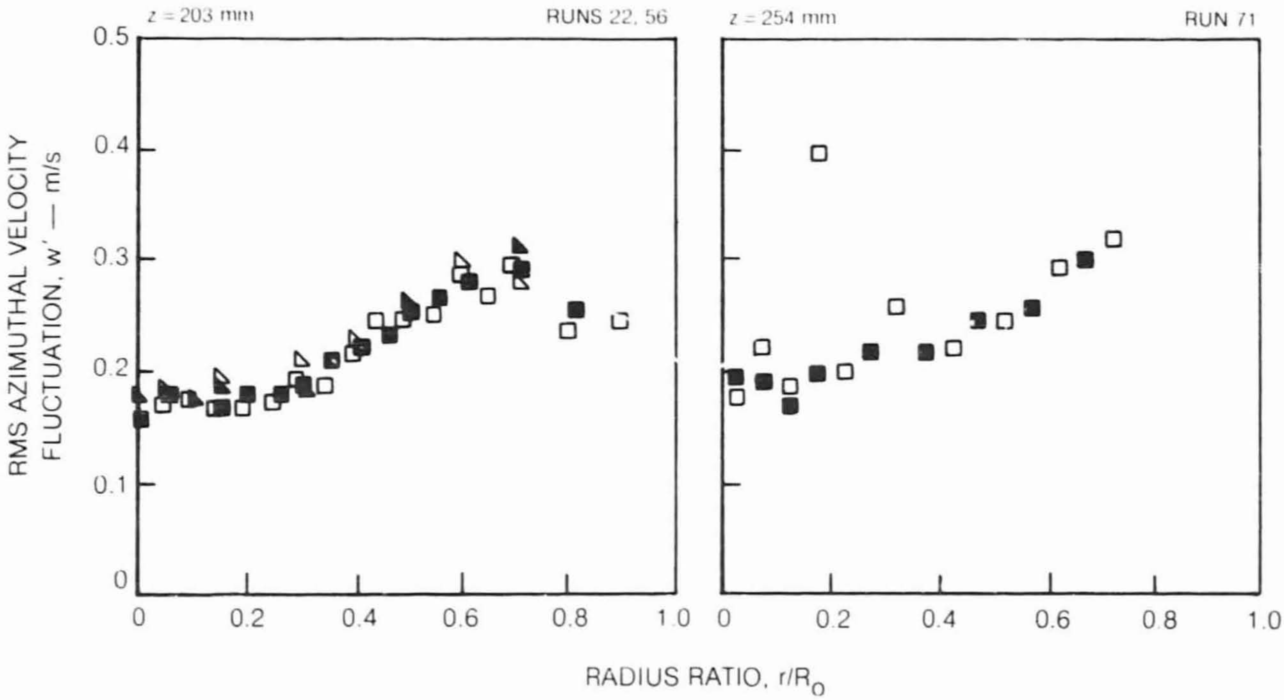

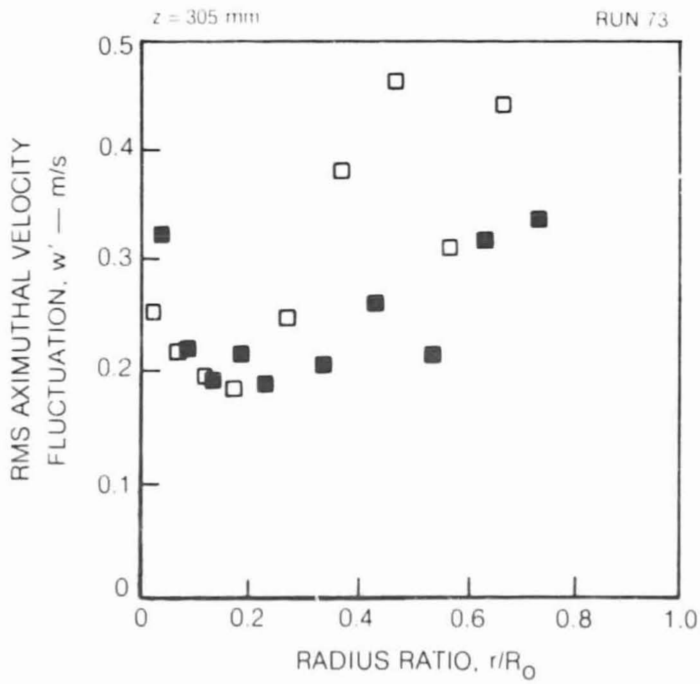

81-12-38-23

MEAN INNER JET FLUID CONCENTRATION PROFILES

SYMBOL	△	▲	◇	◆	◺	◣
LOCATION, θ	0	180	0	180	270	90
RUN NOS	60, 61, 62, 63		45, 47, 52, 51		57, 58, 53, 54	

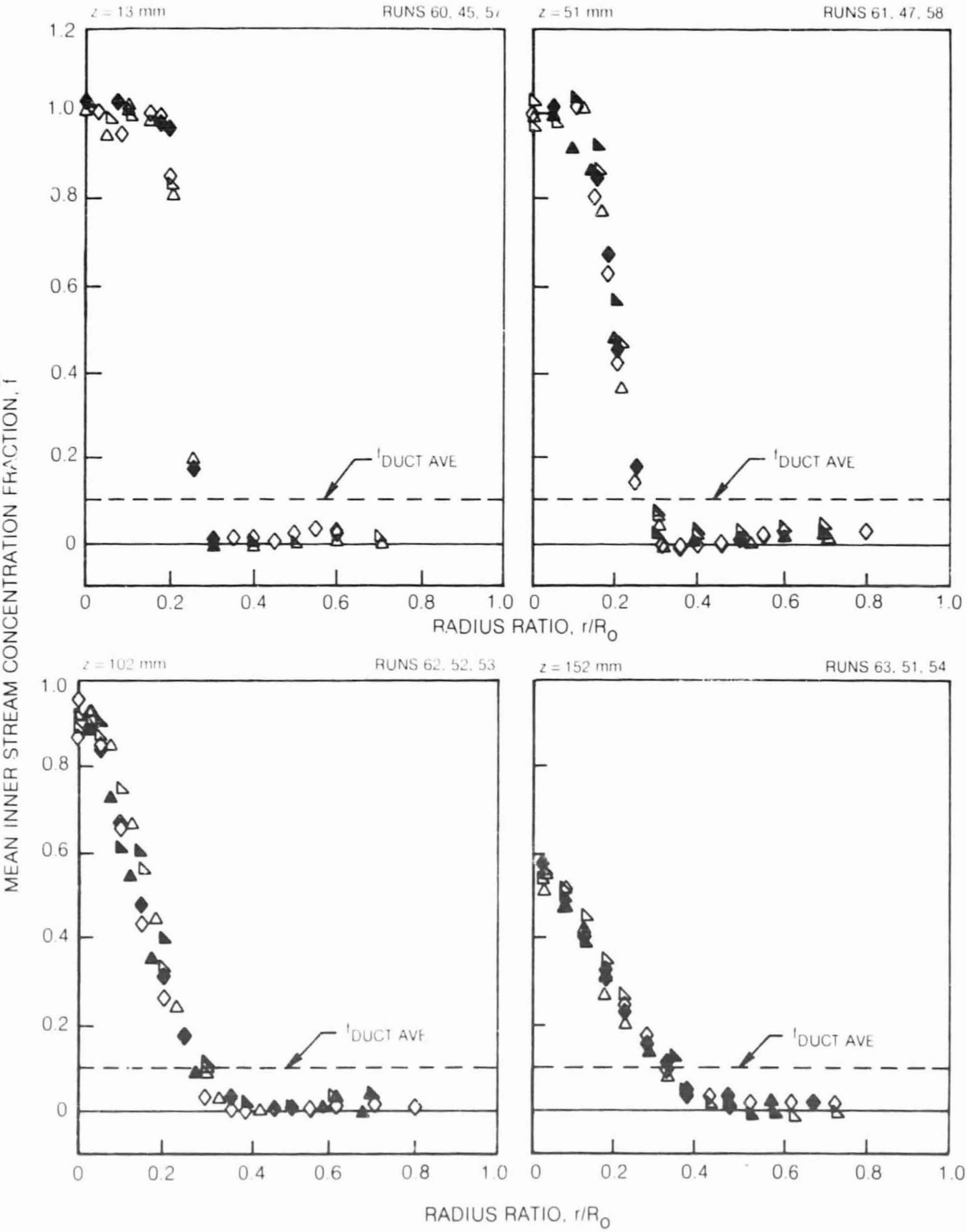

81-12-38-24

MEAN INNER JET FLUID CONCENTRATION PROFILES (CONT.)

SYMBOL	△	▲	◇	◆	◺	◣
LOCATION, θ	0	180	0	180	270	90
RUN NOS	64, 66, 67		50, 69, 70		56	

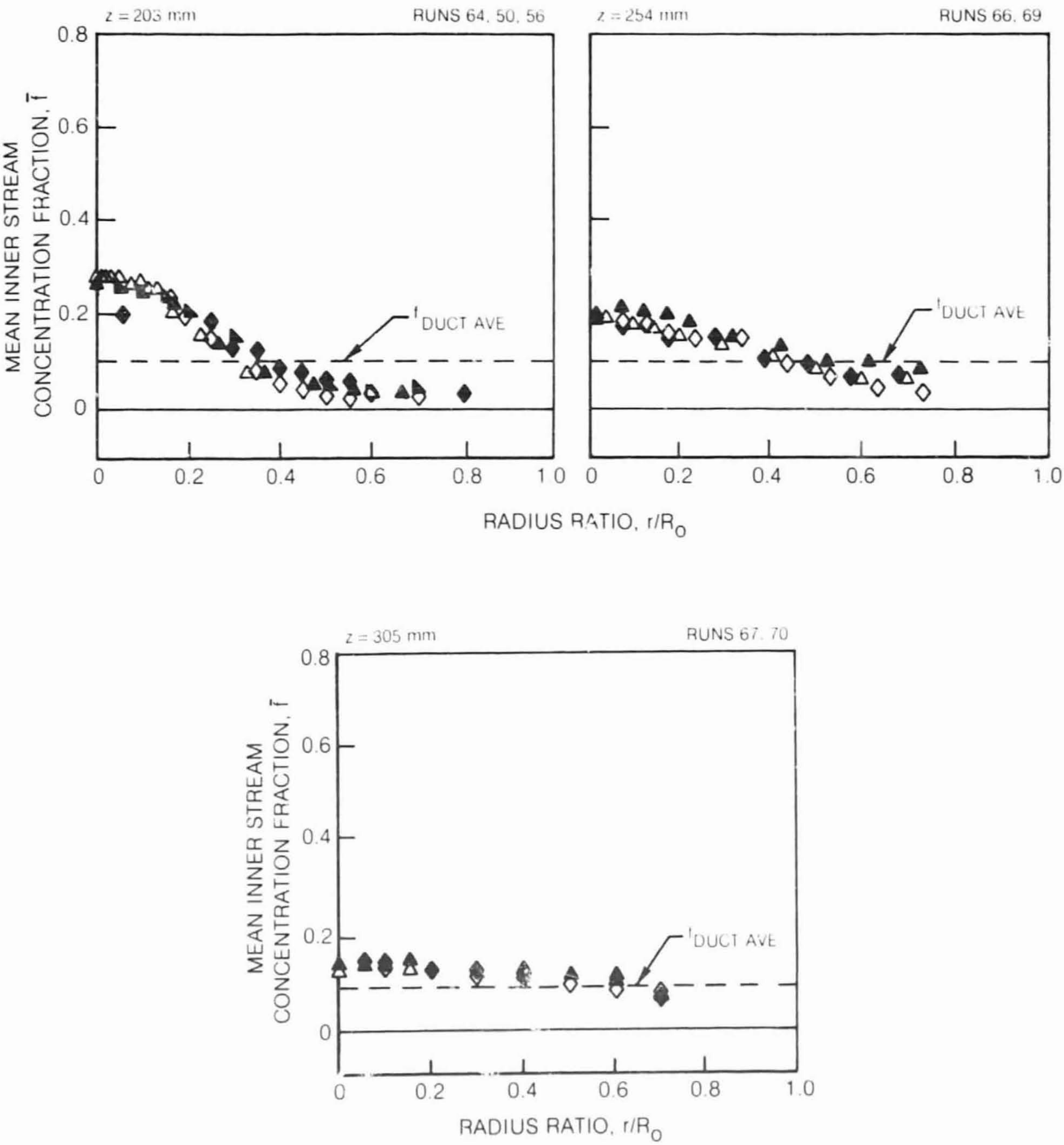

81-12-38-25

FLUCTUATING INNER JET FLUID CONCENTRATION PROFILES

SYMBOL	△	▲	◇	◆	◺	◣
LOCATION, θ	0	180	270	90	0	180
RUN NOS.	60, 61, 62, 63		45, 47, 52, 51		57, 58, 53, 54	

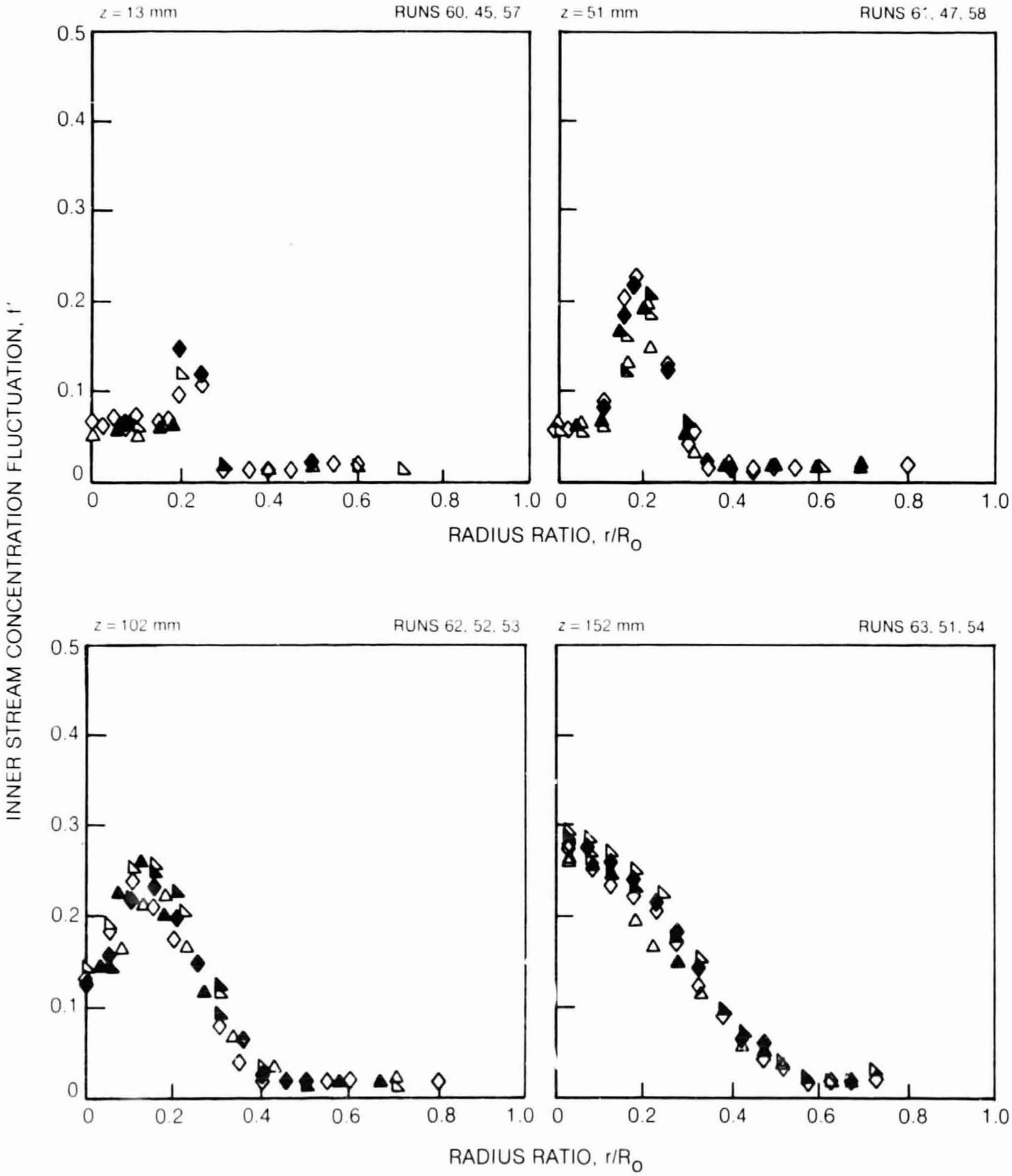

81-12-38-26

FLUCTUATING INNER JET FLUID CONCENTRATION PROFILES (CONT.)

SYMBOL	△	▲	◇	◆	◺	◣
LOCATION, θ	0	180	270	90	0	180
RUN NOS.	64, 66, 67		50, 69, 70		56	

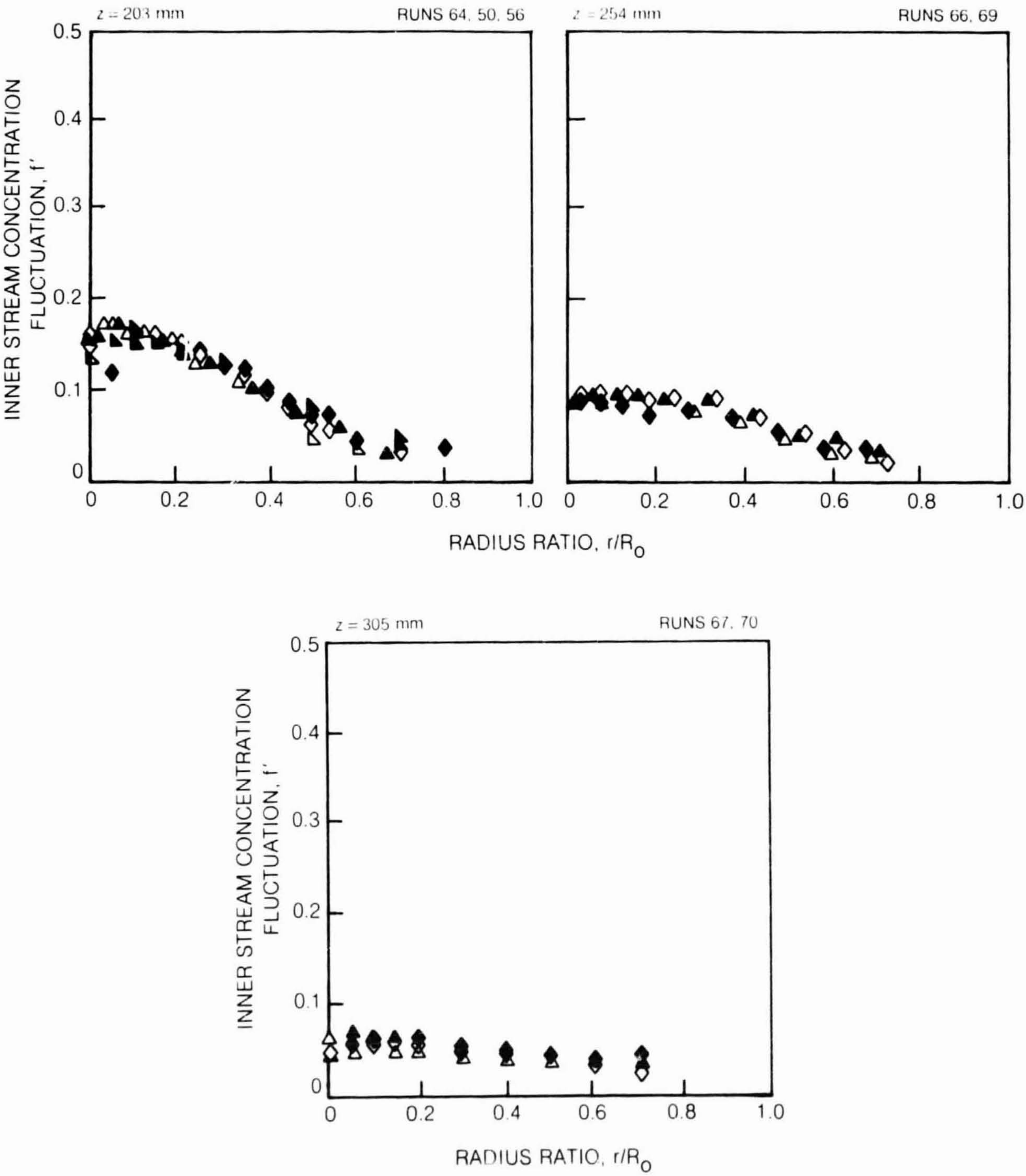

MOMENTUM TRANSPORT RATE, $\overline{uv}$, PROFILES

SYMBOL	○	●
LOCATION, θ	0	180

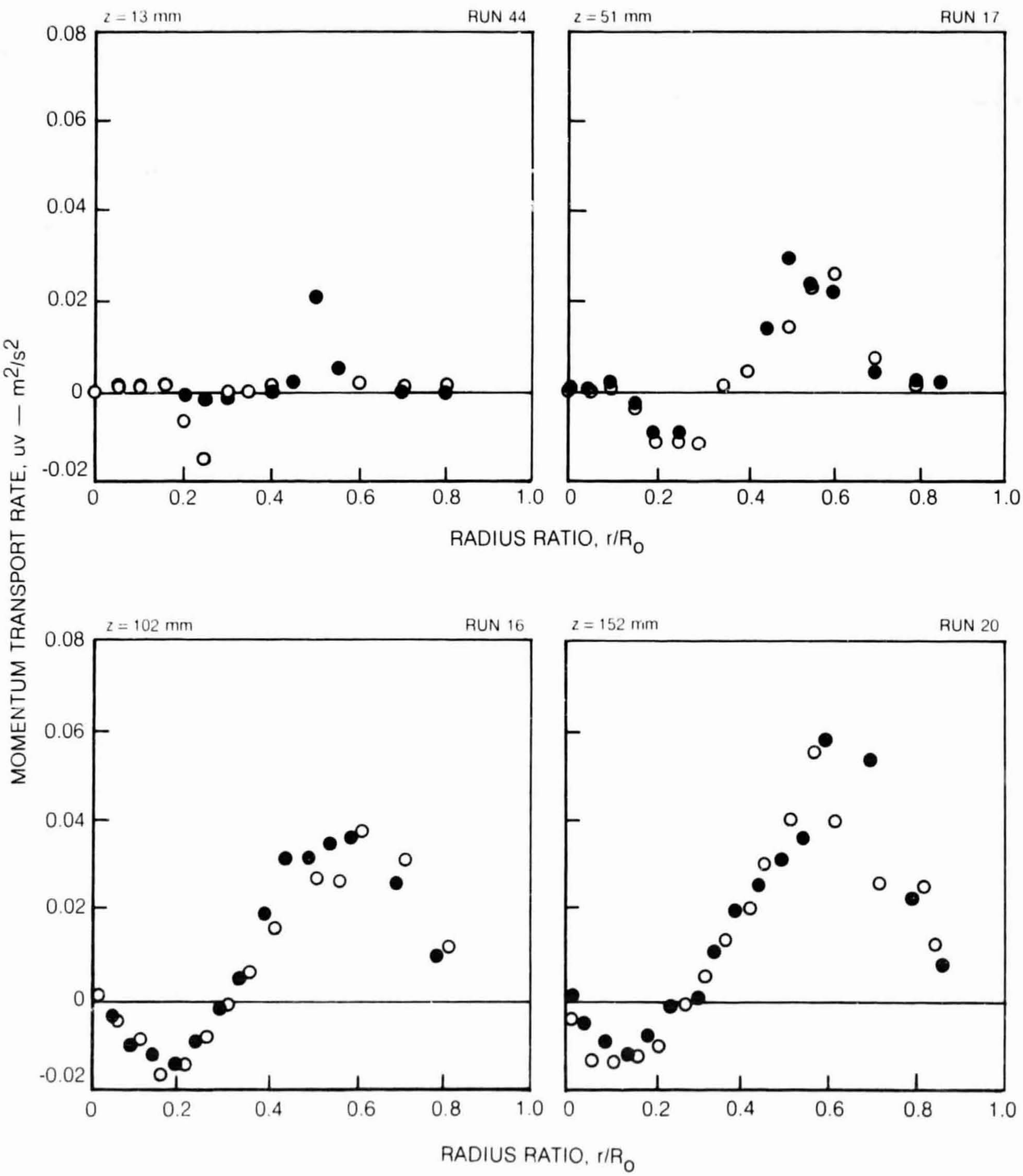

81–12–38–28

MOMENTUM TRANSPORT RATE, $\overline{uv}$, PROFILES (CONT.)

SYMBOL	○	●
LOCATION, θ	0	180

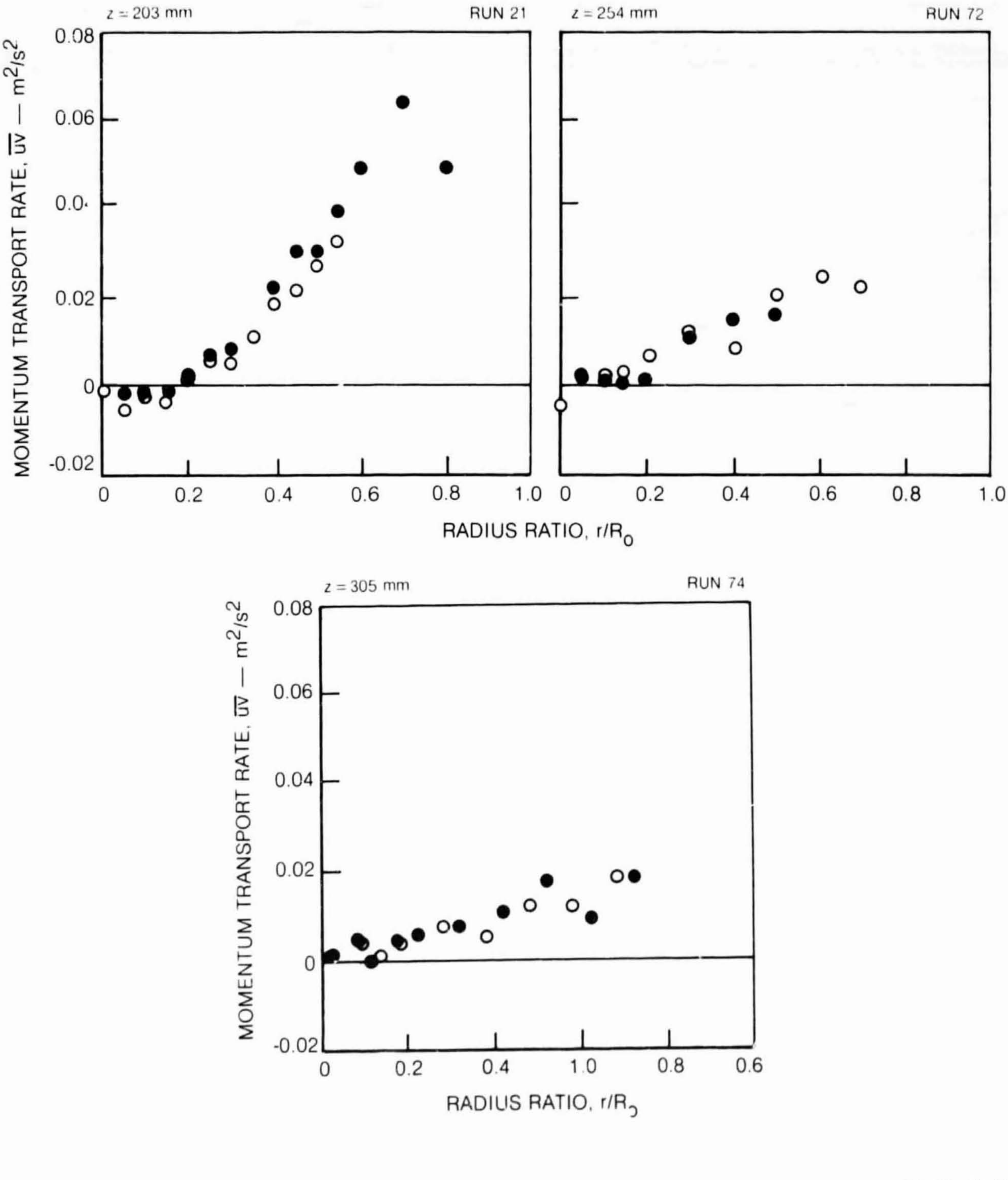

81-12-38-29

MOMENTUM TRANSPORT CORRELATION COEFFICIENT, R_{uv}, PROFILES

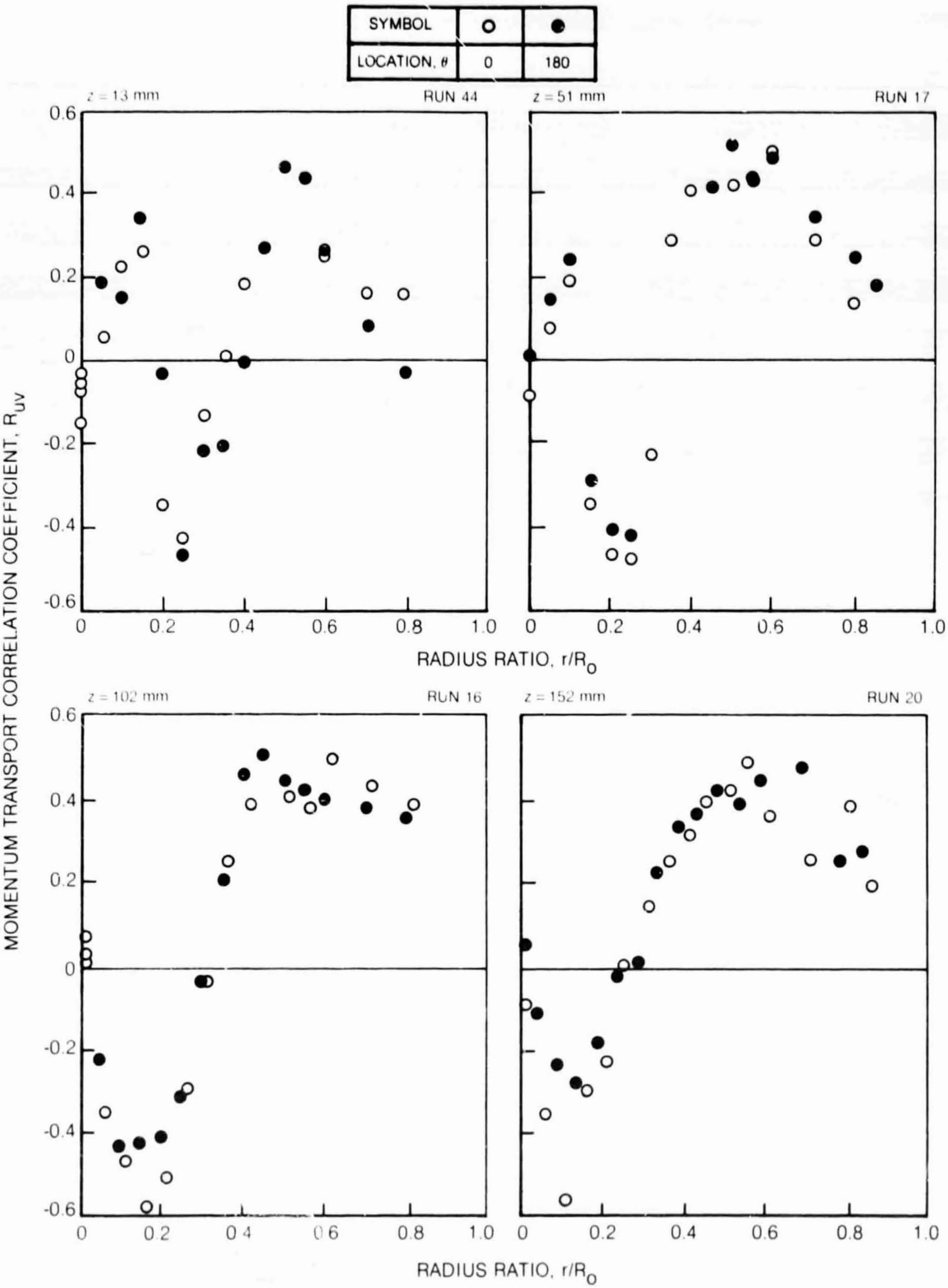

81-12-38-30

MOMENTUM TRANSPORT CORRELATION COEFFICIENT, R_{uv}, PROFILES (CONT.)

SYMBOL	○	●
LOCATION, θ	0	180

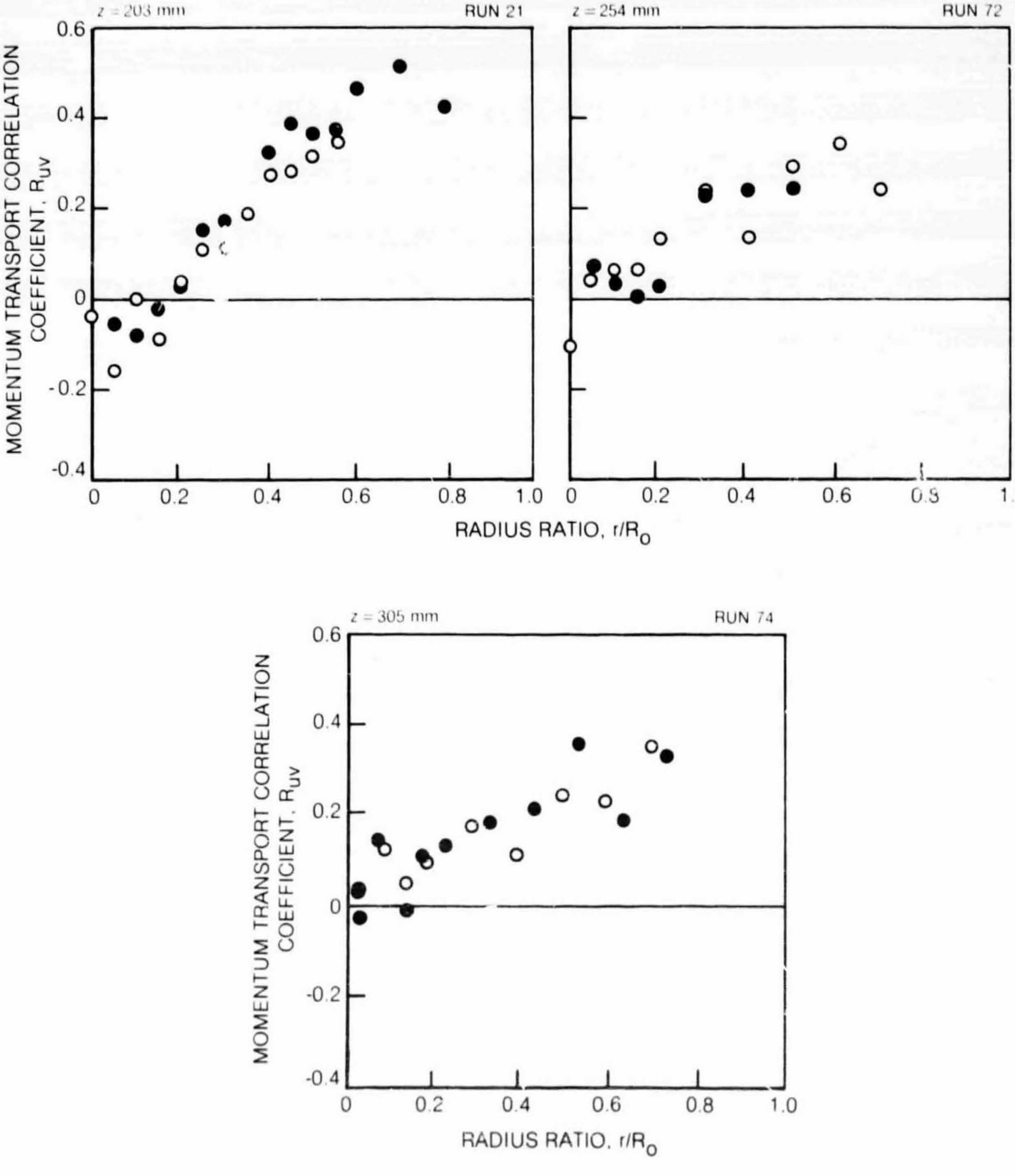

81–12–38–31

MOMENTUM TRANSPORT RATE, $\overline{uw}$, AND CORRELATION COEFFICIENT, R_{uw}, PROFILES

SYMBOL	◪	◩
LOCATION, θ	270	90

AXIAL LOCATION: 102 mm

DATA FROM RUN 23

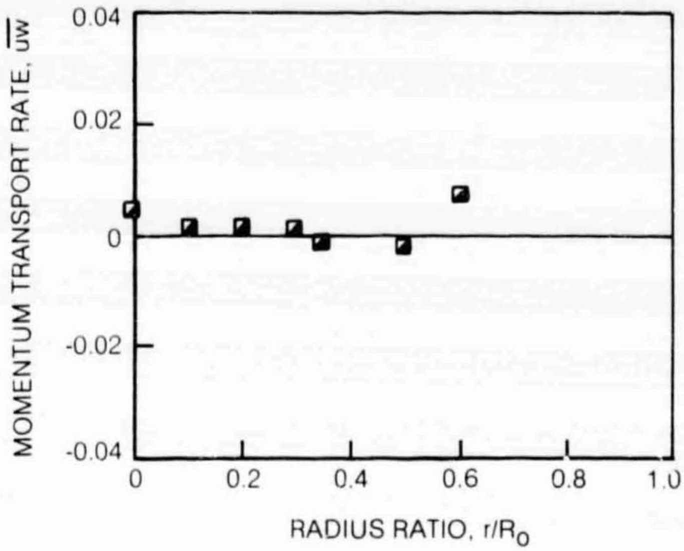

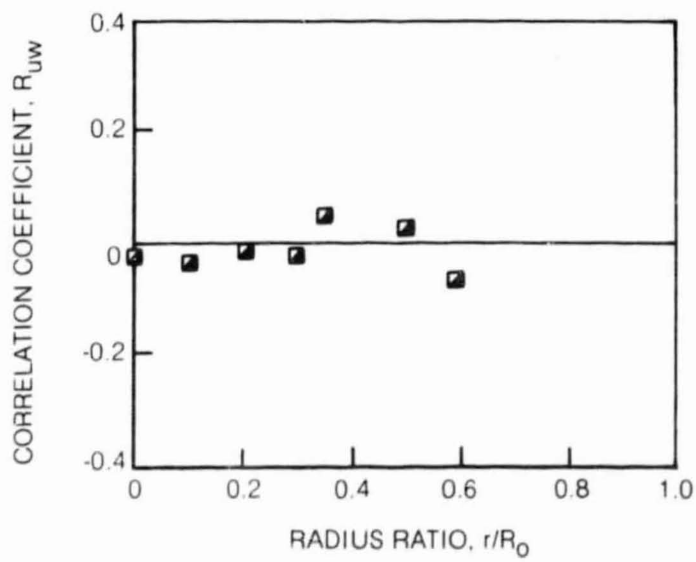

81-12-38-32

RADIAL MASS TRANSPORT RATE, $\overline{vf}$, PROFILES

SYMBOL	◇	◆
LOCATION, θ	0	180

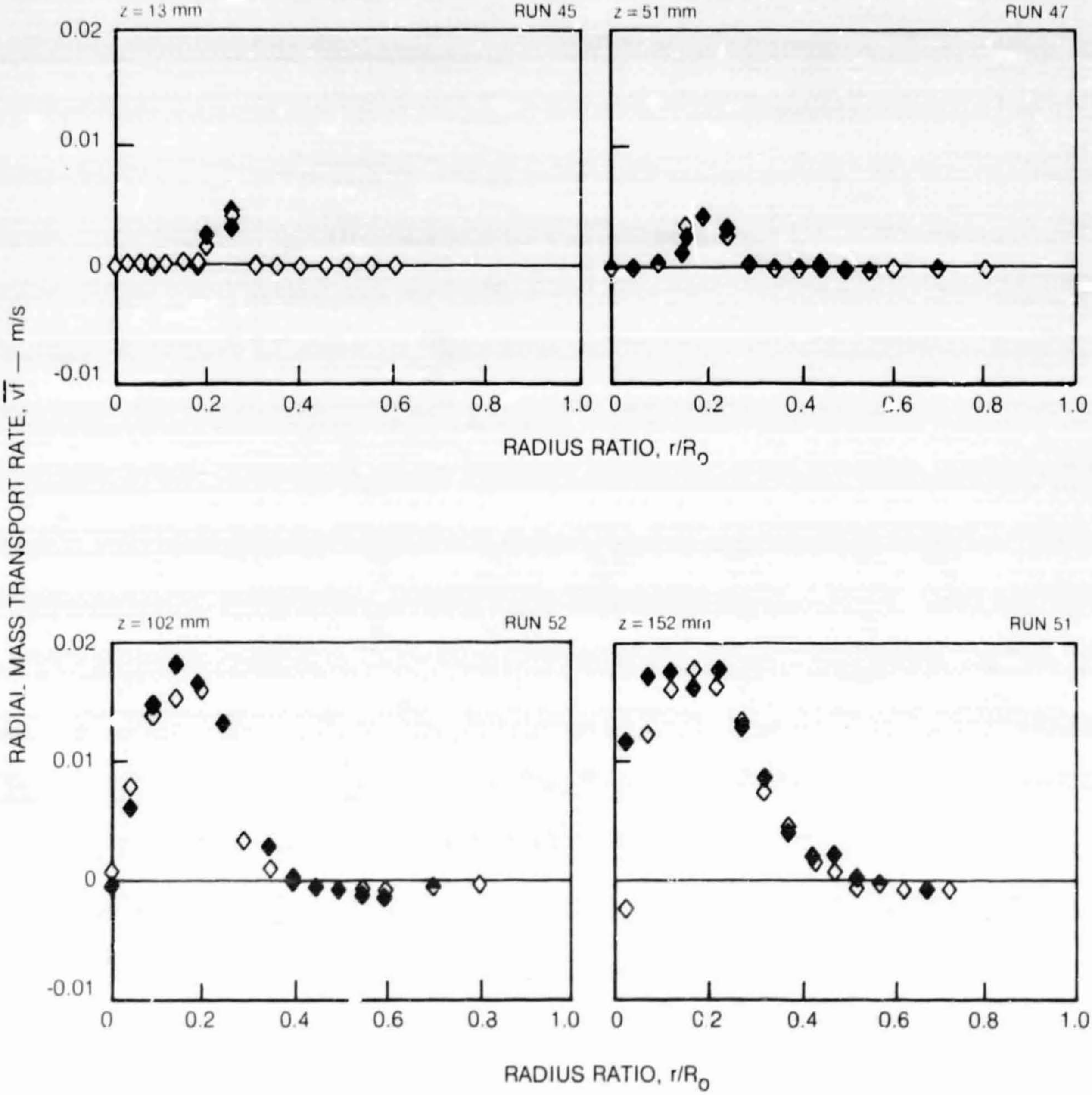

81-12-38-33

RADIAL MASS TRANSPORT RATE, $\overline{vf}$, PROFILES (CONT.)

SYMBOL	◇	◆
LOCATION, θ	0	180

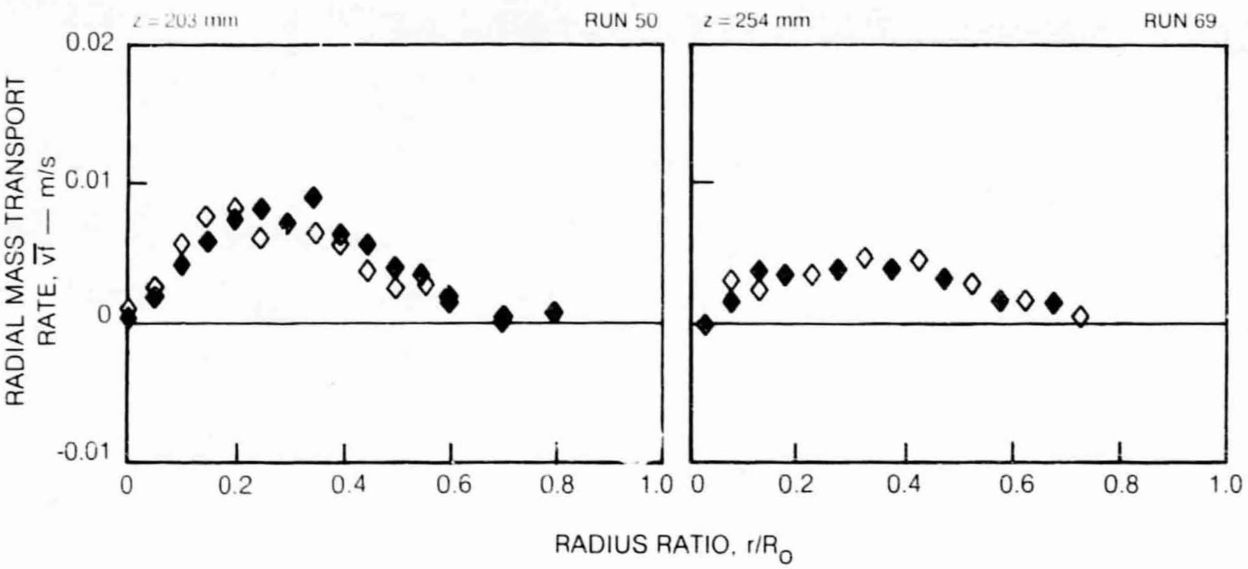

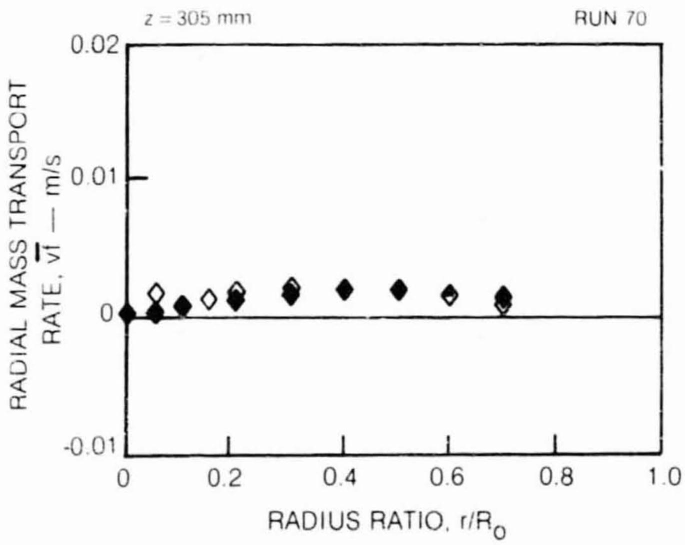

81-12-38-34

RADIAL MASS TRANSPORT CORRELATION COEFFICIENT, R_{vf}, PROFILES

SYMBOL	◇	◆
LOCATION, θ	0	180

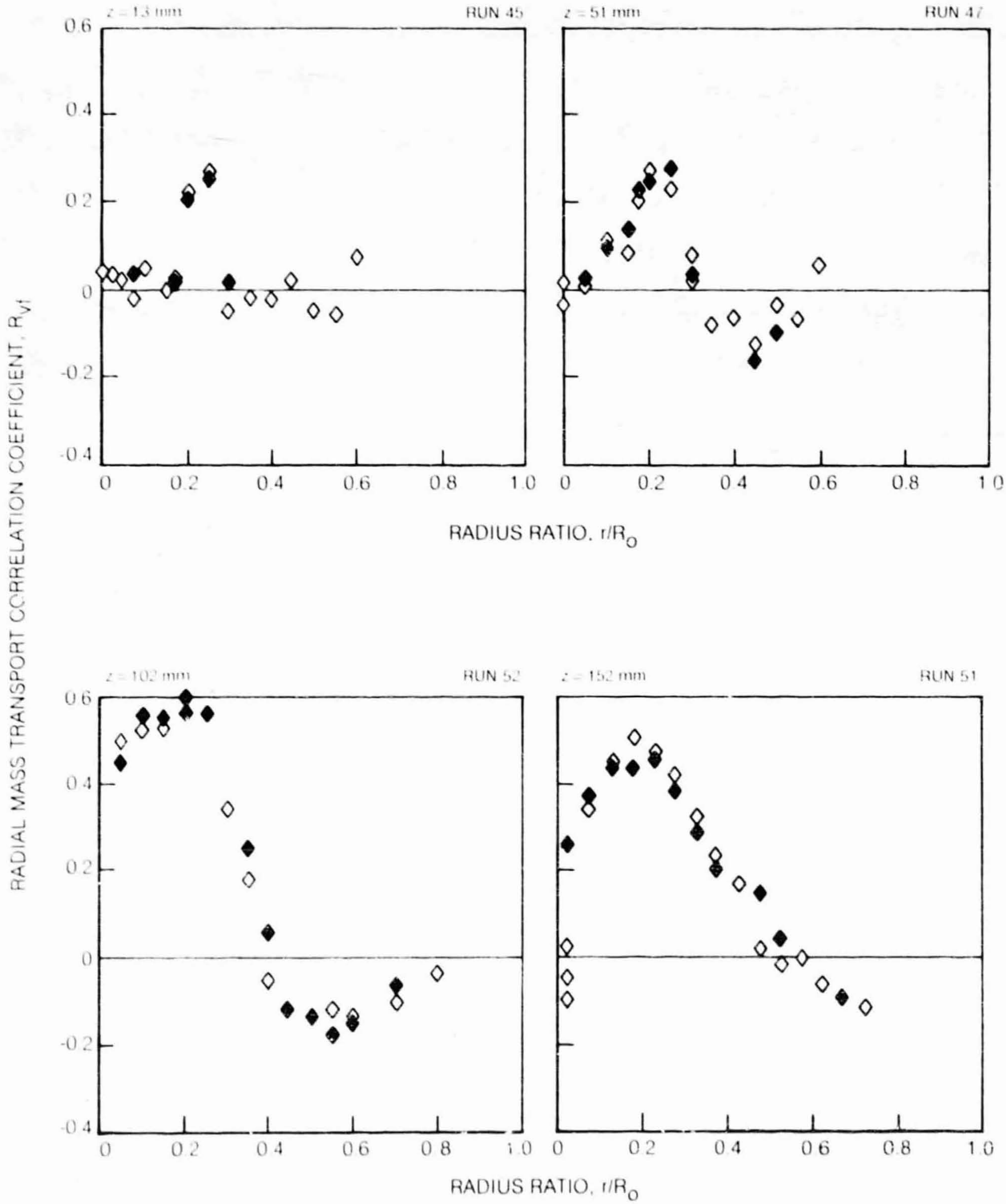

81-12-38-35

RADIAL MASS TRANSPORT CORRELATION COEFFICIENT, R_{vf}, PROFILES (CONT.)

SYMBOL	◇	◆
LOCATION, θ	0	180

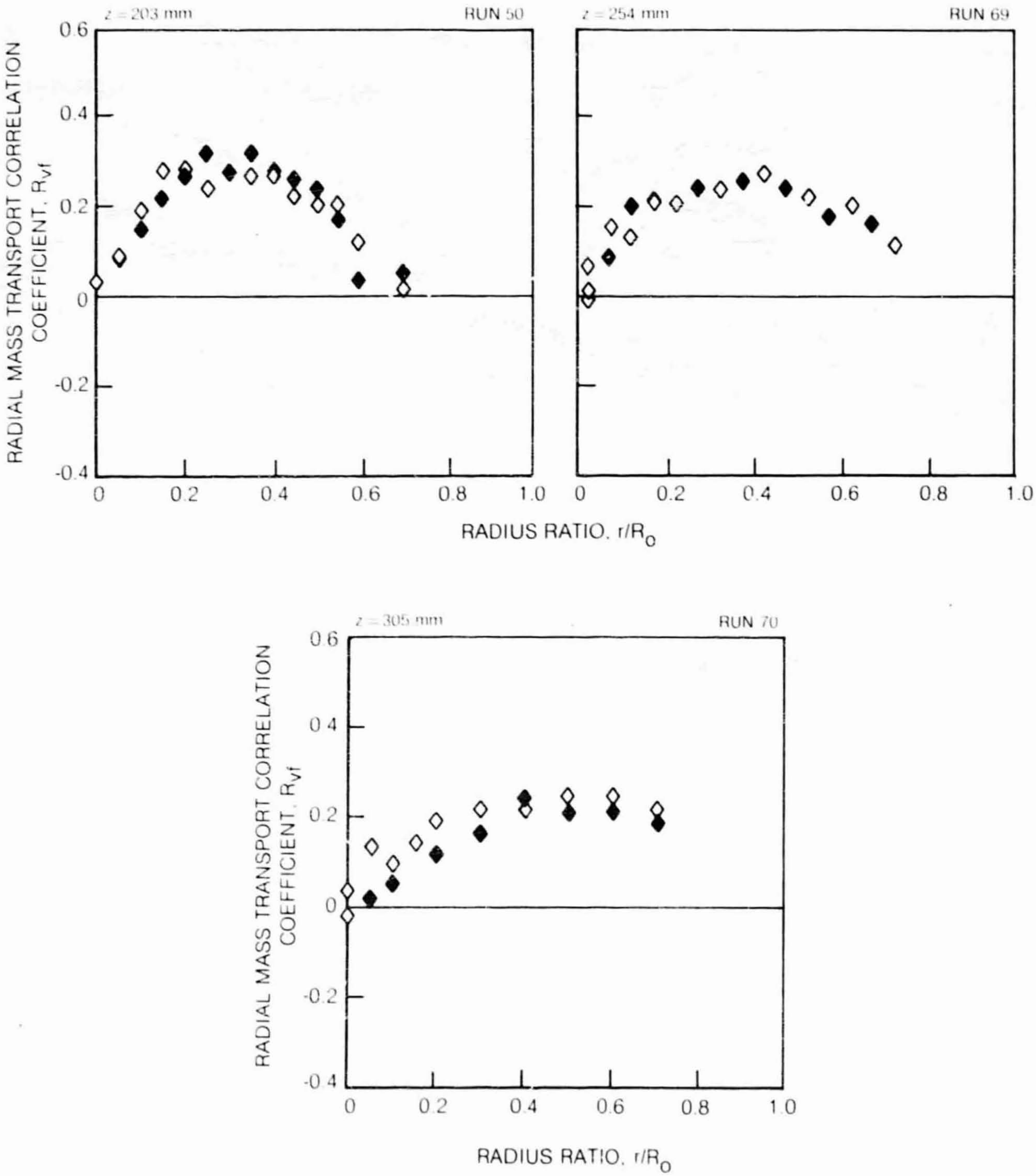

81-12-38-36

AXIAL MASS TRANSPORT RATE, $\overline{uf}$, PROFILES

SYMBOL	△	▲
LOCATION, θ	0	180

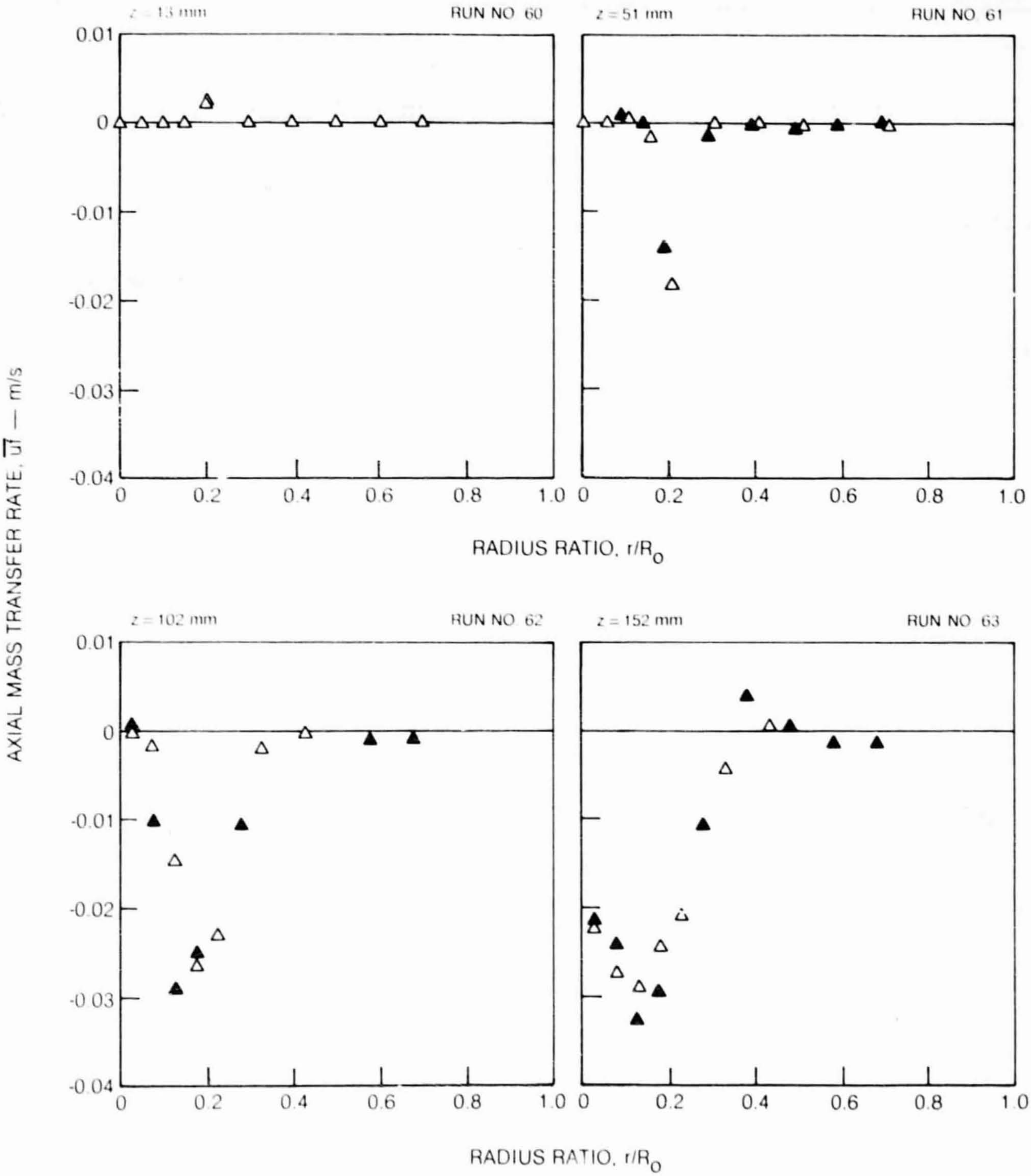

81–9–33–2

AXIAL MASS TRANSPORT RATE, $\overline{uf}$, PROFILES (CONT.)

SYMBOL	△	▲
LOCATION, θ	0	180

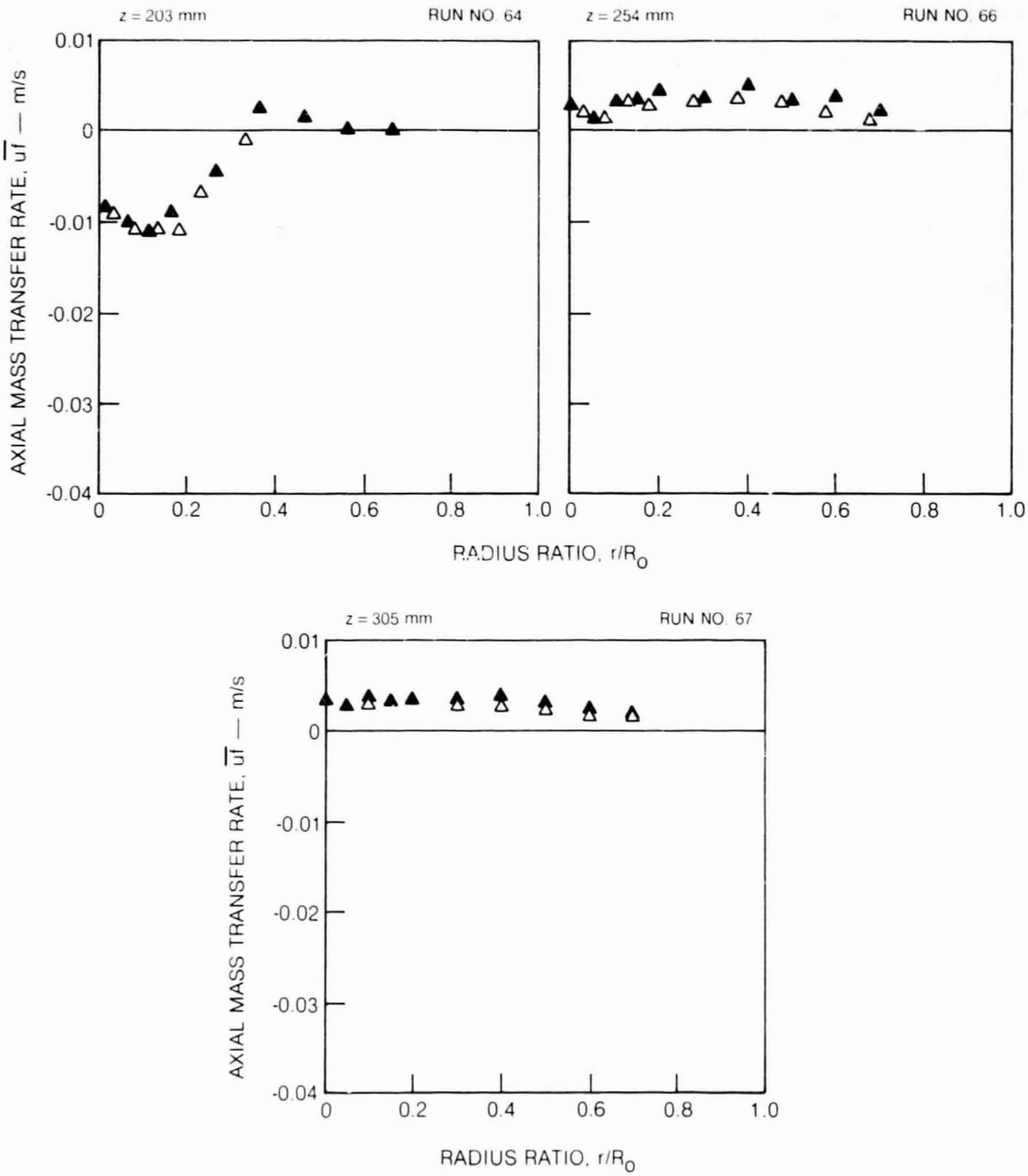

81-9-33-1

SKETCHES OF REGIONS WITH COUNTER-GRADIENT AXIAL TURBULENT MASS TRANSPORT AND AXIAL VELOCITY ACCELERATIONS

ZONE

M1 — CONSTANT CONCENTRATION, NO AXIAL MASS TRANSFER
M2 — COUNTER-GRADIENT MASS TRANSPORT, $\overline{uf}/(-\partial f/\partial z) < 0$
M3 — GRADIENT MASS TRANSPORT, $\overline{uf}/(-\partial f/\partial z) > 0$
M4 — LOW AXIAL TRANSPORT RATE

a) AXIAL TURBULENT MASS TRANSPORT

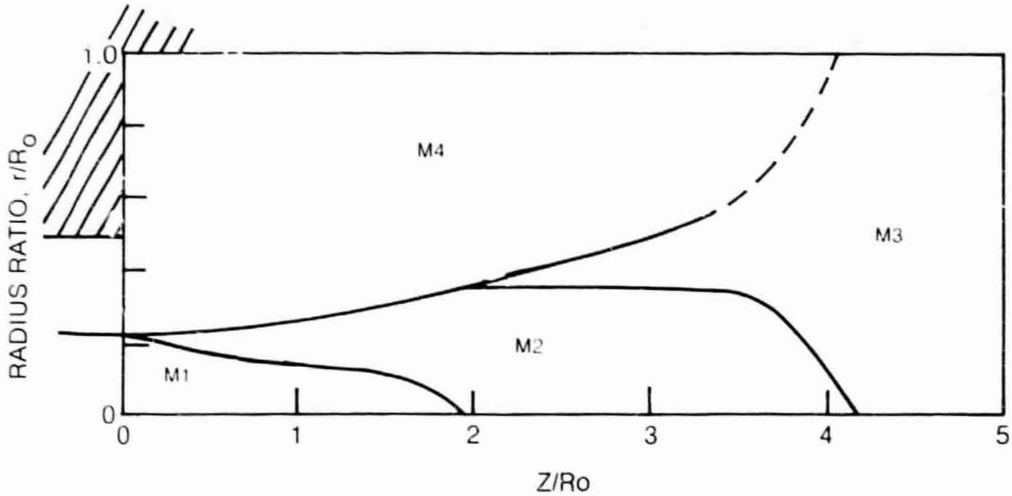

ZONE

V1 — CONSTANT AXIAL VELOCITY
V2 — ACCELERATING AXIAL VELOCITY, $\partial U/\partial z > 0$
V3 — DECELERATING AXIAL VELOCITY, $\partial U/\partial z < 0$
V4 — RECIRCULATION ZONE

b) AXIAL VELOCITY ACCELERATION REGIONS

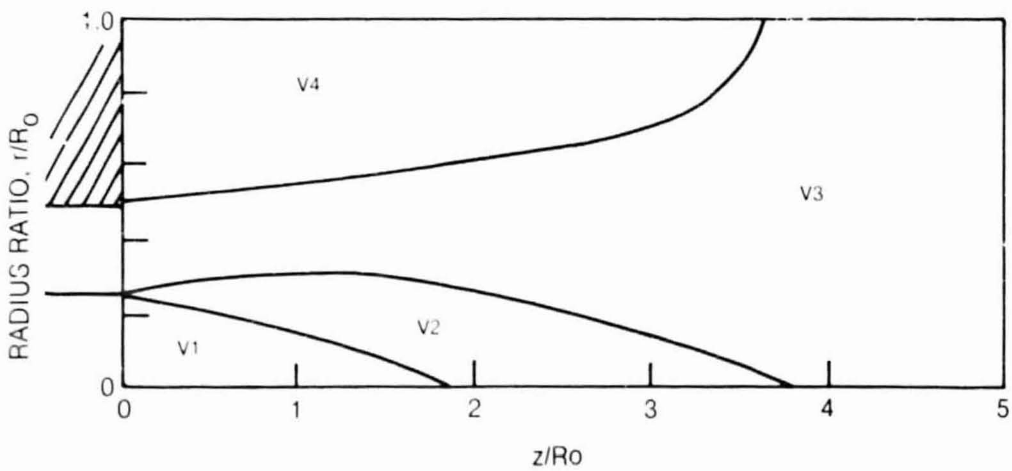

81–9–33–3

AXIAL MASS TRANSPORT CORRELATION COEFFICIENT, R_{uf}, PROFILES

SYMBOL	△	▲
LOCATION, θ	0	180

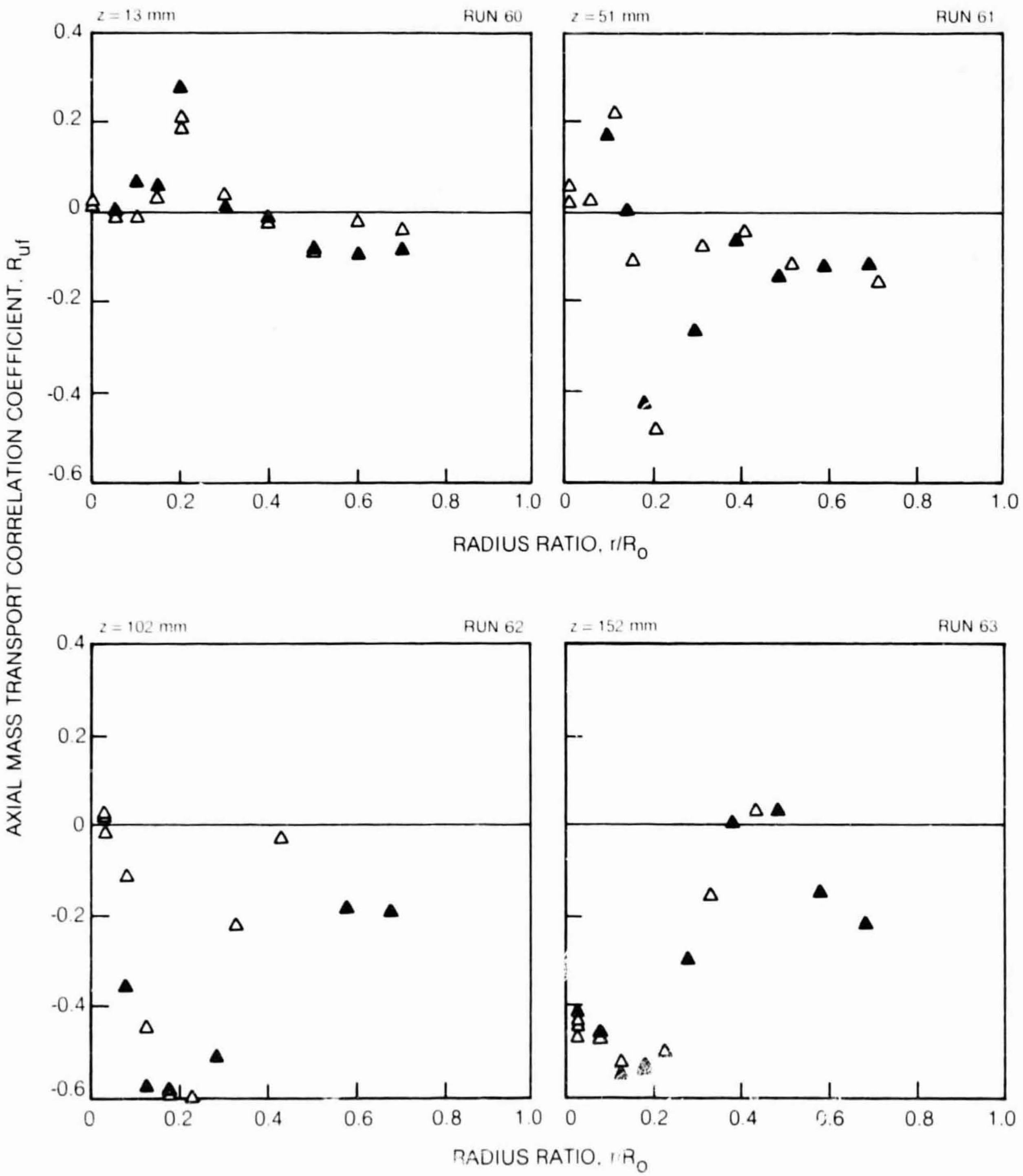

81-12-38-37

AXIAL MASS TRANSPORT CORRELATION COEFFICIENT, R_{uf}, PROFILES (CONT.)

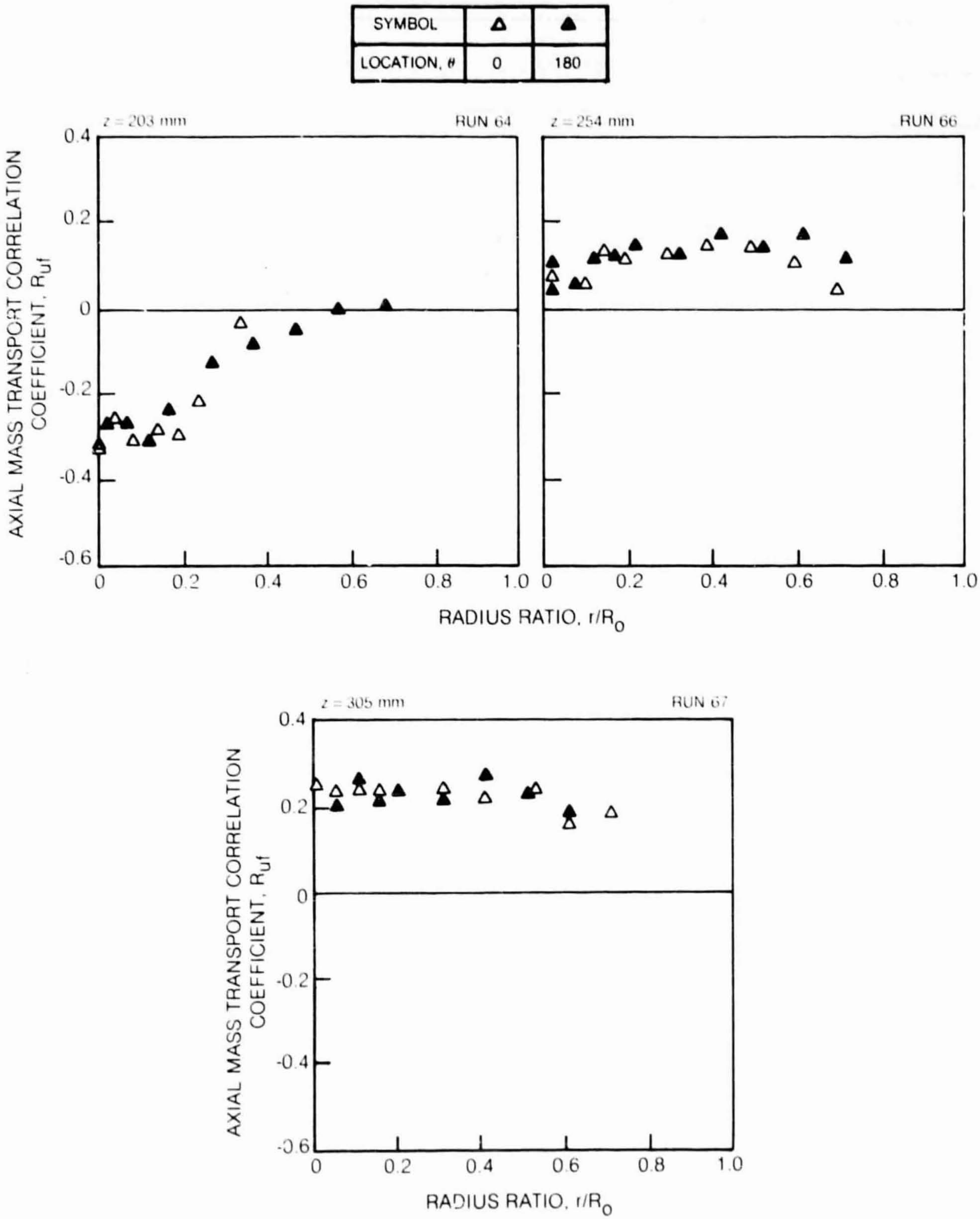

81-12-38-38

AZIMUTHAL MASS TRANSPORT RATE, $\overline{wf}$, AND CORRELATION COEFFICIENT, R_{wf}, PROFILES

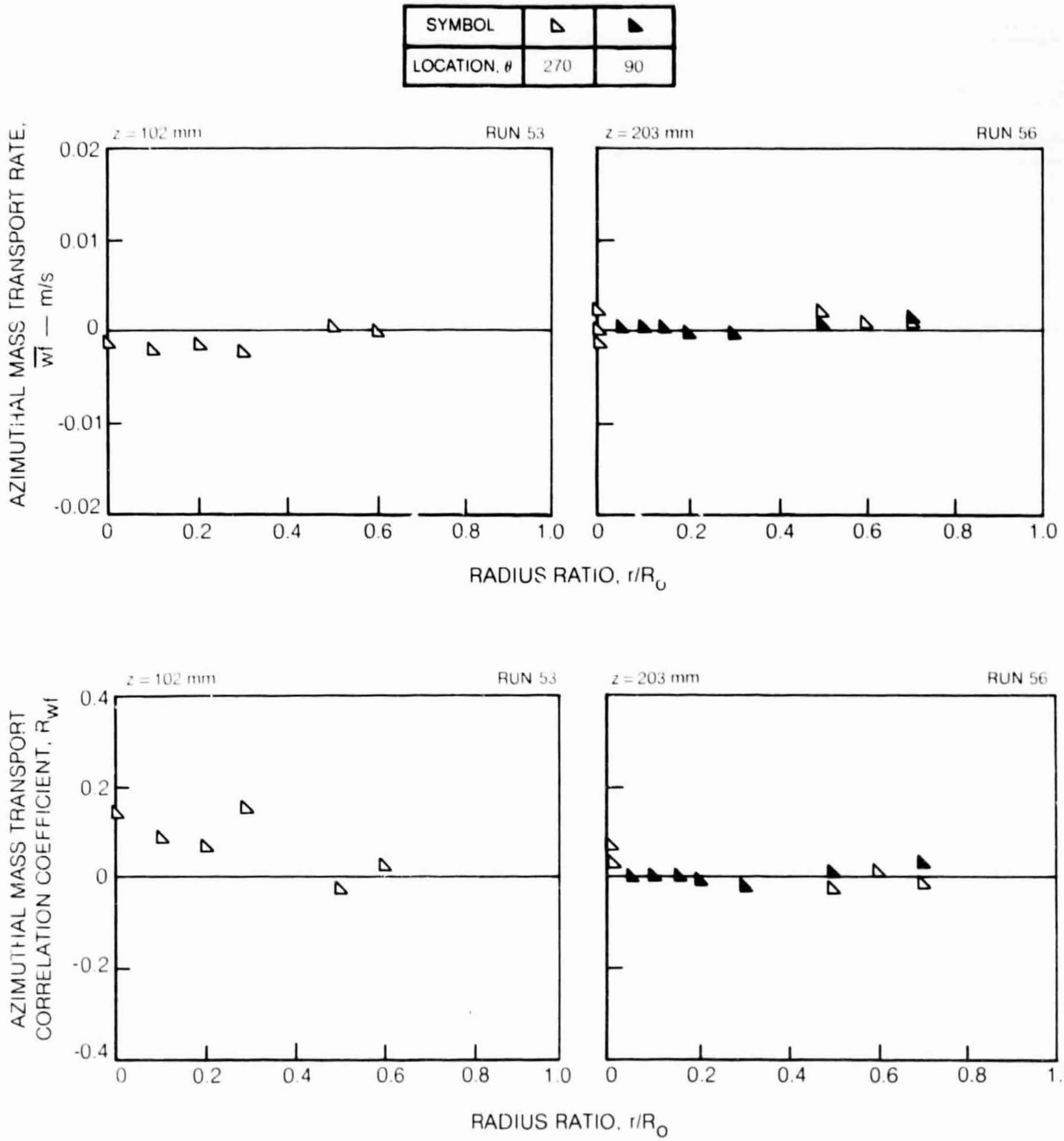

81-12-38-39

AXIAL VELOCITY PROBABILITY DENSITY FUNCTIONS

AXIAL LOCATION 102 mm

DATA FROM RUNS 16 AND 62

r/R_o	U	u'	S_u	K_u
0	0.77	0.11	0.66	5.3
0.1	0.84	0.15	1.01	5.0
0.2	1.20	0.22	-0.15	2.6
0.35	1.50	0.16	-1.62	7.2
0.5	0.86	0.34	-0.42	3.2
0.6	0.45	0.37	-0.15	3.1

$\Delta u = 0.1$ m/s

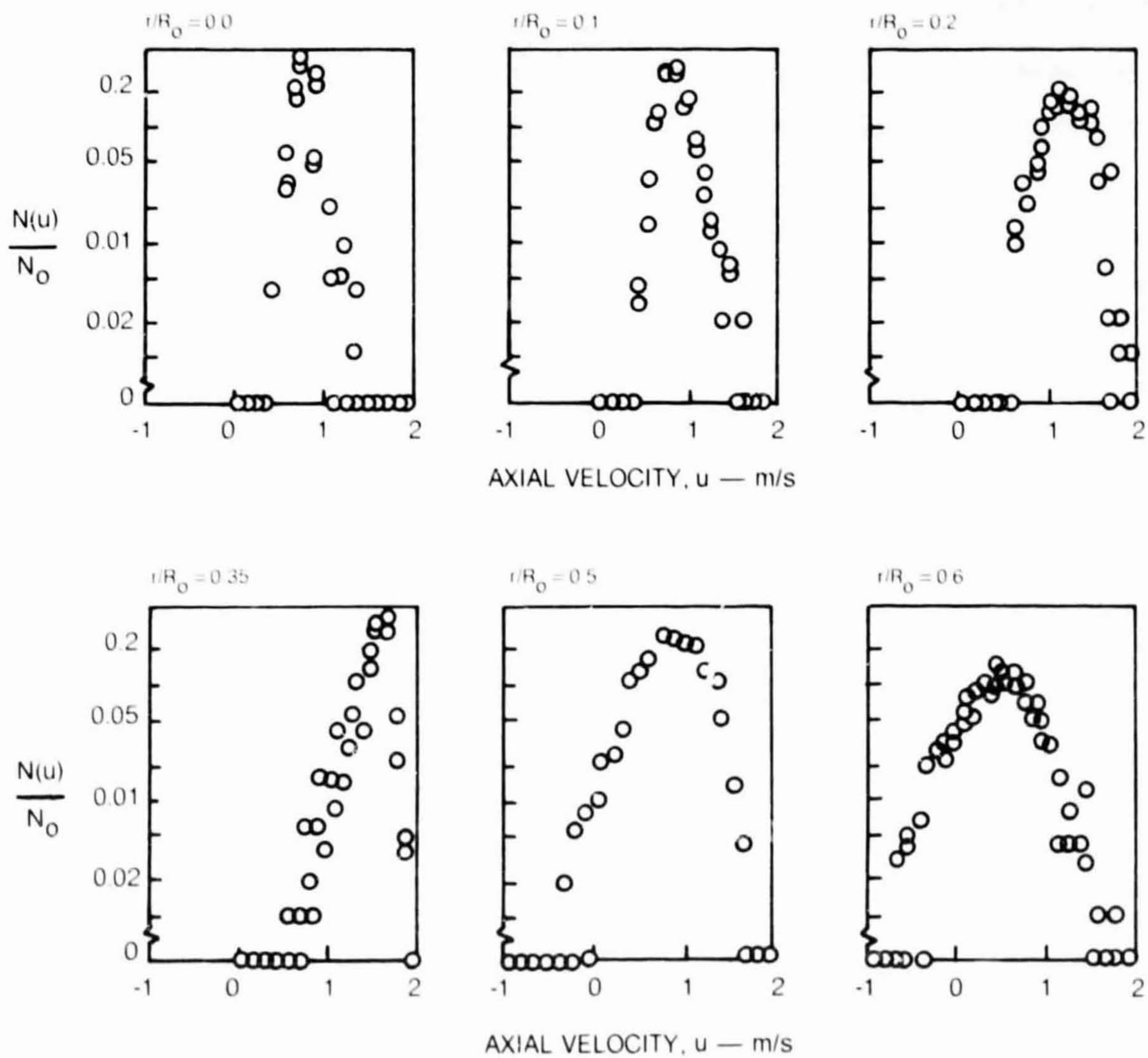

81–12–38–40

RADIAL VELOCITY PROBABILITY DENSITY FUNCTIONS

AXIAL LOCATION 102 mm

DATA FROM RUNS 16 AND 52

r/R_o	V	v'	S_v	K_v
0	-0.01	0.9	0.05	7.2
0.1	-0.05	0.13	-0.90	4.1
0.2	-0.06	0.15	-0.14	3.2
0.35	0	0.15	-0.29	4.8
0.5	0.07	0.22	-0.13	3.2
0.6	0.06	0.26	0.15	2.8

$\Delta v = 0.1$ m/s

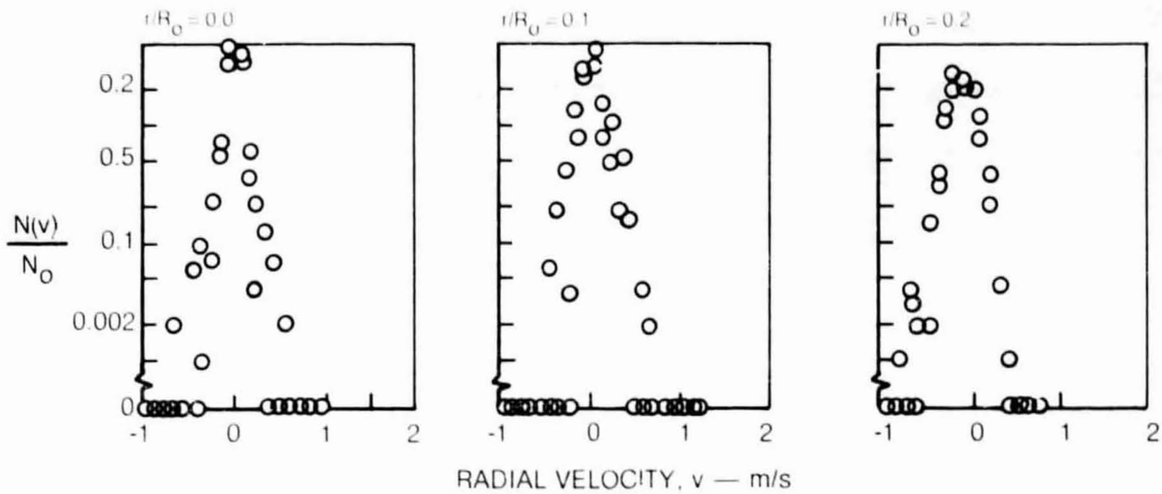

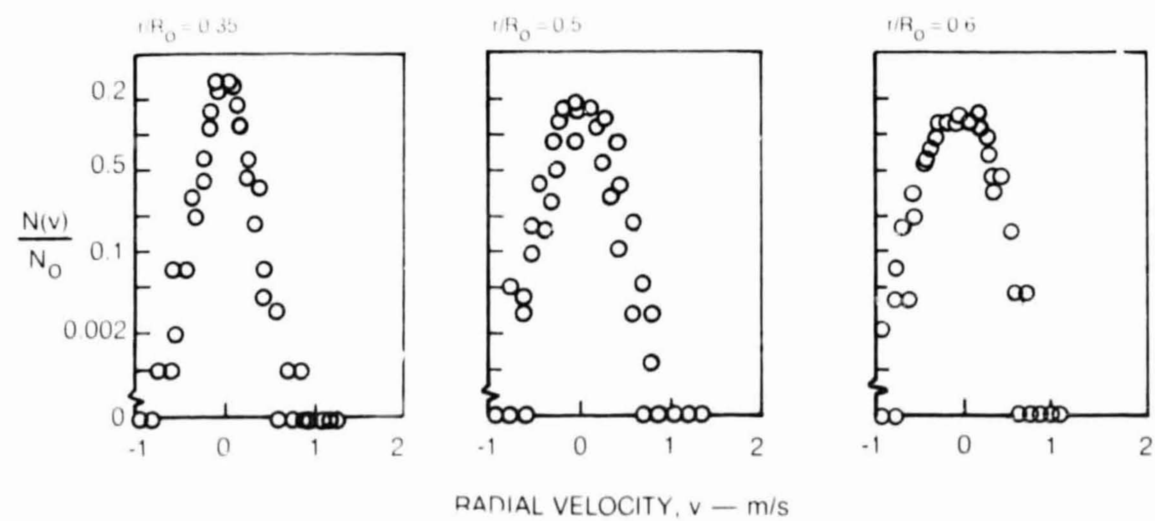

81-12-38-41

AZIMUTHAL VELOCITY PROBABILITY DENSITY FUNCTIONS

AXIAL LOCATION 102 mm

DATA FROM RUNS 53

r/R_o	W	w'	S_w	K_w
0	0.01	0.06	0.28	5.1
0.1	0.01	0.10	0.18	5.0
0.2	0.02	0.14	-0.10	3.3
0.3	0.03	0.12	-0.16	4.5
0.5	0.03	0.26	0.10	3.8
0.6	0.04	0.26	0.12	3.5

$\Delta w = 0.1$ m/s

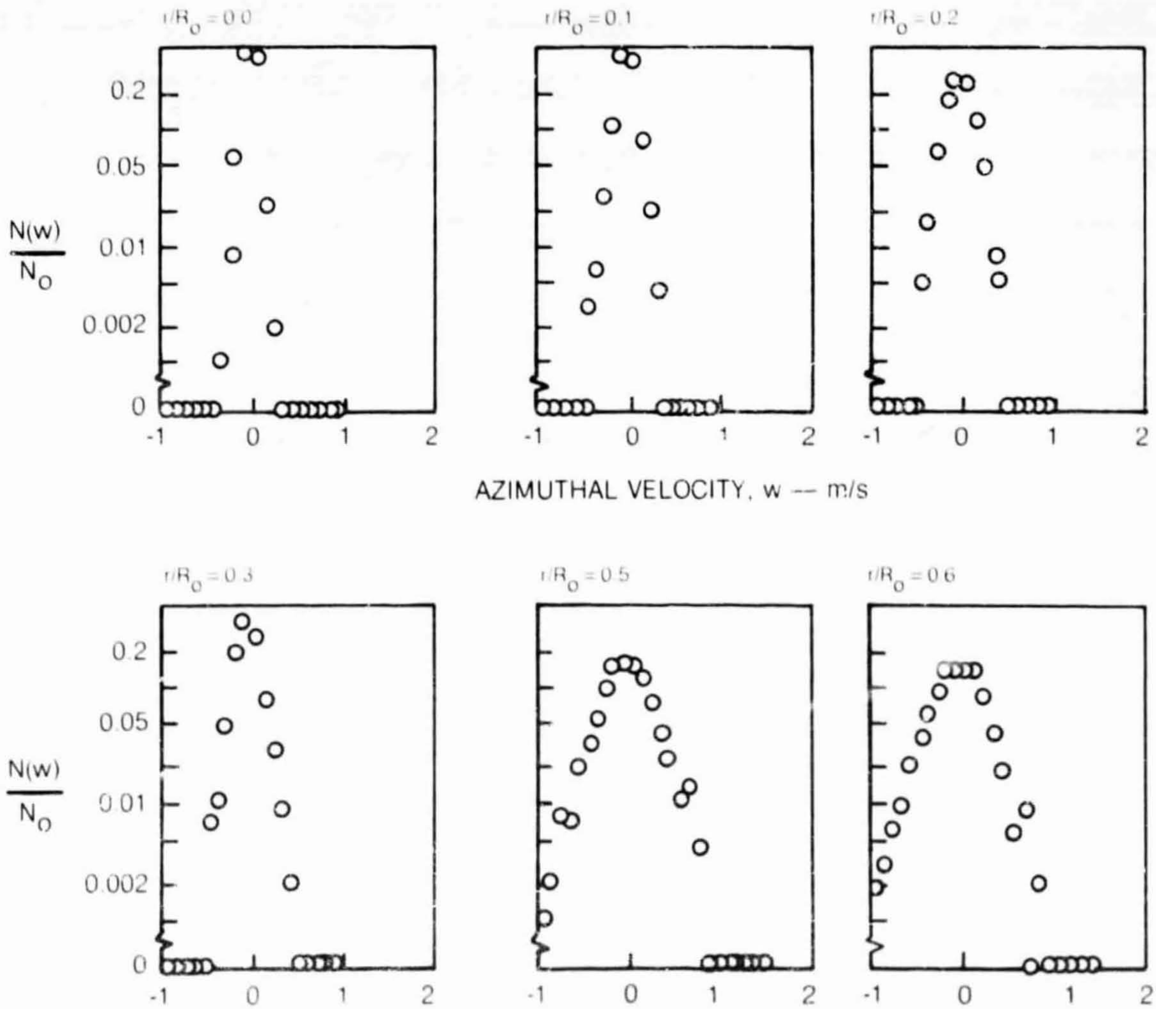

81-12-38-42

INNER JET FLUID CONCENTRATION PROBABILITY DENSITY FUNCTIONS

DATA FROM RUNS 52, 53 AND 62

$\Delta f = 0.02$

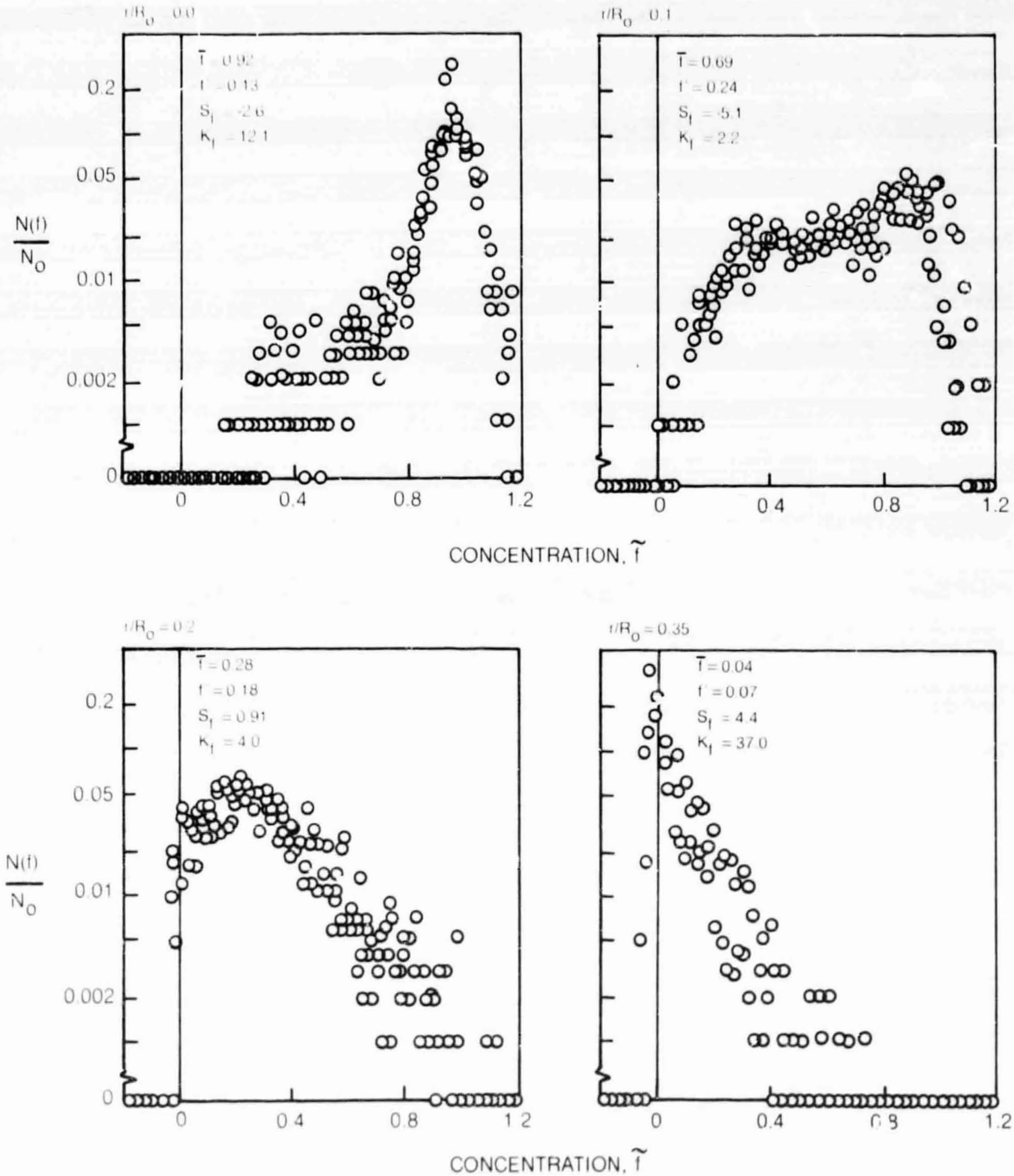

81–12–38–43

SKEWNESS AND KURTOSIS OF AXIAL VELOCITIES PROFILES

SYMBOL	○	●	□	■	△	▲
LOCATION, θ	0	180	270	90	0	180
RUN NOS	16, 21		18, 22		62, 64	

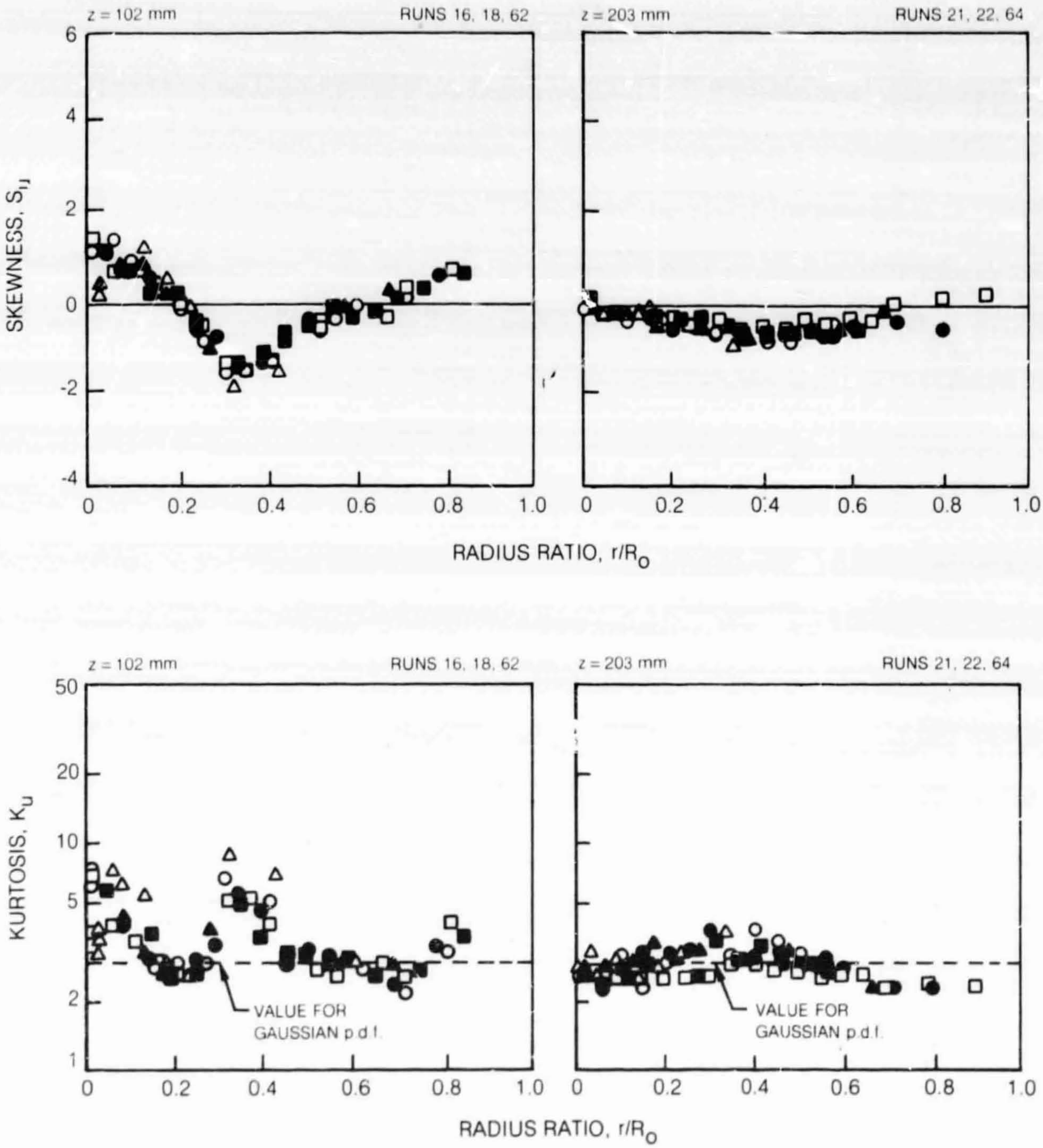

81-12-38-44

SKEWNESS AND KURTOSIS OF RADIAL VELOCITIES PROFILES

SYMBOL	○	●	◇	◆
LOCATION, θ	0	180	0	180
RUN NOS.	16, 21		52, 50	

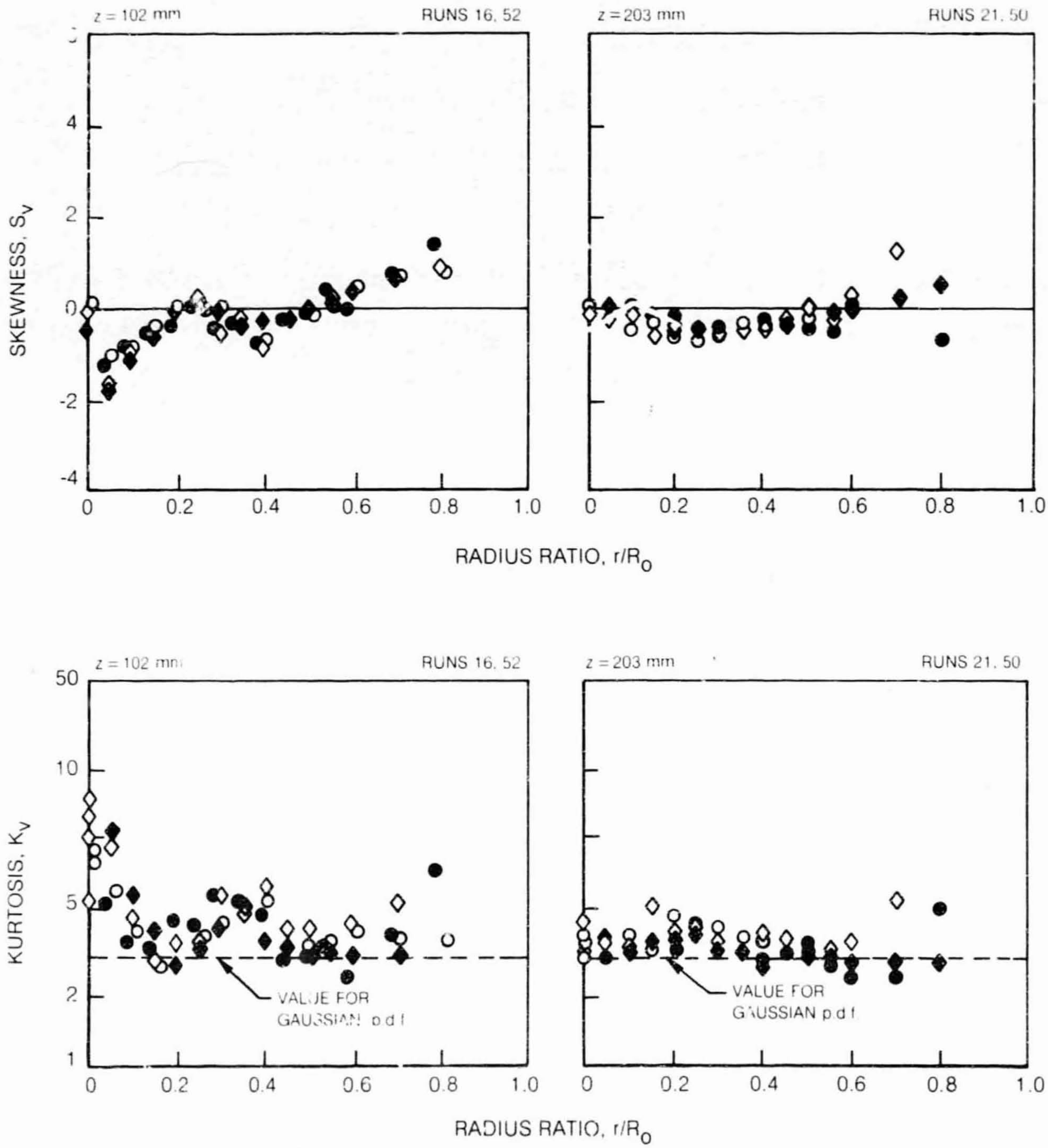

81–12–38–45

SKEWNESS AND KURTOSIS OF AZIMUTHAL VELOCITIES PROFILES

SYMBOL	□	■	◩	◪	◺	◣
LOCATION, θ	270	90	270	90	270	90
RUN NOS	18, 22		23		53, 56	

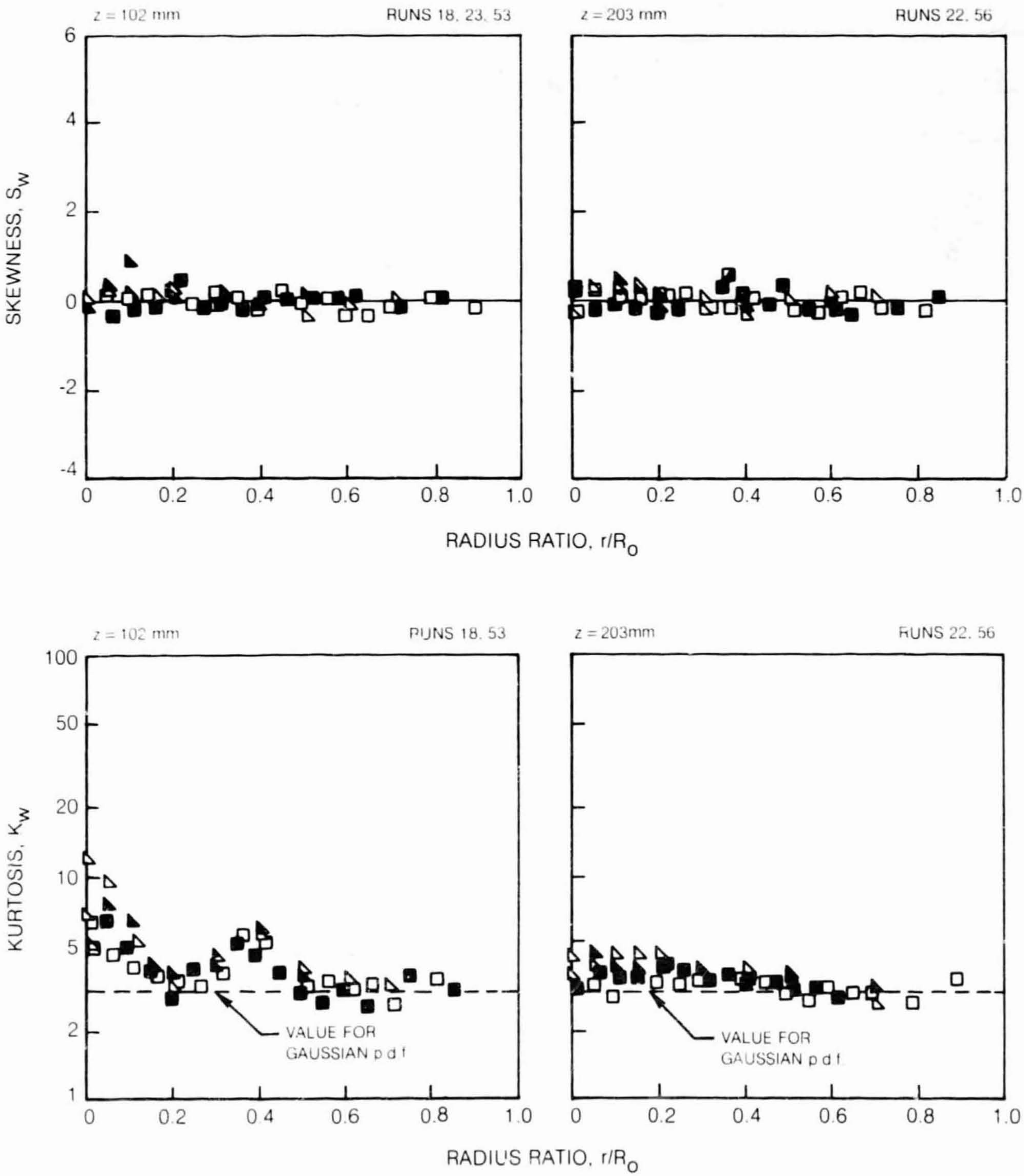

81–12–38–46

SKEWNESS AND KURTOSIS OF INNER JET FLUID CONCENTRATION PROFILES

SYMBOL	△	▲	◇	◆
LOCATION, θ	0	180	0	180
RUN NOS	62, 64		52, 50	

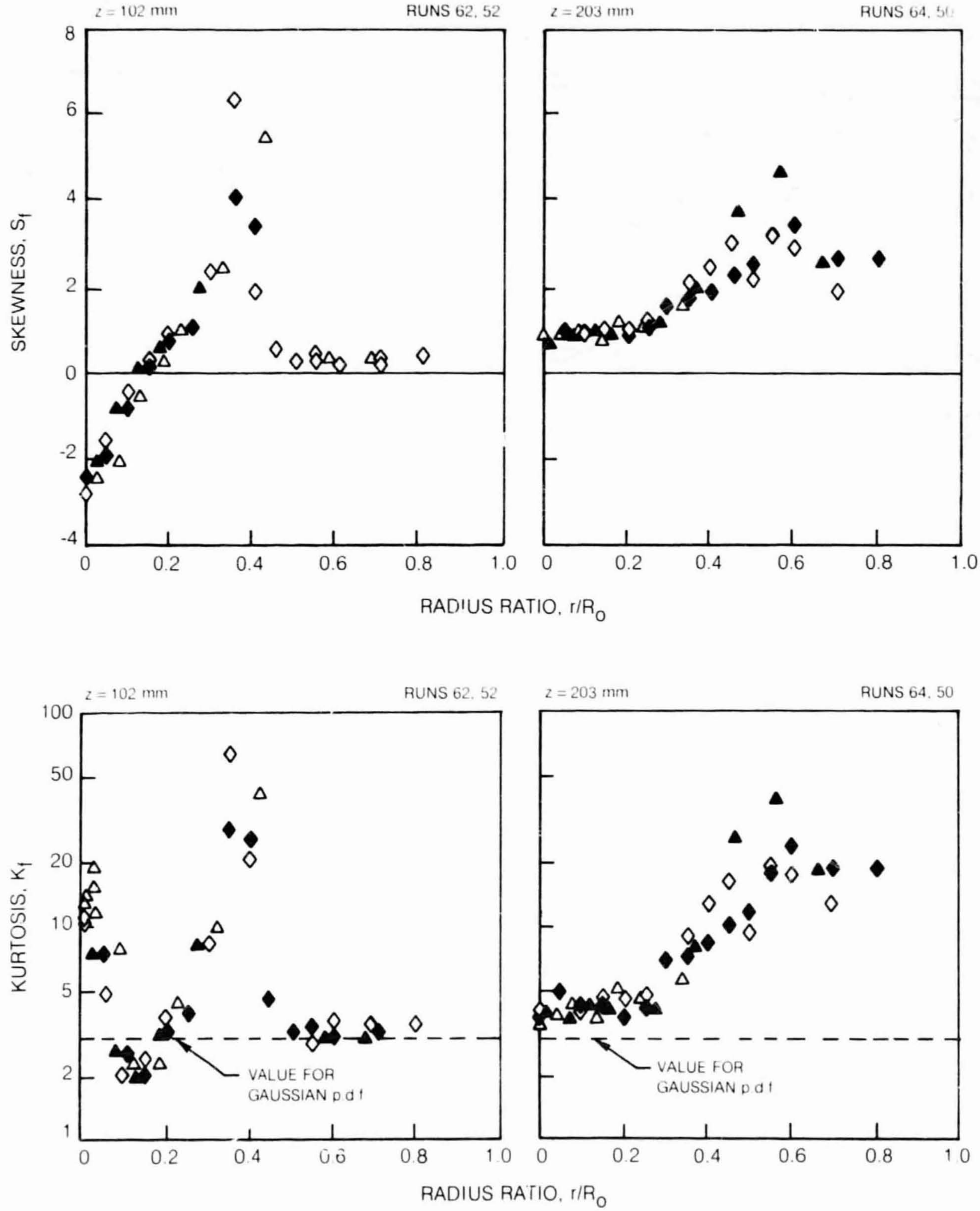

81–12–38–47

AUTOCORRELATION OF LIF SIGNAL

AXIAL LOCATION = 102 mm
SIGNAL DC COUPLED TO SAICOR 42 CORRELATOR

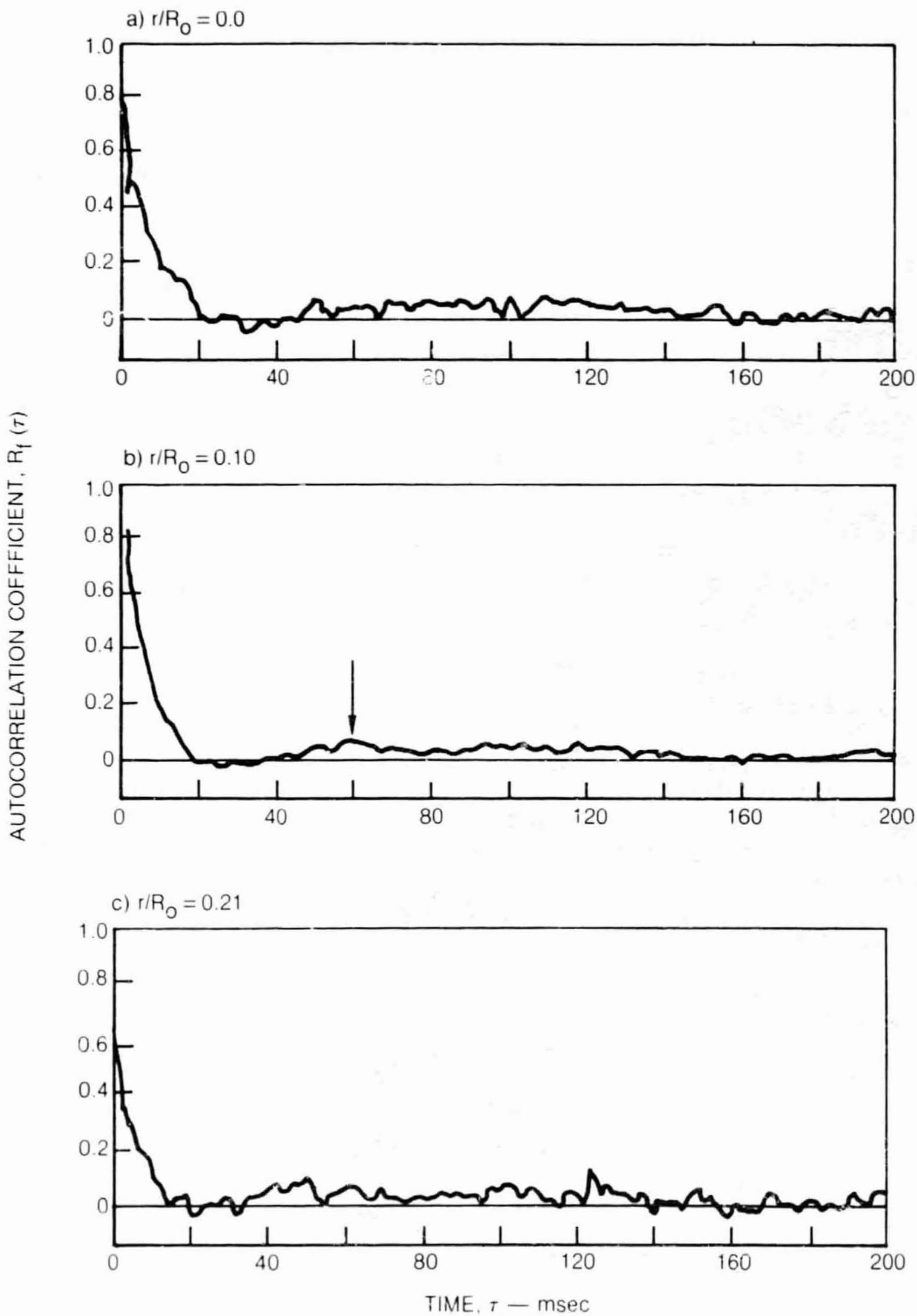

81-12-38-48

TURBULENT MOMENTUM TRANSPORT RATE, uv, PROBABILITY DENSITY FUNCTIONS

AXIAL LOCATION 102 mm

DATA FROM RUN 16

r/R_o	$\overline{uv}$	σ_{uv}	S_{uv}	K_{uv}
0	0.0005	0.030	1.28	41.2
0.1	-0.0096	0.029	-1.79	21.5
0.2	-0.0142	0.030	-2.14	11.9
0.35	0.0064	0.039	3.94	49.9
0.5	0.0277	0.077	1.15	13.2
0.6	0.0371	0.086	1.53	7.2

$\Delta(uv) = 0.1\ m^2/s^2$

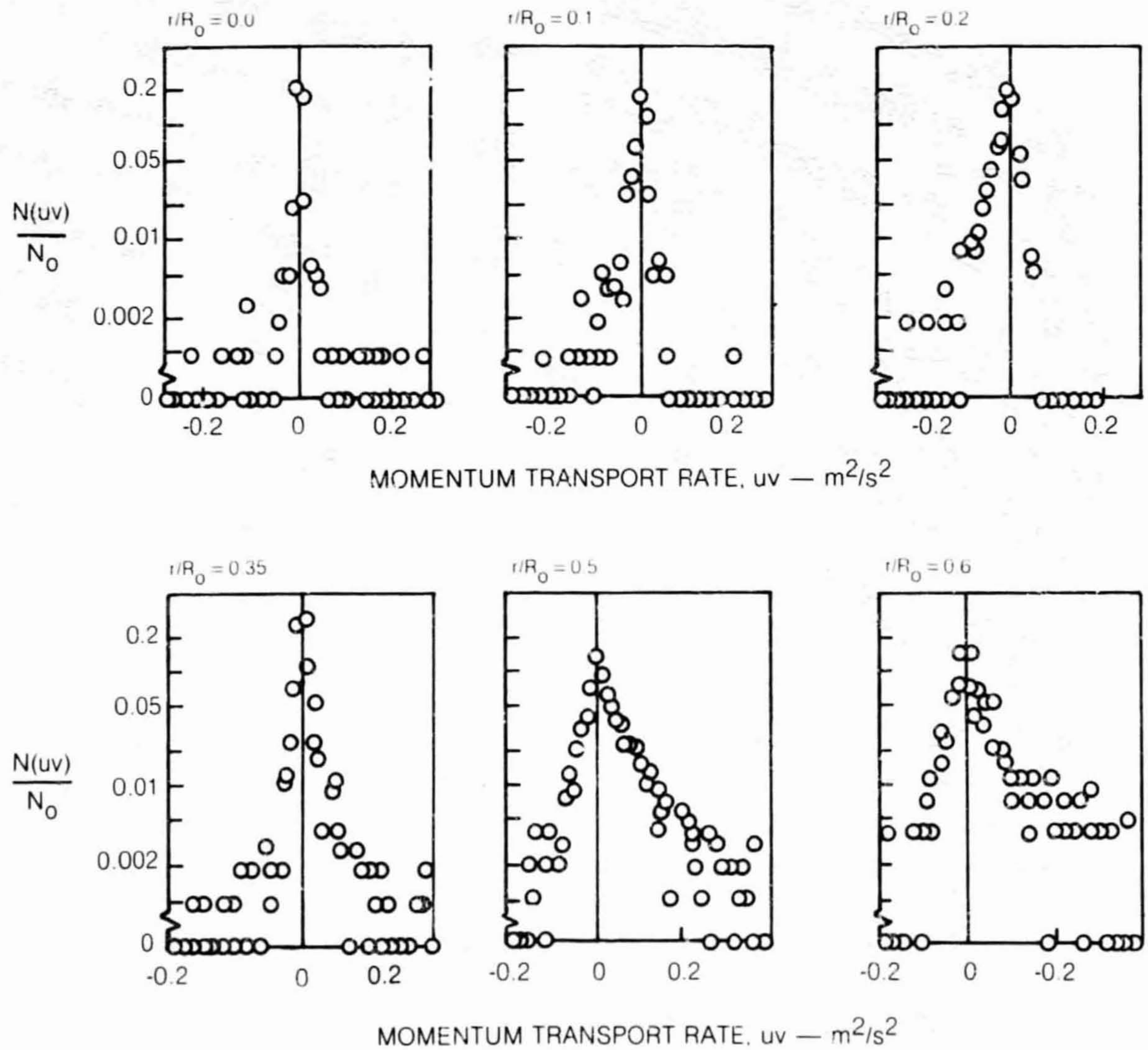

TURBULENT RADIAL MASS TRANSPORT RATE, vf, PROBABILITY DENSITY FUNCTIONS

AXIAL LOCATION 102 mm

DATA FROM RUN 52

r/R_o	$\overline{vf}$	σ_{vf}	S_{vf}	K_{vf}
0	0.0004	0.017	0.16	60.3
0.1	0.0139	0.032	2.60	15.7
0.2	0.0165	0.028	2.23	10.4
0.35	0.0010	0.011	15.96	340.8
0.5	-0.0005	0.004	-0.59	7.65
0.6	-0.0007	0.005	-1.16	9.35

$\Delta(vf) = 0.4$ m/s

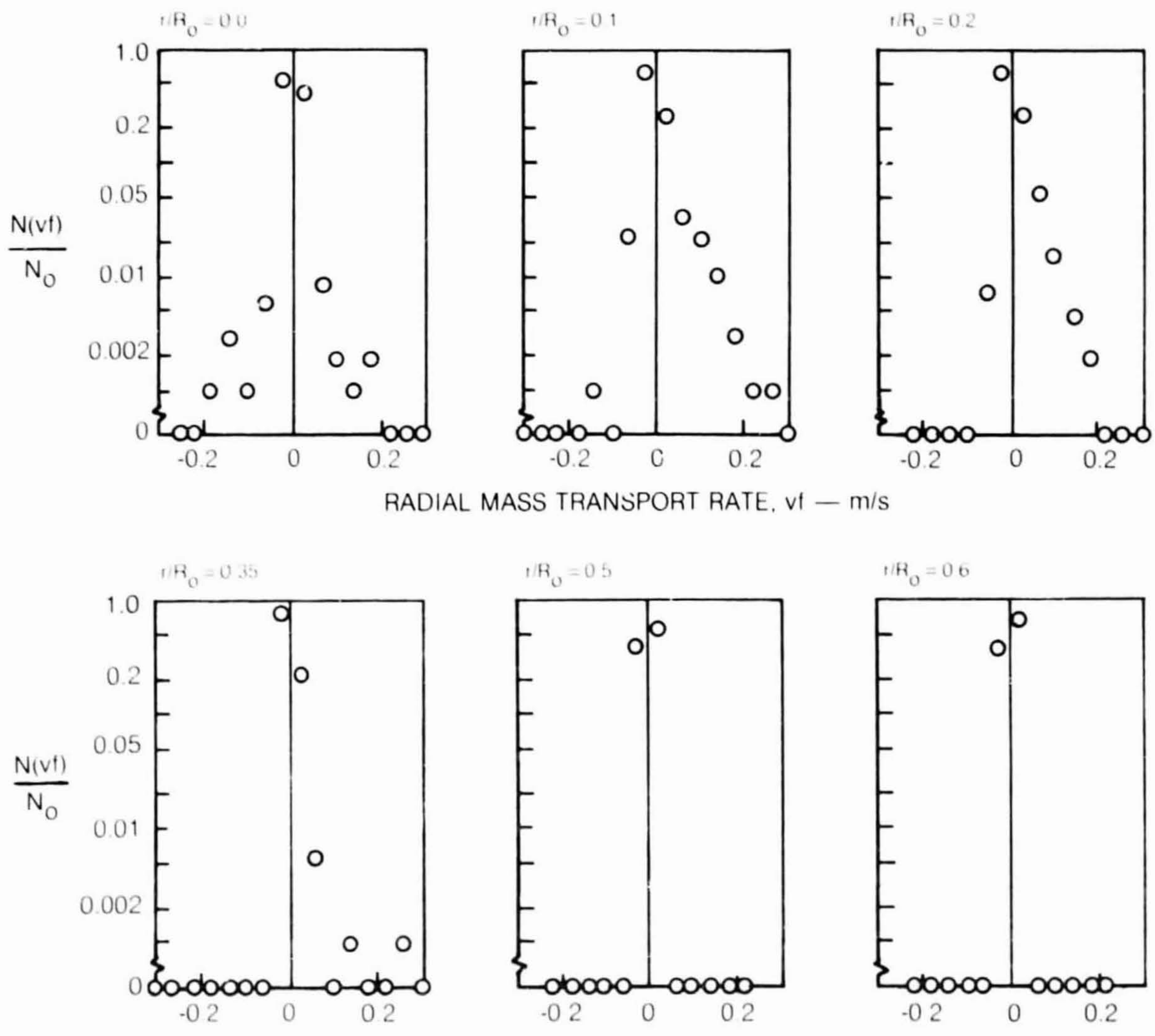

81-12-38-50

TURBULENT AXIAL MASS TRANSPORT RATE, uf, PROBABILITY DENSITY FUNCTIONS

AXIAL LOCATION 102 mm

DATA FROM RUN 62

r/R_o	$\overline{uf}$	σ_{uf}	S_{uf}	K_{uf}
0	-0.0002	0.018	-9.72	175.9
0.1	-0.0146	0.044	-3.74	25.4
0.2	-0.0229	0.044	-2.44	11.5
0.35	-0.0021	0.014	-5.06	54.6
0.6	-0.0011	0.006	-0.65	6.4

$\Delta(uf) = 0.4$ m/s

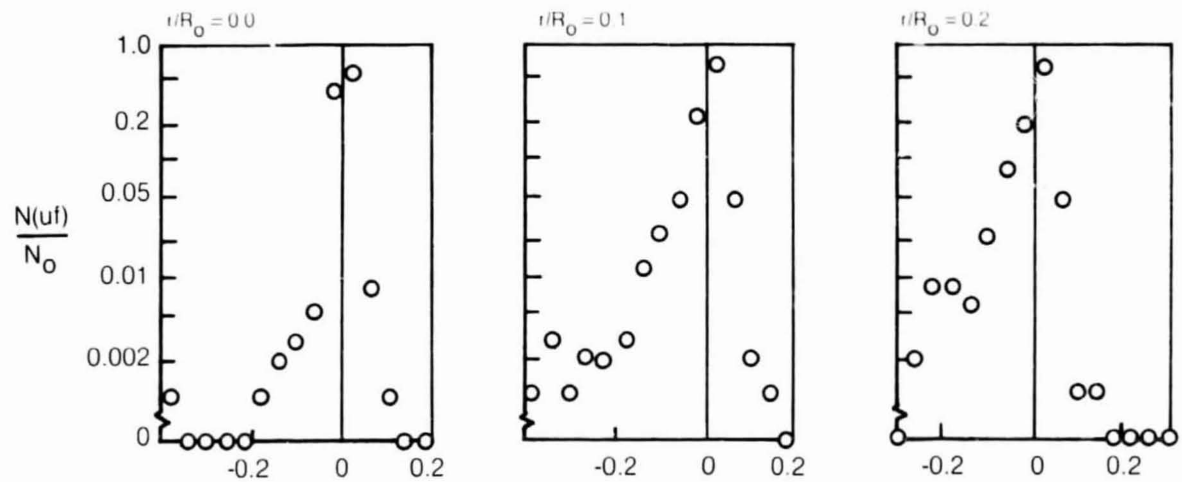

AXIAL MASS TRANSPORT RATE, uf — m/s

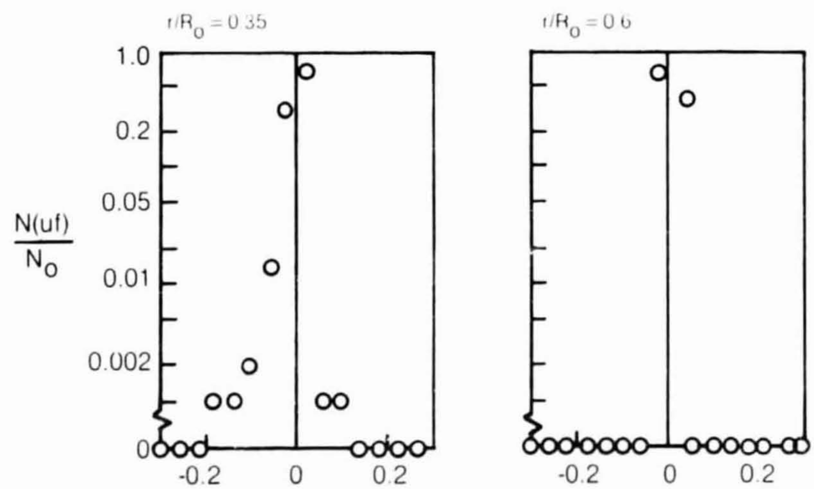

AXIAL MASS TRANSPORT RATE, uf — m/s

81-12-38-51

TURBULENT AZIMUTHAL MASS TRANSPORT RATE, wf, PROBABILITY DENSITY FUNCTIONS

AXIAL LOCATION: 102 mm

DATA FROM RUN 53

r/R_o	$\overline{wf}$	σ_{wf}	S_{wf}	κ_{wf}
0	-0.0012	0.017	-2.66	63.5
0.1	-0.0022	0.033	-0.98	12.6
0.2	-0.0019	0.024	-0.20	7.7
0.3	-0.0022	0.016	-0.72	19.4
0.5	0.0001	0.005	0.29	13.1
0.6	-0.0001	0.004	-0.34	8.2

$\Delta(wf) = 0.4$ m/s

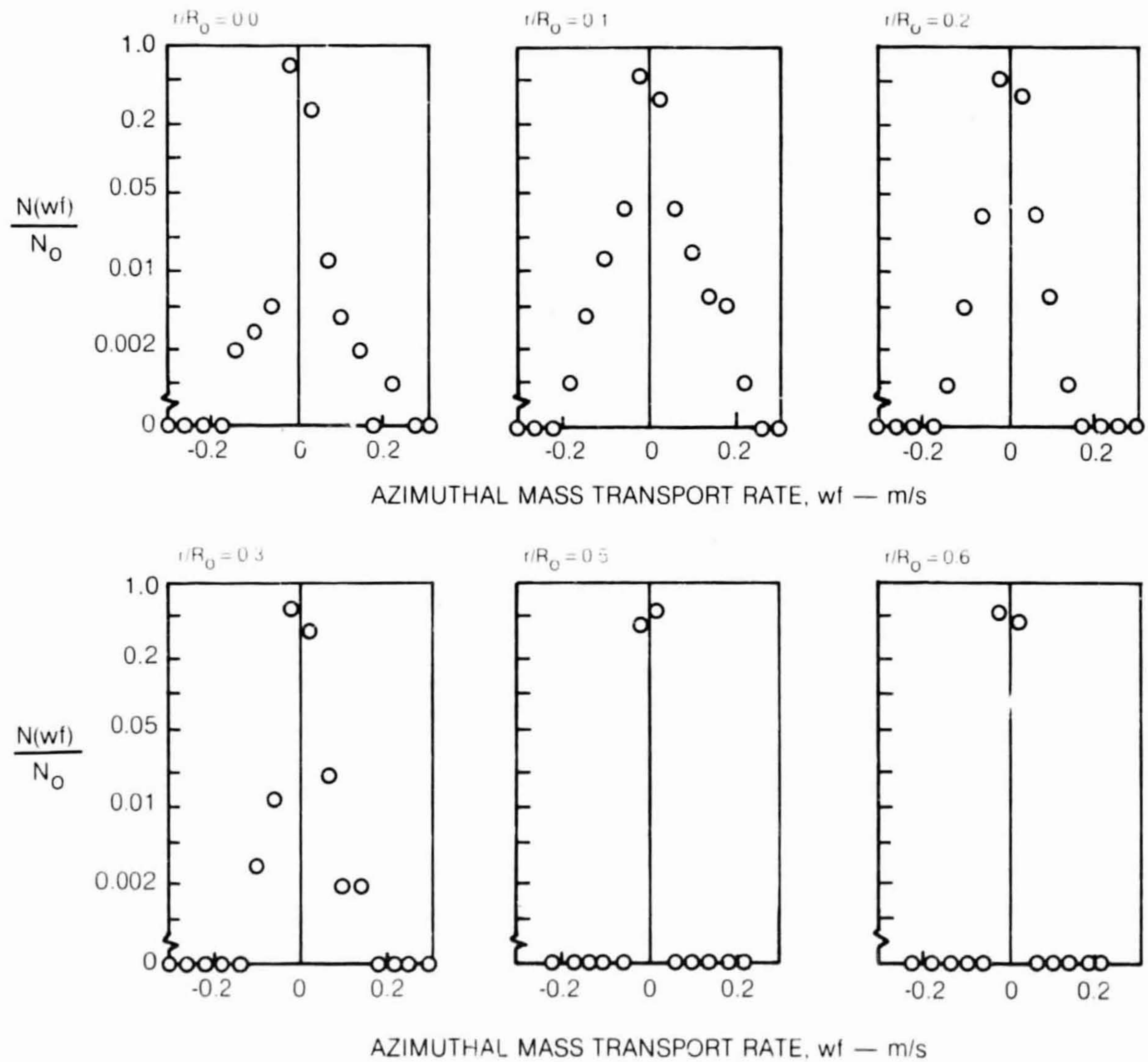

81–12–38–52

SECOND CENTRAL MOMENT OF TURBULENT TRANSPORT RATE PROFILES

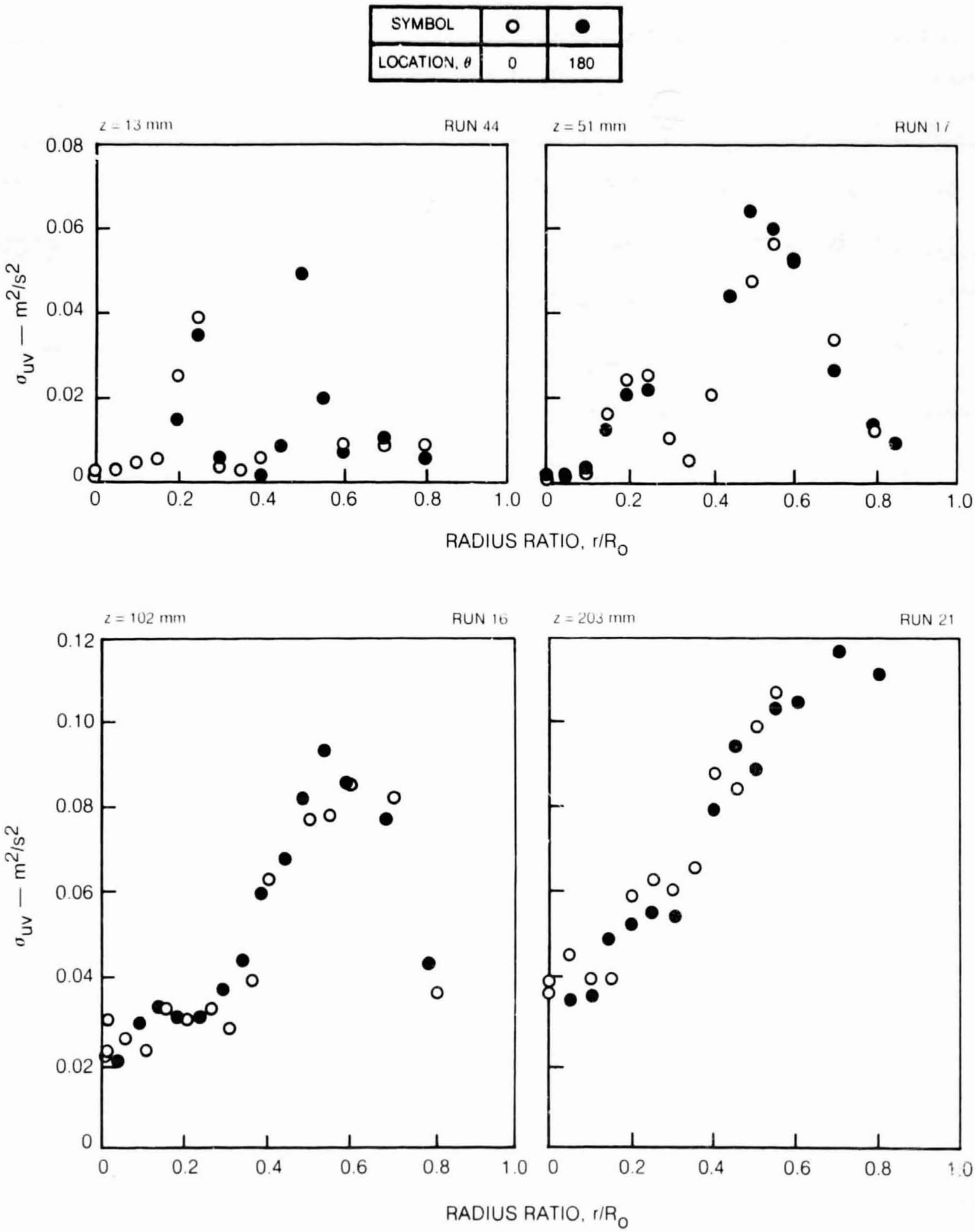

81-12-38-53

SKEWNESS AND KURTOSIS OF TURBULENT MOMENTUM TRANSPORT RATE PROFILES

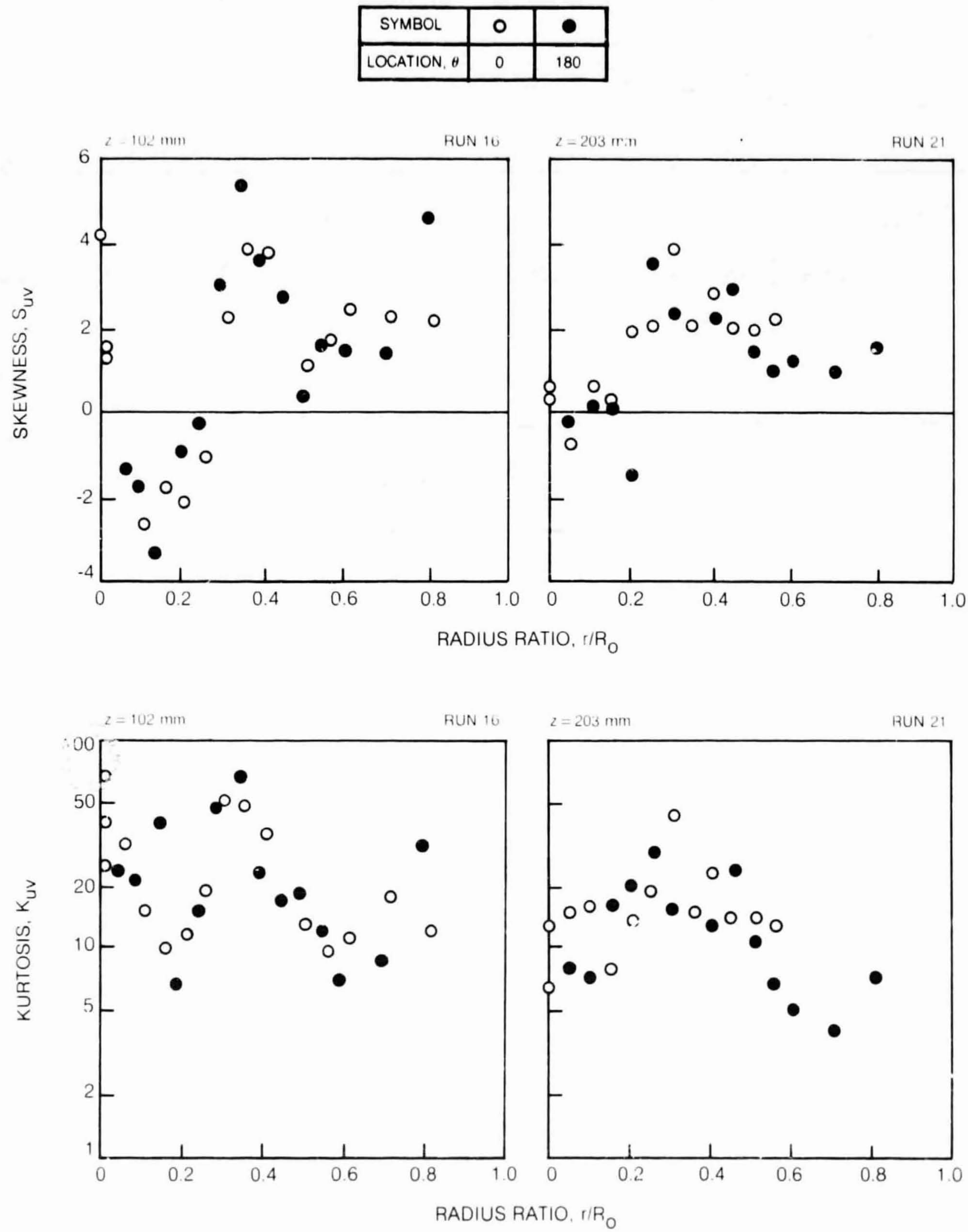

81-12-38-54

SECOND CENTRAL MOMENT OF TURBULENT RADIAL MASS TRANSPORT RATE PROFILES

SYMBOL	△	▲	◇	◆
LOCATION, θ	0	180	0	180

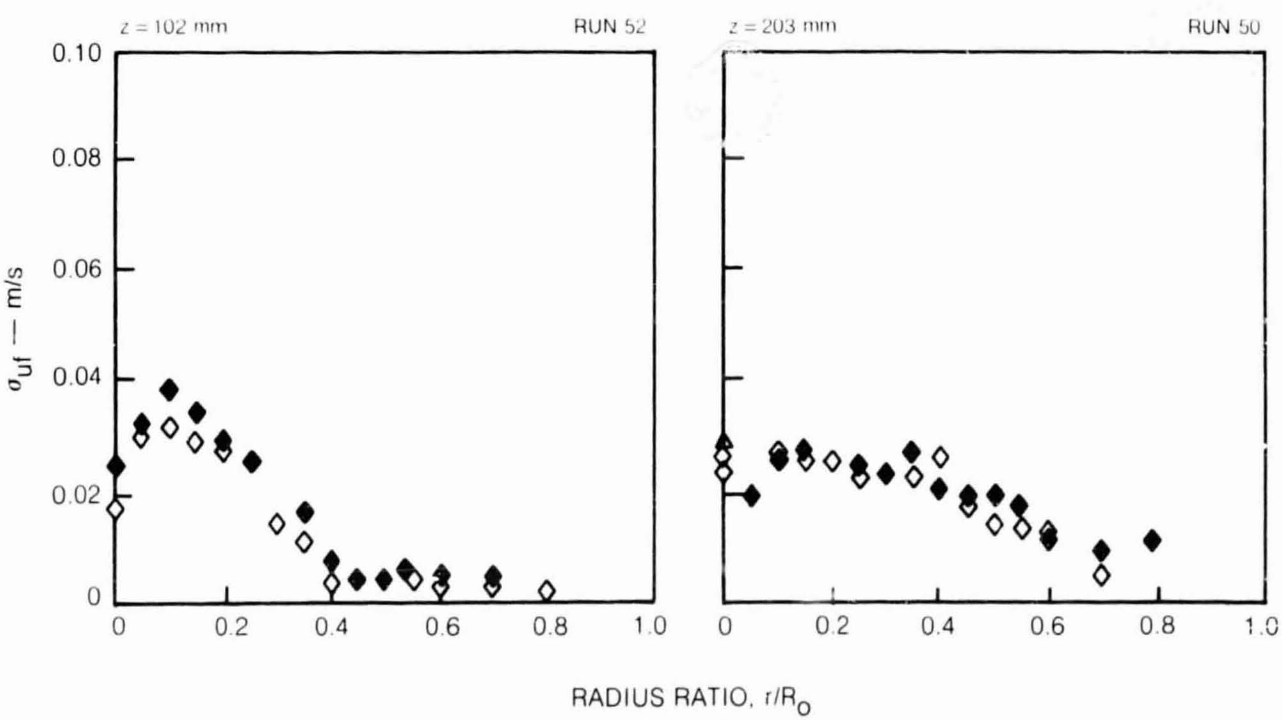

81-12-38-55

SKEWNESS AND KURTOSIS OF TURBULENT RADIAL MASS TRANSPORT RATE PROFILES

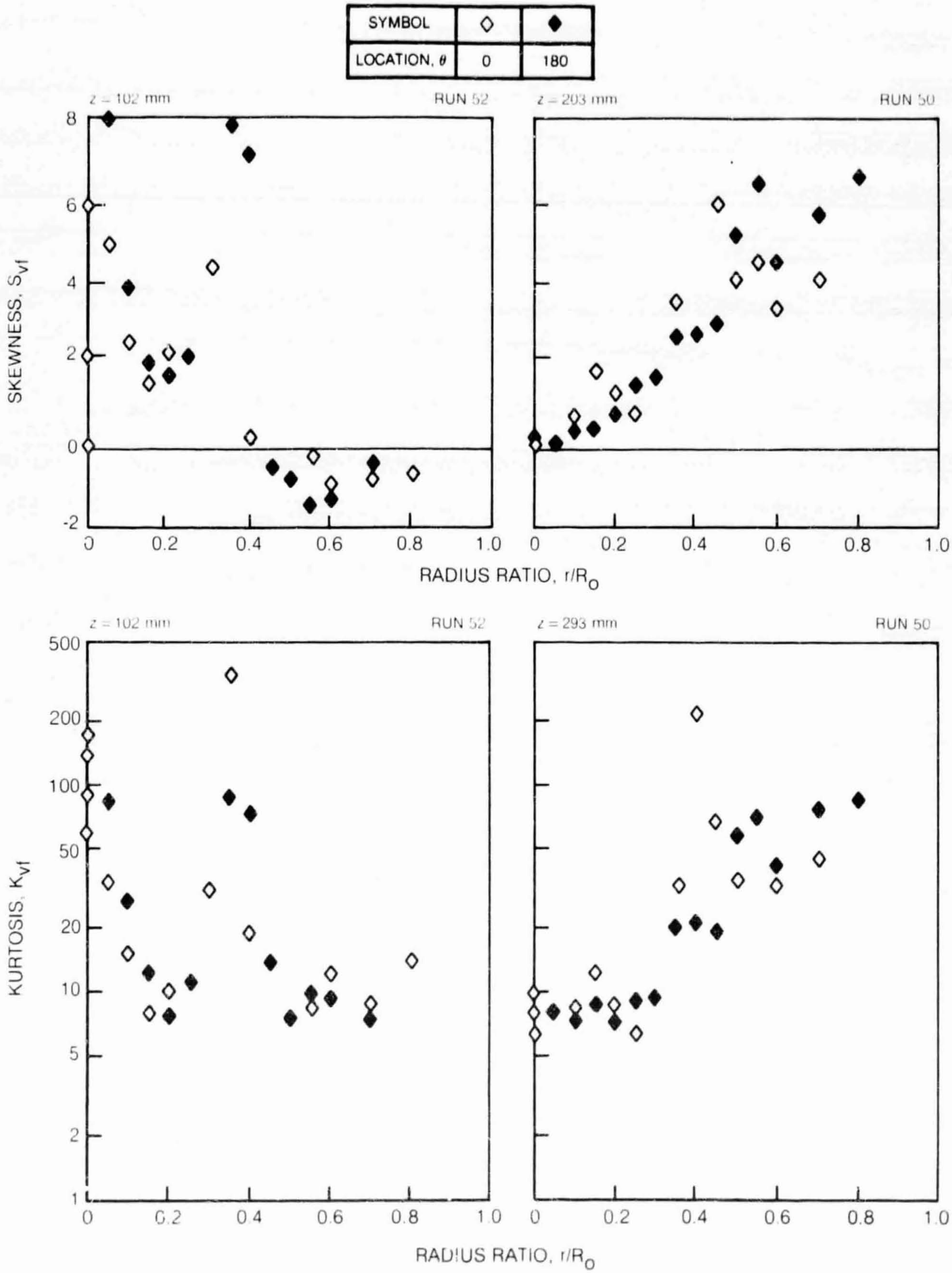

81-12-38-56

SECOND CENTRAL MOMENT OF TURBULENT AXIAL MASS TRANSPORT RATE PROFILES

SYMBOL	△	▲	◊	◆
LOCATION, θ	0	180	0	180

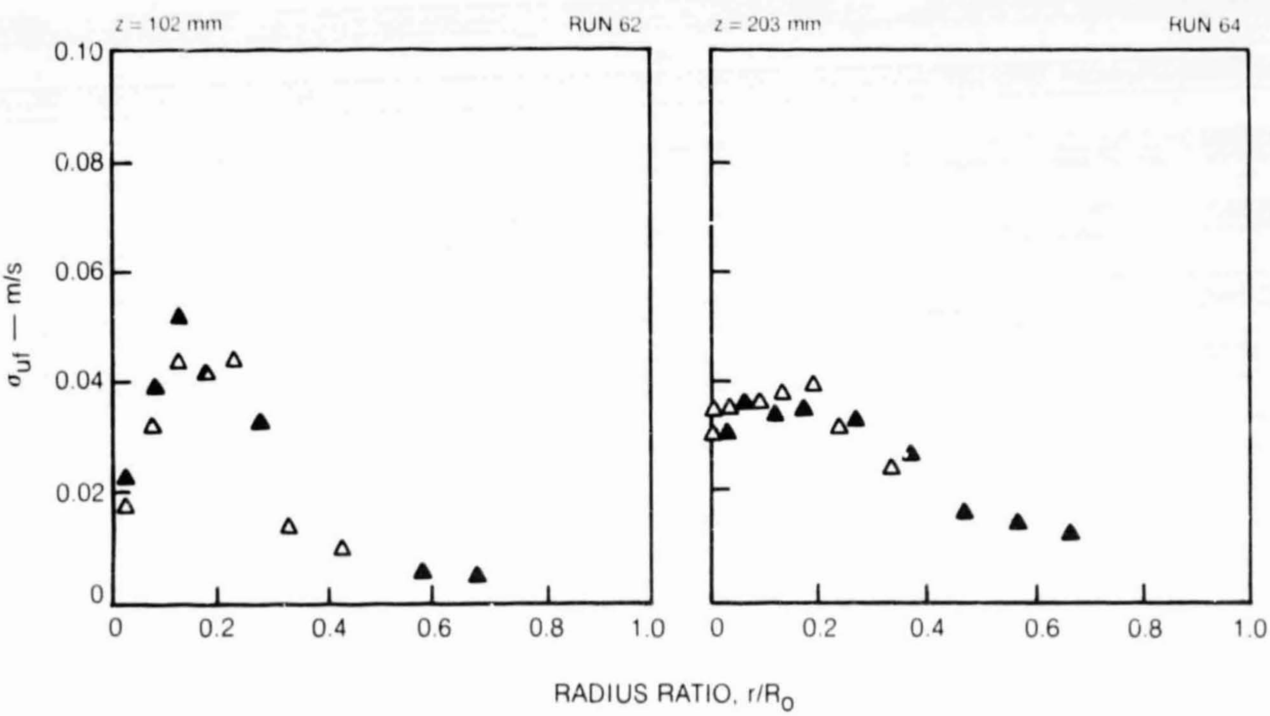

81–12–38–57

SKEWNESS AND KURTOSIS OF TURBULENT AXIAL MASS TRANSPORT RATE PROFILES

SYMBOL	△	▲
LOCATION, θ	0	180

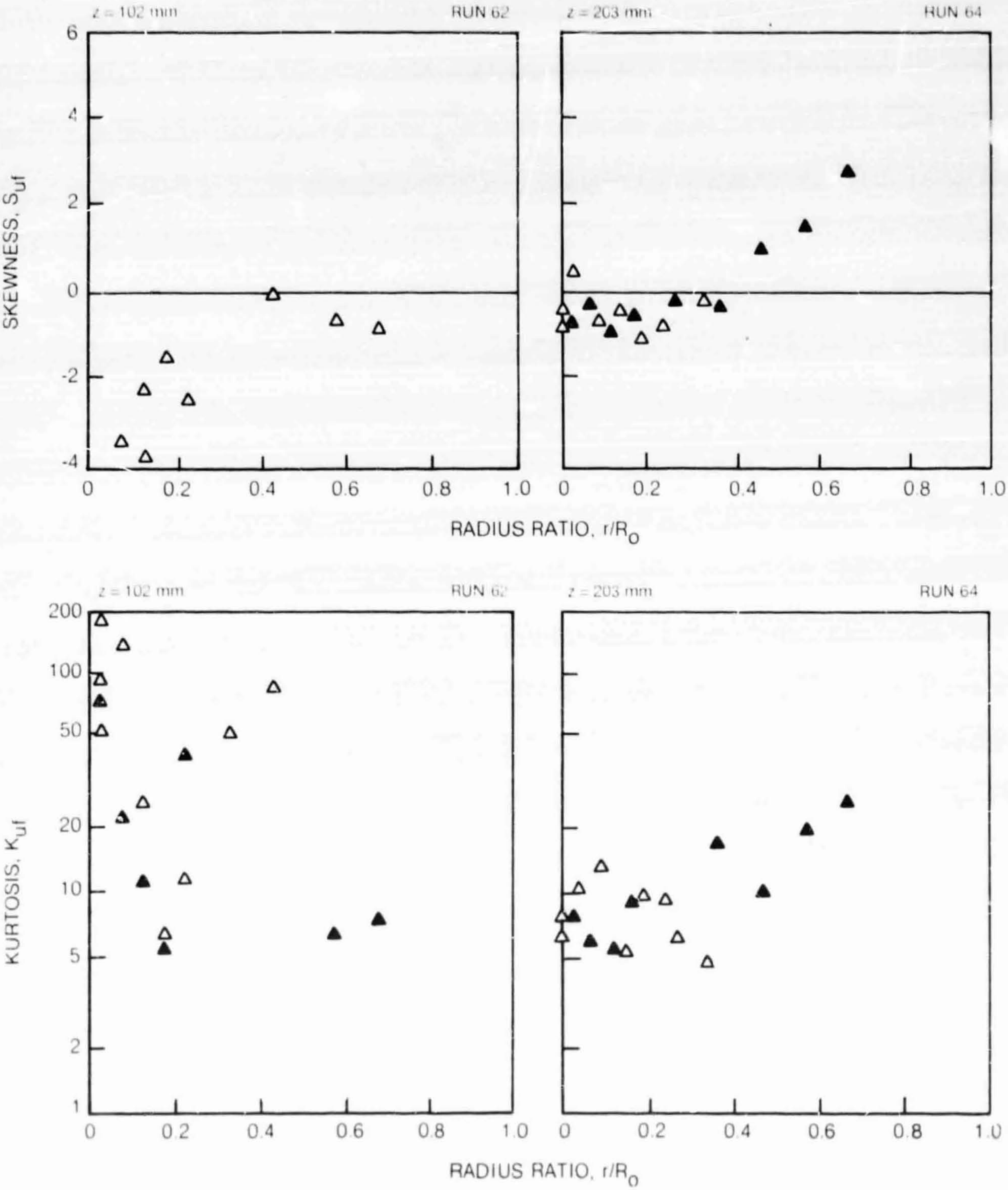

81-12-38-58

SECOND CENTRAL MOMENT, SKEWNESS AND KURTOSIS OF TURBULENT AZIMUTHAL MASS TRANSPORT RATE PROFILES

SYMBOL	△	▲
LOCATION, θ	270	90

AXIAL LOCATION 102 mm

DATA FROM RUN 53

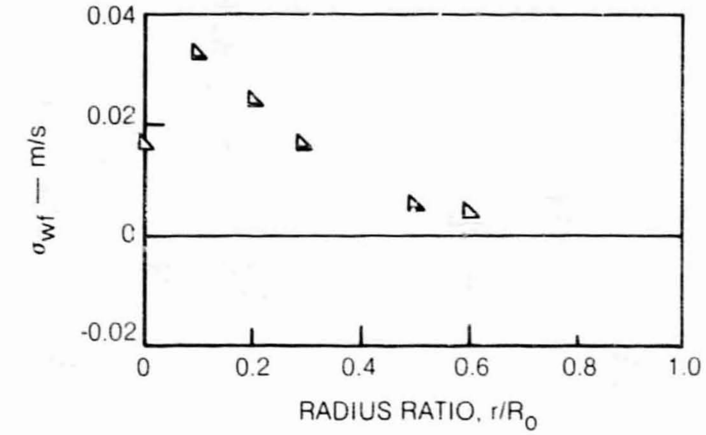

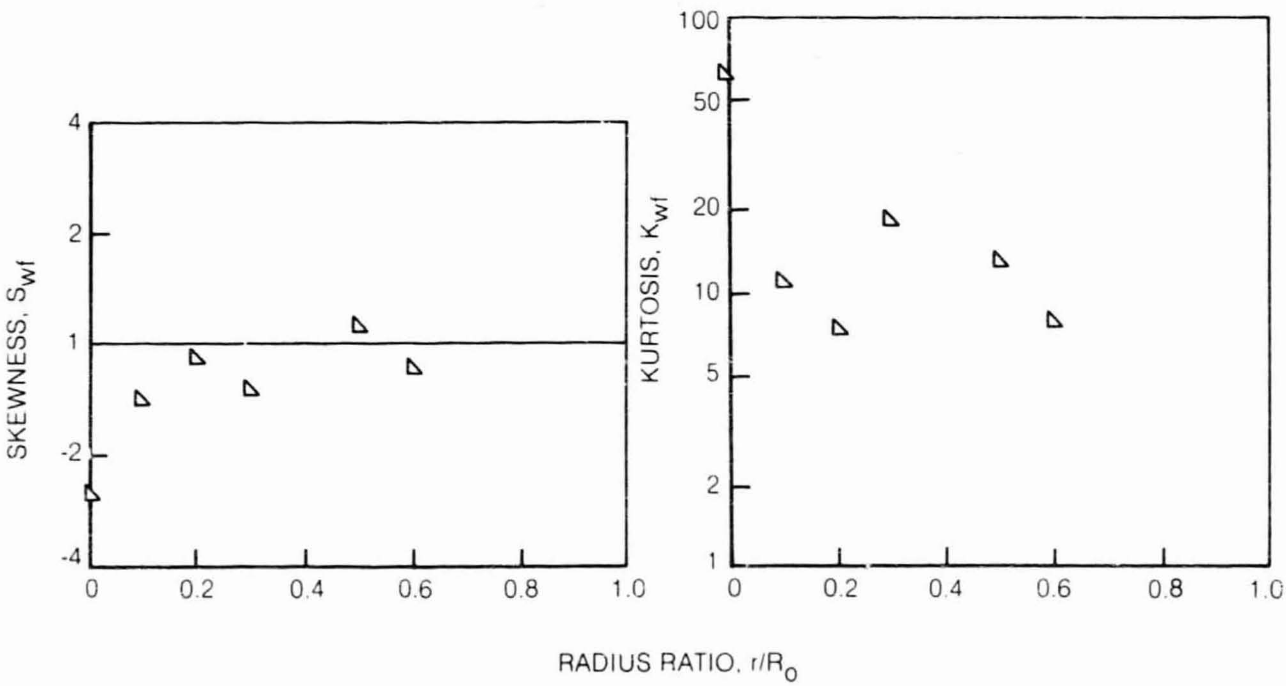

81–12–38–59

VISUALIZATION OF FLOW CONDITION 2 FROM HIGH SPEED MOTION PICTURES

$V_j = 0.27$ m/s $V_a = 1.66$ m/s
$Q_j = 3.1$ gpm $Q_a = 52.8$ gpm

DYE ADDED TO INNER JET FLUID

r-z PLANE

$0 < z < 100$ mm

$100 < z < 250$ mm

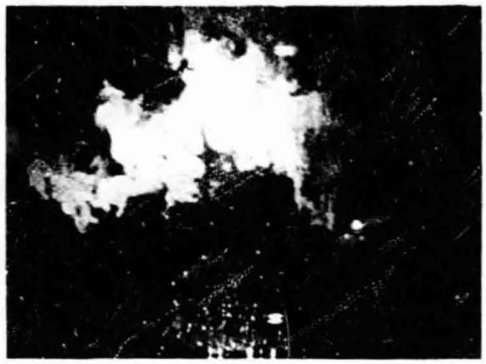

r-θ PLANE

$z = 51$ mm

$z = 102$ mm

$z = 153$ mm

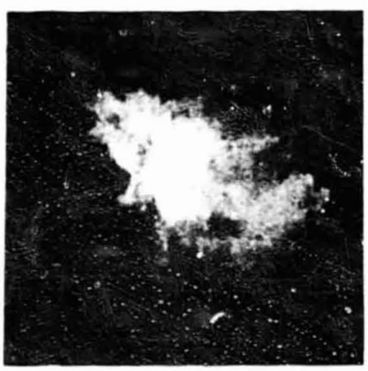

$z = 203$ mm

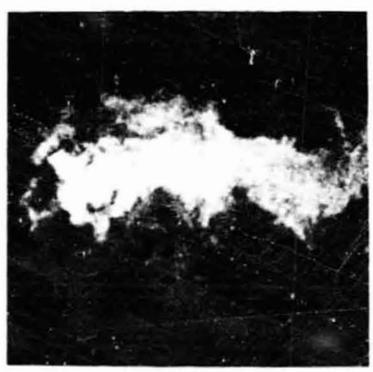

ORIGINAL PAGE
BLACK AND WHITE PHOTOGRAPH

VISUALIZATION OF FLOW CONDITION 3 FROM HIGH SPEED MOTION PICTURES

$V_j = 2.08$ m/s $V_a = 1.66$ m/s
$Q_j = 24.6$ gpm $Q_a = 52.8$ gpm

DYE ADDED TO INNER JET FLUID

r-z PLANE

$0 < z < 100$ mm

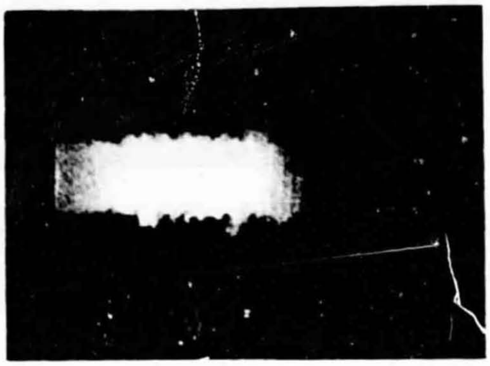

$100 < z < 250$ mm

r-θ PLANE

$z = 51$ mm

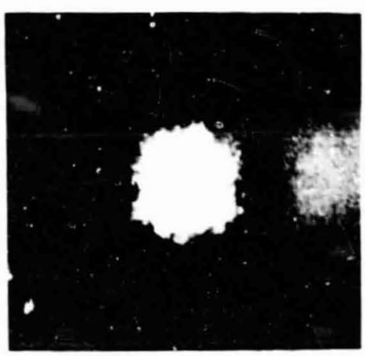

$z = 102$ mm

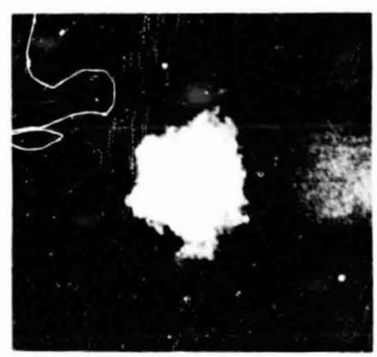

$z = 153$ mm

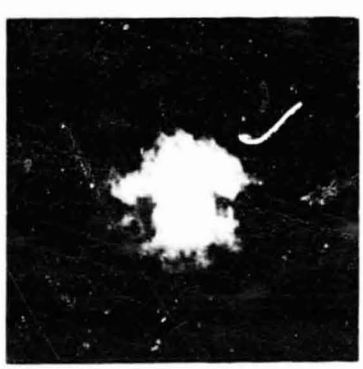

$z = 203$ mm

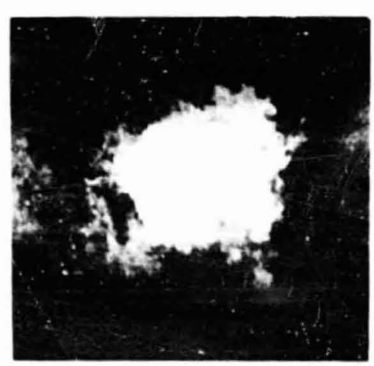

81-12-38-61

ORIGINAL PAGE
BLACK AND WHITE PHOTOGRAPH

FIG. 51

VISUALIZATION OF FLOW CONDITION 4 FROM HIGH SPEED MOTION PICTURES

$V_j = 0.94$ m/s $Va = 1.51$ m/s
$Q_j = 11.1$ gpm $Qa = 48.0$ gpm

DYE ADDED TO INNER JET FLUID

r-z PLANE

$0 < z < 100$ mm

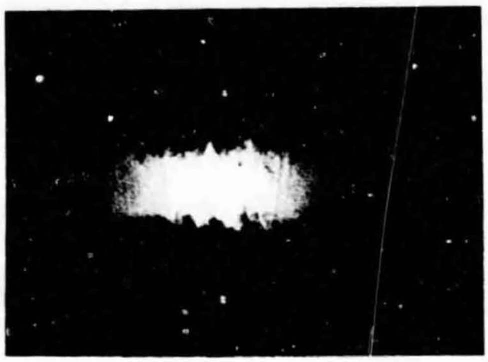

$100 < z < 250$ mm

r-θ PLANE

$z = 51$ mm

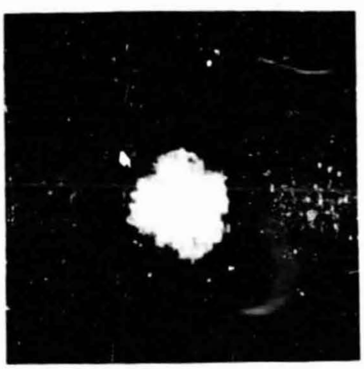

$z = 102$ mm

$z = 153$ mm

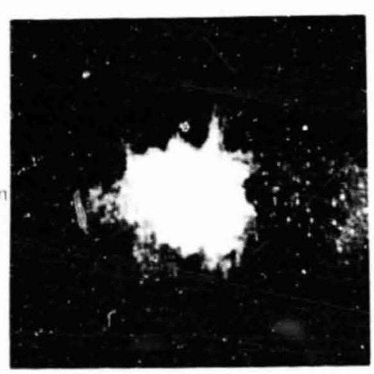

$z = 203$ mm

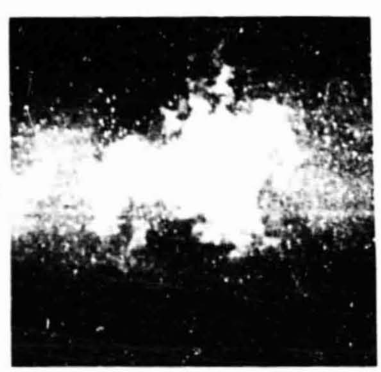

81–12–38–62

VISUALIZATION OF FLOW CONDITION 5 FROM HIGH SPEED MOTION PICTURES

$V_j = 0.94$ m/s $V_a = 2.87$ m/s

$Q_j = 11.1$ gpm $Q_a = 94.8$ gpm

DYE ADDED TO INNER JET FLUID

r-z PLANE

$0 < z < 100$ mm

$100 < z < 250$ mm

r-θ PLANE

$z = 51$ mm

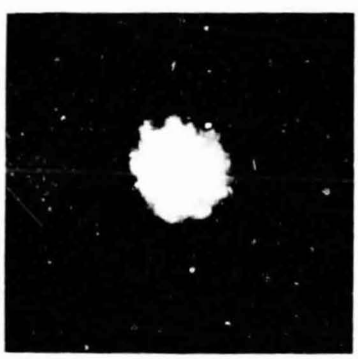

$z = 102$ mm

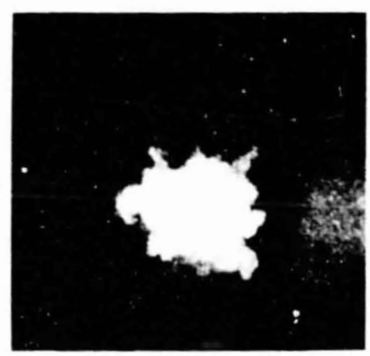

$z = 153$ mm

$z = 203$ mm